FATIGUE CRACK REPAIR FOR OFFSHORE STRUCTURES

José Efraín Rodríguez-Sánchez

Submitted for the Degree of
Doctor of Philosophy

Department of Mechanical Engineering
University College London

March 1999

ABSTRACT

A fatigue crack repair concept based on crack removal by cutting is presented. The aim is to extend the fatigue life of cracked welded connections. The concept developed presents an option to repair fatigue cracks particularly for structures installed in deep waters. Thus, the application of inspection techniques and cutting procedures such as ElectroChemical Machining (ECM) more suited to Remotely Operated Vehicle (ROV) deployment are addressed. Repairs of large fatigue cracks require the use of subsea clamps. A major problem is ensuring that load on stud-bolts is maintained. A second study considered the use of Alternating Current Stress Measurement (ACSM) for stress measurement.

Results from a study of stress analysis of the repair geometry using the finite element method are given. Recommendations for repair profiles were developed based on the analysis and experimental results.

An experimental testing programme was conducted considering welded T-butt and butt specimens. The numerical stress analysis was validated experimentally and conclusions to the application of ROVs and cutting techniques were made. The repair geometry was machined on the specimens using ECM, disc cutting and ROV grinding thus, pros and cons of each technique were identified. Application of compressive residual stresses by shot peening was briefly investigated and some observations are given. Analysis of experimental data was made for the determination of fatigue life extension after repair.

Analysis of the experimental crack shape evolution data was made to propose a crack shape design curve to determine stress intensity factors. Predictions of fatigue cracking after repair using fracture mechanics analysis are made and compared to the experimental results.

Observations of ROV performance on crack repair and stress measurement on bolts for tightening clamps were obtained from full scale trials. This allowed an assessment of ACSM for deep water applications. Finally, conclusions and recommendations for future work are given.

ACKNOWLEDGEMENTS

I would like to acknowledge the invaluable guidance of my supervisors, Professor W. D. Dover and Dr. F. P. Brennan throughout my PhD studies. Under their supervision I always obtained the finest suggestions for this work.

I would also like to acknowledge the support given by Ing. Oscar Valle-Molina especially whilst I was planning this studies.

I am grateful to all my colleagues at the UCL, NDE Centre, especially Peter Myers, Linus Etube and Farid Ud-Din who have been of great support along this time. The technical support given by the workshop personnel, especially Phil Jeavons for his participation preparing the specimens.

Finally, I would like to thank Instituto Mexicano del Petróleo and CONACYT whose financial support made this work possible.

TABLE OF CONTENTS

LIST OF FIGURES

Chapter One

Chapter Two

Chapter Three

Chapter Four

Chapter Five

LIST OF TABLES

Chapter Two

Chapter Three

Chapter Five

NOMENCLATURE

ACPD	Alternating Current Potential Difference
ACFM	Alternating Current Field Measurement
ACSM	Alternating Current Stress Measurement
A_n	constant whose value depends on the strength and ductility of the material
Ap	area of the jack piston
As	stud cross sectional area
a	crack depth
a	crack length
a/c	crack aspect ratio (crack depth / crack length)
a_i	crack depth 'i.'
a_i	initial crack size in metres
a_f	final crack size in metres
B	plate thickness
b	fatigue strength exponent
b	half width of cracked plate in mm
CPU	Central Processor Unit
C, m	material constants used in Paris Law
c	fatigue ductility exponent
c	half length of surface crack in mm
D	fatigue damage
D	repair depth
da/dN	crack growth rate
d	remaining depth after repair (T-D)
E	Young's modulus
ECM	Electrochemical machining
e	nominal strain
FEA	Finite Element Analysis

H	$E/(1+v^2)$ for plane strain and E for plane stress
H	magnetic field
h	half length of cracked plate
I	second moment of area
K	stress intensity factor
K_C	fracture toughness
K_f	fatigue notch factor
K_t	theoretical elastic stress concentration factor
K_{Is}	stress intensity factor sought
K_{Ik}	known stress intensity factor associated with the crack face displacements
k	number of stress ranges
L	repair length
L_{limit}	repair length where $SCF_{surface} = SCF_{edge}$
M	bending moment
M	in plane bending moment referred to unit thickness
M	magnetisation
MPI	Magnetic Particle Inspection
$m(a,x)$	weight function
N	fatigue life in number of cycles
NSC	Non uniform Stress Correction
N_f	cycles to failure
N_i	number of cycles to failure at constant stress range i.
N_i	number of cycles at ΔK_i and a_i
n_i	number of stress cycles in one year of stress range i.
P	total tensile force referred to unit thickness
P	pressure
Q	shape factor for elliptical crack
q	notch sensitivity index
R	stress ratio (Minimum nominal stress / Maximum nominal stress)
R	transverse repair radius

R	notch radius
RR	longitudinal repair radius
RF	reduction factor
S	nominal stress
S	stress range
SCF	Stress Concentration Factor
$SCF_{surface}$	SCF of a surface repair
SCF_{edge}	SCF of an edge repair
$SCF_{bending}$	SCF in bending mode
$SCF_{tension}$	SCF in tension mode
SCF_W	weld toe stress concentration factor
SW	repair surface width
S_t	remote uniform tension stress in Pa
S_b	remote bending stress on outer fibre in Pa
T	plate thickness
t	plate thickness
V_C	potential difference across the crack
V_R	potential difference adjacent to the crack used as reference
W	plate width
W	characteristic dimension that depends on the geometry of the component
x	coordinate parallel to the crack
Y	K modification factor (Y factor), takes in account the geometric characteristics of the crack, component and type of loading.
Y_s	correction for a free front surface
Y_w	correction for finite plate width
Y_e	correction for crack geometry
Y_g	correction for non uniform stress field
Y_k	correction for the presence of geometrical discontinuity
Y_m	correction for changes in structural restraint
Y_i	stress intensity calibration factor 'i.'

Y_{lin}	Y factor solution for a flat plate
Yg	non uniform stress correction factor (Y N&R+DC+NSC)
y	distance from neutral axis to extreme fibre
α	repair orientation
Δ	value normally taken as 1 (fatigue life calculation from Miner's rule)
Δ_C	probe gap across the crack
$\Delta\varepsilon$	strain range
$\Delta\sigma$	surface stress range of the uncracked tubular joint at the crack site
ΔK	stress intensity range K_{max} -K_{min}
Δ_R	probe gap adjacent to the crack used as reference
ΔK_i	stress intensity factor range 'i.'
ΔS	nominal stress range in MPa
Δ_i	stress intensity factor range 'i.'
$\Delta\sigma_i$	notch stress range 'i.'
ε	local strain
ε_a, ε_b and ε_c	strain gauge readings aligned 0^0, 45^0 and 90^0 respectively in a three element rectangular rosette.
ε'_f	fatigue ductility coefficient
ϕ	parametric angle of ellipse in degrees
$\phi_{1,2}$	principal angles
ρ	notch-root radius
ρ	weld toe radius
σ	local stress
σ	nominal surface stress due to bending
σ_a	stress amplitude
σ_b	stress in the uncracked body over infinitesimal length db
σ_b	bending stress at the crack tip
σ_{bo}	bending stress at the surface

$\frac{\sigma_{bi}}{\sigma}$	ratio of the non uniform stress distribution along the line of the crack to a uniformly distributed stress
σ_e	endurance limit
σ_m	mean stress
σ_{max}	maximum local stress
σ_{max}	maximum nominal stress
σ_{min}	minimum nominal stress
σ_{no}	nominal surface stress at the weld toe
σ_{nom}	nominal stress
σ_u	ultimate strength
$\sigma(x)$	through thickness stress distribution in the uncracked body at the prospective crack site produced by a set of applied loads
$\sigma_W(x/T)$	weld toe stress at a non-dimensional depth to thickness ratio x/T
σ_y	yield strength
$\sigma_{1,2}$	principal stresses
σ'_f	fatigue strength coefficient
μ	permeability
υ	Poisson's relation
$v(x)$	known crack face displacements as a function of crack length at the loading point x in the direction of loading for the stress distribution analysed
$2N_f$	reversals to failure

CHAPTER ONE

INTRODUCTION AND BACKGROUND

1.1 Introduction

Fatigue cracking in fixed tubular offshore structures usually takes place at the weld toes of the tubular joints. To maintain the structural integrity of the structure, fatigue cracks have to be repaired to avoid the development of a succession of fatigue related events such as a crack growing through the thickness then propagating around the perimeter of the structural member causing the loss of the member or the eventual loss of several members and finally a possible complete collapse of the structure.

Fatigue crack repair of offshore tubular joints can be achieved by basically two different methods: crack removal by cutting out the crack and mechanical strengthening by clamping the cracked joint. The selection of the repair method depends on the severity of the cracking.

The fatigue design of offshore tubular joints is generally based on the S-N curves considering the joint type and environment. However, S-N curves for repaired joints are non-existent thus, the application of fracture mechanics is required for the fatigue analysis of crack repairs by crack removal.

A background to fracture mechanics is presented in this chapter following a review of the stress analysis of welded connections for offshore underwater applications. The electrochemical machining (ECM) method is presented for the underwater repair of fatigue cracks. The application of residual stresses by a peening method is considered to improve the post repair fatigue performance. The application of ROVs for the deployment of the ECM and peening methods is addressed. Since a repair is a notch, a brief study of the fatigue and stress analysis of notches is reported. To end the chapter, other factors that affect fatigue crack growth in tubular joints are reported and some remarks about the inspection, repair and maintenance of offshore structures are made.

1.2 Tubular Welded Connections

An offshore steel structure for oil production is mainly formed by welded connections of tubular members where fatigue cracks grow from weld imperfections, under the stress produced by the action of ocean waves and winds. This process, has to be monitored and sometimes if not stopped or controlled with the application of fatigue strength improvement methods may lead to a severe stiffness reduction of the welded connection by fatigue cracking and as a consequence may also increase the risk of failure of the overall structure.

Welded tubular connections are structural discontinuities of a space frame where high stress concentrations occur at the weld toes of the connecting welds reducing the fatigue strength of the connection. The tubular member onto which is welded one or more tubes of the same or smaller diameters is known as the chord and the latter members are braces. Configuration and size of a tubular welded connection is determined by its position in the offshore structure which defines the type and magnitude of loading the connection has to withstand.

The tubular welded connections that occur most commonly in structures are the type used in the so called "Template Fixed Platform"; this name is given due to the function of the welded tubular space frame jacket as a template for pile driving. The platform also gives lateral bracing for the piles, which permanently anchor the platform to the foundation, as well as carrying the loads of the superstructure that support the crew, equipment and other facilities.

Although fabrication using square cross-sections is easier, in submerged parts of the structure circular tubes are more appropriate due to their low drag coefficient which results in smaller hydrodynamic forces. Also their uniform symmetrical cross section exhibits no sensitivity to lateral load direction. The latter is especially important in the offshore environment, where wind and wave forces are directionally random.

Tubular joints are highly susceptible to fatigue cracking at the weld toes due to the presence of high stress concentrations, weld defects and residual stresses. The following sections explain in some detail these concepts.

1.2.1 Stress Distributions in Tubular Joints

Stresses in tubular joints arise from three main causes in addition to the residual stresses that may be present:

1. The basic structural response of the joint to the applied load. This is termed the nominal stress.
2. Further, to maintain continuity at the intersection, the tubular walls deform giving rise to deformation stresses.
3. Finally, the weld introduces a geometrical discontinuity, giving rise to notch stresses [1.1].

Nominal stresses are produced by the reaction of the jacket structure under applied external loads, their magnitudes can be calculated from a global analysis of the structure.

Deformation stresses are necessary to satisfy displacement compatibility requirements of the chord around its intersection with the brace. So, the nominal stress distribution in the brace suffers a redistribution to satisfy the non-uniform stiffness distribution of the chord at the intersection.

Notch stresses are the result of the weld and its geometry. The weld stiffens the walls of the chord and brace beyond the weld toe having also an effect on the deformation stresses. The geometry of the weld works as a geometric discontinuity of the tubular walls at the weld toes due to the abrupt change of section. Notch stresses have a highly concentrated effect at the surface, this is the reason why cracks initiate on the surface and propagate through the thickness.

Each one of the three stresses defined above have a particular distribution and location in the tubular joint. The magnitude of each one can be estimated using various techniques but the most commonly used method is based on strain gauge measurements. Figure 1.1 illustrates the redistribution of nominal stress at a tubular joint intersection and the hot-spot stress definition given by the UK Dept. of Energy [1.5].

1.2.2 Fatigue Analysis of Welded Tubular Connections

Fatigue failure is defined as the number of stress cycles taken to reach a pre-defined failure criterion.

Fatigue analysis of welded tubular connections has its main application in offshore structures and this industry has been developed in the last 60 years. However, fatigue problems in welded tubular connections became a major topic of interest more recently when the exploitation of oil and gas reserves started in hostile ocean environments like the North Sea.

The research fields on fatigue of tubular joints can be classified in a simplistic manner as: stress distribution around the welded connection, fatigue life predictions considering service conditions by S-N curves or fracture mechanics approaches, repair to extend or comply with the design fatigue life and inspection, repair and maintenance scheduling.

Prediction of fatigue life of tubular joints depends basically on models representing the wave loads and models representing crack growth. The former are of random nature, so there is always an intrinsic source of error and the latter are highly complicated in terms of material science and are invariably mathematically complicated.

The major factors that affect the fatigue life of a welded connection are:

a) Applied stress range
b) Initial defect shapes, sizes and distribution
c) Notch severity
d) Residual stresses
e) Environment

The higher the magnitude of the applied stress range ($\Delta\sigma = \sigma max - \sigma min$) the lower the capacity of the material to withstand cyclic loads.

In a study of welded components measurement of the depth and radius of initial defects at fillet weld toes and predictions of initiation [1.2] showed a negligible crack initiation life. Therefore, initial defects at fillet weld toes are really initial cracks.

The notch severity influences the rate of growth of the fatigue crack when a notch is subjected to cyclic loading. A measure of the notch severity can be expressed in terms of the fatigue notch factor for cyclic loads and in terms of the stress concentration factor for static loads, both concepts will be explained in section 1.4.

Residual stresses are defined as those stresses which would exist in an elastic solid body if all external loads were removed [1.3]. The level of residual stress determines the fatigue-sensitive portion of the load cycle. So, under a stress cycle that remains completely compressive, a fatigue crack closes and cannot grow.

The underwater environment induce a corrosive effect increasing the effect of the initial defects, thus reducing the fatigue life of the welded component. Additionally, the corrosive effect is more severe in regions with tensile residual stresses like weld toes.

For the design of tubular joints against fatigue failure the magnitudes of the stress concentration factors at the weld toes are needed to determine magnitudes of the hot-spot stresses. Hot-spot stress definition differ substantially from one design code to another. So, to avoid inconsistencies the definition considered and the S-N curves to be used have to be given by the same design code. As an example the hot-spot definition considered for two design codes is presented:

American Petroleum Institute API RP 2A-WSD (20^{th} Edition, 1993)
'C.5: The hot spot stress is the stress in the immediate vicinity of a structural discontinuity'[1.4].
'C.5.4: Although there has been some variation in technique among various investigators contributing to the data base, typical hot spot strain gages were centred within 0.25 inch (6mm) to $0.1\sqrt{Rt}$ of the weld toes, with a gage length of 0.125 inch (3mm) and oriented perpendicular to the weld. Here R and t refer to the outside radius and thickness of the member instrumented either the chord or brace. Due to the steep gradients near intersecting tubes, larger gages further from the weld indicate stresses which are too low. The microscopic notch or stress singularity at the weld toe is excluded from this definition of hot spot stress, but rather is included in the S-N curve. In turn, the S-N curve should be qualified as to the severity of these notches, which are a function of both weld size and profile quality.' [1.4].

UK Department of Energy's Guidance Notes (1984)
'the greatest value around the brace/chord intersection of the extrapolation to the weld toe of the geometric stress distribution near the weld toe. This hot-spot stress incorporates the effects of overall joint geometry (i.e. the relative sizes of the brace and chord) but omits the stress concentrating influence of the weld itself which results in a local stress distribution' [1.5]. See figure 1.1.

As a comment of the above definition, for the study of the fatigue phenomena in tubular welded joints it is not necessary to consider the weld effects in the S-N curves because their influence is only important during the fatigue initiation stage which is a small percentage of the total fatigue life. Moreover, due to the manufacturing differences between welds their effects are difficult to reproduce experimentally.

Once the hot-spot stress has been defined, fatigue life can be calculated considering two different approaches:

a) Stress-life approach based on hot-spot S-N curves obtained usually from tubular joint tests combined with a damage assessment rule (Palmgren-Miner rule). This takes fully into account the geometric effect of the tubular joint and does not consider the weld notch effect due to the impossibility to consider the weld dimensions in all different cases.

b) Fracture mechanics procedures to predict the crack propagation which often accounts for most of the fatigue life of a welded tubular joint.

1.3 Fatigue Crack Inspection and Repair

According to Gurney, 1968 [1.6], there are four alternatives that have to be reviewed during the design stage or in existing structures where fatigue problems are already occurring in service:

1. Remove or reduce the load which is causing the failure
2. Reduce the stress at the critical section
3. Improve the design
4. Application of fatigue strength improvement techniques

Alternatives 1, 2 and 3 are more difficult to implement for existing structures than alternative 4. However, it is important to consider that they could be implemented if a fatigue strength improvement technique is not available.

It is known that there is little difference between the fatigue properties of welded joints made from different grades of steel. However, a fatigue improvement method may allow a higher strength steel to make use of the higher allowable static stress by permitting a higher applied stress range.

During this work only the fatigue performance of fatigue crack repaired welded connections is studied. As will be presented in chapter 2, it has been observed that after a repair has been carried out, the crack can restart in the parent material or in the weld; therefore, the generalised understanding that welded connections perform similarly in fatigue conditions regardless of the steel used for their manufacture cannot be considered if the crack restarts in the parent material.

1.3.1 Fatigue Improvement Techniques

A fatigue improvement technique can be defined as a procedure that extends the fatigue life of a welded joint without changing the applied stresses and without changing the overall joint geometry or shape.

Fatigue improvement techniques can be classified in three groups according to Gurney [1.6] as follows:

1. Modification of the shape of the notch so as to reduce the stress concentration
2. Modification of the residual stress distribution so as to produce beneficial compressive residual stresses at the notch
3. The protection of the notch from the atmosphere or other corrosive medium

Figure 1.2 shows graphically a relationship done by Smith [1.7] in which the three groups mentioned by Gurney are decomposed presenting a variety of methods that have been used to improve the fatigue strength of welded joints.

The modification of the shape of the notch is highly beneficial for transverse butt welds as removal of the stress concentration at the edge of the weld increases the strength to that of the parent material. However, offshore structures have many welded joints and for them it is impossible to restore fatigue strength to that of the parent material, since the deformation stresses are always present, but it is possible to reduce the sharpness of the notch created at the toes and such treatment can still have considerable beneficial effect.

The creation of residual compressive stresses at the notches from which fatigue cracks grow provides a way to make a tensile applied stress cycle partially compressive, considering of course that the applied load is not so great as to relieve the residual stresses by yielding.

The protection of a notch from a corrosive medium also reduces the detrimental increase of crack growth rate due to the corrosion effect.

In service, once a crack is detected its growth can be stopped or delayed if the crack is in the stage of early propagation, but when fatigue damage is severe the repair of a tubular joint is usually carried out by means of strengthening by mechanical clamps or grouted clamps as presented in chapter 5. In this thesis especial attention is given to the repair of cracks in welded joints in the early stages of propagation with the purpose to reinstate, if possible, the original fatigue resistance by means of crack removal.

1.3.2 Underwater Fatigue Crack Inspection and Repair

Due to economical and time constraints the inspection of offshore platforms is performed on a representative sample of the large number of members and joints that exist in a platform. The sample is defined using consistent selection criteria that take into account the probability of the member becoming damaged and its role in the safety of the structure. In a fixed platform fatigue cracks develop in the welded joints of structural members. The inspection of the joints has the purpose of detecting and sizing the effects of fatigue damage which appear in the form of cracks; the most used inspection philosophy considers inspecting all critical nodes over a five year period [1.8].

Fatigue cracks usually start at the weld toes and have to be detected and sized by Non Destructive Testing (NDT) techniques to determine by Non Destructive Evaluation (NDE) methods like fracture mechanics if they have to be repaired in order to extend the fatigue life of the welded connection to a required design life. The selection of the NDT method relies on the operator, the Safety Guidance used or on the advice of the Certifying Authorities. The general situation is that the inspection requirements of the operators are in many cases more stringent than the recommendations given by the certifying authorities.

NDT methods for inspection of offshore platforms are continuously being upgraded due to the necessity to obtain reliable crack detection and sizing information to allow more economic application of repairs and maintain the safety of the platform.

The extent of the NDT methods for underwater inspection of offshore oil and gas production platforms is wide and only the application of MPI (Magnetic Particle Inspection), ACPD (Alternating Current Potential Difference) and ACFM (Alternating Current Field Measurement) for fatigue crack detection and inspection of the repaired profile after the crack has been removed by machining will be addressed in this work. These methods have been used successfully in practice by inspection companies and also during the experimental work presented in chapter 3. Additionally, the ACSM (Alternating Current Stress Measurement) technique for stress measurement on clamp studs is presented in chapter 5.

It is not the purpose of this study to describe the NDT methods mentioned above; however, these have been applied for more than five years by oil rig operators in the North Sea first and in the Gulf of Mexico and have demonstrated their ability to provide reliable results in the field and also in laboratory conditions.

In the offshore industry the modification of the shape of the repair notch is done usually by burr grinding and has become common practice for dry and underwater conditions. However, the creation of residual compressive stresses is still not of frequent underwater application but it should be noted that even gentle grinding can create residual tensile stresses that can actually exceed the ultimate tensile strength of the material, so that cracking occurs [1.9]. The combination of grinding and peening can reverse the detrimental stresses produced by the grinding process. This takes full advantage of the reduction of the stress concentration by the modification of the shape of the notch and creates beneficial compressive stresses in the notch.

Another alternative method applied to modify the shape of the notch is the application of the Electro-Chemical Machining (ECM) technique. Although, residual stresses are also produced using ECM its underwater application using ROVs appears to be more feasible than grinding.

The following sections present the ECM technique for crack removal and the peening technique to induce compressive residual stresses. Finally, the underwater repair of fatigue cracks using Remotely Operated Vehicles (ROVs) will be addressed.

1.3.3 Electrochemical Machining

Electrochemical Machining (ECM) is the controlled dissolution of a metal workpiece using electrolysis.

Using ECM the removal of metal is controlled by anodic dissolution in an electrolytic cell in which the workpiece is the anode and the tool the cathode. The electrolyte is pumped through the gap between the tool and the workpiece, while direct current is passed through the cell at a low voltage, to dissolve metal from the workpiece at approximately 100% efficiency [1.10].

ECM is generally used in the industry to do work that would be difficult by mechanical machining; such as, machining hard metals or producing odd-shaped profiles; although it is best suited to mass production applications, because of high set-up costs, it is sometimes applicable to small lot production. The most frequent application of ECM is in the production of jet engine, aerospace and automotive parts. Figure 1.3a) shows a typical set-up for ECM, and figure 1.3b) shows the application of ECM on a T-butt used for the experimental work presented later in this thesis. Figure 1.4a) shows a slotted U shaped tool electrode and figure 1.4b) the ECM system operating on a T-butt used in the experiments described in chapter 3.

Set-up

Only a brief description of the set-up required will be given as it is outside of the scope of this work and may vary depending on the particular application. The tool may be made of brass, cooper, stainless steel, titanium, platinum, aluminium or graphite. The workpiece must be an electrically conductive material. The set-up must be rigid enough to withstand the forces caused by the high pressure of the electrolyte which tend to separate the tool from the workpiece. A servomechanism can be used to control the movement of the tool.

Settings

Control of many variables is needed for good results in ECM, the most important of these are: a) tool feed rate, b) current density, c) electrolyte composition, suspended solids content, temperature, and flow rate, d) tool and fixture material, e) workpiece material and condition, and f) cutting gap [1.10].

The current density in amperes per square units of cutting area is the most important factor in determining the permissible rate of tool feed and surface finish.

The electrolyte has three main functions: carrying the current between the tool and the workpiece, removing the products of the reaction from the cutting region, and removing heat produced during the operation. The electrolyte usually should not contain more than 2% by weight of sludge.

Surface Finish

Surface finish is important since it is a key factor for components under fatigue loading. The greater the current density at the cutting face the finer the surface finish. Important variables that affect surface finish are: feed rate, gap dimensions, and electrolyte composition, viscosity, temperature and flow.

Microscopic surface defects may be caused by selective attack on certain constituents in an alloy. They are usually associated with low current densities and with metallic precipitates at grain boundaries. One kind of surface defect is associated with inter-granular attack, which can shorten the fatigue life of metal, and cannot be accepted in parts subjected to high stress [1.10].

Hydrogen Embrittlement

Hydrogen embrittlement does not occur during ECM because hydrogen is given off at the tool and not at the workpiece. Neutral electrolytes such as salt solutions, are unlikely to cause hydrogen embrittlement [1.10].

Application

The following settings were given by D. Clifton from Edinburgh University [1.11] during the application of ECM in a laboratory sampling experiment which presents similarities to a fatigue crack repair in a welded connection.

Average tool feed rate	1.5 mm per min
Machining voltage	18 volts

Machining current at max. tool depth	98 amps
Flow pressure	4 MPa
Temperature	20^0 C
Electrolyte composition	20% $NaNO_3$ solution
Tool material	Copper
Tool width	20 mm
Tool height	40 mm
Tool slot width	0.6 mm
Tool slot length	50 mm
Workpiece material	Steel
Overcut	0.4 mm
Gap	0.3-0.7 mm

1.3.4 Peening

Peening is the process of impacting a metal surface with hard objects causing plastic deformation in the surface. The impact objects can be hard small particles, a bunch of needles or even a simple hammer and the process would be known as shot peening, needle peening or hammer peening respectively.

The mechanisms of fatigue improvement using peening are:
-Cold work
-Residual compressive stress

The cold work process is used in the industry to improve the strength of metals changing the metallurgy of the surface resulting in an increased surface hardness and refined grain structure; however the brittleness is also increased and consequently there is a limit to which cold working may be carried without danger of fracture.

The residual compressive stress is probably the most important benefit of peening in terms of fatigue improvement. The residual stress is produced since the surface layer of material is deformed beyond its yield point by peening; however, it cannot deform freely as the material underneath is not affected by the peening and therefore has not been plastically deformed. So, a residual stress is kept in the surface material due to the constraint imposed by the deeper layers. A graphical representation of this effect can be represented in a two bar system as shown in figure 1.5 [1.9] and the resultant stress distribution in a metal bar after peening is presented in figure 1.6 [1.12]

It, has been found by researchers that the fatigue improvement by peening is mainly due to the residual compressive stress rather than due to the cold work hardening process. Occasional high tensile loads, such as many components experience in service, reduce the beneficial effects of peening since plastic deformation is caused at points of high stress concentration when the loading is applied.

Residual compressive stresses reduce the effective range of fatigue stress and reduces crack growth and can even stop cracks growing entirely. However, there are still difficulties in making quantitative predictions of the effect on fatigue life as a result of a particular peening process. Fracture Mechanics procedures have not been easily applied for peened components; moreover, peeneing has a greater effect on the crack initiation phase where fracture mechanics cannot be applied. Is more likely that fading of residual stress has a less effect in high yield stress materials since they can sustain higher tensile loads before deforming plastically.

Peening leaves a surface far from being smooth which may cause crack starting points. Once a crack starts to propagate across the residually compressed layers, the magnitudes of the residual stresses are needed to make predictions of crack growth, but there is not a generally reliable and practical method to obtain residual stress information.

The following rule of thumb is recommended for the application of shot peening but the concept can be extended for other methods of peening. If the component under consideration is achieving a reversed bending endurance limit close to 0.5 of the tensile strength in steels or 0.25 in other alloys, further improvement by peening is unlikely [1.9].

The maximum residual compressive stress induced by shot peening is aproximately 60% of the ultimate tensile strength in compression. This ratio is common to all metallic materials [1.9].

The general conclusion on the behaviour of cracks growing from a peened surface in fatigue is that surface effects, which may be regarded as minute cracks, already exist in the surface but that their initial growth rate is considerably slower than that of cracks which are eventually initiated in a normal well prepared (unpeened) surface. Their progress is further reduced by the increased compressive stress represented by the peak value below the surface, see figure 1.6. The reason why the crack eventually starts to grow again is probably due to the relaxation in the residual stress due to the imposed alternating stress [1.9].

The magnitude and depth of the residual stress field are the major factors controlling the fatigue effect of peening and these will depend on the process applied, particularly the intensity of peening. For the case of shot peening the size of the pellets determines the depth of the residual stress field as can be seen in figure 1.7 [1.13].

Intensity will vary greatly with circumstances, one technique used in a wide variety of circumstances is to peen a flat strip of metal on one side while it is clamped to the component and then measure how much it curves when it is released. This is the Almen strip method. The strips have to be of certain dimensions and made from metal with specified properties. Peening intensity is linked to this curvature, which is easily measured, as an arc-height. Large curvatures and therefore large arc-height values go with higher intensities, see figure 1.8.

Almen strips are seen as a very good way of monitoring consistency of a peening process, but not a fundamental way of comparing processes with different parameters. Because the same effect could be obtained increasing one or two of the following parameters and keeping one or two constant: Time of exposure, blast pressure and shot size.

Another approach which is regularly used and which is still linked to the amount of surface deformation is an estimate of coverage. Coverage is defined as the ratio of dimpled surface to the total surface and this is still fairly laborious since irregular areas need to be measured and compared but is easier to establish the exposure time needed to just create a surface with no unpeened regions. This is defined as 100% coverage condition and can be found by simple visual inspection. If twenty seconds of exposure gives 100% coverage, for instance, forty seconds under the same conditions is described as 200% coverage, and ten seconds as 50% coverage.

Most of the metal working processes, unless very carefully controlled, have a detrimental effect on fatigue life and resistance to stress corrosion cracking (SCC). Welding is the worst of them: welding creates very high residual tensile stresses, introduces a mechanical stress concentration area, a very hard brittle layer and an annealed area, all in the heat affected zone (HAZ) adjacent to the weld metal. This combination can lower the fatigue strength to a small percentage of that of an integrally machined component (rather than welded). Peening can be applied to reduce the tensile stresses produced during the welding process improving the performance of the component. Figure 1.9 shows a T-butt specimen used in the experimental work described in chapter 3 under shot peening.

1.3.5 ROV Underwater Inspection and Repair

The need to exploit oil reservoirs in deeper waters and the trend to reduce diver intervention has increased the attention towards the application of Remotely Operated Vehicles (ROV).

An ROV system comprises the following components:
a) Delivery vehicle or ROV
b) Deployment system or arm manipulator
c) Tools to perform the required tasks like ACFM, ECM, ACSM, etc.
d) Control system to command the components a) to c)

This work will only address the techniques and tools to perform inspection and repair of fatigue cracks with the application of ACFM and ECM and the stress measurement on clamp studs using the ACSM technique.

Grinding performed by divers can be considered as a common practice for the removal of fatigue cracks in underwater conditions. It requires a considerable force to drive the grinding tool and in some cases one does not obtain the desired precision of the repair profile. ROV application of grinding induces cyclic loading on the arm manipulator which produces fatigue damage to this expensive component.

Deployment of ECM by an ROV has been considered a more suitable technique to produce a repair profile to remove fatigue cracks rather than by grinding as it requires no force on the tool and it is possible to obtain the required precision of the profile. Moreover, since a sample of the material is obtained, it may provide the following additional advantages over grinding:
a) Identification of the nature of the defect removed; this would provide confirmation that the defect is a fatigue crack.

b) Confirmation that all the fatigue crack has been removed

c) Determination of the steel characteristics and metal condition

Clifton, 1996 [1.14], mentioned that the application of ECM in underwater conditions does not have technical problems and even sea water can be used as an electrolyte giving feed rates of 0.7 mm/min; however, it is recommended to use an enriched NaCl solution to improve the performance.

The successfulness of fatigue crack repair relies on the fatigue life extension obtained which depends on the following factors:

a) Amount of metal removed beyond the crack tip

b) Groove profile

c) Groove surface finish

d) Service stress level

Etube, 1994 [1.15] demonstrated that for crack sizing using ACFM and removal by grinding the recommended amount of metal cut out beyond the crack tip is 2 mm to account for sizing and cutting inaccuracies. The development of a recommended groove profile is presented in chapter 2 and the effects of surface finish and stress level on crack initiation are studied in chapter 3.

Sugunan et al, 1990 [1.16] noted that the fatigue crack repair problem in tubular joints would be less severe for cracks in the size range 0-5 mm (crack depth) and 0-50 mm (crack length), but that deeper cracks and factors such as high β ratio (brace diameter/chord diameter) could make the problem more difficult. Additionally, it was also noted that crack removal in tubular joints would change the initial stress distribution leading to peak stress regions adjacent to the repair ends, see figure 1.10.

Application of the ACFM technique in underwater conditions by divers has been used extensively for fatigue crack inspection. For the case of ROV arm deployment the ACFM technique uses an array for scanning along a certain length. This prevents the arm doing the difficult operation of following the weld toe path around the joint and only performing 'pick and place' operations for which the ROV arm is fully capable. However, a new probe has to be designed for the inspection of the repaired profile. Dover [1.14] has explained that cracks in tubular joints seldom grow as simple planar cracks, instead they are often doubly curved growing along the curved weld toe and curving under the weld. This could create problems for cutting and for re-inspection. Figure 1.11 shows the effect of a crack curving under the weld and a prototype of an ACFM array for inspection of repaired cracks is shown in figure 1.12 [1.14].

Finally for the case of clamp repair the deployment of the ACSM technique is quite simple since stress measurement of clamp studs requires only spot measurements. Therefore, the 'pick and place' capability of the ROV arm is ideal for the operation as presented in chapter 5.

1.4. Stress Analysis of Notches

A notch is a localised change in shape which has a definite depth and root radius. Notches are important because they are a common source of fatigue cracks leading to failure.

A practical classification of notches would be:

Form part of the component

- Screw threads
- Bolt holes
- Grooves

Consequence of Manufacturing

- Weld toes
- Machining marks
- Grinding scratches

- Weld defects

Notch weld defects are basically caused by the absence of material as in the case of slag inclusions, cold laps, cracks, porosity, undercuts and lack of penetration.

1.4.1 Stress concentration factor

The theoretical elastic stress concentration factor K_t relates the maximum elastic stress at the root of a notch to far-field loading and is defined as the ratio of the maximum local stress σ_{max} to the nominal stress σ_{nom}.

$$K_t = \frac{\sigma_{max}}{\sigma_{nom}} \tag{1.1}$$

The subscript t indicates that the stress concentration factor is always a theoretical factor because it is based on assumptions in the theory of elasticity like Hooke's law, homogeneity, etc. The basic subscript t distinguishes theoretical factors from experimentally determined factors such as fatigue notch factor K_f. The K_t values depend strongly on notch depth and root radius. Various compendiums of K_t values have been published with useful data for strength calculations, among them is Peterson's [1.17].

1.4.2 Stress distribution ahead of a notch

The presence of notches in stress fields produce a high stress localisation known as stress concentration. In practice, the stress concentrating effect of the notch can raise the local stress above the yield stress of the material for relatively small applied stresses. Yielding then occurs at the notch root which leads to a redistribution of stress and a breakdown of SCF known as blunting effect. Due to yielding at the notch root the peak stresses predicted by the SCF are never attained.

The size effect of the notch root radius can be attributed to the volume effect. As the size of the notch increases, the volume of highly stressed material near the notch increases. This result is a greater probability of fatigue failure, see figure 1.15, [1.18].

1.4.3 Fatigue notch factor

Under fatigue loading conditions, the elastic stress concentration factor is replaced by the so called fatigue notch factor

$$K_f = \frac{\text{unnotched component endurance limit}}{\text{notched component endurance limit}} \qquad (1.2)$$

In general, fatigue experiments suggest that notches produce a less stress concentrating effect than predicted by theoretical elastic analysis such that Kf < Kt and Kf→Kt for large notch-root radii and for higher strength materials.

The degree of agreement between theoretical predictions of elastic stress concentration and actual effects is often measured by the so-called notch sensitivity index [1.19] which is defined as

$$q = \frac{K_f - 1}{K_t - 1} \qquad (1.3)$$

q varies from zero for no notch effect (K_f=1) to unity for the full effect predicted by the elasticity theory ($K_f = K_t$).

Whereas the theoretical stress concentration factor, K_t is a function of the notch size, notch shape, component geometry and loading mode; the fatigue stress concentration factor, K_f is dependent additionally on material. It is determined from experimental measurements or empirical relations. An example of such a measure of K_f is the well known Peterson equation for ferrous wrought alloys [1.17]

$$K_f \approx 1 + \frac{(K_t - 1)}{(1 + A_n / \rho)} \qquad (1.4)$$

or in terms of notch sensitivity factor

$$q \approx \frac{1}{(1 + A_n / \rho)} \tag{1.5}$$

where

A_n constant whose value depends on the strength and ductility of the material

ρ notch-root radius.

Two rectangular plates of the same material and under the same loading mode, each one with a circular hole in the middle, would have identical theoretical stress concentration factor values if the relation of plate width versus hole diameter and loading mode is the same. But Applying Peterson's relation reveals that the notches will have different fatigue stress concentration values, the value of K_f for the wider plate would be larger. This result shows that for geometrically similar notches, notch sensitivity increases with increasing notch root radius.

The value of K_f can be used to correct the entire S-N curve for notched members, results tend to be conservative. A general trend is that the value of fatigue notch factor decreases with increasing stress level. This trend is material dependent and can probably be explained by the blunting effect near the notch. In most design cases the fatigue notch factor needs to be corrected for shorter lives. This concept is expanded in section 1.5.1.

1.4.4 Mean stress effects

Cyclic fatigue properties of a material are obtained from completely reversed, constant amplitude strain-controlled tests. Components in practice seldom experience this type of loading, as some mean stress is usually present and it may have a significant effect on the fatigue life.

The fatigue notch factor K_f is not necessarily always less than the elastic stress concentration factor K_t. It may be less or it may be more depending on the mean stress considered, tensile mean stress can increase the notch factor above the stress concentration factor K_t.

Plotting the results of a nonzero mean stress on a Haigh diagram (alternating stress versus mean stress) with lines of constant life through the data points may appear as in figure 1.14.

Since reproducing the Haigh diagram can be expensive, empirical relationships have been developed to connect the endurance limit on the alternating stress axis to either the yield strength σ_y or ultimate strength σ_u on the mean axis[1.18]

Sodeberg (USA, 1930) $\quad \sigma_a / \sigma_e + \sigma_m / \sigma_y = 1 \quad$ (1.6)

Goodman (England, 1899) $\quad \sigma_a / \sigma_e + \sigma_m / \sigma_u = 1 \quad$ (1.7)

Gerber (Germany, 1874) $\quad \sigma_a / \sigma_e + (\sigma_m / \sigma_u)^2 = 1 \quad$ (1.8)

where

$$\text{Stress amplitude} = \sigma_a = (\sigma_{max} - \sigma_{min})/2 \tag{1.9}$$

$$\text{Mean stress} = \sigma_m = (\sigma_{max} + \sigma_{min})/2 \tag{1.10}$$

$$\text{Endurance limit} = \sigma_e \approx 0.5\,\sigma_u \ \text{ for } \sigma_u \leq 200 \text{ ksi} \tag{1.11}$$

$$\text{if } \sigma_u \geq 200 \text{ ksi then } \sigma_e \approx 100 \text{ ksi} \tag{1.12}$$

1.5 Fatigue Life Calculation at Notches

Fatigue life in a notched component can be determined using three different approaches and each one has its particular range of validity.

- The stress-life, S-N, method
- The strain-life method
- Fracture mechanics approach

The fatigue life of a component is made up of initiation and propagation stages. Usually the strain-life method is applied during the initiation stage where plasticity has a significant role. Fracture mechanics approaches are considered for an estimate of the fatigue life spent in crack propagation. At long lives, where plastic strain is negligible and stress and strain are easily related, the strain-life and stress-life approaches are essentially the same. The growth of a fatigue crack from a notch covers the whole range from a short crack in a yielded region to a long crack in an elastic body.

1.5.1 Stress-Life Approach

The stress-life, S-N method was the first approach used in an attempt to understand and quantify metal fatigue. This approach is widely used in design applications where the applied stress is primarily within the elastic range of the material, the resultant lives (cycles to failure) are long and loading is essentially constant amplitude. The stress-life method does not work well in low cycle applications, where the applied strains have a significant plastic component. In this range a strain-based approach is more appropriate. This method is unsuitable to account for load sequence effects, changes in notch mean or residual stresses. Nevertheless, this method is still widely used in fatigue analyses.

S-N curves are generally produced for unnotched specimens under fully reversal loading and in order to correct a S-N curve for a notched member the fatigue notch factor K_f can be used. The modified Juvinall approach [1.20] considers that to modify a S-N curve for notched components two points are needed as the S-N curve has two changes in slope. The first point corresponds to life to failure of 10^6 cycles and the stress range is obtained dividing the endurance limit Se by K_f. The second point corresponds to life to failure of 10^3 cycles and the ordinate is obtained dividing the stress range at 10^3 cycles by K'_f which is the fatigue notch factor for stresses corresponding to lives of 1000 cycles, figure 1.15.

An alternative more conservative method with the disadvantage that it defines the S-N curve in the low cycle region where the approach is inappropriate, considers the trend that the notch effect decreases with decreasing fatigue life. The method requires only one point at life 10^6 cycles with a corresponding alternating stress of

Se/K_f., this point is connected with a straight line to the true fracture stress, σ_f at one cycle [1.18].

1.5.2 Strain-Life Approach

The strain-life method is based on the observation that in many components the response of the material in notches is strain or deformation dependant. This method assumes that smooth specimens tested under strain-control can simulate fatigue damage at the notch root of an engineering component. Crack growth is not explicitly accounted for, therefore, the strain-life method is often considered for initiation life estimates.

The strain-life method accounts for notch-root plasticity. By knowing the notch root strain history and smooth specimen strain-life data, fatigue-life evaluations may be performed for notched members. One of the advantages of this method is that it accounts for changes in local mean and residual stresses which make it suitable for calculating fatigue-life of a notched component considering constant amplitude loading, variable amplitude loading, sequence and mean stress effects.

The strain-life method requires that notch root stresses and strains be known. These may be determined by the following methods: Strain gauge measurements, finite element analysis and methods that relate local stresses and strains to nominal values (Neuber's rule).

The least time-consuming and least expensive method of determining these values is by relating the local stresses and strains to nominal values. The procedure is based on the assumption that upon yielding, the local stress, σ, and local strain, ε, are no longer linearly related and the local values are no longer related to the nominal values by K_t. Instead, the nominal and local values are related in terms of stress and strain concentration factors

$$K_\sigma = \frac{\sigma}{S} \tag{1.13}$$

$$K_\varepsilon = \frac{\varepsilon}{e} \tag{1.14}$$

where

S and e are nominal stress and strain respectively

σ and ε are local stress and strain respectively

After yielding occurs, the local stress concentration, K_σ, decreases with respect to K_t, and K_ε increases with respect to K_t see figure 1.19. Thus, after yielding the actual local stress is less than that predicted using K_t, while the actual local strain is greater than predicted using K_t. Neuber analysed a specific notch geometry and derived the following relationship

$$K_t = \sqrt{K_\sigma K_\varepsilon} \tag{1.15}$$

substituting equations (1.13) and (1.14) and rearranging

$$\begin{gathered} K_t^2 = \frac{\sigma}{S}\frac{\varepsilon}{e} \\ K_t^2 S e = \sigma\varepsilon \end{gathered} \tag{1.16}$$

Application of this rule requires satisfy at the same time a cyclic stress-strain curve of the material, so the problem is reduced to the solution of two simultaneous equations. The most common stress-strain curve is in the following form proposed by Morrow [1.21]

$$\frac{\Delta\varepsilon}{2} = \frac{\sigma'_f}{E}(2N_f)^b + \varepsilon'_f\,(2N_f)^c \tag{1.17}$$

where

$2N_f$ Reversals to failure

E Young's modulus

$\Delta\varepsilon$ Strain range

and the following four empirical constants known as fatigue constants are:

σ'_f Fatigue strength coefficient b Fatigue strength exponent

ε'_f Fatigue ductility coefficient

c Fatigue ductility exponent

The first term represents the elastic strain component; the second, the plastic strain component. Knowing these material constants, the strain-life relationship can be evaluated, and then used to predict the onset of fatigue cracking. The consistency of published cyclic material properties should be examined before adopting values for insertion into strain-life approximations. For conservative estimates of high-cycle fatigue failure, the lower value of fatigue strength coefficient and the higher value of fatigue strength exponent should be chosen from any appropriate set of cyclic material values [1.22]

1.6 Fatigue Crack Growth

Life prediction involves calculating stresses and strains in highly stressed areas from the input loads for a given material and geometry. The calculated stresses and strains are transformed into fatigue damage or crack growth. Integrating damage or crack growth subject to an empirical failure criterion, through some service history, leads to a predicted life.

The fatigue process involves a period of damage accumulation leading to crack initiation (Stage I), followed by a period of crack growth (Stage II), until the critical flaw size is reached (Stage III). Total life is thus the sum of an initiation and propagation phase.

The differentiation of crack initiation and crack propagation is important in life prediction, because the presence of a crack alters the stress field in a component. Once this stress field is disturbed significantly by the crack, the slip process concentrates at the crack tip, and fracture mechanics approaches are used to predict the life including the crack effect on the stress field.

1.6.1 Crack initiation

Crack initiation is the process of plastic deformation caused by a dislocation movement represented as intensified slip bands in the body of the material and as intrusions-extrusions on the surface.

Fatigue cracks initiate only in regions where plastic deformation occurs. Consequently, fatigue cracks do not initiate in a component whose strain field everywhere including regions of strain concentrations and of residual stresses is elastic [1.23].

Fatigue crack initiation occurs by the process of reversed-slip or reversed-plastic strain. The amount of slip that develops under the action of a given strain depends on how easy it is for two planes of atoms to move past each other along the slip plane. Thus, the component of force applied normal to the slip plane makes slip easier if it is tensile, by separating the planes, and correspondingly harder if it is compression. Where such intense slip bands intersect a free surface, intrusions and extrusions can form due to the cyclic irreversibility of plastic deformation. This is what is called Stage I of fatigue crack growth which has a crystallographic nature because although it grows 45^0 respect to the normal maximum principal stress, its plane and growth speed depends on grain boundaries.

Crack initiation has different interpretations depending on the surface quality of the component under study, for example, for welded structures crack initiation is almost neglected due to the propagation of defects introduced during the welding procedure. On the other hand, for machined components with very smooth surfaces the crack initiation stage takes an important part of the fatigue life of the component.

Frost, Marsh and Pook [1.24] commenting on metals in which fatigue cracks are initiated at a free surface presented the following arguments explaining that damage in a polycrystalline ductile metal is associated with grains having free surface rather than those within the body of the metal

1. Surface grains are in contact with the atmosphere; thus, if environment is a factor in the damage process, they are obviously the more susceptible.
2. A surface grain is the only part of a polycrystal not wholly supported by adjoining grains. Because the slip systems in neighbouring grains of a polycrystal are not related to each other, a grain having a free surface will be able to deform plastically more easily than a grain in the body of metal which is surrounded by other grains.
3. It has been shown that if a fatigue test is stopped after some fraction (say, 20 per cent) of the expected life of the specimen, a thin layer of metal is removed from the test-section, and the test continued at the same stress level, the total life of the specimen is longer than the expected life of the original specimen [1.25]. If a surface layer is removed at frequent intervals throughout a test, the expected life may be exceeded many times; in fact, provided that the stress amplitude is maintained constant and the frequency of removal and depth of removed layer are sufficient, the life will be limited only by the initial cross-sectional area of the specimen.
4. The fatigue strength of small specimens cut from the interior of the test-section of a larger specimen broken in reversed direct stress (that is, cut from material which has been subjected to a stress level greater than the plain fatigue limit) is not inferior to that of the virgin material [1.26].
5. If the surface of a specimen is hardened, either metallurgical or by surface working, the fatigue strength of the specimen as a whole may be increased. Similarly, any procedure which softens the surface decreases the fatigue strength of the specimen.

6. Metallurgical examination of broken fatigue specimens of nominally homogeneous metallic specimens which have been subjected to a uniform stress distribution over their cross-section does not reveal cracks in the body of the specimen. In certain circumstances, however, cracks may form in the interior of a specimen at inclusions or flaws or beneath hardened surface layers.

Stresses inside the notch region are undoubtedly important in describing fatigue crack initiation and early growth at the hot spot, but these phenomena form only a small part of the total fatigue life of a welded connection. Such stresses decay rapidly as crack growth takes place into the welded connection from the weld toe [1.27] .

For the case of tubular welded connections, the weld toe radius ρ mainly effects the fatigue crack initiation life, while the weld toe angle may affect both initiation and propagation lives [1.28].

1.6.2 Crack Propagation

The three Stages of fatigue crack growth are related to the three fundamental modes of crack surface displacements defined in fracture mechanics, see figure 1.17. Stage I corresponds to Mode II or shearing with a Mode I superimposed, Stage II is only Mode I or tensile opening of the crack and finally Stage III corresponds to Mode III or tearing.

Crack growth in Stage I after crossing one or two grains change to a Stage II crack mode. During this stage which is essentially non-crystallographic and stable crack propagation takes place, the crack now turns from 45^0 to a plane normal to the maximum principal stress; striation markings are characteristic of Stage II.

The final phase where rupture occurs or Stage III presents ductile tearing with an inclined mode of fracture as the crack tears through the material. The point of transition from Stage II to Stage III is dependent on the yield strength of the material, stress intensity factor and stress ratio.

1.7 Fracture Mechanics Calculations

The aim of Fracture Mechanics is to calculate whether or not a defect of given size will propagate in a catastrophic manner under service loading and hence to determine the degree of safety that the structure possesses with respect to failure by fracture [1.29].

Fracture mechanics seeks to define the local conditions of stress and strain around a crack, in terms of global parameters such as: load, shape and size of the crack, geometry of the component and material properties [1.30]. Various approaches have been employed in the analysis of fracture problems, leading to the introduction of various fracture mechanics parameters. However, the most popular of them is the stress intensity factor (K), it can characterise the stress field ahead of a sharp crack according with the linear-elastic fracture mechanics theory.

1.7.1 Determination of Stress Intensity Factors

Various methods for the determination of stress intensity factors (K), can be considered ranging from the consultation of handbooks to the application of complicated mathematical analysis with integral transforms and complex variables; numerical methods can also be considered such as the finite element method and the boundary element method and a final option can be the use of experimental techniques.

Chapter 4 will describe the application of two analytical methods and the extraction of ΔK from experimental data. With the application of equipment able to provide crack growth measurements, the crack growth rate per cycle (da/dN) can be determined experimentally and knowing the fatigue constants of the material (C and m), it is possible to apply the Paris law [1.32] expressed in equation (1.18).

$$\frac{da}{dN} = C(\Delta K)^m \tag{1.18}$$

$$\Delta K = \left(\frac{1}{C}\frac{da}{dN}\right)^{\frac{1}{m}}$$

Using the crack growth data collected during the experimental fatigue testing of a component, the stress intensity factor calculated would correspond to the specific conditions of loading, geometry of the component and crack size variation during the test.

Life to failure can be determined rearranging the Paris equation proposed in the 1960s and is still considered as the most widely accepted expression

$$N_f = \int_{ai}^{af} \frac{da}{C(\Delta K)^m} \tag{1.19}$$

where

da/dN	crack growth rate
C	material constant
m	material constant
ΔK	stress intensity range K_{max}-K_{min}
N_f	cycles to failure
a_i	initial crack length
a_f	final crack length

1.7.2 Fracture Toughness

As a crack grows the storage capacity of energy in the material reduces and when the material cannot store more energy the crack growth transforms from stable to unstable behaviour leading to a brittle failure of the component.

The material resistance to brittle fracture is characterised in terms of fracture toughness. The plane stress fracture toughness of a material (K_C) is the maximum value of the stress intensity factor a crack can assume before it propagates like a brittle failure. Fracture toughness can be considered the limiting value of the stress intensity factor.

Since the fracture toughness of a material will depend on the volume of material capable of plastically deforming prior to fracture, and since this volume depends on specimen thickness, it follows that the fracture toughness will vary with thickness [1.31]. The plane stress fracture toughness depends on metallurgical and specimen thickness. Maximum constraint conditions occur in the plane strain state. The plane strain fracture toughness (K_{IC}) is dependent only on metallurgical factors. When plane strain state conditions are not reached the fracture toughness at the given conditions is obtained instead.

One very important aspect of this lower level of toughness known as plane strain fracture toughness is that it does not decrease further with increasing thickness, thereby making this value a conservative lower limit of material toughness in any given engineering applications [1.31].

The interaction of the fracture toughness with the design stress and crack size controls the conditions of fracture in a component as can be observed in the relation

$$K_C = \sigma\sqrt{\pi a} \tag{1.20}$$

where

K_C Fracture toughness depends on the material selection

σ Stress level depends on the design stress

a Crack size depends on the allowable flaw size or NDT flaw detection

The above relation may be used in several ways to design against fatigue failure but once a combination of two variables is defined, the third is fixed.

1.8 Fatigue Analysis of Tubular Joints

Fatigue analysis of an offshore structure should be made considering the recommended methods in the design codes. Note that the design codes have validity within given limits, especially in terms of environmental parameters. Although, the recommendations derived from this thesis can be applied to any geographical region, the stress level associated with wave loading considered in the fatigue analysis should be determined for the particular region where the structure is operating.

The fatigue analysis methods for offshore structures are broadly classified as: deterministic and probabilistic, since they are not the central to this work only a brief description of them is given.

1.8.1 Deterministic Analysis

In the deterministic method of fatigue analysis the structural response is determined for a group of average stress ranges determined from wave heights that characterise the wave environment in a region within a period of time. The response of each structural member is computed from a global stress analysis of the structure for each wave height and its associated wave period. The allowable number of cycles for the various average stress ranges can be determined from the S-N curves given in the design code. The number of cycles experienced by the structural member can be determined from the wave period correspondent to the average stress range. The fatigue damage is calculated for each stress range using the Miner-Palmgren linear cumulative theory [1.33] expressed as

$$D = \sum_{i=1}^{k} \frac{n_i}{N_i} \qquad (1.21)$$

where

k number of stress ranges

n_i number of stress cycles in one year of stress range i.

N_i number of cycles to failure at constant stress range i.

The fatigue life in years can be calculated as

$$\text{Total Life} = \Delta / D \tag{1.22}$$

where

Δ value normally taken as 1 or smaller to increase the safety margin

The Miner-Palmgren equation assumes fatigue failure for a damage ratio D=1.This equation does not consider sequence effects thus, the damage caused by a stress cycle is independent of where it occurs in the load history.

1.8.2 Probabilistic Analysis

To predict the fatigue life of a component subjected to variable amplitude loading, cycle counting techniques can be applied to reduce a complex load history into a number of events which can be compared to the available constant amplitude data. Among the most common techniques for cycle counting are: Rainflow counting, Peak counting, Range counting and level crossing counting. These procedures have the aim of finding the most damaging combination of counts from a fatigue point of view.

The Rainflow cycle counting technique has derived in many other techniques [1.36, 1.37] however, it is has become a generic term that describes any cycle counting method which attempts to identify closed hysterisis loops in the stress-strain response of a material subjected to cyclic loading as expressed in equation (1.17). Each time a hysteresis loop is closed a cyclic count is made.

In the probabilistic method the Miner-Palmgren equation is generally also applied. Thus to determine the fatigue life, the stress range probability density function is usually considered in the form of a Rayleigh distribution. Integration of the distribution for damage calculation and determination of other parameters involved is explained in [1.35].

1.8.3 Fracture Mechanics Analysis

The deterministic and probabilistic fatigue analysis methods described before both rely on the S-N curves provided by a design code to determine the fatigue life from the Miner-Palmgren equation. However, for the case of a fatigue crack repaired tubular joint by crack removal as proposed in this work, the design codes do not provide S-N curves. Therefore, fatigue life determination has to be carried out by fracture mechanics procedures as presented in chapter 4.

The fatigue crack growth in tubular joints can be described by equation (1.18) and the stress intensity factor range ΔK can be expressed as

$$\Delta K = Y\Delta\sigma\sqrt{\pi a} \tag{1.23}$$

where

$\Delta\sigma$ surface stress range of the uncracked tubular joint at the crack site

a crack depth

Y modification factor (Y factor)

Equation (1.23) is a general expression that can be applied to any crack geometry and loading mode by considering the corresponding Y factor. The Y factor can remain constant through all the crack growth but in general and especially for the case of the crack geometries present in tubular joints, it varies as a function of various parameters as is presented in chapter 4.

For the calculation of the fatigue life of a crack repaired tubular joint by crack removal, the Y factor should include the particular characteristics of the crack growing in the repair notch and propagating through the thickness of the tubular member under the membrane and bending stresses produced by the wave loading on the structure. Thus, fatigue life can be calculated from equation (1.18), for a corresponding final crack depth a_f considering the deterministically or probabilistically determined stress ranges for the particular tubular joint and crack site.

1.9 Factors Affecting Fatigue Crack Growth in Tubular Joints

From the conclusions obtained in the United Kingdom Offshore Steels Research Project-phase I, UKOSRP-I [1.34], for this work it was considered that the principal factors that could effect the fatigue crack growth of a fatigue crack repaired tubular joint are:

a) Thickness effect
b) Environmental factors
c) Weld factors
d) Variable amplitude and damage accountancy

The thickness effect is that thicker specimens have shorter fatigue endurance, so an adequate correction to the S-N curves has been included in the Department of Energy Guidance.

Environmental factors such as corrosion can reduce the endurance under freely corroding conditions by a factor of two compared with air tests. An optimal cathodic protection potential of -0.85 V tends to restore the endurance to the air value.

Weld factors such as weld improvement techniques are beneficial. At lower levels of stress range the effect is marked. However in freely corroding conditions, the benefit from toe grinding reduces, although it is still significant.

Experimental tests support the use of Miner-Palmgren summation to calculate variable amplitude endurance. However, there was evidence that the mean summation value could be less than unity (0.8 approx.).

1.10 Generalities about Inspection, Repair and Maintenance

An offshore structure is required to operate safely during its uninterrupted operation until the reserves are exhausted or until further production becomes uneconomic.

Loss of structural integrity and the resulting inability of the structure to support some of the loads can occur in a number of ways, such as [1.38]

a) Foundation failure
b) Overall instability
c) General plasticity
d) Fatigue
e) Fracture
f) Corrosion, etc

or by a combination of these mechanisms.

The process of inspection, repair and maintenance has the intention to guarantee to a certain extent the integrity of the structure against the mechanisms described above. Additionally, this process allows the statutory requirements for certification to be met. The cost involved in inspection, repair and maintenance represents a major element in the operational cost of an offshore structure. However, it is accepted by the operators as an unavoidable cost.

Jacket structures have some components whose integrity is critical to the reliability of the structure, while others do not have a great effect on the system reliability. Therefore, these type of structures are suitable candidates for targeted risk-based inspection planning strategies where both the probability and consequences of failure of each component are taken into account [1.39].

Fatigue damage has been identified as the most important factor in causing degradation of structural integrity of offshore structures in the North Sea. During the operational life, the structural tubular joints can experience up to 200 million wave induced stress cycles of variable amplitude [1.40].

The current practice is to repair whenever a fatigue crack is found, offshore repair is very expensive but this has been considered the only way for the offshore industry to ensure the integrity of the structure as required by the UK Department of Energy.

1.11 EDICS Project

The Evaluation of Diverless IRM for subsea Completions and deepsea Structures (EDICS) [1.41], became necessary since there is in the offshore industry the tendency to reduce diver intervention and increase the use of deeper water production and subsea completions.

In the EDICS project the ROV execution of Inspection, Repair and Maintenace (IRM) is evaluated considering the following three components:

A) Delivery vehicle (ROV)
B) Deployment system (Computed Aided Telemanipulator CAT addressed in this thesis as arm)
C) Tools for IRM

There are various commercial versions of each of the three components presented above but their performance is not well established. Thus, the aim of the EDICS project was to evaluate them for assuring safe operations and cost reductions.

The project was carried out by seven companies from France and Britain and it was founded by the European Commission and industrial sponsors. The total cost of the project was 2.82 MECU. The work was executed from April 1995 to June 1998.

The interventions on subsea installations evaluated in the EDICS project were:

- Inspection: Visual inspection and NDT (ACFM, ACSM)
- Repair: Grinding
- Maintenance: Checking and valve operating (torque)

Only the most demanding activities identified in subsea interventions were evaluated and extrapolations were made to evaluate others.

The deployment systems evaluated were:
B.1) ARM by Slignsby (UK)
B.2) MAESTRO by Cybernetix (France)

The docking of the ROV against the structure plays an important role on the successfulness of the IRM activities. Two docking systems were evaluated: three docking points using sticky feet and two docking points using claws.

Full scale trials in steady water and with turbulent water conditions using an ROV and deployment system were carried out in Aberdeen (UK) at the National Hyperbaric Centre and in Brest (France) at IFREMER (Institut Francais de Recherche pour l'Exploitation de la MER). The IRM tasks selected for evaluation required a 50-100 hp work ROV. The ROVs used in the trials were:

A.1) MRV6 for trials in UK
A.2) SCS (Stolt Comex Seaway)Constructor for trials in France

The tools used during the EDICS trials were:

C.1) Inspection (NDT): For crack detection and sizing ACFM array and ACFM single probe, both probes designed for pick and place deployment.

	For stress measurement the ACSM array also designed for pick and place deployment.
C.2) Repair:	Grinding
C.3) Maintenance:	Valve operating (Torque)

The Inspection trials were performed with high level of accuracy since the arm has good level of performance on pick and place activities. The Repair, grinding trials were not as successful since under the action of current there is a residual motion (+/- 30mm) transmitted to the tip of the burr affecting the desired shape of the repair. Maintenance trials, valve operating was performed easily, the ROV arm system was able to apply a force or 50 kg.

During the development of this thesis, the EDICS project provided the opportunity for ROV arm grinding one of the specimens used in the experimental programme presented in chapter 3. Due to the high costs involved in ROV arm trials, the opportunity given in the EDICS project was invaluable for assessing the performance of an ROV arm machining the repair profile proposed in this thesis.

Additionally, the EDICS project gave also the possibility to participate in the validation of the ACSM technique described in chapter 5. The ACSM is a novel technique for stress measurement and has an important application in the verification of the load level on stud-bolts in clamps. Clamps are widely used for the repair of severely cracked tubular joints in the offshore industry. The integrity of the clamp providing an alternate load path avoiding the cracked joint, relies on the friction between the clamp and the tubular joint surface. The friction is induced by the force applied by the stud-bolts. Thus, the load level on the studs-bolts has to be checked regularly to satisfy safety requirements demanded by the Certification Authorities and the operators. However, there is an absence of commercial equipment for stress/load measurement in underwater conditions. This situation heightened the need to consider the application of the ACSM technique in the fatigue crack repair activities presented in this thesis.

1.12 Summary

The assessment of ROV based interventions for IRM activities in offshore structures installed in deep waters was considered in the scope of the EDICS project. From the results it was observed that the ROV arm system had difficulties in performing a burr grinding repair procedure (based on a diver procedure) for crack removal. This situation led to considering the possibility of utilising the ECM technique as a metal removal procedure to substitute the burr grinder. This substitution avoids for the ROV the difficult task to follow repair paths since the ECM technique can be incorporated into a self contained unit. Thus, the ROV is then only required for its ideal 'pick and place' function.

The explanation given above provides an available solution for repairing a fatigue cracked welded connection by an ROV system. However, the geometry of the repair has to be considered carefully. The repair profile has to be simpler compared with the repairs performed by divers since it has to be produced with a restricted number of degrees of freedom. Additionally, the repair geometry has to facilitate the inspection and extend to the maximum possible the fatigue life of the repaired component.

In the remaining of this section, the strategy considered for determining a procedure based on ROV systems for the repair of fatigue cracked welded connections in deep underwater conditions is presented. Establishing the validity of the procedure for ROV repair in deep water structures will form the main work of this thesis. Since fatigue cracks can only be removed until they have reached certain depth, the fatigue crack repair problem consists of two parts:

1) Design of a repair geometry to remove shallow cracks
2) For the repair of deep cracks, the ROV system has to be capable of assuring that the loads acting on the structure are bypassing the cracked connection by using a clamp system.

For the design of the repair profile it is considered necessary to determine the stress distribution of the burr ground repairs commonly performed by divers. This can be achieved by finite element stress analysis of long repair profiles. The optimisation of the repair profile will be based on the following considerations:

a) Crack initiation takes place where the higher value of stress concentration is located.
b) Fatigue life after repair extends in inverse relation to the stress concentration value.

Thus, variation of repair geometry parameters such as depth, radius and length can be used to minimise the stress concentration, identify the crack initiation location and determine an optimum repair profile.

The optimum repair design for crack removal has to be proven experimentally and determine the fatigue life extension obtained. The analytical assumptions made in a) and b) have to be verified. For the cases were the fatigue life extension is not as desired it is maybe possible to increase the fatigue life after repair inducing compressive residual stresses on the repaired surface by shot peening. Assessment of the benefits obtained by shot peening has to be made.

Since ECM is a new technique for crack removal it is convenient to make a comparison with a technique that provides the best possible control whilst machining a repair. It is considered appropriate that the best available machining technique to compare ECM with is using disc cutters driven by a numerically control machine. Thus, comparisons of fatigue lives obtained from ECM and disc cut repaired specimens have to be made to determine the effect of ECM on the fatigue life extension of fatigue cracked repaired components.

It is also considered appropriate to compare the ECM and disc cut repair profiles with profiles obtained by ROV arm grinding to validate the application of ECM for ROV systems.

The experimental work can also provide information to define a crack depth to plate thickness ratio for the transition from shallow crack removal to clamping deep cracked connections.

Predictions of remaining fatigue life of crack repaired welded connections using fracture mechanics methods are required by operators since the available S-N curves do not consider fatigue crack repaired components. Thus, fracture mechanics predictions of remaining fatigue life after repair have to be made and comparisons with the experimental data can be used to validate the predictions.

For deep cracked tubular joints the ROV system has to be capable of assuring that the loads acting on the structure are bypassing the cracked connection by using a clamp system.

The integrity of the clamp system depends on the friction between the clamp and tubular joint and the friction is induced by the load on the stud-bolts. Thus, the load/stress level has to be checked regularly to verify that the alternate load path is provided avoiding the cracked connection. The lack of commercial equipment for underwater load/stress inspection led to consider in this thesis the assessment of the ACSM technique.

1.13 References

[1.1] UEG Offshore Research, "Design of Tubular Joints for Offshore Structures", *UEG/CIRIA*, 1985.

[1.2] I. J. Smith, I.F. Smith and S. J. Hurworth, "A 3-D analysis of the longitudinal non-load carrying fillet welded fatigue specimen", *Welding Institute Members Report*, Cambridge, UK, No. 184, 1982.

[1.3] J. O. Almen, P. H. Black. *Residual Stresses and Fatigue in Metals*, Mc. Graw- Hill Book Company, New York, 1963, p.6.

[1.4] "Recommended Practice for Planning, Designing and Constructing Fixed Offshore Platforms-Working Stress Design", 20th Edition, *American Petroleum Institute,* Washington, July 1993.

[1.5] Department of Energy, "Offshore Installations: Guidance on design and construction", *HMSO*, London, April 1984.

[1.6] T. R. Gurney, *Fatigue of Welded Structures*, Cambridge University Press, 1968.

[1.7] I. F. Smith and M. A. Hirst, "A review of fatigue strength improvements methods", *Can. Journal Civil Engineering.*, Vol. 12, 1985.

[1.8] Lyons, G. J., Brown, D. T., Editors, *Inspection, Assessment and Recertification of Offshore Platforms*, Bentham Press London, 1995.

[1.9] K. J. Marsh, *Shoot Peening: Techniques and Applications*, Engineering Materials Advisory Services Ltd., 1993.

[1.10] *Metals Handbook*, American Society of Materials, Vol. 3, 1967.

[1.11] D. Clifton, M.B. Barker, R.W. Gusthart and J.A. McGeough, "An Automated System for Weld Sampling and Defect Removal", *Underwater Technology*, Vol. 17, No. 4, 1991.

[1.12] *Shot Peening Applications*, Metal Improvement Company, Inc. 7th Ed., 1995.

[1.13] A. Bignonnet, et al, "Improvement on the Fatigue Life of Offshore

Welded Connections", *Institut de Recherches de la Siderurgie Francaise (IRSID)*, P.E. 3758.

[1.14] W. D. Dover, *Minutes of DIRECT kick-off meeting*, UCL, 2nd July 1996.

[1.15] L. Etube, *Optimisation of Weld Toe Grind Repair Profiles to Improve Fatigue Life using NDT Procedures*, 3rd Year Project, Mechanical Engineering, UCL, 1994.

[1.16] N. Sugunan, D. McDiarmid, W.D. Dover, "Fatigue Strength of Tubular Joints Subjected to Extensive Repair Grinding", *Final Report UCL NDE Centre*, 1990.

[1.17] R. E. Peterson, *Stress Concentration Factors*, John Wiley & Sons., 1973.

[1.18] J. A. Bannantine, J. J. Comer, J. L. Hanrock, *Fundamentals of Metal Fatigue Analysis*, Prentice Hall, New Jersey, 1990.

[1.19] G. E. Dieter, *Mechanical Metallurgy*, Mc Graw Hill, 1988.

[1.20] R.C. Juvinall, *Engineering Considerations of Stress, Strain and Strength*, McGraw Hill, New York, 1967.

[1.21] J. Morrow, ASTM STP 378, *American Society for Testing Materials*, 1965.

[1.22] F. P. Brennan, "The use of approximate strain-life fatigue crack initiation predictions", *Fatigue Journal*, Vol. 16, July 1994.

[1.23] J. M. Barsom, S.T. Rolfe, *Fracture and Fatigue Control in Structures*, Second Edition, Prentice Hall, Inc., 1987, pp. 272.

[1.24] N.E. Frost, K.J. Marsh, L.P. Pook, *Metal Fatigue,* Clarendon Press, Oxford, 1974, p. 6.

[1.25] J. M. Young, A. P. Greenough, *J. Inst. Metals*, Vol. 89, 1960-1, p. 241.

[1.26] G. F. Molden, G. C. Smith, *J. Iron Steel Inst.*, Vol. 194, 1960, p. 459.

[1.27] N. M. Irvine, "Review of stress analysis techniques used in UKORSP", *Fatigue in offshore structural steels*, Thomas Telford Ltd., London, 1981.

[1.28] X. Niu, *Effects of local stresses on fatigue strength of tubular welded joints*, PhD. Thesis, University College London, 1987.

[1.29] J. Knott and P. Withey, *Fracture Mechanics Worked Examples,* The Institute of Materials, 1993.

[1.30] A. Almar-Naess, *Fatigue Handbook,* Tapir, 1985.

[1.31] R. Hertzberg, *Deformation and Fracture Mechanics of Engineering Materials,* Wiley, 1989.

[1.32] P. C. Paris and F. Erdogan, "A critical analysis of crack propagation laws", *Trans. ASME, J. Basic Eng.*, Vol. D85, 1963

[1.33] M. A. Miner, "Cumulative Damage in Fatigue", Journal of Applied Mechanics, Vol. 112, 1945.

[1.34] United Kingdom Offshore Steels Research Project-phase I, *Final Report,* Dept. of Energy, OTH 88 282, 1988.

[1.35] H. O. Madsen, R. Skjong and M. Moghtaderi-Zadeh, "Experience on Probabilistic Fatigue Analysis of Offshore Structures", Proc. 5th Int. Symposium and Exhibit on Offshore Mechanics and Arctic Engineering (OMAE), Tokyo Japan, pp 1-8, 1986.

[1.36] M. Matsuishi, T. Endo, "Fatigue of Metals Subjected to Varying Stress", *Japan society of Mechanical Engineers*, Fukuoka Japan, March 1968.

[1.37] American Society for Testing Materials, Annual Book of ASTM Standards, Section 3: Metals Test Methods and Analytical Procedures, Vol. 03.01-Metals Mechanical Testing; Elevated and Low Temperature Tests, ASTM, Philadelphia, 1986.

[1.38] M. J. Baker, "The Reliability Concept as an Aid to Decition Making in Offshore Engineering", *Behaviour of Offshore Structures*, 1985.

[1.39] K. Woolley, "Targeted risk-based inspection planning", *Offshore*

Engineer, June 1996.

[1.40] P. W. Marshall, "Problems in Long Life Fatigue Assessment for Fixed Offshore Structures", Preprint 2638, ASCE National Water Resources and Ocean Engineering Convention, San Diego Ca., 1976,

[1.41] EDICS Project, "Evaluation of Diverless IRM for subsea Completions and deepsea Structures", Final Technical Report, Cybernetix, Doris Eng., GRL, IFREMER, SCS, TSC, UCL., UK, September 1998.

Figures

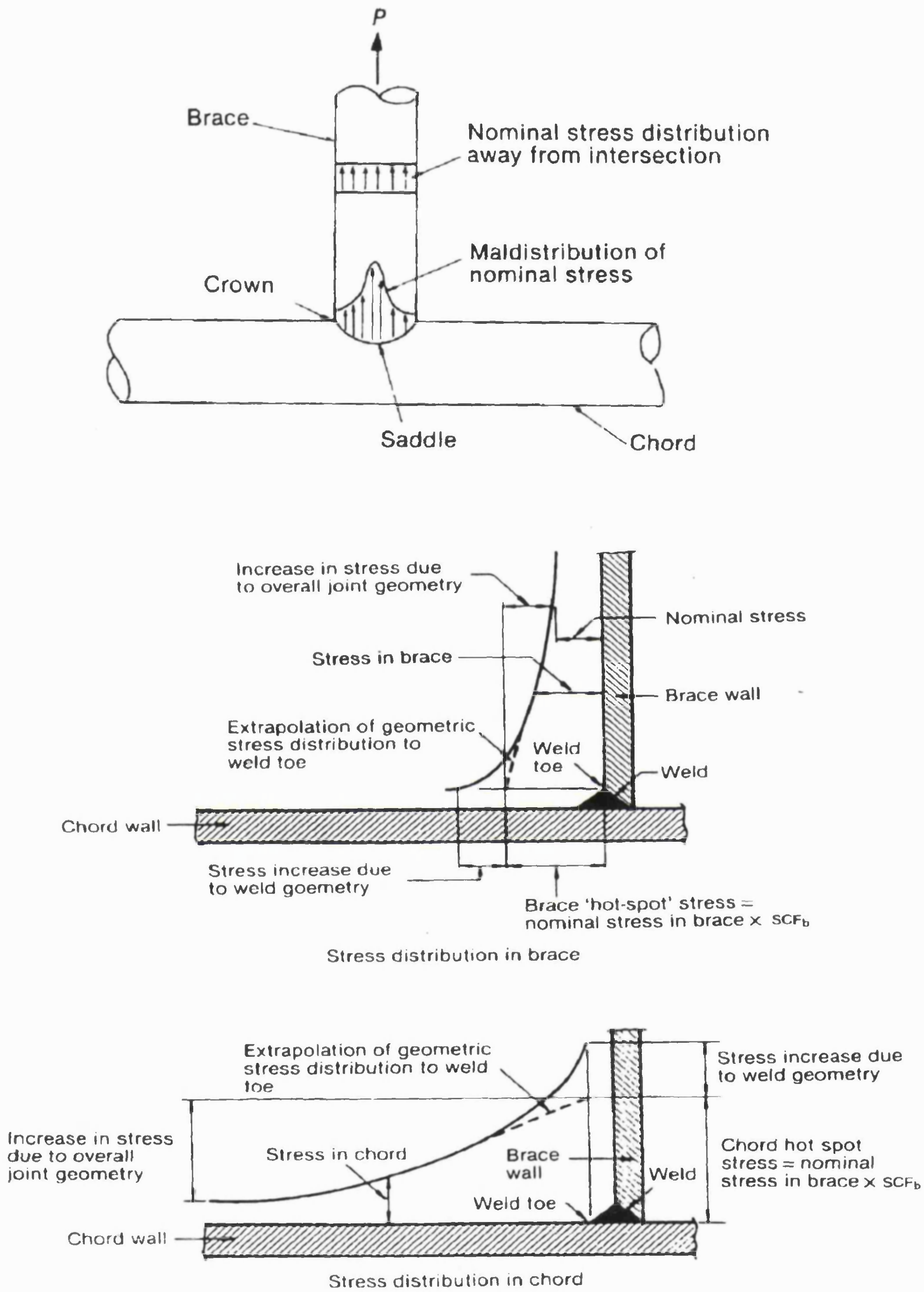

Figure 1.1 Redistribution of nominal stress in a tubular joint intersection and hot-spot stress definition by UK Dept. of Energy [1.1]

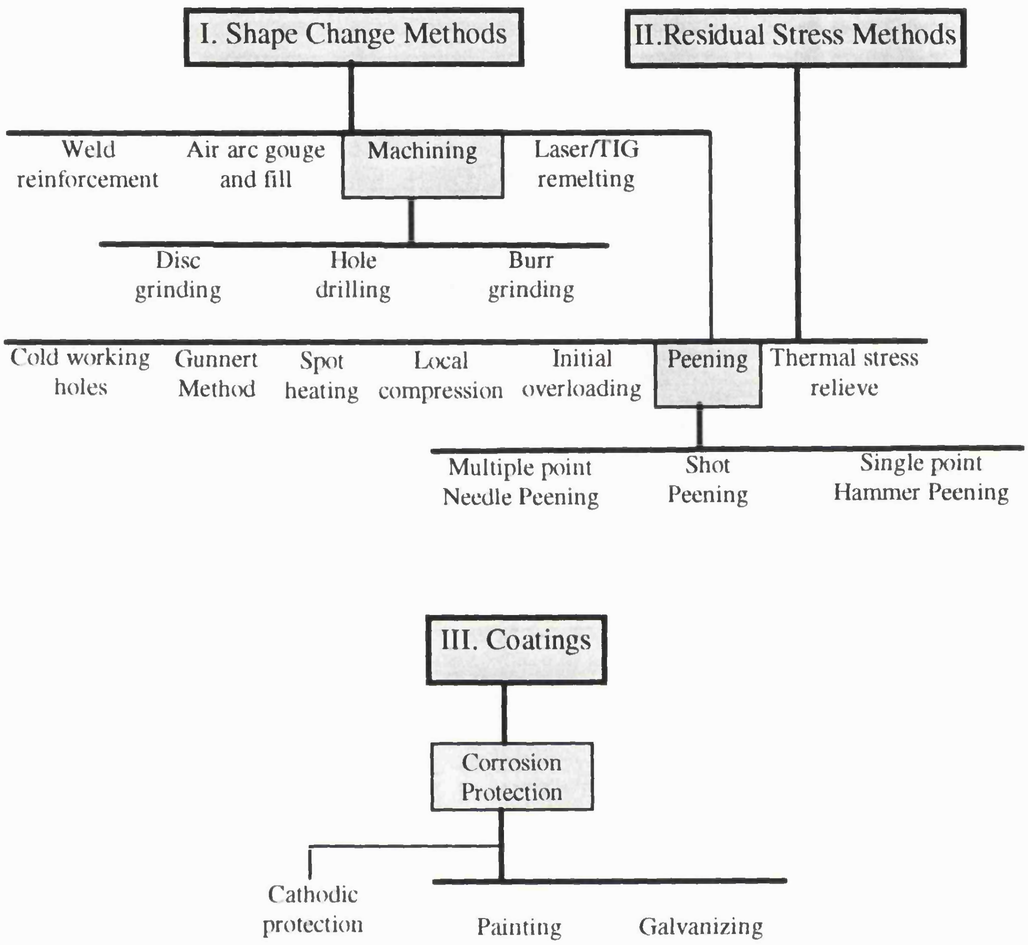

Figure 1.2 Fatigue improvement methods classified in three basic categories

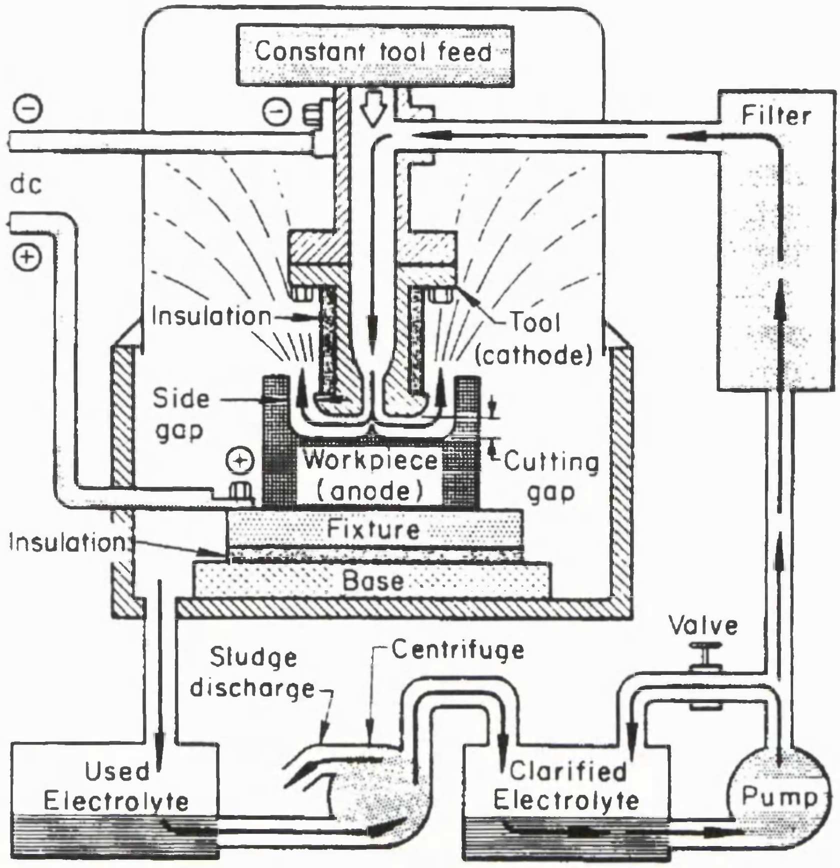

Figure 1. 3a) Typical set-up for electrochemical machining [1.10]

Figure 1. 3b) Electrochemical machining set-up for a T-butt

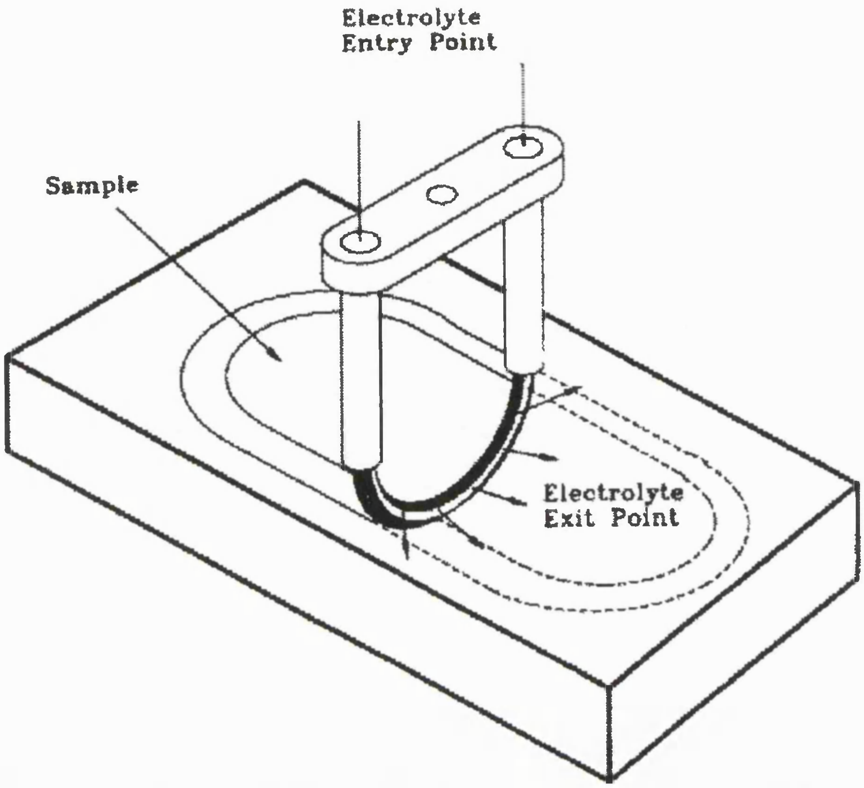

Figure 1. 4a) Slotted tool electrode showing electrolyte flow [1.11]

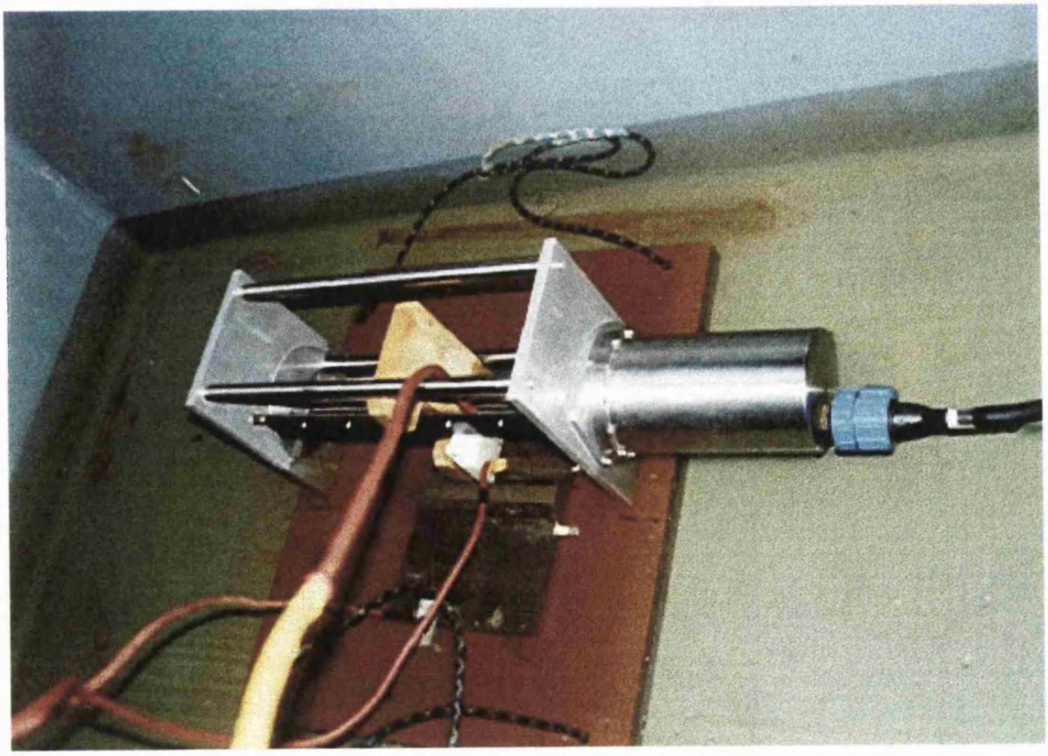

Figure 1. 4b) ECM system operating on a T-butt connection

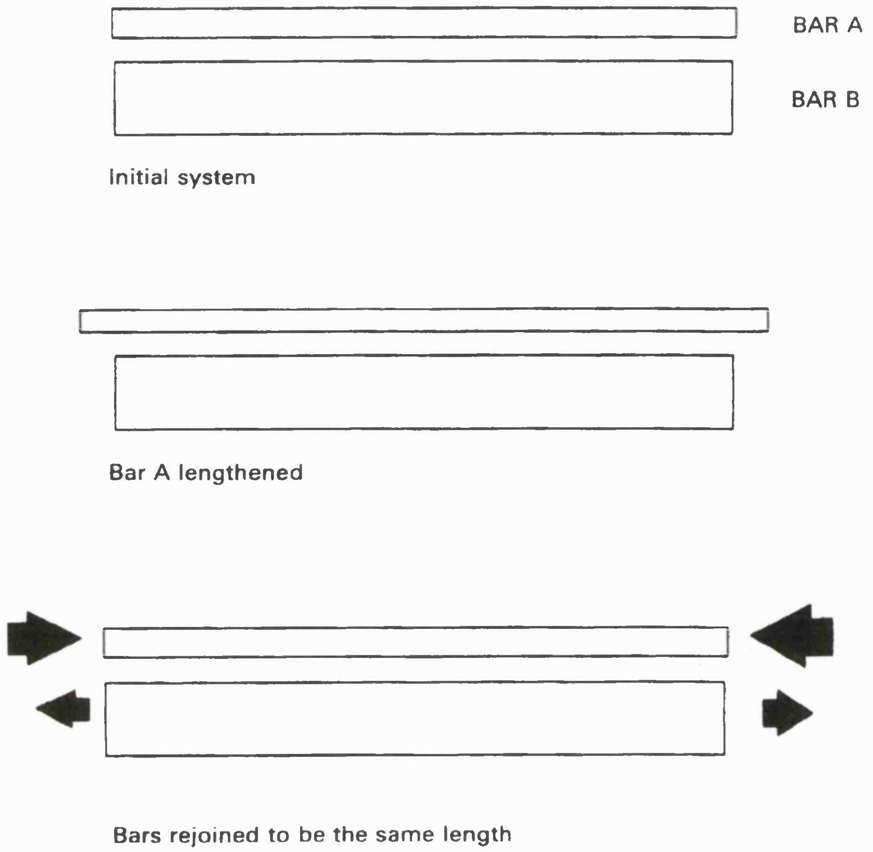

Figure 1.5 Creation of residual stress in a two bar system [1.9]

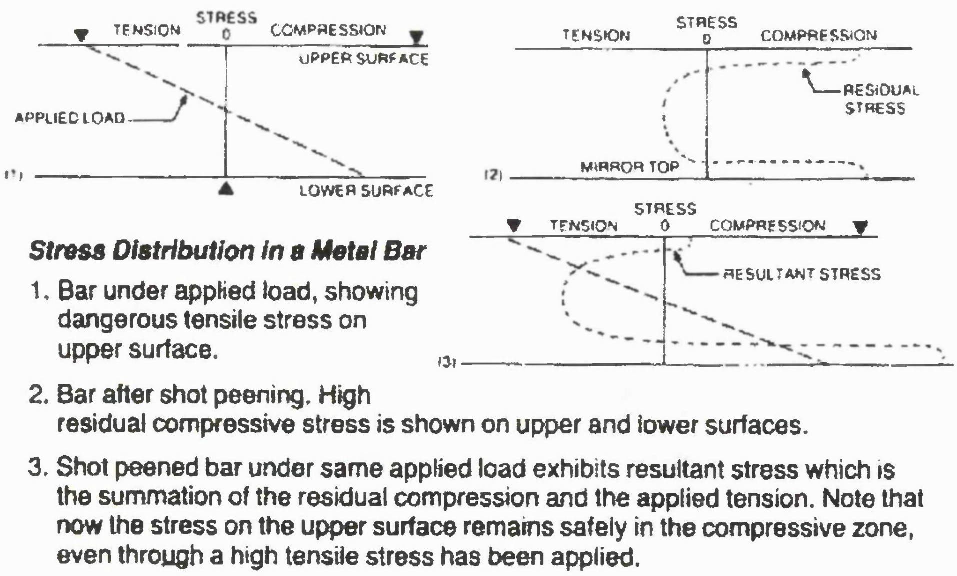

Figure 1. 6 Stress Distribution in a Metal Bar After Peening [1.12]

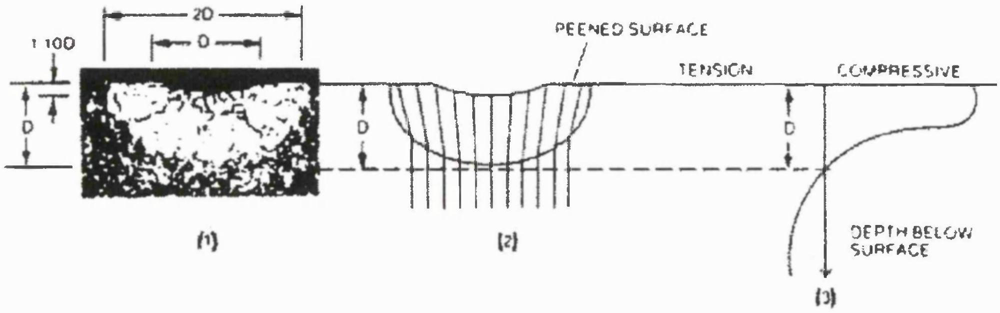

1. Impact of a high speed pellet creates a dimple of diameter "D". The depression is about 1/10 D.

2. The surface is stretched by the impact. The depth of the stretching is approximately "D".

3. The "not stretched" core exerts a compressive force in attempting to restore the surface to its original condition.

Figure 1. 7 Depth of the residual stress field produced by shot peening [1.9]

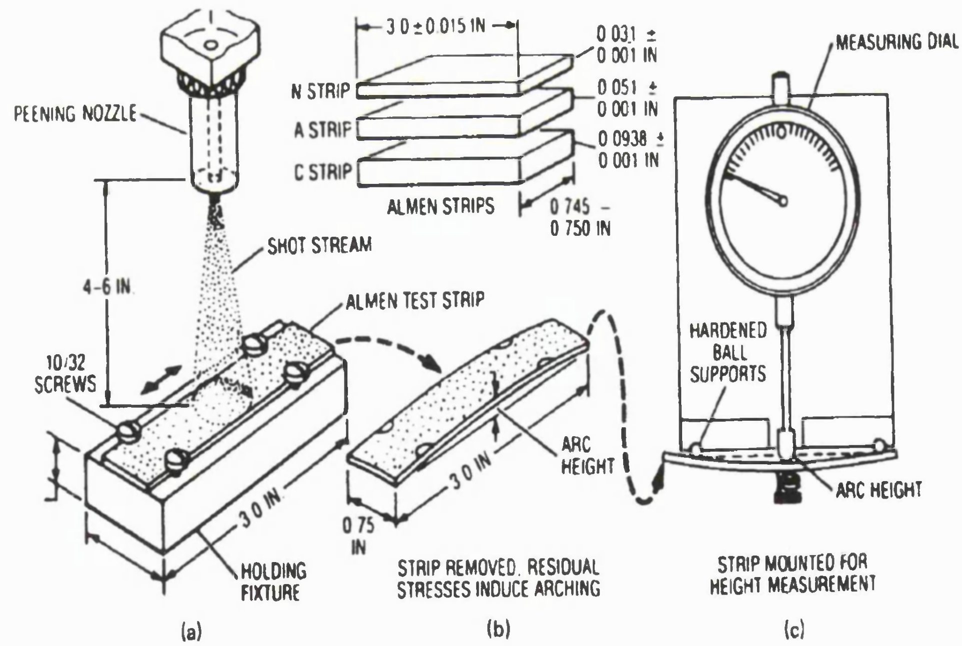

Figure 1. 8 The Almen strip system to measure intensity of shot peening in terms of curvature [1.9]

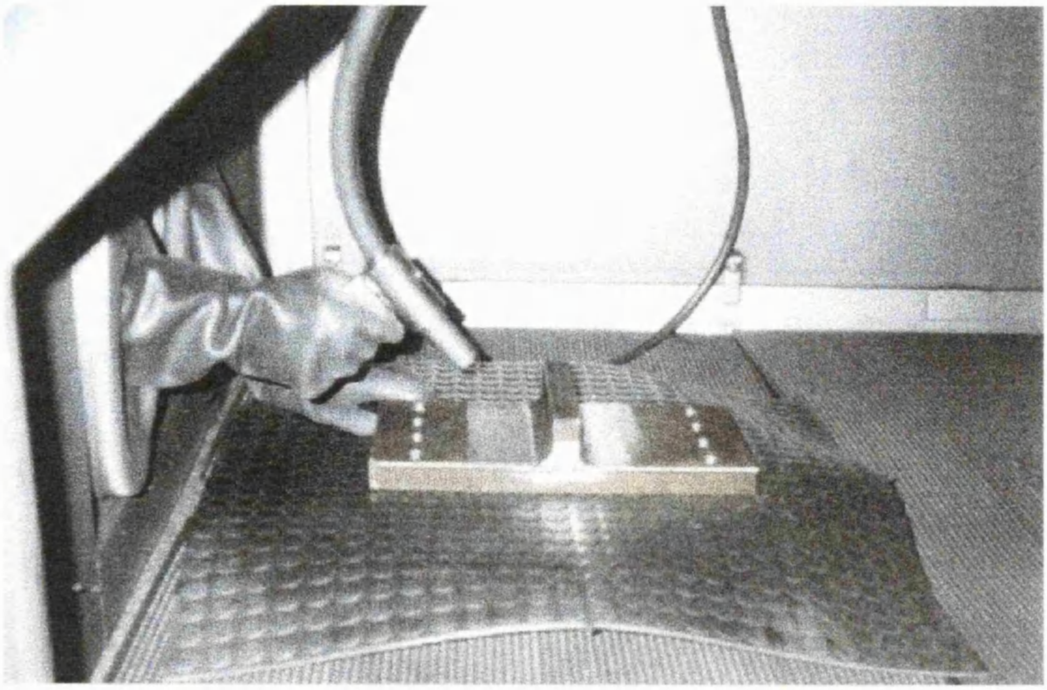

Figure 1. 9 T-butt specimen under shot peening (blast suspended)

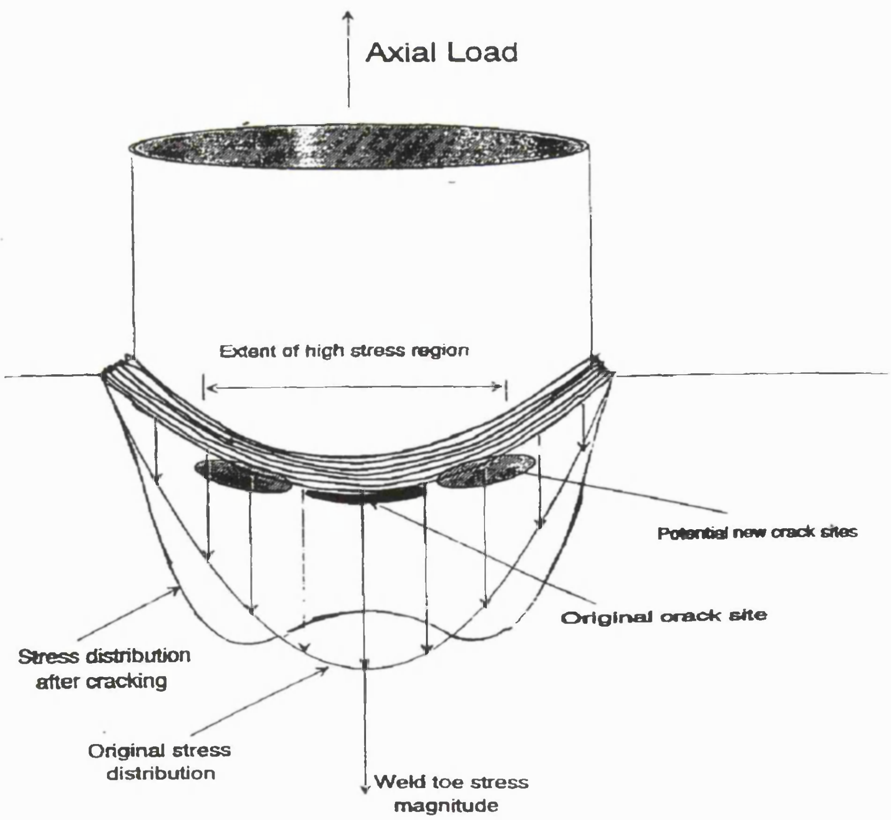

Figure 1. 10 Changes in stress distribution due to repairing [1.16]

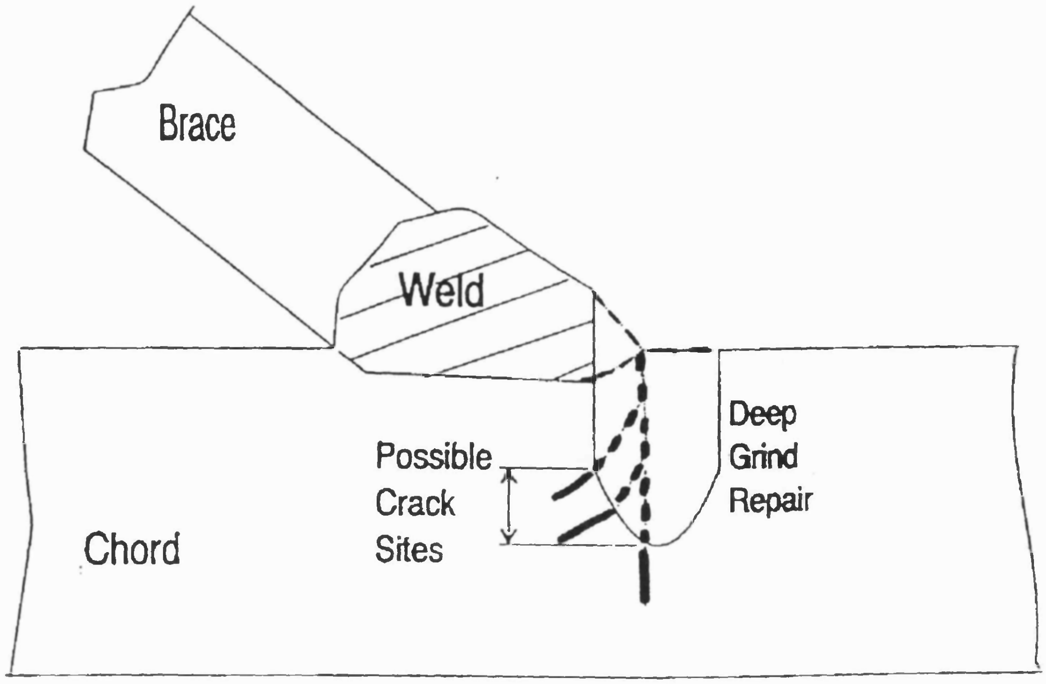

Figure 1. 11 Crack curving under the weld [1.14]

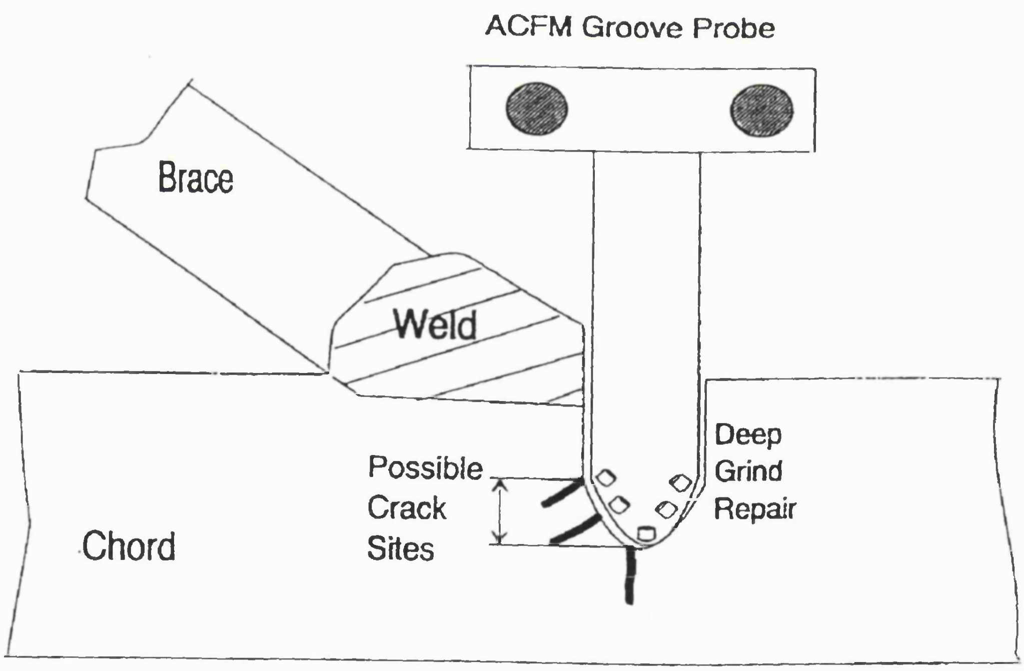

Figure 1. 12 ACFM probe configuration for inspection of repaired profiles[1.14]

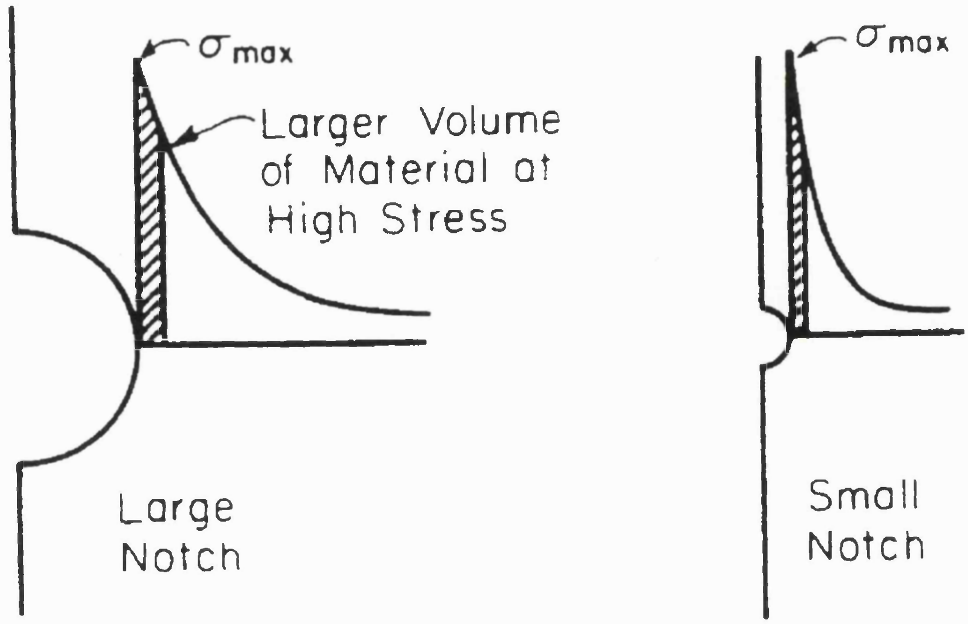

Figure 1. 13 Volume of stressed material at large and small notches [1.18]

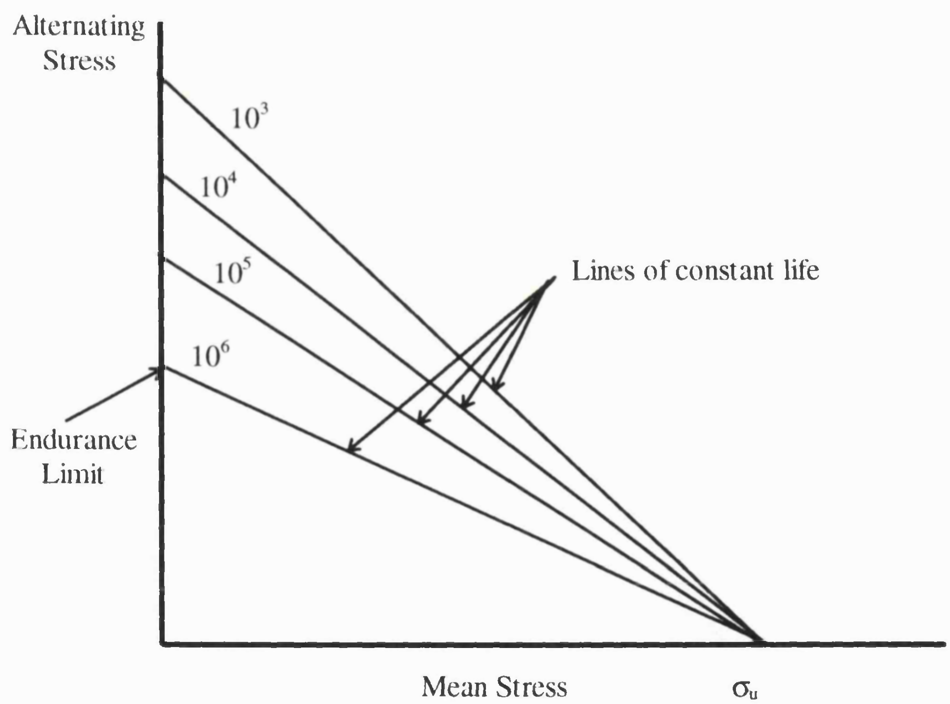

Figure 1. 14 Haigh Diagram

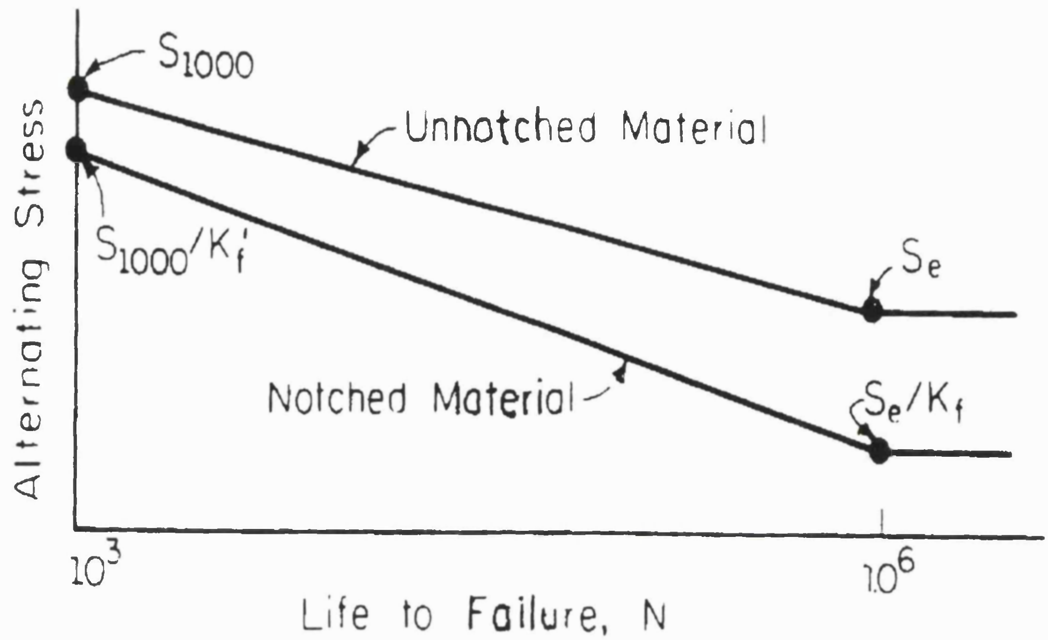

Figure 1. 15 Modification of S-N curve for notched components [1.18]

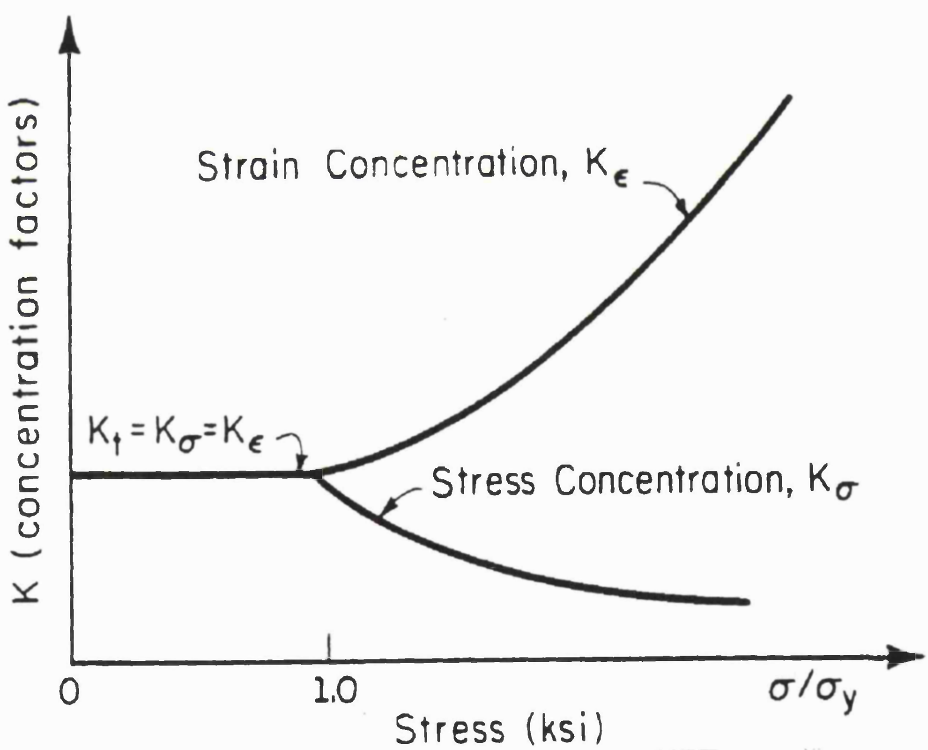

Figure 1. 16 Effect of yielding on $K\sigma$ and $K\varepsilon$ [1.18]

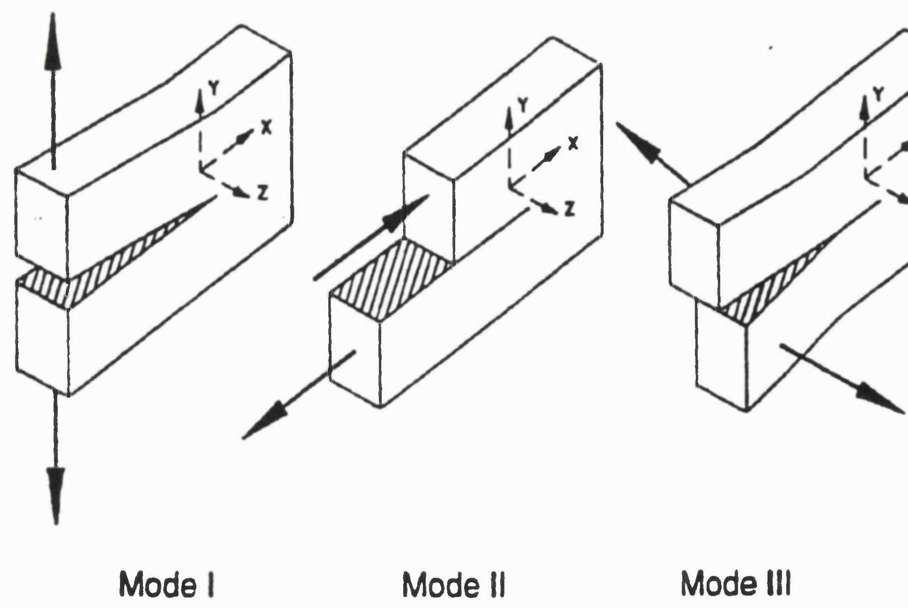

Figure 1. 17 The three fundamental modes of crack surface displacement

CHAPTER TWO

DESIGN AND STRESS ANALYSIS OF A CRACK REPAIR FOR WELDED CONNECTIONS

2.1 Introduction

Repair of flaws like fatigue cracks in welded connections can be carried out by removing the material which contains the crack according to a prescribed repair profile. The selection of the repair profile for cutting out the material for minimising the Stress Concentration Factor (SCF) depends on the crack and joint geometry. A repaired crack may have a lower SCF than in the as-welded condition, therefore crack initiation life can be reinstated and extended by repairing. Reasonably accurate predictions of fatigue crack re-initiation life can be made knowing the SCF of a welded connection [2.1].

Two and three dimensional repair profiles are studied here, both repair profiles have a U-shaped notch configuration which for the three dimensional case varies in depth along the third dimension following a longitudinal profile within a defined repair length. Although U-shaped notches are common geometries, the SCF data published e.g. Peterson [2.2], is not frequently appropriate for fatigue life prediction of welded connections where, applied to a three dimensional situation, these are likely to result in over conservative predictions of fatigue life [2.3]

The fatigue crack repair profile presented in this chapter is intended to be applied on tubular connections typical of those used in offshore structures for oil production. These connections develop fatigue cracks at the weld toes and if repairs are made in the early stages of crack growth, the fatigue life can be reinstated. Figure 2.1 shows a repaired fatigue crack on a typical offshore tubular joint using the repair procedure presented in this chapter.

Stress analysis of crack repair profiles was made on flat plates and T-butts and not on tubular joints since the former are simpler for Finite Element Analysis (FEA) modelling and the results can be extrapolated to tubular joints. Kare [2.4] demonstrated that Finite Element (FE) determined weld toe stress distributions of T-butts in tension and bending can be combined to determine stress distributions at the weld toe in tubular joints providing that the weld geometries are the same in both cases. The FEA of crack repair profiles presented in this chapter was made using the Integrated Design Engineering Analysis Software (IDEAS) package [2.5].

Previous research on the repair of fatigue cracks proposed a different repair profile to the one presented in this chapter. The repair profile proposed by Dover et al [2.6] was longer and had a shape suitable for manual burr grinding, see figure 2.2. The repair profile presented here has only the minimum required repair length (crack length plus allowance)and relies to certain extent on the capability of the Electrochemical Machining (ECM) technique to cut at any angle without the need to increase the depth of cut as in the case of manual burr grinding.

2.2 Repair Profile Definition

Considering work done by Neuber [2.7], it is possible to conclude that the SCF in a two dimensional notch is a function of the notch radius (R) and notch depth (D). In this thesis D is defined as the crack depth plus an extra depth which allows for inspection and repair inaccuracies, see figure 2.3. The relationship between D and R leads to the definition of the repair profile geometry in two dimensions. Considering different ratios of D to R can result in geometries like hyperbolic, elliptical, U-shaped or part-circular (a special case of U-shaped). In this thesis a U-shaped geometry is defined as a circular segment connected to the surface by vertical walls. It can be defined for this study that an U-shaped profile is used when $R/D < 1$ and a part-circular profile when $R/D \geq 1$.

The concept of equivalent notch configuration defined by Bowie et al [2.8], establishes that for any given notch geometry there is always an equivalent U-notch with the same maximum stress at the notch root. Applying the concept of equivalent notch configuration, see figure 2.4, it was considered that profiles with shapes ranging from part circular to U-shaped are simple and convenient for the repair of fatigue cracks in welded connections. For simplicity the notches will be described as U-shaped throughout this thesis.

Increasing R, reduces the SCF value, but it is important to consider the amount of material that is removed. This affects the local collapse capacity of the repaired zone against Punching Shear. This mechanism is explained in guidance for the design of tubular joints for fixed offshore platforms [2.9].

2.2.1 Two Dimensional Edge Repair

To define a convenient position for the U-shaped repair with respect to the crack, it can be seen from figure 2.5 that for a given crack depth the repair can be made considering two cases:

a. D is considerably deeper than the crack depth. To balance the rise of the SCF value produced by the increment in D, R has to be increased (R2). The result is a repair that removes a considerable amount of material and as a consequence the connection becomes weak as explained above.
b. The repair depth is equal to D (R1). For this case the amount of material removed is minimised with respect to the crack deviation from the vertical and required SCF value, see figure 2.3.

Thus, it can be inferred that removal of a crack in a welded connection using a U-shaped profile to optimise SCF requires that the centre of the semicircle has to lie on a line perpendicular to the surface passing through the weld toe.

The practicality of machining the optimum repair was also considered with respect to access of a machining tool. In certain cases there may be insufficient space between the weld toe and attachment plate to allow for machining. Therefore, to reach the weld toe with the cutting tool, the orientation of the walls of the U-shaped profile may be inclined with respect to the surface($\alpha<90^0$), see figure 2.3

and 2.4(e). Additionally, another possible reason to recommend an inclined U-shaped repair is that fatigue cracks tend to grow inclined through the thickness towards the weld. The former reason is justified in terms of operational feasibility to perform the repair, however the latter can be overcome by increasing R.

Although, inclined repairs ($\alpha<90^0$) may have to be considered for operational reasons, these have not been studied here since the SCF values of vertical repairs ($\alpha=90^0$) are the same according to the concept of equivalent notch configuration, see figure 2.4. Caution has to be exercised as a limiting value of α exists were the concept of equivalent notch configuration is no longer valid.

The above has only considered the geometry of the repair but the SCF also depends on the loading mode. Hence, the arguments given above were numerically validated for a vertical repair ($\alpha=90^0$) under tension and bending conditions and are reported in the following sections.

2.2.2 Three Dimensional Surface Repair

A two dimensional finite element analysis of a U-shaped notch is only applicable to the case of an edge repair. Therefore, it was considered necessary to study the case of a surface repair to determine the effect of the repair length and longitudinal profile. The surface repair considered in this study is a three dimensional repair with a transverse U-shaped profile, as defined in previous sections, that varies in depth along the third dimension following a longitudinal repair profile within a defined repair length.

The longitudinal repair profile can be semielliptical since fatigue cracks propagate through the thickness following a semielliptical shape. However, in order to minimise the number of variables to define a longitudinal profile and knowing that SCFs of semielliptical and semicircular grooves are similar [2.2], the profile for the longitudinal repair is considered in this study as an arc (circular segment). The repair depth defines the arc's height and the repair length defines the arc's chord, in these conditions a longitudinal semicircular profile can cut out any semielliptical crack. The notation to define the longitudinal repair profile is shown in figure 2.6. The repair length (L) is defined as the crack length plus an extra length which allows for inspection and repair inaccuracies. Figure 2.7 shows a surface repair with a semicircular longitudinal profile in the z-y plane and a transverse U-shaped profile in the x-y plane.

To fix the position of the longitudinal repair profile it is considered that the planes of the transverse and longitudinal profiles are perpendicular to each other and also that the deepest point of both profiles is common.

2.3 Finite Element Analysis of Repair Profiles

The FE method applied to stress analysis seeks to calculate the displacement or stress field and usually the results of greatest interest are peak values. The FE method allows an approximate numerical solution to a specific problem [2.10].

The FE method was used in this work to determine SCF values and stress field distributions of repaired specimens. The FEA assisted in the understanding of the experimental results obtained and confirmed the location of crack initiation of the repaired profiles tested. Two and three dimensional FEA were performed and relations between the different models were investigated.

2.3.1 Two Dimensional FEA of Edge Repairs on T-Butts

To determine the variation of SCFs versus R and D, a parametric two dimensional FEA was conducted. Although, there is a third parameter involved in the definition of a two dimensional repair it can be expressed as a function of R and D. The repair surface width (SW) in a U-shaped repair, see figure 2.3, varies in relation to R and D according to equations (2.1) and (2.2).

$$SW = 2R \tag{2.1}$$

for $R < D$ ($R/D<1$ U-shaped)

$$SW = 2\sqrt{2RD - D^2} \tag{2.2}$$

for R ≥ D (R/D≥ 1 Part circular shape)

where

R transverse repair radius

D repair depth

The number of combinations of D versus R was limited to a number of cases considered as possible practical solutions for a typical welded T-butt. Fifteen combinations of D/T and eight combinations of R/T were selected and analysed under bending and tension loading modes giving a total of 240 different finite element models. Only half of the T-butt was analysed considering the symmetry in geometry and loading thus, two different sets of boundary conditions were defined for the analysis of tension and bending. Eight-noded shell elements were used in the mesh definition. From the analysis output the position on the repaired surface and magnitude of the maximum principal stresses were reviewed. Figures 2.8 and 2.9 show a model used and the principal stress distributions under tension and bending respectively. In all the cases studied varying R and D for tension and bending loading modes, the highest SCF was always located in the bottom of the groove.

The nominal stress considered was the stress magnitude on the surface of the primary plate unaffected by the weld and repair. The results provided by the FEA were verified at points not affected by the weld geometry and repair using simple beam theory. The SCFs reported for tension and bending were determined as

$$SCF = \text{Maximum principal stress} / \text{Nominal stress} \tag{2.3}$$

A sample of the data obtained for T=30 is presented in table 2.1. A graphical representation of the data is shown in figures 2.10 and 2.11, it can be seen that for a given depth the SCF value decreases as the radius is increased, and that for the tension mode the SCF values are larger than in bending. On the same graphs it is also shown the SCF values of four weld toe radius/plate thickness ratios for the same T-butt joints in an as-welded condition obtained by Brennan et al, [2.11], to compare as-welded SCFs with SCFs after repair.

2.3.2 Three Dimensional FEA of Surface Repairs on Flat Plates

A three dimensional FEA of U-shaped surface repairs was made initially on plain plates to evaluate the weld geometry effect. Three repair lengths (L) were analysed (60, 40 and 20 mm) in order to obtain the SCFs trend. The plate thickness considered was 30 mm, extrapolation to other repair lengths and thickness values is possible using the parametric equations presented in following sections.

The plate width (W) modelled was 100 mm for the L values analysed, the use of wider plates showed no difference in the SCFs obtained. Thus, it was considered that the plate width parameter can be ignored for purposes of SCFs calculations if $L/W \leq 0.6$. This can be explained in terms of the perturbation caused by the notch to the lines of force. It is observed that progressively increasing the plate width, a threshold point is reached beyond which the deflection of the lines of force at the ends of the notch do not change.

Solid finite elements were used for the mesh definition which was required to have different densities to reduce the element distortion on the curved surface. Tension and bending loading modes were analysed separately. A four point bending arrangement was considered in order to avoid the effect of shearing forces. A particular set of boundary conditions was applied to the model depending on the loading condition. An example of a finite element model showing a plain plate with a surface repair, boundary conditions and forces is presented in figure 2.7.

The SCFs obtained from three dimensional FEA of surface repairs on flat plates are shown in tables 2.2 and 2.3 for tension and bending respectively in three columns headed “SCF surface”. A typical stress distribution for bending is shown in figure

2.12. A graphical representation of the tension SCFs obtained for T=30mm, including the sample data of edge repairs is shown in figure 2.13. It can be observed in this figure that the SCFs for edge repairs are maximum values.

The weld effect and the relation between edge and surface repairs is explained in the following sections.

2.3.3. Three Dimensional FEA of Surface Repairs on T-Butts

To complete the three dimensional FEA, surface repaired T-butt models with a 45^0 weld angle were analysed. It is important to note that when the weld is considered in the model, a weld toe radius > 0 has to be introduced to obtain reliable FEA results. Otherwise, the results are not correct due to a mathematical singularity along the line where the weld merges with the parent plate surface. In practice this singularity never occurs but analytically as in a FE model it is always present if it is not corrected. The radius considered at the weld toe in all the models analysed was R, the same used for the repair. Although, as welded weld toes never have radii of magnitude R it was considered convenient to include such radii in the finite element model to demonstrate that the concentration at the ends of the repair is due to the repair and not due to the weld toe. Additionally, it was considered that when machining a crack repair, extension of the repair profile sideways to remove possible weld defects is feasible.

In the FE models the weld toe radius was made by cutting out material 0.5mm deep on the parent plate by extruding a circumference of radius R with its centre on a line passing at the weld toe and perpendicular to the main plate. Figure 2.14 shows a surface repair on a T-butt with a weld toe radius = 0 and figure 2.15 shows the same T-butt after a weld toe radius = R has been included in the FE model.

As in the cases mentioned above, only half of the model was analysed and different sets of boundary conditions were used for tension and bending. The mesh had different densities to consider the curvature of the repaired surface whilst minimising distortion.

For tension loading the stress distribution obtained was very similar to the distribution obtained for edge repairs, i.e. high tensile stresses concentrated in the bottom of the groove, see figure 2.17. However, for bending loading, the region with maximum principal tensile stresses was concentrated at the repair ends where the groove merges with the weld toe. This stress distribution is completely different as compared with the distribution obtained for edge repairs, see figure 2.16. This finding showed that the two dimensional FEA results of edge repairs on T-butts could not be extrapolated to the case of three dimensional edge repairs. Therefore, FEA of T-plates with a 45^0 weld angle for various combinations of R and D for L=60 mm and T=30 mm were carried out. Results from the analysis are presented in table 2.4 for tension and bending. These analyses were particularly time consuming and on average each FE model took 4 hours of CPU to provide stresses and displacements.

Discrete stress distributions along the longitudinal surface repair centre-line on flat plates under bending are shown in figure 2.18. It can be seen that even on a flat plate under bending there is a tendency to have a stress concentration at the repair ends for deeper repairs (D8R8L60). This effect is amplified for a T-butt as shown in figure 2.19. This figure also shows that for tension the maximum stress is always in the bottom of the repair. Comparison of figures 2.18 and 2.20 at the repair ends show the weld effect on the SCF.

2.4 SCF Parametric Equations for Crack Repair Profiles

Studying the relationship of the SCFs obtained by FEA and the geometrical and loading parameters it is possible to represent the SCF in the form of parametric equations. The parametric equations allow interpolation of the SCF within the parametric limits of validity.

2.4.1 Equations for Edge U-Shaped Repairs on T-Butts

A set of parametric equations were obtained for tension and bending respectively, for the SCF values obtained from the FEA described in 2.4.1. Pearson's correlation coefficient between the SCF values obtained from the parametric equations (2.4) for tension and (2.5) for bending and the two dimensional SCF FEA values is 0.99. The parametric SCF equations for edge U-shaped repaired profiles on T-butts are

$$SCF_{Tension} = 45.983\,C_{2T}(D/T)^2 - 3.5494\,C_{1T}(D/T) + 2.8815\,C_T \qquad (2.4)$$

$C_{2T} = -12.059(R/T)^3 + 13.743(R/T)^2 - 4.4426(R/T) + 1.3768$
$C_{1T} = -15.471(R/T)^3 + 14.787(R/T)^2 + 1.8413(R/T) + 0.2795$
$C_T = -16.288(R/T)^3 + 17.895(R/T)^2 - 5.9832(R/T) + 1.5678$
for
$0.08 < D/T < 0.533$ and $0.08 < R/T < 0.533$

$$SCF_{Bending} = 17.438C_{2B}(D/T)^{\wedge}2 - 2.0919C_{1B}(D/T) + 2.9696C_B \qquad (2.5)$$

$C_{2B} = -9.2188(R/T)^3 + 12.077(R/T)^2 - 3.8901(R/T) + 1.3249$
$C_{1B} = 16.523(R/T)^3 - 5.3881(R/T)^2 + 3.3809(R/T) + 0.4853$
$C_B = -10.061(R/T)^3 + 14.155(R/T)^2 - 6.1172(R/T) + 1.6646$
for
$0.08 < D/T < 0.533$ and $0.08 < R/T < 0.533$

By presenting the equations in a non-dimensional parametric form, the results obtained from the FEA, are valid for any combination of D, R and T within the specified ranges. A graphical representation of equations (2.4) and (2.5) is shown in figures 2.20 and 2.21.

2.4.2 Weld Size Effect on SCFs for Edge Repairs

In order to investigate whether or not the equations (2.4) and (2.5) are applicable to any weld geometry, a two dimensional FEA study was conducted to determine the weld geometry effect on the SCF repair profiles. The study determined SCFs on flat plates of T=30mm with the edge repair profiles presented in table 2.1 and subsequently compared those SCFs with the values presented in table 2.1. These correspond to the T-butt with the welded geometry presented in figure 2.3, (weld angle=45^0 and attachment length=2T). The comparison showed that the SCFs obtained from the flat plates and T-butts are very similar. For the plain plate in tension, the SCFs are overestimated in the range 0%-8%, and in bending are underestimated in the range 0%-2%. Therefore, it can be considered that equations (2.4) and (2.5) when used for any weld geometry would reduce the ranges of overestimation and underestimation presented since the equations were developed for a welded geometry with 45^0 weld angle and the error ranges were obtained from comparison with a flat plate. Note that this comparison was made only for T=30mm thus, the error ranges presented above could change for other thicknesses. However, no large discrepancy is expected.

Finally, equations developed for edge repairs on T-butts can be applied to flat plates since the weld influence is negligible for repairs with D/T>0.13 and R/T> 0.13

2.4.3 SCF Relation between Edge Repairs on T-Butts and Surface Repairs on Flat Plates

It was expected that SCFs for edge repairs would be larger than SCFs for surface repairs, as shown in figure 2.13. Since for the latter case, the lines of force can pass around the repair reducing the stress at the bottom of the notch. A relationship between the edge and surface repair SCF was sought so that equations (2.4) and (2.5) developed for edge repairs on T-butts might be used to obtain SCFs for surface repairs on flat plates. This was thought to be possible since the weld influence is negligible for D/T>0.13 and R/T> 0.13 as explained in 2.4.2. The relation was called reduction factor (RF) and it was defined as

$$RF = SCF\ surface / SCF\ edge \tag{2.6}$$

The SCFs obtained from the three dimensional FEA of surface repair profiles on flat plates presented in section 2.3.2 were arranged as presented in tables 2.2 and 2.3 for tension and bending loading modes respectively. It can be observed on the right hand side of tables 2.2 and 2.3 the RF values calculated using the expression presented in equation 2.6. RF was obtained considering the same D and R values for SCF surface and SCF edge repair for a given L value from tables 2.2 and 2.3.

It can be seen on the RF section of tables 2.2 and 2.3 that for a given L the RFs remain practically constant while R varies. Therefore, an average RF value is presented at the bottom of each L column for each block of constant D. The average RF values obtained can be used to modify equations (2.4) and (2.5 to obtain surface repair SCFs on flat plates.

2.4.4 Equations for Surface Repair Profiles on Flat Plates

From the average RF values presented in tables 2.2 and 2.3, a set of parametric equations was obtained for tension and bending loading modes respectively. The parametric RF equations for tension and bending for T=30mm are:

$$RF_{tension} = -0.0913(L/T)^2 C_2 + 0.4506(L/T)C_1 + 0.4291C$$

$$(2.7)$$

$$C_2 = -82.804(D/T)^2 + 30.082(D/T) - 1.7043$$

$$C_1 = -46.688(D/T)^2 + 18.895(D/T) - 0.9115$$

$$C = 29.18(D/T)^2 - 15.83(D/T) + 2.9988$$

for $L/T \geq 0.67$ and $0.13 \leq D/T \leq 0.27$

$$RF_{bending} = -0.0167(L/T)^2 C2 + 0.1841(L/T)C1 + 0.5311C$$

(2.8)

$C_2 = 51.198(D/T)^2 - 73.743(D/T) + 13.701$

$C_1 = -39.965(D/T)^2 + 3.1287(D/T) + 1.9728$

$C = 33.023(D/T)^2 - 13.256(D/T) + 2.3303$

for $L/T \geq 0.67$ and $0.13 \leq D/T \leq 0.27$

The parametric equations to determine SCF surface U-shaped repair profiles on flat plates can be obtained as:

$$\text{SCF surface} = \text{RF(SCF edge)} \quad (2.9)$$

where

SCF edge   SCF for a edge repair on a T-butt from equations (2.4) and (2.5)

Pearson's correlation coefficient was obtained comparing surface SCF values from equations (2.7), (2.8) and (2.9) against the SCF surface values presented in tables 2.2 and 2.3. The correlation obtained was 0.999 for tension and 0.9887 for bending.

2.4.5 Equations for Surface Repair Profiles on T-Butts

It has been demonstrated that the weld effect on the SCF values is negligible for edge repaired T-butts. This situation allowed the use of SCF parametric equations (2.4) and (2.5) for edge repaired T-butts to determine SCF values for surface repaired flat plates by considering a RF. So, it seemed possible to also determine SCF values for surface repaired T-butts from equations (2.4) and (2.5). However, this was not possible since for the case of surface repairs on T-butts, the weld effect cannot be neglected.

From the SCF FEA values for a surface repair L=60mm on a T-butt T=30mm presented in table 2.4, parametric equations (2.10) and (2.11) were developed.

$$SCF_{bending} = 9.2812\, C_{2b}\, (R/T)^2 - 8.8125\, C_{1b}\, (R/T) + 4.37\, C_b \qquad (2.10)$$

$C_{2b} = -57.951\ (D/T)^2 + 28.408\ (D/T) - 2.3635$

$C_{1b} = -51.223\ (D/T)^2 + 24.223\ (D/T) - 1.7957$

$C_b = -18.535\ (D/T)^2 + 9.4394\ (D/T) - 0.1465$

for

$0.13 \le R/T \le 0.4$, $0.13 \le D/T \le 0.27$, $L = 60$ and $T=30$

$$SCF_{tension} = 7.3125\, C_{2t}\, (R/T)^2 - 7.2\, C_{1t}\, (R/T) + 4.07\, C_t \qquad (2.11)$$

$C_{2t} = 116.82(D/T)^2 - 43.556(D/T) + 5.0384$

$C_{1t} = 70.891(D/T)^2 - 26.13(D/T) + 3.3904$

$C_t = 15.756(D/T)^2 - 4.7359(D/T) + 1.31$

for

$0.13 \le R/T \le 0.4$, $0.13 \le D/T \le 0.27$, $L=60$ and $T=30$

Note that the above equations provide SCF values located at the repair ends for bending and at the bottom of the repair for tension.

2.5 Discussion

Figures 2.10 and 2.11 show the sample data for edge repairs on T-butts with T=30 mm plotted in terms of the variation of SCF for different radii giving three curves for repair depths 4, 6, and 8 mm. Inserted on the figures are SCF values for the as-welded joint prior to any repair. For these values the weld toe radii are lower than the repair radii (from 0.3 to 1.98 mm) and obviously do not follow a similar trend to the repair data. Two important observations can be made from Figures 2.10 and 2.11:

a) A wide range of SCF values associated with the crack repair geometries analysed have similar magnitudes to the as-welded SCF values. This means that it is possible to reinstate the original as-welded SCF value if a crack is repaired using the proposed repair geometries.

b) In the case where a crack has re-initiated in a repaired profile, it is still possible to make a second repair and in some cases even obtain a lower SCF than in the first repair depending on the depth and notch radius of the first repair. The latter might be more appropriate to improving the fatigue resistance of a narrow corrosion groove.

From figures 2.10 and 2.11 it would appear that the SCF values can be correlated on the basis of two main non-dimensional parameters D/T and R/T. Extending this work to surface groove repairs of limited length requires a third parameter L/T expressed as RF as given in equation (2.9).

The transverse repair profile proposed in this study changes automatically for a given D from U-shaped to part circular as R is increased. From table 2.1, it can be observed that there is a trend showing that SCF U-shaped > SCF part circular. However, it can be observed from figures 2.10, 2.11, 2.20 and 2.21 that the SCF distribution is continuous the SCF curve merging smoothly from U-shaped to part circular model for a given depth. The limits shown on equations (2.4), (2.5), (2.7) and (2.8) correspond to the cases analysed using the finite element method, however, higher ratios of D/T and R/T can be used since the curve trend is clearly apparent. Since the influence of the remaining thickness (d = T-D) has not been studied, it is recommended that equations (2.4), (2.5), (2.7) and (2.8) are applied for repair depths less than 40% of the thickness.

The results obtained from the FEA of grooves in plain plates showed that the weld geometry effect on the SCF values of T-butts with edge repairs is small. Therefore, equations (2.4), (2.5), (2.7) and (2.8) for the determination of edge SCF on T-butts can be used for flat plates and can be also applied to any weld geometry on T-butt connections with edge repairs.

For a U-shaped repair profile on a flat plate, the SCF surface value is the same as the SCF edge if L is longer than a repair length called L_{limit}. However, in general the SCF surface is less than SCF edge as shown in figure 2.13. A repair profile on a flat plate which has a repair length shorter than L_{limit} can be called a short repair and one with a repair length longer than L_{limit} can be called long repair. Short repairs on flat plates may increase the fatigue initiation life of a component since SCF values are smaller than for long repair SCF values. Additionally, short repairs on flat plates tend to have the same stress level on a considerable area of the repaired surface profile thus, crack initiation may occur in any part of this region increasing the probability of detection during inspection. However, the crack geometry will generally be the limiting factor in choosing the repair length. For a crack aspect ratio of 10/1 and a crack depth of say 3mm, the repair length would have to be much greater than 30mm. Thus, D=4 and R=6 with L=60 would be appropriate for the 3mm crack.

The above has considered only the results and parametric equations obtained for edge and surface repairs on flat plates and edge repairs on T-butts. The next part of the discussion will consider the case of surface repairs on T-butts.

Surface repairs on T-butts differ from the previous cases because they have a different stress distribution on the surface of the repair groove especially under bending loading. This different stress distribution is caused by the stiffness imposed by the weld at the ends of the repair. For the case of an edge repair there is no material at the repair ends, therefore the position of the highest stress must be at the bottom of the groove. However, but for the case of a surface repair, the material at the ends of the repair restrains the deformations increasing the stress in that region.

During the FEA it was required to incorporate a radius at the weld toe to overcome a mathematical singularity however, it was also thought that a transition from the repair to the surface where the repair merges with the weld toe is required. Usually the as-welded repair radius is smaller than R therefore, the change of radii from the weld toe to the repair would be abrupt if a transition is not considered. Finally, it was considered that a weld toe radius of the same magnitude as R would avoid changing tools while machining the repair profile and the transition.

The principal limitation of the parametric equations for surface repair profiles on T-butt plates is that only the repair length L=60 for T=30 was analysed therefore, the equations do not consider L and T as parameters that can be modified to obtain SCF values for different repair lengths and plate thicknesses.

2.6 Conclusions

1. Parametric equations have been developed for the determination of SCF repair profiles for the removal of flaw like fatigue cracks for the cases of edge and surface repairs on welded T-butt connections and flat butt welded plates. Additionally a set of parametric equations for surface repairs on T-butts is also available for L=60 and T=30.
2. Fatigue crack initiation life of welded connections can be reinstated by using a U-shaped or part circular repair profile.
3. Fatigue initiation life after repair can in some cases be larger than in the as-welded condition since a lower SCF after repair can be achieved.
4. SCFs of repair profiles are in general larger for tension loading than for bending.
5. On welded T-butt connections with edge repairs it can be considered that the weld geometry has no effect on the SCFs of U-shaped or Part circular repairs with depths of at least 4mm.
6. On flat plates for a given set of D and R values, surface SCFs approach edge SCF values as L increases.
7. Long repair profiles to remove fatigue cracks should be avoided since they may weaken the component and increase the SCF values.

8. U-shaped and Part circular surface SCF distributions for a particular depth are the same.
9. Under bending loading stress distributions of T-butts and flat plates with surface repairs are substantially different. As opposed to T-butts and flat plates with surface repairs under tension and T-butts and flat butt plates with edge repairs under tension and bending.

2.7 References

[2.1] N. E. Dowling, "Notched Member Fatigue Life Predictions Combining Crack Initiation and Propagation ," *Fatigue of Engineering Materials and Structures*, Vol. 2, 1979.

[2.2] R. E. Peterson, *Stress Concentration Factors*, John Wiley & Sons, 1973.

[2.3] J.E. Rodriguez, F.P. Brennan and W.D. Dover, "Minimization of stress concentration factors in fatigue crack repairs", *International Journal of Fatigue*, Vol. 20, No. 10, pp. 719-725, 1998.

[2.4] R.F.Kare, *Influence of weld profile on fatigue crack growth in tubular welded connections*, PhD. Thesis, The City University, London, 1989.

[2.5] IDEAS (Integrated Design Engineering Analysis Software), User's Manual, Finite Element Modelling, *Structural Dynamics Research Corporation*, USA, 1994.

[2.6] W.D. Dover, D. Broad, A. Lopez, F.P. Brennan, "Effectiveness of Grind Repair NDT Procedures", *University College London*, 1995.

[2.7] H. Neuber, "Theoretical Determination of Fatigue Strength at Stress Concentration," *Report AFML-TR-68-20 Air Force Materials Lab*, Wright -Paterson Air Force Base Dayton , Ohio 1968.

[2.8] O. L. Bowie and C. E. Freese, "Analysis of notches using conformal mapping", *Mechanics of Fracture vol. 5, Stress analysis of notch problems*, Editor G. C. Sih, Noordhoff Int. Publishing, 1978.

[2.9] "Recommended Practice for Planning, Designing and Constructing Fixed Offshore Platforms-Working Stress Design", 20th Edition, *American*

Petroleum Institute, Washington, July 1993.

[2.10] R. D. Cook, *Finite Element Modelling for Stress Analysis,* John Wiley and Sons, Inc. 1995.

[2.11] F. P. Brennan, W. D. Dover, R. F. Kare, A. K. Hellier, *Development of Parametric Equations for Weld Toe Stress Intensity Factors*, Technical Software Consultants and University College London, 1995.

Tables

Profile	R/D	D/T	R/T	SCF-Tension	SCF-Bending-
D8R2	0.25*	0.27	0.067	6.94	4.78
D6R2	0.33*	0.20	0.067	5.42	4.12
D4R2	0.5*	0.13	0.067	4.09	3.47
D8R4	0.5*	0.27	0.13	5.71	3.82
D6R4	0.67*	0.20	0.13	4.51	3.34
D4R4	1**	0.13	0.13	3.49	2.89
D8R6	0.75*	0.27	0.2	4.98	3.29
D6R6	1**	0.20	0.2	3.93	2.87
D4R6	1.5**	0.13	0.2	3.05	2.48
D8R8	1**	0.27	0.27	4.56	3
D6R8	1.33**	0.20	0.27	3.58	2.6
D4R8	2**	0.13	0.27	2.78	2.24
D8R10	1.25**	0.27	0.33	4.28	2.81
D6R10	1.67**	0.20	0.33	3.36	2.43
D4R10	2.5**	0.13	0.33	2.63	2.11
D8R12	1.5**	0.27	0.4	4.07	2.67
D6R12	2**	0.20	0.4	3.19	2.3
D4R12	3**	0.13	0.4	2.51	2

*D (Depth in mm), R (Radius in mm), * U-shaped profile, ** Part-circular profile*

Table 2.1 SCF values for edge repairs on a T-butt (T= 30mm) under tension and bending using two dimensional FEA

Profile	SCF edge	SCF surface			Reduction Factor (RF)		
T=30	From Table2.1	L=60	L=40	L=20	L=60	L=40	L=20
D4R4	3.49	3.5	3.25	2.77	1	0.9312	0.7936
D4R8	2.78	2.83	2.6	2.28	1	0.9353	0.8201
D4R12	2.51	2.53	2.36	2	1	0.9402	0.7968
					Average RF		
					1	0.9356	0.8035
D6R4	4.51	4.32	3.87	3.08	0.9578	0.8581	0.6829
D6R8	3.58	3.41	3.08	2.42	0.9525	0.8603	0.6759
D6R12	3.19	3.14	2.82	2.26	0.9843	0.884	0.708
					Average RF		
					0.9649	0.8675	0.6889
D8R4	5.71	5.45	4.45	3.37	0.9545	0.7793	0.5902
D8R8	4.56	4.23	3.56		0.9276	0.7807	
D8R12	4.07	3.79	3.24		0.9312	0.7961	
					Average RF		
					0.9378	0.7854	0.5902

D (Depth in mm), R (Radius in mm), L(Repair length in mm)

Table 2.2 SCF values for surface repairs on a fat plate (T= 30mm) under tension using three dimensional FEA

Profile	SCF edge	SCF surface			Reduction Factor (RF)		
	From Table2.1	L=60	L=40	L=20	L=60	L=40	L=20
D4R4	2.89						
D4R8	2.24	2.04	2.01	1.72	0.9107	0.8973	0.7678
D4R12	2.00	1.82	1.73	1.59	0.91	0.865	0.795
					Average RF		
					0.91	0.88115	0.7814
D6R4	3.34	2.8	2.42	2.02	0.8383	0.7246	0.6047
D6R8	2.6	2.15	2.00	1.79	0.8269	0.7692	0.688
D6R12	2.3						
					Average RF		
					0.8326	0.7469	0.6464
D8R4	3.82	2.89	2.62	2.37	0.7565	0.6858	0.6204
D8R8	3	2.23	1.95		0.7433	0.65	
D8R12	2.67						
					Average RF		
					0.7499	0.6679	0.6204

D (Depth in mm), R (Radius in mm), L(Repair length in mm)

Table 2.3 SCF values for surface repairs on a fat plate (T= 30mm) under bending using three dimensional FEA

Profile	R/D	D/T	R/T	SCF-Tension	SCF-Bending-
D8R4	0.5*	0.27	0.13	3.60	3.58
D6R4	0.67*	0.20	0.13	3.24	3.36
D4R4	1**	0.13	0.13	2.98	2.87
D8R8	1**	0.27	0.27	2.87	2.92
D6R8	1.33**	0.20	0.27	2.67	2.68
D4R8	2**	0.13	0.27	2.37	2.45
D8R12	1.5**	0.27	0.4	2.59	2.62
D6R12	2**	0.20	0.4	2.36	2.33
D4R12	3**	0.13	0.4	2.10	2.16

*D (Depth in mm), R (Radius in mm), * U-shaped profile, ** Part-circular profile*

Table 2.4 SCF values for surface repairs on a T-butt (L=60, T= 30mm) under tension and bending using three dimensional FEA

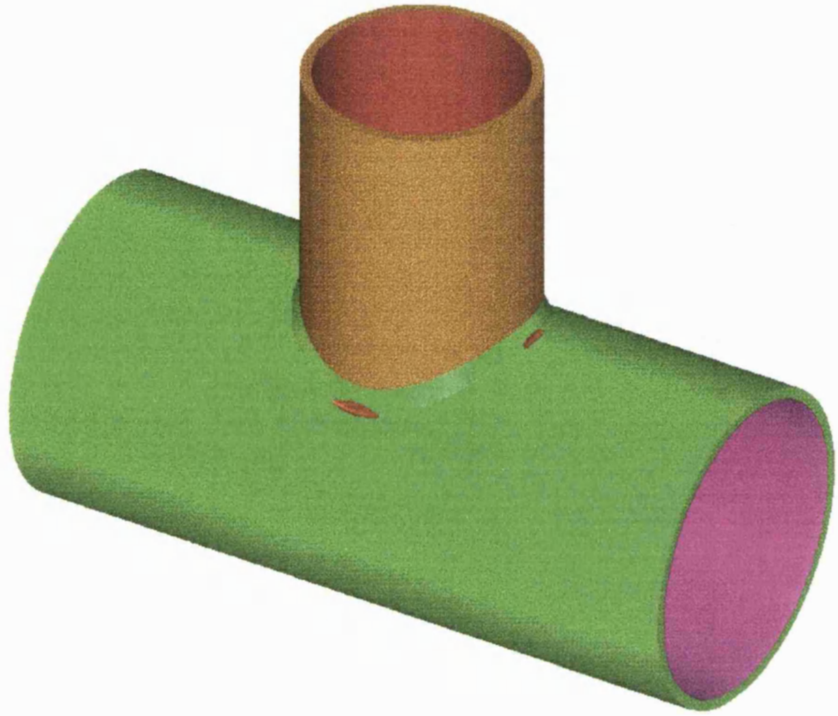

Figure 2.1 Fatigue crack repair profiles on a typical offshore tubular joint

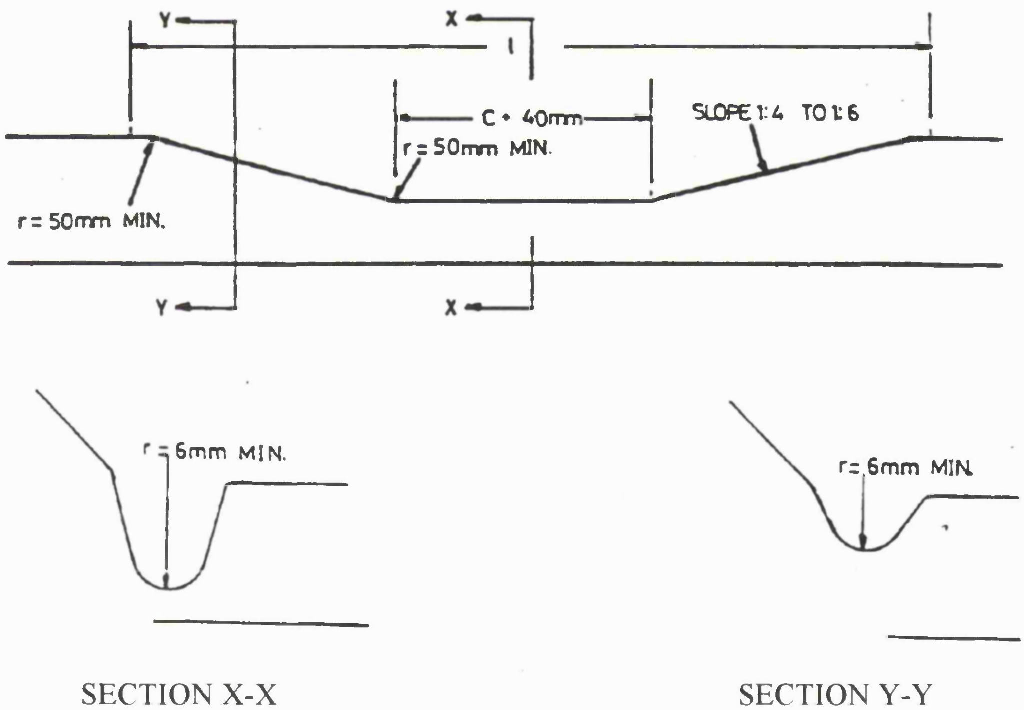

Figure 2.2 Grind repair used with manual bur grinding on tubular joints [2.6] (C= crack length, r= radius, l= repair length, repair depth = crack depth+2mm)

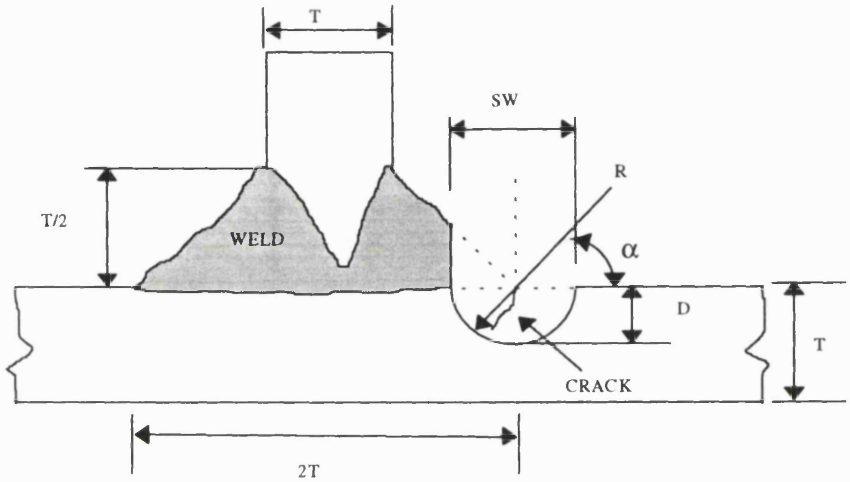

Figure 2.3 Edge U-Shaped Repair Profile and Parameters

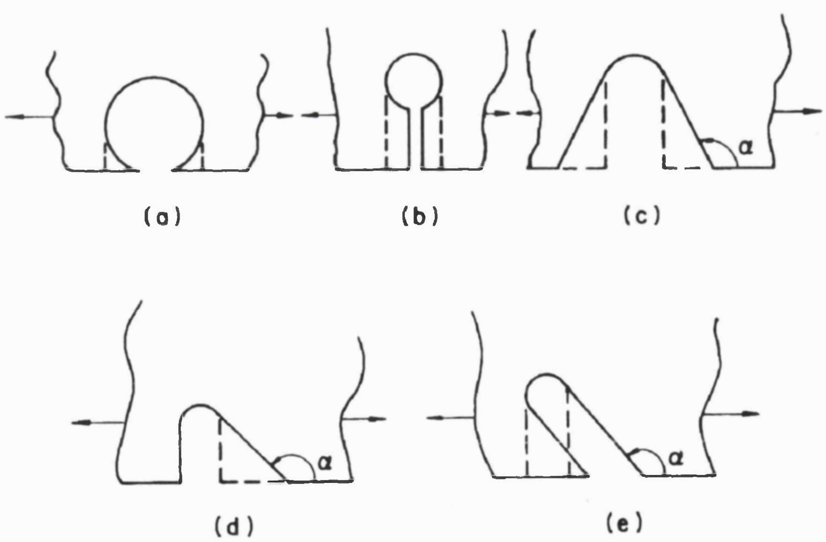

Figure 2.4 Equivalent notch configurations [2.8]

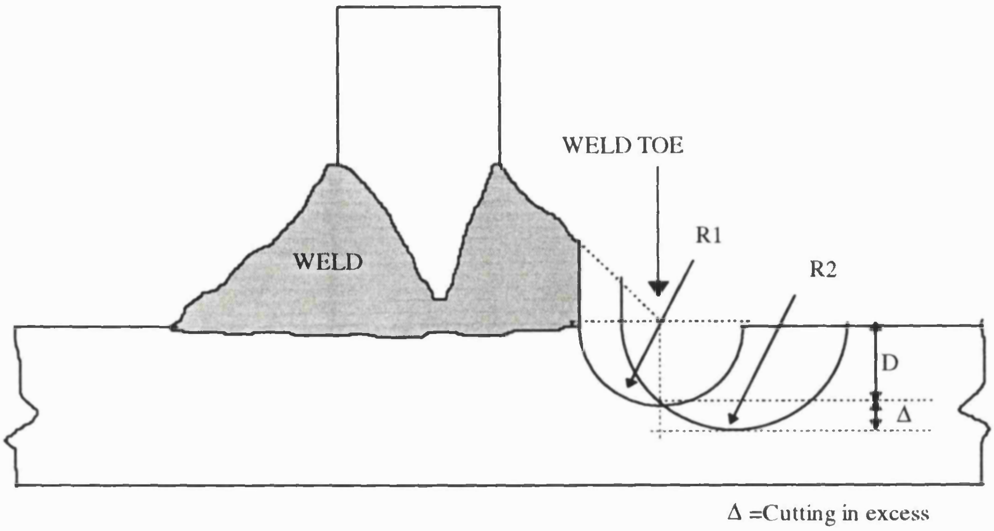

Figure 2.5 U-shaped repair profile position at the weld toe

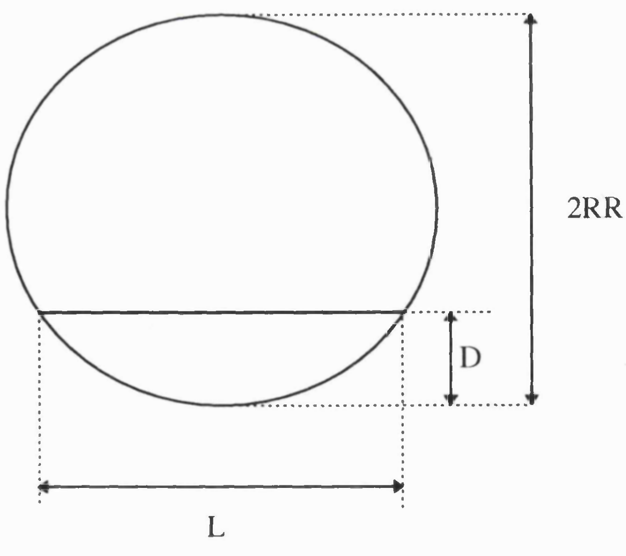

Figure 2.6 Longitudinal Semicircular Repair Profile
(D= repair depth, L= repair length and RR= longitudinal repair radius)

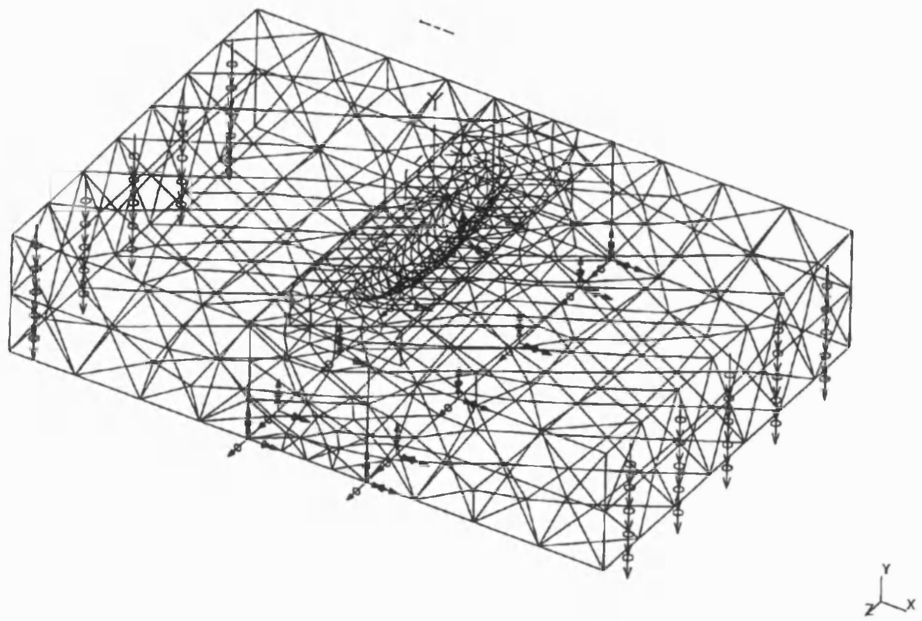

Figure 2.7 Finite Element Model of a surface U-Shaped repair profile on a flat plate

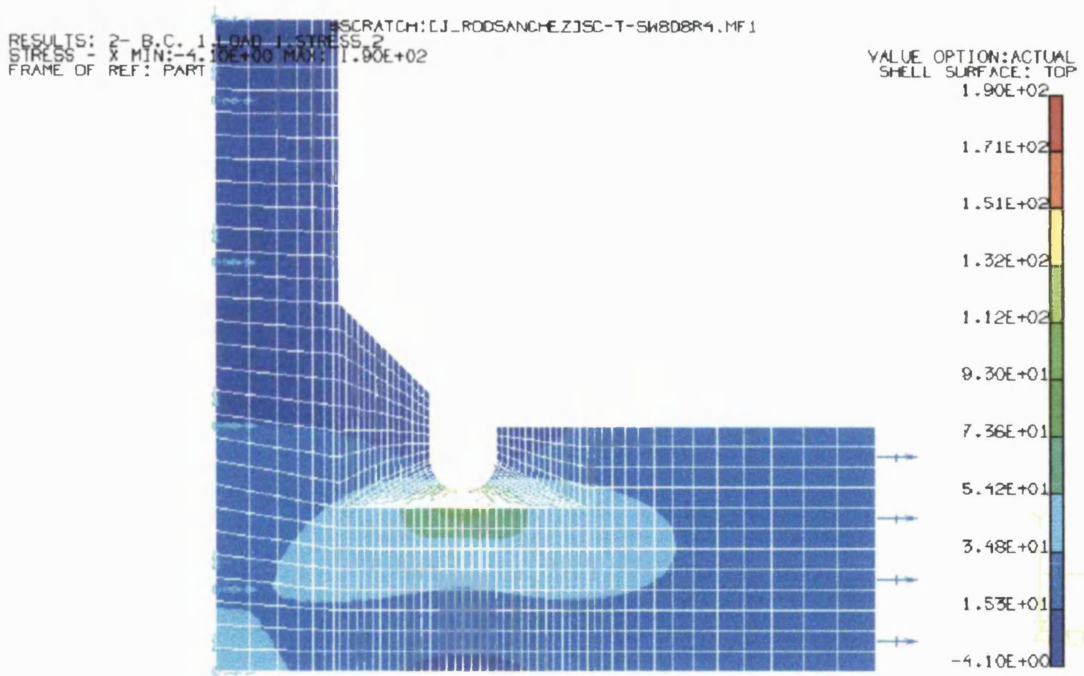

Figure 2.8 Edge repair 2D principal stresses distribution on a T-butt under tension

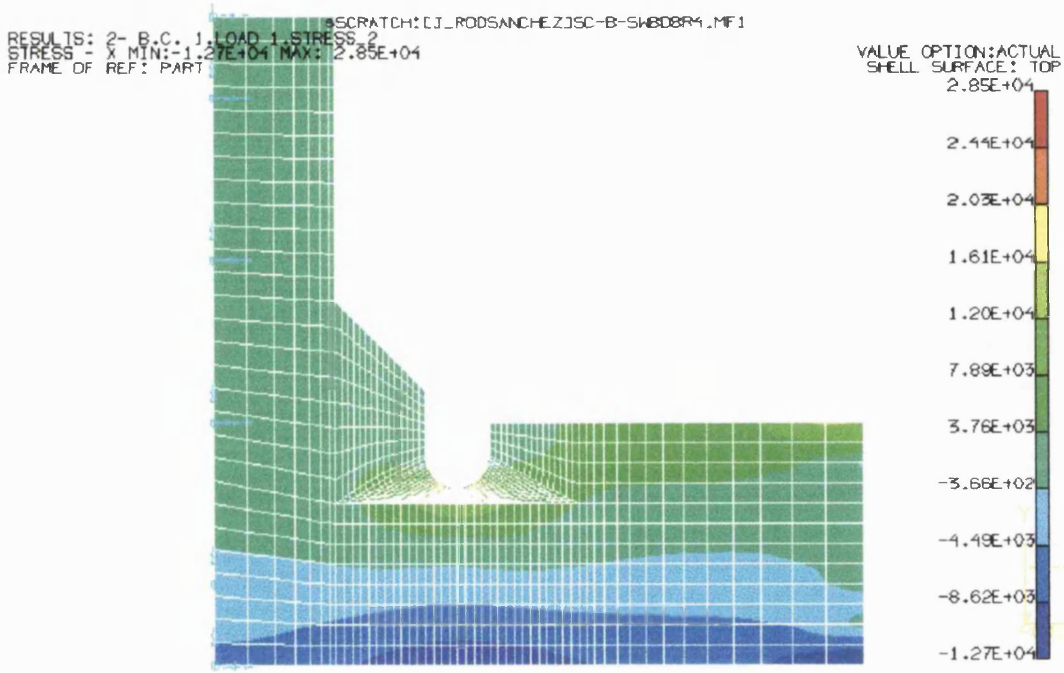

Figure 2.9 Edge repair 2D principal stresses distribution on a T-butt under bending

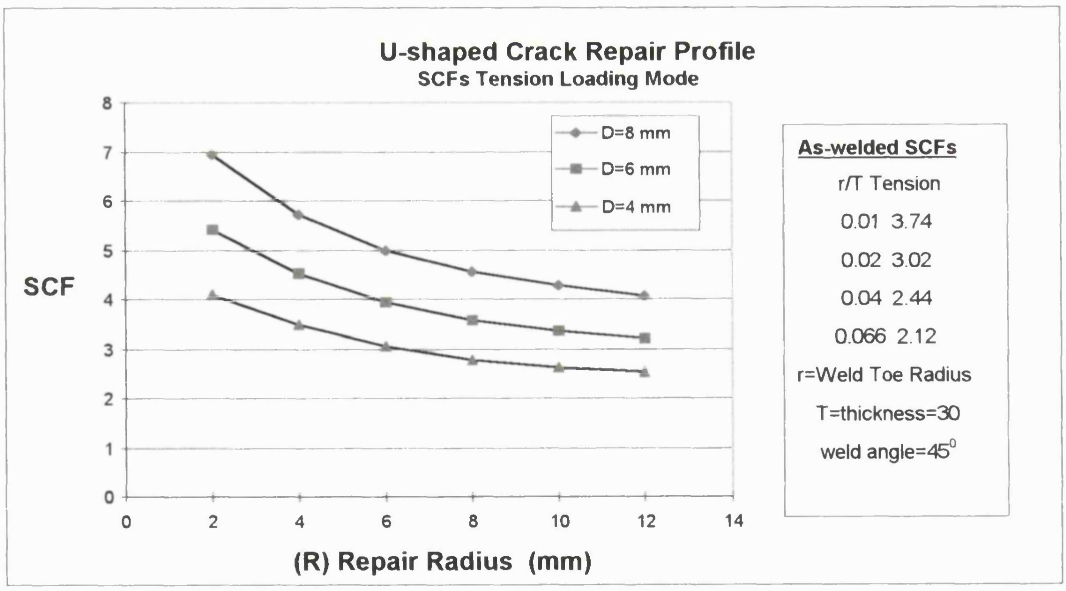

Figure 2.10 SCFs for Edge U-Shaped Repair Profiles on T-Butts under Tension (T=30mm)

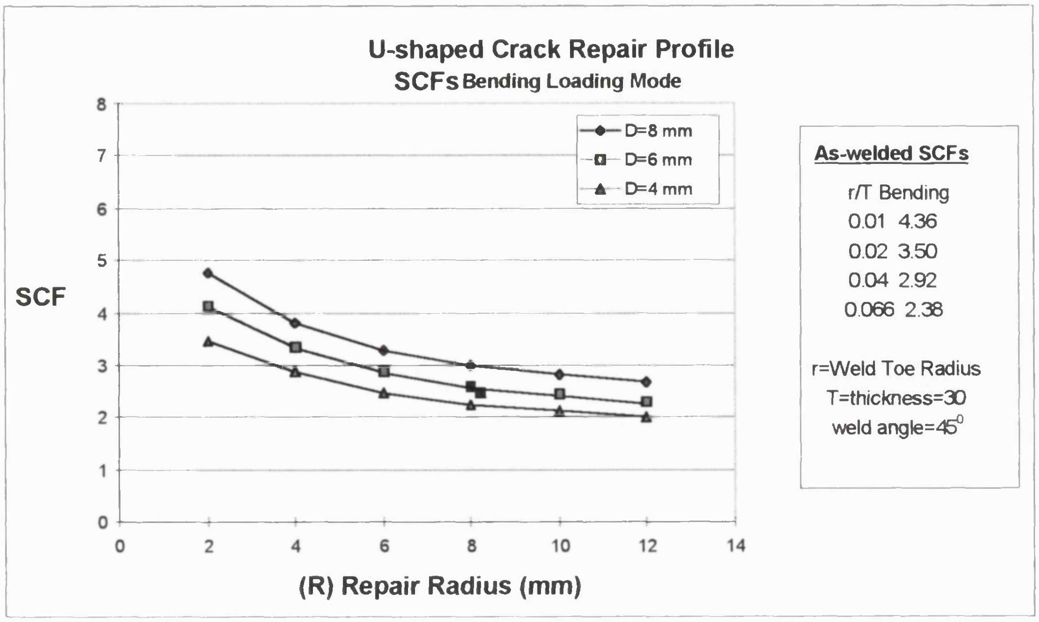

Figure 2.11 SCFs for Edge U-Shaped Repair Profiles on T-Butts under Bending (T=30mm)

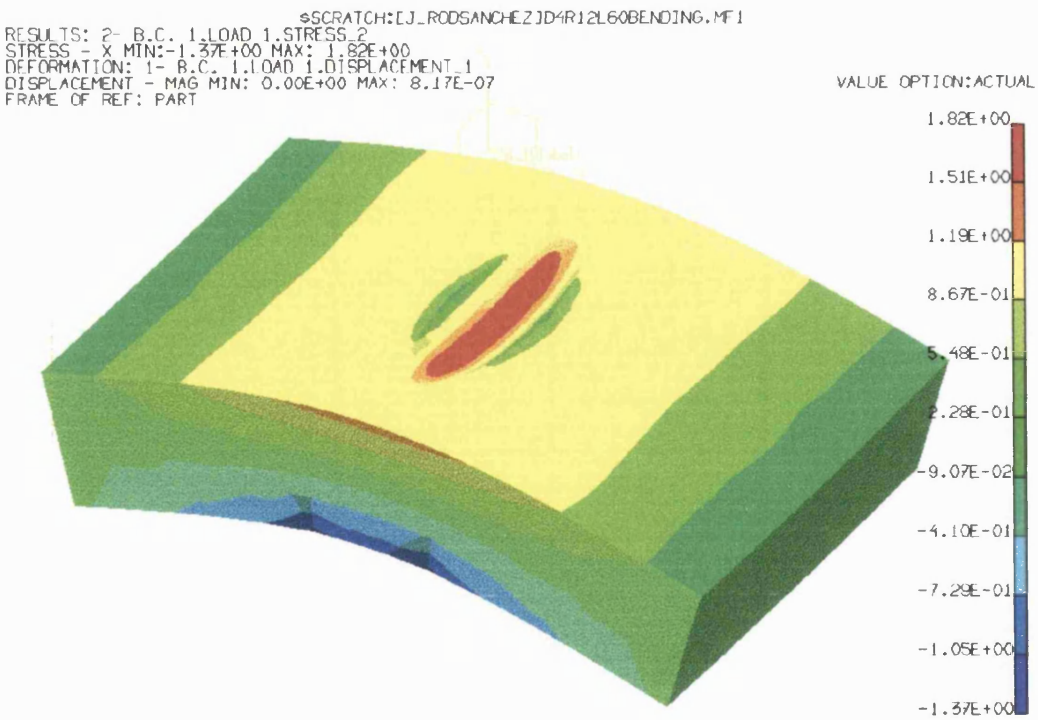

Figure 2.12 Stress distribution of a flat plate with a surface repair under bending

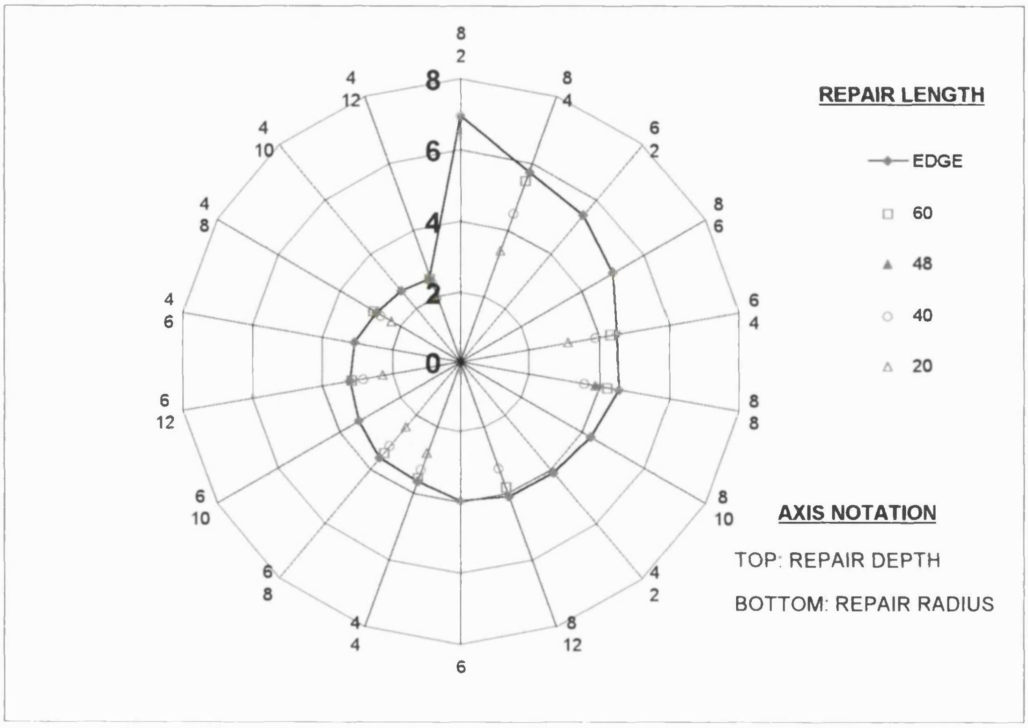

Figure 2.13 SCFs of edge repairs on T-butts and surface repairs on flat plates, both cases under tension(T=30mm)

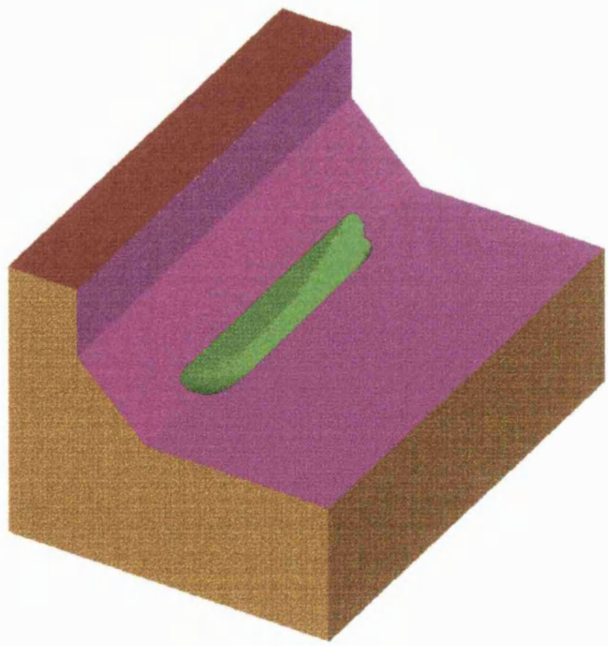

Figure 2.14 Surface repair on a T-butt with weld toe radius=0 in FEA model

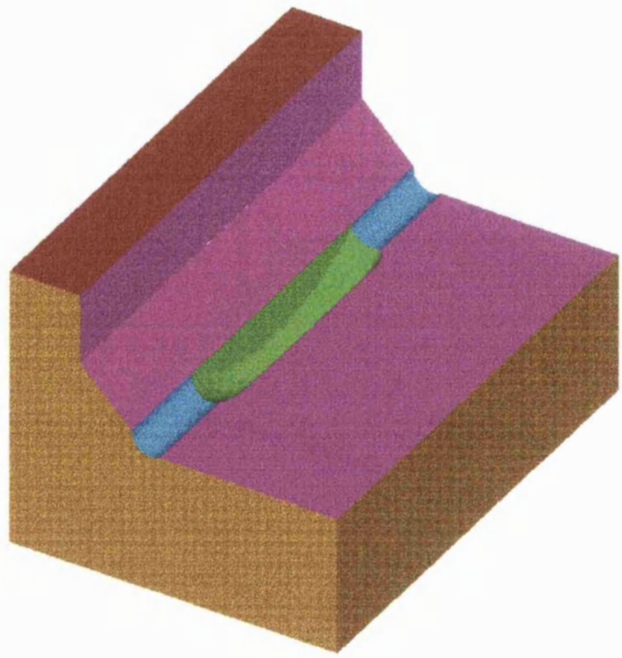

Figure 2.15 Surface repair on a T-butt with weld toe radius = R in FEA model

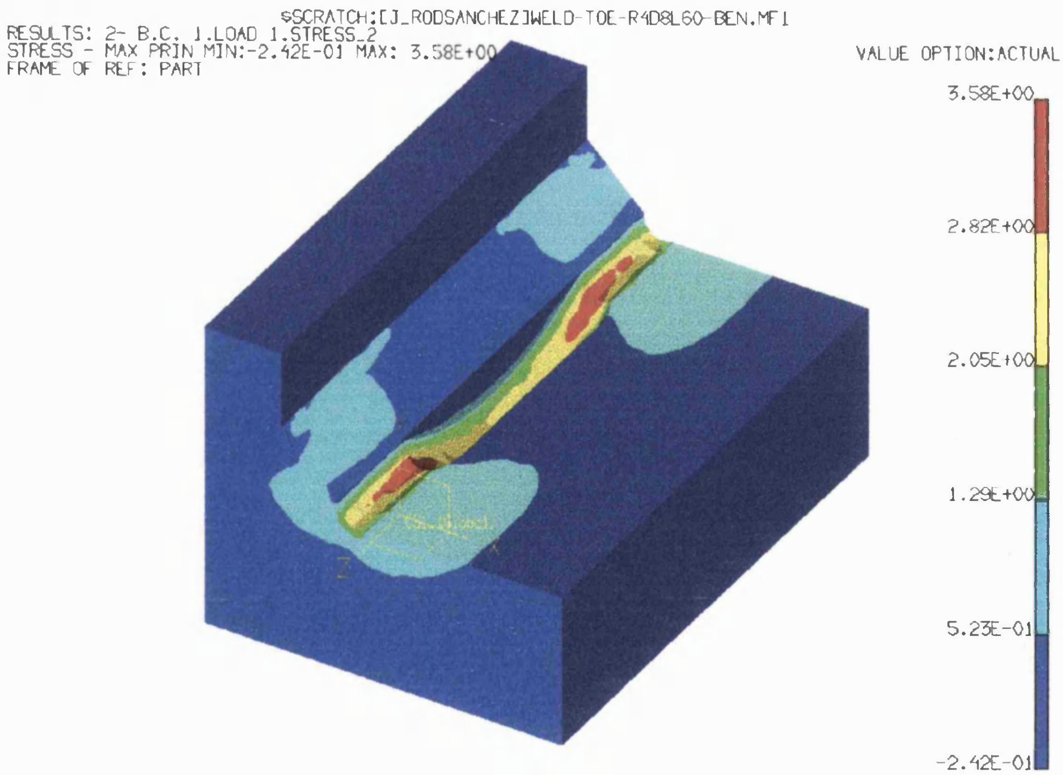

Figure 2.16 Stress distribution of a surface repair on a T-butt under bending

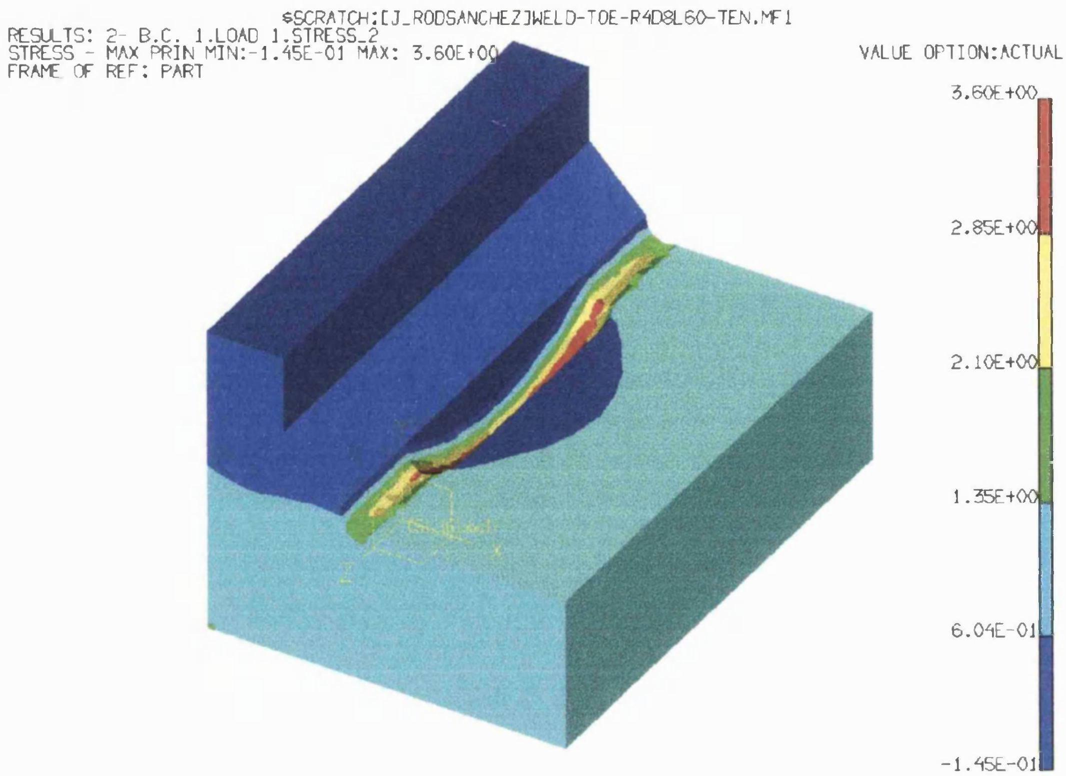

Figure 2.17 Stress distribution of a surface repair on a T-butt under tension

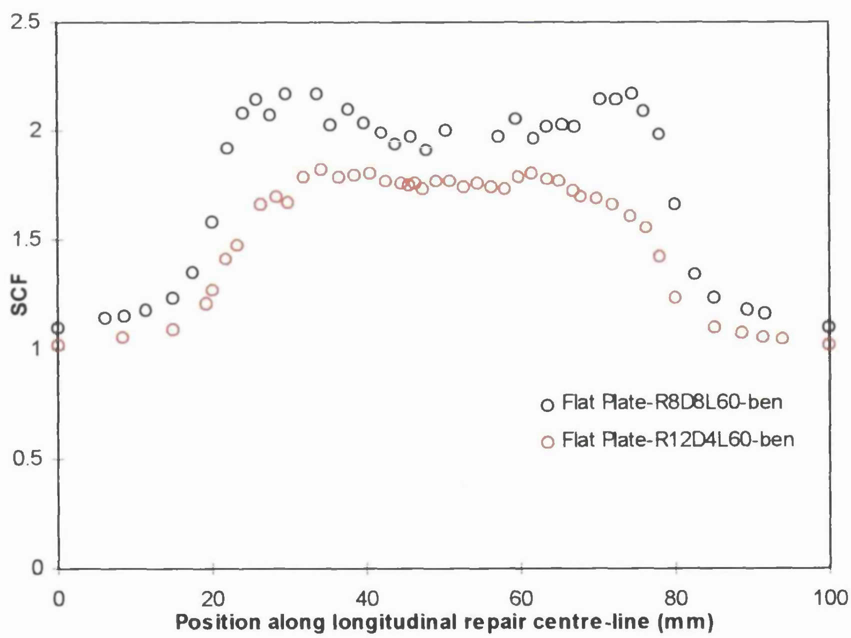

Figure 2.18 SCF distribution along two surface crack repairs on a flat plate under bending (At 20mm repair starts and at 80mm repair ends)

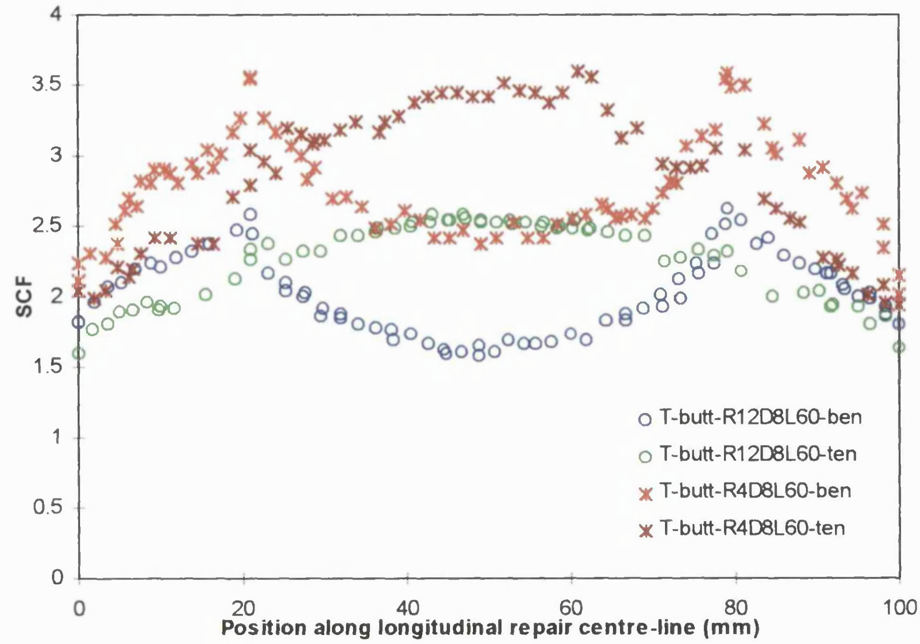

Figure 2.19 SCF distribution along two surface crack repairs on a T-butt under bending and tension (At 20mm repair starts and at 80mm repair ends)

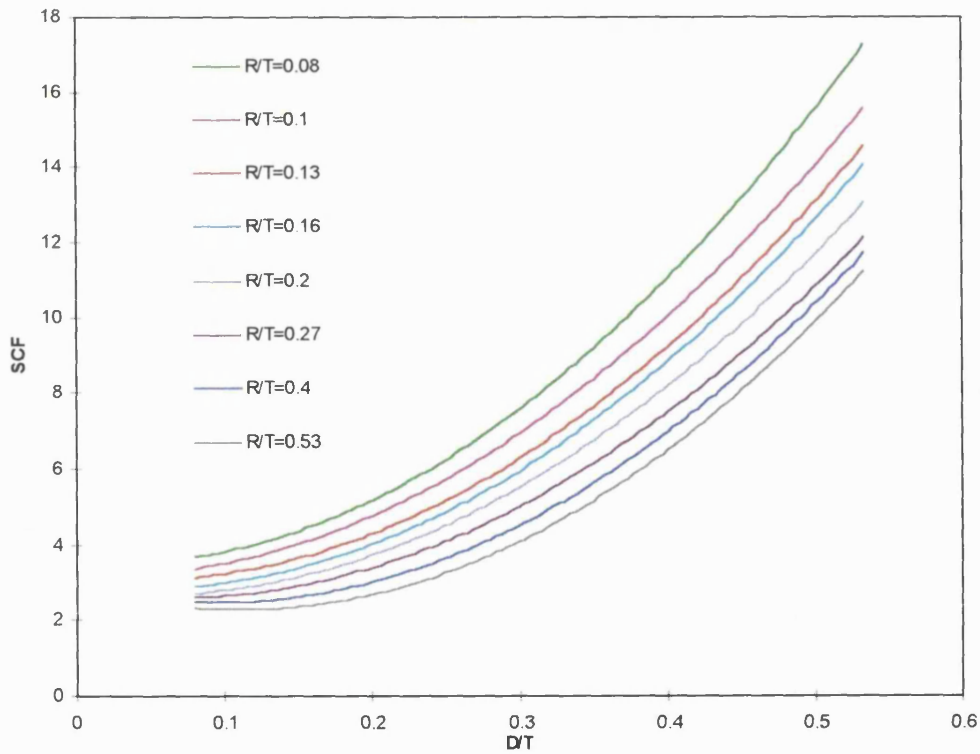

Figure 2.20 SCFs for edge repaired T-butts under tension

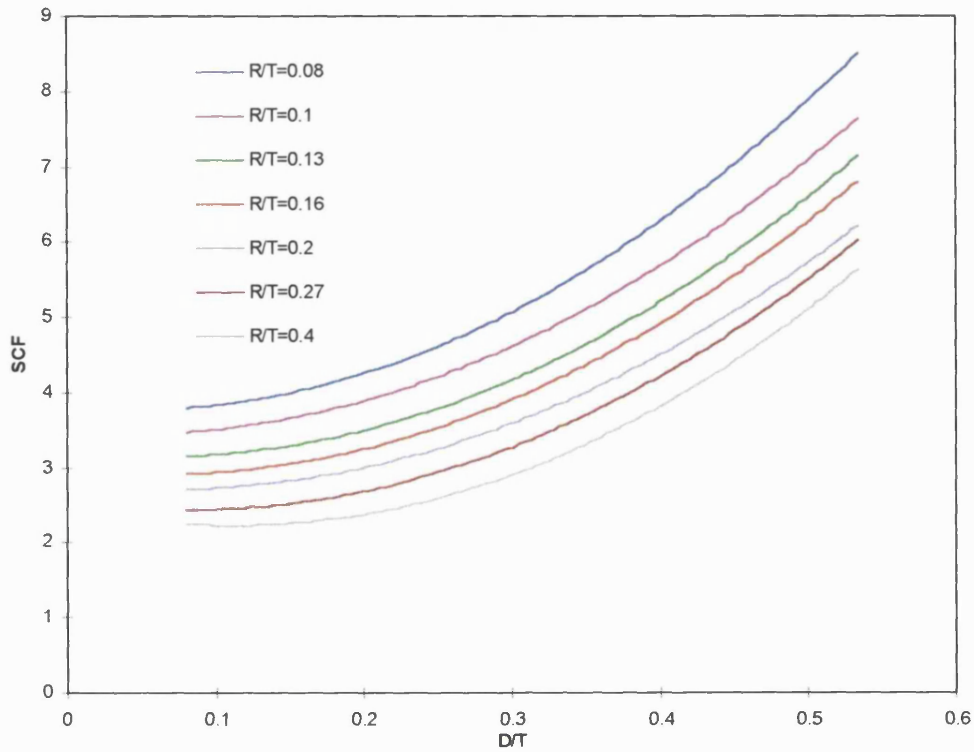

Figure 2.21 SCFs for edge repaired T-butts under bending

CHAPTER THREE

EXPERIMENTAL FATIGUE TESTING OF REPAIRED WELDED JOINTS

3.1 Introduction

Results obtained during experimental fatigue testing of as-welded specimens and specimens with the repair geometry analysed in chapter two will be presented. The repair geometry was machined on butt and T-butt plates by electrochemical machining, disc cutting or ROV grinding and in some cases residual compressive stresses were introduced by shot peening.

An automated state of the art inspection technique was used for monitoring and sizing cracks during fatigue testing. Full description of testing procedures, data acquisition equipment, data processing and repair procedure is given. Data obtained has been analysed to determine crack growth rates, crack initiation behaviour, crack shape evolution and fatigue life extension after crack repair. Analysis of the data was made to provide stress intensity factors. This has the intention to compare in chapter 4 with recently developed stress intensity factor models to identify an appropriate fracture mechanics model for the repaired condition.

3.2 Butt and T-butt Welded Specimens

Experimentation on butts and T-butts welded plate specimens has been used extensively to explain fatigue behaviour of more complex welded structures. The specimens used for the experimental work here are butt and T-butt welded plate connections in the as-welded condition and of fatigue crack repaired geometries. Testing butt and T-butt specimens was considered convenient since it is more economical than on full scale tubular connections. Additionally, transportability of the specimens was an important aspect during testing since various repair machining techniques were considered and not all of them could be implemented at UCL. Although, particular stress distributions found in tubular connections (geometric stresses) are not reproduced when testing on butt and T-butt specimens, extrapolation of the results to tubular welded connections is possible.

Dimensions, material, manufacture and specimen design are presented in the following sections.

3.2.1 Specimens Design

Design of the specimens was an ongoing process due to the nature of the results pursued. Although the basic geometry of a butt or T-butt welded connection was never changed, adjustments had to be made to produce the desired cracking pattern for this study.

During the experiments it was observed that fatigue cracks in butt and T-butt welded connections subjected to bending loading with a uniform distribution of stress along the width always develop into edge cracks. Edge cracks can be repaired with the procedures presented in this work, but they were not ideal for the purposes of this research since the intention is to repair surfaces similar to those found in tubular joints under fatigue loading. It was found that surface cracks on butts and T-butts under bending loading can be obtained by:

a) Improving the fatigue resistance in unwanted regions of cracked weld toes.
   - a.1) Inducing compressive residual stresses.
   - a.2) Reducing the stress concentration at the weld toe.

Option a.1) was not considered to be convenient due to the possible relaxation of compressive stresses during cyclic loading therefore, option a.2) was implemented by machining the weld toe to increase the weld toe radius reducing the SCF where cracking was not wanted.

Increasing the weld toe radius where cracking is not wanted is a reliable procedure to obtain surface cracks on T-butts whilst maintaining a uniform distribution of nominal stress along the plate width. A uniform distribution of nominal stress along the plate width makes fracture mechanics calculations and extrapolation of the results easier. Tubular joint repair could well include crack removal and removal of adjacent weld toe regions.

3.2.2 Dimensions

Selection of plate thickness and specimen width has a significant effect on the results obtained. It is known that for welded connections fatigue life reduces as plate thickness is increased [3.1]. Specimen width becomes important if crack shape evolution is considered important since a certain width is required for the crack shape to fully develop. Additionally, the finite width factor for typical laboratory size plate specimens used for studying fatigue crack growth of surface elliptic cracks in bending causes the surface point stress intensity factor to increase as the crack size increases, and hence the crack growth rate also increases [3.2].

Plate thickness and specimen width were the principal dimensions varied during testing. For T-butt welded specimens 20 and 30mm plate thickness was used, main and attachment plates were always of the same thickness for a specimen; the specimen width was 300mm for specimens series TB300 and 200mm for the others. For butt welded specimens 20mm plate thickness and 200mm specimen width were used for the only two specimens tested. Figure 3.1 shows the range of specimen dimensions considered during testing. Weld dimensions will be described in section 3.2.3.

Weld shape and weld toe radius are the main sources of dimensional scatter. Many specimens were tested having the weld toe machined, thus record of weld shape and weld toe radius was only made for specimens tested with weld toes in as welded condition. However, for repair depths $\geq$ 4 mm, like all the cases studied in this thesis, the weld geometry has negligible effect as was demonstrated in chapter 2 section 2.4.2.

3.2.3 Manufacture and Material Properties

All specimens were manufactured using a steel which had to comply with the requirements defined in BS EN 10025 Grade S355J2G4 [3.3]. Chemical composition and mechanical properties are given in tables 3.1 and 3.2 respectively.

T-butt specimens manually welded were welded from plates which had been machined to the final dimensions. The attachment plate was bevelled to 45^0 to allow a full penetration weld according to AWS [3.4] as shown in figure 3.2. After preheating to 70^0 C a general purpose electrode E6013 was used for welding. Electrodes of 3.2 mm were used for root penetration and 4.0 mm for dressing. No restraint was applied to the attachment during fabrication although welding was balanced on both sides. Average bowing obtained was 2.5 mm/m along the specimen width direction. Poor weld quality was found in many specimens at the weld toe plate ends thus, specimens TB300 were manufactured following a different procedure.

T-butt specimens series TB300 were cut out in pairs from a T-butt welded joint 400 mm wide x 700 mm long which had 50mm from both longitudinal ends cut-off. The purpose was to eliminate the plate ends where defects accumulate due to poor fusion during welding. The attachment plate was bevelled to 45^0 for a full penetration weld as in the previous case. Preheating to 70^0 C and automatic welding with a rod 5mm diameter EV50 was used for assembling. No restraint was applied to the attachment during fabrication and welding was balanced as in the previous case. Average bowing obtained was 3.0 mm/m along the specimen width direction.

T-butt machined specimens were manufactured from thick plates by cutting off the excess material using a numerically controlled machine. Weld toes were machined simulating the weld shape described in figure 3.2. However, the round weld cap was made flat instead. Bowing of the parent plate was eliminated and precise control of the dimensions was achieved.

Butt specimens manually welded were welded from plates which had been machined to the final dimensions. The plates were bevelled to 45^0 to allow a full penetration weld as shown in figure 3.2. After preheating to 70^0 C a general purpose electrode E6013 was used for welding. No restraint was applied to the attachment during fabrication although welding was balanced on both sides.

3.3 Experimental Set Up

The following sections will describe a set-up designed and manufactured for loading the specimens used for this study. Equipment, instrumentation and software used to control the test and monitor crack growth during testing will also be described.

3.3.1 Applied Loading

Due to limitations of time for experimentation it was considered convenient for the purposes of the research to test only under bending loading since, it was identified that for tubular joints, the stress field near the weld is predominantly bending, even under axial loading [3.5].

In order to avoid relying on precise positioning of the specimens on the loading set-up to produce the same stress level before and after repair a four point bending set-up was considered recommended for testing. A four point bending set-up produces a constant moment distribution between the two internal loading points. The set-up was designed specifically for the specimens and manufactured at UCL Mechanical Engineering workshop, see figure 3.3.

The set-up consists basically of a top and bottom set of hardened rollers mounted on supports which are bolted to a framework. The bottom set of roller supports sits on a plate which has a hinge connection to a framework on top of the actuator.

The hinge has the purpose of adjusting the set-up to the lack of flatness of the specimens. This adjustment is especially important in a four point bending set-up to assure that each roller applies equal load to the specimen. The top set of roller supports is fixed to the loading machine framework. The fatigue load is applied with a 1 Mega-Newton servo-hydraulic INSTRON actuator controlled with a DARTEC 9600 controller, see figure 3.4. The controller is able to work on load or position controls. All the tests were performed under load control, so even when the stiffness of the specimen changed the magnitude of the load cycle applied did not change.

3.3.2 Fatigue Crack Depth Monitoring

Crack depth evolution was monitored from early stages of growth using the Alternating Current Potential Difference (ACPD) technique applied by the U-10 Crack Microgauge. The technique requires the injection of an alternating current on the surface of the specimen. The current follows the contour of surface breaking defects like cracks and since the potential gradient on the metal surface and on the crack faces is assumed to be linear, measurements of the potential difference across the crack and adjacent to the crack can be used for the calculation of the crack depth, see figure 3.5. Crack depth can be calculated from the following expressions:

$$\begin{aligned} &V_R a \Delta_R \\ &V_C \alpha(\Delta_C + 2d) \\ &\frac{V_C}{V_R} = \frac{\Delta_C + 2d}{\Delta_R} \end{aligned} \tag{3.1}$$

Thus,

$$d = \frac{\Delta_R}{2}\left[\frac{V_C}{V_R} - \frac{\Delta_C}{\Delta_R}\right] \tag{3.2}$$

For the case when $\Delta_C = \Delta_R$:

$$d = \frac{\Delta_R}{2}\left[\frac{V_C}{V_R} - 1\right] \tag{3.3a}$$

where:

d Crack depth

Δ_C Probe gap across the crack

Δ_R Probe gap adjacent to the crack used as reference

V_C Potential difference across the crack

V_R Potential difference adjacent to the crack used as reference

The above equation is strictly valid for an infinitely long crack in an infinite plate. Therefore, crack depths have to be corrected to consider other aspect ratios (crack depth/crack length) such as semi-elliptical cracks. Modifiers to correct crack depths for cracks with low aspect ratios are minimal, thus no corrections were applied.

Spot welded probes are fixed to the specimen along the weld toe region. Since the spot welding is done manually variations in dimensions of Δ_C and Δ_R are always present affecting the accuracy of the crack depth calculations. An alternative procedure to monitor crack growth not taking in account Δ_C into the calculations is by determining for a given site the difference of crack depth between two subsequent readings sub-scripted as 1 and 2. From equation (3.2) calculating the difference of crack depth between readings 1 and 2 the following equation can be established:

$$d_2 - d_1 = \frac{\Delta_{R2}}{2}\left[\frac{V_{C2}}{V_{R2}} - \frac{\Delta_{C2}}{\Delta_{R2}}\right] - \frac{\Delta_{R1}}{2}\left[\frac{V_{C1}}{V_{R1}} - \frac{\Delta_{C1}}{\Delta_{R1}}\right] \quad (3.3b)$$

but for a given site along the crack path: $\Delta_{R_2} = \Delta_{R_1}$ and $\Delta_{C_2} = \Delta_{C_1}$

Hence:

$$d_2 - d_1 = \frac{\Delta_{R2}}{2}\left[\frac{V_{C2}}{V_{R_2}} - \frac{V_{C1}}{V_{R_1}}\right] \quad (3.4)$$

Equation (3.4) is particularly useful when monitoring cracks in regions where a crack repair has already been made. The cumbersome manual measurement of Δ_C

which contains the transverse groove section at various sites along the repair length is not required. The Δ_R distance is only needed and can be set to a constant value without complication since it is placed beside the repair groove on the main plate, see figure 3.6. To determine crack growth evolution using equation (3.4) it is required to provide an initial crack depth value because the equation only provides a crack depth difference between two subsequent readings. The initial crack depth value is usually zero in the absence of a crack or the crack depth value if the monitoring starts on a pre-cracked condition.

It is especially important to locate the spot welded probes outside the repaired surface since, on the grooved surface the stress distribution is high and spot welded probes act as stress risers therefore causing cracks to initiate at the spot welded sites invalidating the test. This situation was observed in specimen S12R12D4.

To avoid the time consuming activity of spot welding probes twice on each specimen (before and after repair) an ACPD array with six sites of spring loaded pins was manufactured by TSC. The array has a shape that fits grooves up to 15mm deep with transverse repair radii in the range 8- 12mm. The probe spacing, Δ_C and Δ_R were set to 5mm, see figure 3.7.

The idea of using the array was to position it in the groove and monitor crack growth anticipating that crack initiation would take place in the bottom of the groove. Problems were found with the time in service the spring loaded pins could sustain. The spring loaded pins were also cycling as the probe was always in contact with the specimen surface during testing. Sometimes springs in more than one site did not last to complete a specimen test and valuable data was missed.

A possible solution to overcome the service life of the spring pins would be to mount the probe on a rotor that could lift the probe during cycling and press it against the specimen while scanning. The lifting and pressing process could have been included in the software which controlled the test to maintain full automation. This solution was not attempted and spot welding was continued instead. However, manual use of the array provides a fast and convenient alternative for data collection especially useful after the crack had been repaired as a verification that the entire crack had been removed.

3.3.3 Test Control and Data Collection

Test control and data collection was carried out by a computer running software written at UCL by D. Faulke, 1993 [3.6]. Some modifications were made to the software to include parameters required for this particular testing programme. During testing the computer sends signals to the DARTEC controller after a predetermined number of cycles to stop fatigue cycling and to hold the specimen at mean load while scanning the spot welded sites along the crack path with the U-10 Crack Microgauge. The data obtained during the test was printed in situ and saved in the hard disk of the computer in a spreadsheet format for post processing. The data collected consists of: time, number of cycles undergone at the moment of scanning, crack voltage, reference voltage and crack depth for each of the sites scanned on the specimen. Figure 3.8 presents a diagram of the testing system and the interactions between the components.

The convenience of the test control and data collection system is that it can be left operating continuously with minimal supervision. The system also allows modifications of the scanning frequency during testing if more data is required near failure when cracks are growing rapidly.

3.4 Experimental Stress Analysis

Experimental measurement of stress by strain gauging in the bottom of a repair profile was attempted on a specimen with a repair groove D4R8L60. A difference of 30% was obtained when the experimental and finite element determined stress magnitudes were compared. However, experimental readings were not highly reliable since strain gauge positioning and bonding in the bottom of the repair was difficult. An optimum strain gauge bonding seemed difficult to be achieved due to the high curvature in the bottom of the repair groove. The narrow groove surface opening made it difficult to properly place a rectangular rosette in the bottom, even using gauges of 2 mm length.

Highest stress concentration was found to be located at the repair ends and not in the bottom of the repair after a more detailed stress analysis using the finite element method was made as presented in chapter 2. However, no more experimental stress analysis was carried out thus, a comparison between experimental and finite element method stress values was not made.

Conversion of strain readings to principal stresses was done using equation (3.5)

$$\sigma_{1,2} = E\left[\frac{\varepsilon_a + \varepsilon_c}{2(1-\upsilon)} \pm \frac{1}{2(1-\upsilon)}\sqrt{(\varepsilon_a - \varepsilon_c)^2 + (2\varepsilon_b - \varepsilon_a - \varepsilon_c)^2}\right] \tag{3.5}$$

The principal angles measured from axis a are given by:

$$\tan 2\phi_{1,2} = \frac{2\varepsilon_b - \varepsilon_a - \varepsilon_c}{\varepsilon_a - \varepsilon_c} \tag{3.6}$$

where:

$\sigma_{1,2}$ Principal stresses

$\phi_{1,2}$ Principal angles

E Young's modulus

υ Poisson's relation

ε_a, ε_b and ε_c Strain gauge readings aligned 0^0, 45^0 and 90^0 respectively in a three element rectangular rosette.

During the stress analysis various strain readings were recorded for a loading and unloading process at different applied load levels. The load levels were always in the elastic range in order to avoid plastic deformations before the specimen was tested.

3.4.1 Experimental Set Up Calibration

An additional application of the experimental stress analysis was the calibration of the experimental set up.

For the calibration of the test set-up, two strain gauges were bonded on a T-butt welded specimen 50mm from the weld toe and equally spaced along the width. The T-butt was one of the manually welded specimens for the testing programme. The specimen dimensions were: W=200mm, T=30mm and L=400mm. Strain readings were obtained for various stress levels to verify that the set-up was imposing a uniform bending loading along the specimen width. Additionally, it was verified that the nominal stress magnitude on the specimen surface at the section where the strain gauges were placed was according with the calculated using equation (3.7).

$$\sigma = \frac{M}{I} y \tag{3.7}$$

where:

σ   stress due to bending
M   bending moment
I   second moment of area
y   distance from neutral axis to extreme fibre

It was observed that the stress distribution across the specimen was not uniform. This is thought to have been mainly influenced by the specimen bow in the width direction. The bowing was produced by deformations induced during the welding process. Although, the magnitude of the bow was not considerable (2.5mm/m) the set-up rollers applied the load unevenly along its 200 mm length. This situation encouraged crack initiation at the specimen ends.

To overcome the situation explained above, a solution was considered to machine flats on the specimens where the rollers apply the load. A second solution was to reduce the roller length to concentrate the application of the load on the specimen.

This latter option relies on the specimen stiffness to distribute the load along the width avoiding a non-uniform stress distribution.

This option was employed reducing the roller length to 75 mm. From the strain gauged specimen the strain readings confirmed that the load was distributed uniformly along the specimen width. Additionally, experimentally determined nominal stresses using equation (3.5) showed a maximum difference of 4% with respect to the theoretical values obtained using equation (3.7).

As part of the calibration process the distance between the middle rollers was maximised to have a uniform distribution of bending moment in the longest possible distance of the specimen. The distance between an external and internal roller is 35mm, see figure 3.4. After the set-up calibration no additional experimental stress analysis was carried out on the specimens prior to fatigue testing.

3.5 Fatigue Test Programme

The fatigue testing programme and adjustments made to it as results were obtained will be presented in this section. Additionally, the stress levels used and analysis of the data collected are also explained.

A testing programme was originally planned to determine the fatigue life improvement of repaired fatigue cracked T-butt joints, see table 3.3. The programme comprised of 12 specimens, 30mm thick, all with repair profiles. The repair profiles were manufactured by disc cutting.

All the repair profiles were longitudinally semicircular 60 mm long. This is shorter than previously proposed repair profiles, see figure 2.2 in chapter 2, and was deliberately chosen to be more representative of non-manual repairs. These can be considered to be uncommon profiles but in many cases could be realistic profiles as is explained in the discussion when referring to crack shape evolution.

Repair depths and transverse radii for the 60 mm long profiles are presented in table 3.3. Compressive residual stresses were applied by shot peening 6 of the 12 disc cut specimens. Since there is available data from previous studies of fatigue life of T-butts in the as-welded condition it was considered convenient to start the testing programme using specimens not previously fatigued cracked but with repair grooves. This situation simulated specimens where the cracks were fully removed by repair before subsequent fatigue testing.

The specimens were subdivided into sets of different repair radii, the smallest being 4mm. Each specimen during the testing process had to undergo two fatigue testing stages, at the end of the first fatigue stage the testing was planned to stop when crack depth was 7 mm to make a repair 9 mm deep maintaining the same repair radius and in some cases compressive residual treatment was planned to be applied again. A graphical representation of the expected experimental crack growth curves can be seen in figure 3.9. The extreme left curve represents the as-welded condition to which the fatigue improvements will be referred to, and the four following curves represent the average of three specimens. Since this is only a qualitative representation of the expected results three curves have been superimposed and the specimen number is indicated on top of the curve. The difference between the three superimposed curves is that each one will shift to the right as the transverse radius of the groove is increased.

The testing programme tried to simulate a critical but possible condition where a crack is detected, sized, repaired and then after some time an inspection reveals that a new crack has initiated and a new repair has to be done. This testing programme intended to demonstrate that after repair the fatigue life obtained is longer than if the crack was not repaired at all and that further repair could improve the benefit.

After starting the testing programme, the first specimens tested showed unexpected cracking patterns. The cracks were not initiating in the bottom of the repairs but at the repair ends where the repair merges with the plate surface. This situation lead to the suspicion that the set up was not applying a uniform load along the specimen width therefore, a full calibration of the set up was made as was described in section 3.4.1. The calibration showed that with 75mm roller length the specimens have sufficient stiffness to produce a uniform stress along the specimen width in the weld toe region thus, no evident explanation of the cracking not initiating in the bottom of the repair was obtained.

In the search for an explanation of the unexpected cracking location a review of the finite element results was made. The review revealed that all finite element cases analysed before the testing programme was initiated showed maximum stress concentration in the bottom of the repair groove, and it was therefore, expected crack initiation in such place, see chapter 2. However, the finite element models analysed were only two dimensional idealisations of repair profiles on T-butt joints, so full three dimensional models of repair profiles on butt welded plates were analysed.

To understand the unexpected cracking pattern a three dimensional finite element analysis of a repair profile on a T-butt joint was carried out having the exact geometry of the specimen and repair profile experimentally tested. The results showed that the maximum concentration of stresses was at the repair ends due to the stiffening effect of the vertical plate therefore, crack initiation would initiate in those regions. Before resuming the experimental testing it was consider convenient to conduct an exhaustive finite element stress analysis study of various combinations of repair depths, radii and plate thickness in three dimensional models that required in some cases more than 4 hours of CPU for obtaining stress distributions, see chapter 2. These analysis identified the crack initiation places and the stress concentration variation with respect to repair depth, repair radius and plate thickness.

An additional finding whilst experimentally testing was that in some specimens corner cracks were obtained at the point where the weld toe reaches the edge of the specimen. Inspecting the weld toes at the edges of the specimens it was found that weld quality was poor. This was explained due to the insufficient fusion when the electrode is initially placed on the metal. The problem is aggravated when the weld runs start and stop at the same place, as happens at the ends of narrow plates like the specimens.

To eliminate the corner cracking problem it was considered that a 10 mm slice of the specimen be cut-off at both ends. However the specimens were already narrow (200mm wide) thus, it was decided to manufacture new wider specimens instead with the ends cut-off. The new specimens were 300mm wide with 20mm thickness and were named TB300 series, see section 3.2.3.

The fact that crack initiated at the repair ends in T-butt welded joints suggested that the testing programme had to be adjusted since it was based on the hypothesis of cracks initiating in the bottom of the repair.

A modified testing programme was made of 6 Groups of specimens. Each group has the aim to explain or verify a particular situation identified in the finite element analysis or in the original testing programme. Obtaining information by groups allowed to gradually build up a general view of fatigue crack repairing welded connections using short repair profiles. The 6 Groups presented below were formed considering the findings presented in this section and in sections 3.5.1, 3.6.4 and 3.6.5.

Table 3.4 contains all the fatigue tested specimens that will be introduced through the remainder of this chapter and relevant experimental parameters. Specimens in lines 1 to 18 are contained in Groups 1 to 6. Specimens in lines 19 to 25 did not provide relevant information to be considered in Groups 1 to 6 but were considered in the S-N curves presented in section 3.7. The interpretation of the coloured shades is as follows:

Grey: Specimens that were fatigue cycled, repaired and re-tested.

Green: Type of specimen and manufacture

Yellow: Repair dimensions, Radius (R), Depth (D), Length (L) and procedure used to machine the repair.

Pink: Crack monitoring technique, number of sites and spacing

Blue: As-welded/As-machined mean in this context that the specimen was tested without any crack repair however, an artificial notch might be used to avoid multiple crack initiation and coalescence (this is specified in Groups 1-6). F means if the specimen failed or BF not failed whilst testing. SP shot peened applied. RR specimen was repaired and re-tested. FA fractured surface analysed (section 3.7.6). SC, EC, CC refer to how the crack initiated on the specimen: surface crack, edge crack, corner crack.

Additionally, table 3.4 provides: specimens dimensions, Thickness (T) and Width (W), nominal stress used for testing, accumulated fatigue life and the stress ratio (R).

Although, in many cases the name given to the specimens contains relevant information it can lead to confusions thus, *to avoid misinterpretations about particular characteristics of a specimen it is convenient <u>not</u> to rely on the specimen name but on the information provided in table 3.4, especially on the comments (blue column).*

GROUP 1

The finite element analysis identified that butt welded specimens (analysed as flat plates) have a more uniform distribution of stress in the groove as opposed to T-butts due to the absence of the stiffening provided by the vertical attachment. However, even on butt specimens cracks can initiate from the repair ends. Thus, to confirm the cracking pattern initiating at the repair ends, butt welded specimens LI2ASWB and LI3ASWB were tested for this purpose. These specimens are butt welded plates. The weld toes were machined R8D1 except in a centred 30 mm long region to force crack initiation to take place in the as-welded region, avoiding multiple initiation and coalescence. It was planned to remove the cracks by repairs and re-test the specimens. Dimensions and other experimental parameters are presented in table 3.4. Results will be presented in section 3.7.

GROUP 2

The finite element analysis identified that the stiffening effect of the vertical attachment was still present with 20 mm thick plates (cracking at the repair ends was first observed on specimens 30 mm thick). Additionally, there was the suspicion that crack initiation at the repair ends was enhanced by weld defects. Thus, the cracking pattern initiating at the repair ends was verified on non-welded specimens but machined. The specimens NOW1 and NOW3 were obtained by machining a plate into a T-butt shape. These specimens had simulated weld toes of radius 1.5 mm. These specimens were tested with a 10 mm long notch of approx. 1 mm deep made with a manual blade. The notch would force crack initiation to take place at the centre of the specimen avoiding multiple crack initiation. It was planned to remove the cracks using repairs and re-test the specimens. Dimensions and other experimental parameters are presented in table 3.4. Results will be presented in section 3.7.

GROUP 3

This group considers the first tested specimens. Specimens ASWEL001, SPE3R4D4 and SPE2R4D4 were T-butts fatigue cycled using various stress ranges throughout the test. The incremental stress range was applied to avoid very long fatigue tests due to the low stress ranges applied at the start of the test. Specimens SPE3R4D4 and SPE2R4D4 had centred repairs machined with disc cutters in as-welded condition and the weld toes were machined R4D0.5. The aim of this Group is to determine the fatigue life extension of repaired specimens

SPE3R4D4 and SPE2R4D4 versus the fatigue life of an as-welded specimen ASWEL001which was fatigue cycled until failure was reached without any crack repair made. Specimens SPE3R4D4 and SPE2R4D4 were planned to be repaired for a second time and re-tested. Although, SPE3R4D4 was shot peened no reliable data was collected to evaluate the effects of compressive residual stresses. Dimensions and other experimental parameters are presented in table 3.4. Results will be presented in section 3.7.

GROUP 4

In this group the effects of compressive residual stresses are studied. It was also considered convenient to verify that edge repaired (constant depth repair across the total width) specimens would show multiple crack initiation in the bottom of the repair as shown in the two dimensional finite element analysis. Specimens UPD4R2 and LPD4R2 were tested to verify that crack initiation takes place in the bottom of edge repairs and to analyse the effects of compressive residual stresses in the fatigue crack growth of repaired specimens. These specimens are T-butt welded plates, the repair profile was grooved using traditional cutting tools at UCL Engineering Workshop, specimen UPD4R2 was tested in as-welded condition, specimen LPD4R2 was tested after shot peening at MIC [3.7], dimensions and other experimental parameters are presented in table 3.4. Results will be explained in section 3.7 and in chapter 4, section 4.3.2.

GROUP 5

In this group only specimen MACHR4D4 is considered. Although, this specimen is not welded but machined it was not considered in Group 2 since it was repaired using an ROV arm. This specimen was fatigue re-tested after ROV burr grinding to verify the fatigue life extension. The simulated weld toes had a radius of 4 mm. Previous to ROV burr grinding the specimen had a centred repair R4D4L60 machined with a disc cutter in as-machined condition and after fatigue cycling, cracks initiated from the repair ends. Thus, the ROV burr grinding had the intention to remove such cracks. Dimensions and other experimental parameters are presented in table 3.4. Results will be presented in section 3.7.

GROUP 6

With the experience gained from the previous groups a comparison study was planned in this group considering four T-butt specimens TB300 series. The purpose was to quantify the fatigue life extension of repaired specimens against specimens in as-welded condition. Thus, specimens TB300001 and TB300002 represented the case of as-welded condition. These specimens had prior to testing the weld toes machined R4D0.5 except in a centred 30mm long region on one side of the specimen. This forced crack initiation at the centre of the specimen avoiding multiple initiation. The average measured weld toe radius of the as-welded region was 0.8 mm. The repaired condition was represented by specimens TB300003 and TB300004, they had machined repairs prior to testing of dimensions R4D6L60 and R4D9L60 respectively. Repairs were made with a disc cutter. The weld toes were left in as-welded condition and the average measured weld toe radius was 0.8 mm. Dimensions and other experimental parameters are presented in table 3.4. Results will be presented in section 3.7.

GROUP 7

In this group three electrochemically machined specimens have been considered, they are EM3R12D4, EM01R8D4 and ECM6R8D4. The aim is to quantify the fatigue life extension an crack initiation location when using ECM repairs and make a comparison with repairs made using disc cut machining. The specimen ECM6R8D4 had the weld toes machined R8D0.5 prior to testing and the other two were tested with weld toes in as-welded condition. Dimensions and other experimental parameters are presented in table 3.4. Results will be presented in section 3.7.

3.5.1 Test Stress Levels

For the first tested specimens a low stress range level was applied, thus specimens ASWEL001, SPE3R4D4 and SPE2R4D4 showed that the number of load cycles was extending further than $3.5X10^6$ without signs of cracking, see figure 3.10. The results obtained from these specimens are considered in the study Group 3 presented in section 3.5. The experience obtained experimentally from these three specimens lead to set the stress range levels for testing between 180 and 300 MPa with the exception of one fatigue cracked specimen which was repaired and tested at 157 MPa, see table 3.4. Since the determination of an S-N curve was not a concern the stress levels for fatigue testing were kept as high as possible to shorten testing time.

3.5.2 ACPD Data Analysis

Raw experimental crack growth evolution data in the form of voltages was collected by ACPD using the U-10 Microgauge controlled by the software routine. The data was saved on a spreadsheet after every scan and was processed according to the following procedure:

a) Determination of crack growth evolution along the crack path. A plot of number of cycles versus crack depth is obtained, see for example figure 3.11. Equation (3.4) is applied for crack depth calculations. Identification of the deepest crack section for subsequent data analysis is made.

b) Data smoothing for the deepest crack section by adjusting to each data point a second order polynomial expression. The polynomial expression for a particular data point is adjusted considering three data points before and after the particular data point. The procedure is repeated for each experimental data point except for the first three and the last three since less than three data points are before and after respectively. This procedure is known as the seven point incremental polynomial technique [3.8]. The experimental data obtained using ACPD has very low scatter thus, plotting number of cycles versus crack depth for the smoothed data and the experimental data on the same axes a superimposed graph is obtained.

c) Determination of crack growth rates. da/dN is determined by evaluating the first derivative of the second order polynomial expression for each data point. Plots of da/dN versus crack depth will be presented in chapter 4.

d) Determination of stress intensity range factors ΔK is obtained for each data point from Paris equation presented in chapter 1, since da/dN has been already determined. The parameters C and m in the Paris equation were set to C= $4.5X10^{-12}$ and m= 3.3 for da/dN in m/cycle and ΔK in MN $m^{-3/2}$. The C and m values correspond to the upper bound obtained from a least squares geometric regression from experimental results obtained for BS 4360 50D steel in a laboratory air environment [3.9]. Plots of ΔK versus crack depth are presented in chapter 4.

e) Determination of Y values. Y values take in account the geometric characteristics of the crack, component and type of loading. Y values for each data point can be determined from $Y= \Delta K /(\Delta\sigma \sqrt{a})$ since ΔK, $\Delta\sigma$ and a are known. Plots of Y versus crack depth are presented in chapter 4.

The computational work involved during the data process is extensive. Thus, a template spread sheet was designed to do the calculations. In some cases data collected during testing was invalidated since cracking not relevant to the case of study was obtained due to poor weld quality at the plate ends.

3.6 Fatigue Crack Repair

As was mentioned before, the first specimens tested did not have a fatigue crack prior to machining of the repair groove. The unexpected crack initiation out of the repair groove obtained on those specimens lead to a comprehensive finite element analysis and the position where crack initiation takes place on a repaired specimen was verified.

A complete definition of the geometrical parameters of the crack repair profiles used in the experimental work described in this chapter was made in chapter 2. The objective pursued during the design of the repair profile was to reduce the repair SCF to remove a given crack depth. During the experiments three repair radii of dimensions 4mm, 8mm and 12mm were used and from the amount of weld cut when using radius 12mm it is considered that in practice a review of the static load capacity of the member should be conducted prior to use of a cutting tool with radius equal or greater than 12mm.

The longitudinal repair profile of the grooves machined on the specimens was always semicircular and the transverse repair profile varied from semicircular to U-shaped depending on the depth/radius ratio, see chapter 2.

3.6.1 Electrochemical Machining

The ECM technique described in chapter 1 was used for machining repair profiles at the facilities of Edinburgh University. Repairs by ECM were only machined on manually welded uncracked specimens 30mm thick. Dimensions of the repair profiles machined are shown in table 3.4 and a typical ECM repair is shown in figure 3.12.

It is known that surface finish is a key factor in fatigue. Several variables during ECM affect the surface finish, the most important of those being: tool feed rate, current density, electrolyte composition, tool characteristics, workpiece characteristics and cutting gap. So, a complete control of the surface roughness and irregularities is extremely difficult. Therefore, comparisons of nominal repair dimensions and positioning accuracy versus nominal values were made using three ECM repaired specimens, as will be explained in section 3.6.3.

Weld quality was also identified as a factor that affects the repair surface. Some of the specimens repaired had welds with inclusions of considerable size. The tool had difficulties travelling through regions that contained inclusions, some tools even broke in the cutting process. To overcome this situation 20% N_aNO_3 was used as electrolyte to reduce feed rate but the surface quality obtained in specimens with weld inclusions was poor.

ECM is considered a more suitable technique than burr grinding to be deployed by an ROV arm. This is due to the lack of forces and vibrations involved during the application of ECM which make the technique more controllable by an ROV. On the contrary, as will be mentioned in section 3.6.5, the forces required during grinding are considerable. ECM also provides a sample of the material which among many other applications it can be used to verify that the crack has been completely removed, see figure 3.15.

3.6.2 Disc Cutter Machining

The use of ECM for the repair of fatigue cracked joints is a novel application of the technique. Thus, it was considered convenient to compare the ECM repaired profiles with profiles obtained using a machining technique that can be controlled with high precision. The technique considered for the comparison with ECM was cutting the repair profiles using disc blade cutters driven by a numerically controlled machine, figure 3.13 show disc cutters radii 4, 8 and 12mm used during the study. It is obvious that this technique could not possibly be applied to a real underwater repair of a fatigue crack, but repair profiles obtained using this technique could provide a good base line to evaluate ECM. The disc blade machining technique was used to make repairs on uncracked and cracked specimens. Dimensions of the repair profiles machined are shown in table 3.4 and a disc cut repair D4R8L60 is shown in figure 3.14.

The use of disc blade cutters driven by a numerically controlled machine provided the opportunity of obtaining optimum quality repair profiles since it was possible to have: precise positioning of the repair in the specimen, good quality surface repair and total control of the longitudinal and transverse repair profile dimensions. The numerically controlled machine used is at UCL Mechanical Engineering Workshop.

3.6.3 Dimensional Control of Machined Repairs

A dimensional study of three representative repair grooves electrochemically machined on T-butts was conducted to determine the achievable dimensional control during the machining of repair grooves for crack removal. At the same time three disc cut machined repairs were also dimensionally studied to compare the differences between the two manufacture methods with the nominal repair groove dimensions.

Initially it was considered to determine the surface roughness of the repairs however, the roughness of the repair grooves (ECM and disc cut) exceeded the roughness range of the instrument available. However, as will be demonstrated in section 3.7 the repair surface roughness was not relevant for the cases experimentally tested because the crack reinitiated on the parent plate surface weld toes outside of the repaired surface.

A vernier scale can only provide discrete measurements along the repair groove. Consequently, it was thought that a replica of the groove could provide more precise measurements when amplified using a shadow graph projector. Replicas of the six grooves studied were made and magnified plots of the deepest longitudinal section of the grooves were drawn using the shadow graph projector. Unfortunately, the continuous plots had to be transformed into discrete data to make the comparisons but these provided the opportunity to verify the consistency of the data by superimposing various plots from the same specimen.

Three parameters were considered during the dimensional study: repair depth, repair length and repair positioning on the specimen. Distortion from the semicircular shape was found to be nil for the disc machined grooves and in general was negligible for the electrochemically machined specimens when the cutting process was continuous. However, noticeable shape distortions were observed when the cutting process was altered by for example, problems with the electrolyte flow and welding inclusions. Figures 3.15 show the surface quality obtained when welding inclusions are found during the cutting process.

The deepest longitudinal sections of the three electrochemically machined repair grooves dimensionally studied are shown in figure 3.16, it can be observed that only one repair groove was found out of shape in a sample of three specimens. The disc machined repair grooves are shown in figure 3.17. Table 3.5 presents the differences of electrochemically machined repaired and disc machined grooves with respect to the nominal dimensions. It can be observed that the absolute largest differences encountered with respect to the nominal values were in the electrochemically machined specimens: 27.5% in repair depth, 15% in repair length and 0.9% in repair positioning.

All the electrochemically machined repair grooves dimensionally studied were nominally 4 mm deep and 60 mm long so, an absolute error in depth of 27.5% corresponds to +/- 1.1 mm. Although, it is always recommended to remove an extra 2mm in depth to consider inaccuracies during crack dimensioning, this allowance will have to be reviewed to also cover inaccuracies during electrochemical machining. The absolute repair positioning error 15% added to the absolute repair length error 0.9% is 15.9% and applied to 60 mm long corresponds to +/- 9.5 mm so, an extension of the repair length has to be considered to overcome this inaccuracy. This dimensional study was made in a late stage of the experimental work, thus the specimens used for the study were not tested with the exception of specimen LI2ASWB. The errors described above were obtained from a very limited study and a larger study is recommended to determine more reliable ECM performance data.

3.6.4 Compressive Residual Stresses for Fatigue Improvement

Within the scope of this research the application of compressive residual stresses to the repair surface was considered. These reduce the magnitude of tensile stresses on the repaired surfaces to improve the fatigue life of repaired connections.

As mentioned in chapter 1 when peening was discussed, various methods for inducing residual stresses are available but only a few of these are suitable for offshore underwater applications. Needle peening and hammer peening are among the recommended techniques for underwater application when compressive residual stresses are desired [3.10]. Due to the unavailability of needle peening and hammer peening equipment a very similar procedure, the shot peening technique was investigated.

Although, underwater shot peening for the improvement of fatigue crack resistance has not been used in practice it was considered convenient to include it in this study since other applications of shot blasting such as marine growth removal are currently in use in underwater conditions. Hence, adjustments to currently used techniques based on shot blasting suggest that shot peening in underwater conditions might be possible.

T-butt specimens were brought to the facilities of Metal Improvement Company, Inc (MIC) at Newbury, England where light peening was applied. The magnitude of the compressive residual stress was not determined. Instead, the magnitude of peening was quantified in terms of the permanent deformation that make the Almen strips sag, [3.11]. MIC personnel recommended that for optimum results the striking material should hit the surface perpendicularly and for narrow grooves, like the one in the specimen, the striking material would not hit the walls of the groove at 90^0 due to interference produced by the opposite wall when directing the nozzle to the target wall [3.12]. Fortunately, fatigue cracks do not generally start at the repair lateral walls and to induce compressive residual stresses on the surfaces where the crack is prone to start (bottom of the groove for long repairs and on the surface end of the groove for short repairs), the shot stream could be directed without any difficulty. However, it should be noted that problems may be encountered with peening of skewed joints.

To study the effects of compressive residual stresses in fatigue crack repaired connections, the study Group 4 was presented in section 3.5.

3.6.5 ROV Arm Burr Grinding

Repair of fatigue cracks of offshore structures in underwater conditions has been done traditionally by divers. However, for structures installed in deep waters risk is considerable for divers and costs of operations increase considerably so, the application of ROVs for deep water operations has become an option to overcome such problems.

Within the scope of the EDICS project [3.13], which partly supported this research work, the evaluation of various techniques for crack inspection and repair using ROVs was reviewed. An opportunity arose under the EDICS scope of work to repair two fatigue cracked specimens in underwater conditions. The repair trials were conducted at the premises of Slingsby Engineering Limited, in Yorkshire, England and the grinding tool was supplied by the French research institute IFREMER along with one grinding burr of 8 mm head radius.

The specimens repaired using the ROV arm from General Robotics Ltd. [3.14] were SPE7R8D4 and MACHR4D4, dimensions and stress levels to produce the cracks are presented in table 3.4. The specimens had already a fatigue crack repair groove from where new cracks had initiated. Previous to the trial a repair procedure for the complete removal of the cracks was prepared thus, crack location and dimensioning was conducted prior to the experiment.

It had been planned to re-test the specimens in fatigue after grinding for the determination of fatigue life extension. However, a constrained budget limited the time for the trial and the repair procedure was not completed. Additionally, no inspection operations were performed therefore, no verification of full crack removal after grinding was carried out. At the end of the one day trial it was not known whether or not complete removal of the cracks was achieved however, specimen MACHR4D4 was subjected to subsequent fatigue loading.

To study the fatigue life extension after ROV burr grinding specimen MACHR4D4, the study Group 5 was presented in section 3.5.

A complete description of the arm grinding trials is described in a report prepared by Larkum, Rodriguez and Rivas [3.15] and a resume is as follows:

Tests began on T-butt welded sample SPE7R8D4 submerged in the bottom of a small water tank. The arrangement is shown in figure 3.19. Test runs were conducted under automatic control of the arm moving across the plate in a straight line. The repair depth was increased gradually on each run by positioning the burr just sufficient to ensure contact with the plate. The first runs were conducted at a considerable distance from the weld toe at a travel speed of 1cm/s, typical speed used for inspection but it was found that the tool skipped somewhat on the surface rather than biting into the metal. Over the length of a run the ground path was distinctly curved and uneven. Further runs were conducted at the lower speed of 1mm/s and generally 1mm deeper each time. The quality of the cut improved dramatically being almost perfectly straight and consistent.

On completion of these preliminary grinding runs it became clear that the grinding burr had become damaged, with most of its cutting teeth broken on the end face. Unfortunately, it was not possible to acquire another burr and the decision was taken to continue with the trial using the damaged burr. The damage was probably caused by the high speed and high force with which the burr was made to contact the metal at the start of each run (estimated to be equivalent to about 10cm per second this is 25% of manipulator maximum speed).

A distinct bounce had been noticed in the manipulator arm during the approach to the start of each grinding run, partly due to the arm being at a position near its maximum reach. To alleviate this, the arm shoulder was extended towards the tank using the toolskid's telescopic boom and this gave a much more balanced arm configuration, see figure 3.20. This significantly improved the arm motion during the approach.

Once the optimum settings were identified a grind was conducted on SPE7R8D4 but along the weld toe to a point just past halfway along the weld. The run was made at 1mm/s and the results were good, with comparatively good surface finish considering the poor state of the grinding burr. A final run was conducted from the centre of the weld to the far end. The tool travelled slightly too deeply possibly due to the plate not being sufficiently level and started to bounce and spark, and came loose in its chuck. On completing the run the tool spindle was found to be pinched and damaged. Since there was no other tool available, the spindle was sawn down and refitted into the chuck for testing to continue. Figure 3.21 shows a slice of specimen SPE7R8D4 with cracks at the weld toes. The groove on the right was produced by disc cutting and that on the left the repair produced by grinding.

To conclude the trial the specimen MACHR4D4 was ground along the machined toe to a point just at the bottom of the previous groove (located at the centre of the specimen) and then to a point 20 mm before the far end. The results were still good, and comparable to those achieved in SPE7R8D4. The repair was generally straight with consistent depth and fairly good surface finish, see figure 3.7.

If a dedicated software for controlling the arm during grinding is developed it is envisaged that the quality of the results could be greatly improved. It has to be noted that during the trial the arm was attached to a skid resting on the floor. This is equivalent to an ideal docking situation with no wave forces acting on the arm. Controlling software must be able to compensate for the ROV movements amplified at the tool end of the arm.

3.7 Fatigue Test Results

The following sections present the results obtained during experimental testing the specimens that make the 6 Groups described in section 3.5.

3.7.1 Crack Growth Curves

Crack growth curves relate the number of cycles to crack depth. For surface cracks the crack growth at the deepest section is usually presented. In some cases for comparison purposes, the crack growth at the repair ends and in the bottom of the repair are presented together to illustrate how cracks develop in short repairs.

GROUP 1

This group is formed by specimens LI2ASWB and LI3ASWB. These specimens are butt welded plates tested in as-welded condition. An unmachined centred region of as-welded weld toe forced the initiation of surface cracks, otherwise multiple crack initiation would take place. Figure 3.23 shows the crack growth of both specimens among some other specimens, the legend in the figure provides stress level and specimen thickness. Although, the same stress level was used for testing both specimens, scatter in crack growth can be observed. Some data was lost starting the test of LI2ASWB so the curve is missing from a=0 to a=1. The aim of the test was to confirm that cracking can initiate from the repair ends even on butt welded specimens. Thus, specimen LI3ASWB was repaired using a centred repair R8D8L60 and then named LI3ASWB2, the weld toes were re-machined using an edge repair R8D0.5, for removing possible crack initiation places and avoid specimen failure from such places. Crack growth before and after repair is shown in figure 3.24, the legend in the figure provides stress level and specimen thickness.

The specimen LI3ASWB2 cracked at a repair end confirming the aim of Group 1. After repair a long crack initiation stage was obtained before cracking on the border of the weld cap and a repair end. This explains why the crack growth curve after repair starts from the specimen surface. However, embedded weld defects lead to subsurface crack initiation. The interpretation of the fractured surface was required to deduce the complicated cracking pattern observed, see figure 3.35, details are described in section 3.7.6.

A more detailed analysis of the fatigue life extension obtained is made in the discussion presented in section 3.9.

<u>GROUP 2</u>

This group contains the specimens NOW1 and NOW3. These specimens are T-butt machined plates with a simulated weld toe radius of 1.5 mm. A centred notch 10 mm long and approx. 1 mm deep was made with a blade in both specimens to force crack initiation at such places avoiding multiple initiation. Figure 3.23 shows the crack growth of both specimens among some other specimens, the legend in the figure provides stress level and specimen thickness. The crack growth curve for specimen NOW1 is shown before repair (0-3.5mm) and after (5.5-8.2mm). As in Group1, the same stress level was used for testing both specimens and a scatter in crack growth can be observed. The purpose of the test was to confirm that cracking can initiate from the repair ends without the enhancement of weld defects on T-butt plates with plates 20 mm thick. Thus, specimen NOW1 was repaired using a centred repair R4D4L60, specimen NOW1 becomes NOW12 after repair. In both specimens, in addition to the centred crack initiated at the artificial notch, multiple initiation was also found along the machined weld toe. Thus, for specimen NOW1 an edge repair R8D5.5 was required all across the specimen width to remove the multiple crack initiation. MPI inspection was used to verify that crack remains were not left. In the centre of the edge repair an additional repair R4D4L60 was also machined to continue with the aim of study in Group 2.

Specimen NOW12 was re-tested under an equivalent nominal stress of 300 MPa which correspond for the reduced section to 157 MPa. Figure 3.23 shows crack initiation from a=5.5, this crack growth curve corresponds to a crack that initiated at a repaired end of specimen NOW12 confirming the aim of the study in Group 2.

The specimen NOW3 was similarly repaired using an edge repair R8D3 and centred in the edge repair an additional R4D4L60 was machined. Then it was re-tested under 217 MPa nominal stress which is also equivalent to 300 MPa in the reduced section. To confirm the benefits of the practice of re-machining the weld toes before re-testing, the weld toe on the other side of the vertical plate was left unmachined. This is the weld toe where no artificial notch was made. The specimen failed on this side after 4.7×10^5 accumulated cycles but no cracks were found on the repaired side. This is why no crack growth is shown after repair in figure 3.23. This experiment although, out of the aim of Group 2 allowed to verify in one specimen that fatigue life can be extended by crack removal.

A more detailed analysis of the fatigue life extension obtained is made in the discussion presented in section 3.9.

GROUP 3

This group has the specimens ASWEL001, SPE3R4D4 and SPE2R4D4. These specimens are T-butt welded plates. Specimen ASWEL001 was tested in as-welded condition and cycled until it failed. Specimens SPE3R4D4 and SPE2R4D4 had centred repairs machined in as-welded condition and the weld toes were machined R4D0.5. Figure 3.10 shows the crack growth of these three specimens, the legend in the figure provides the specimens thickness and the various stress levels used with the accumulated fatigue life for each stress level. The purpose for testing these three specimens was to determine the fatigue life extension of repaired specimens SPE3R4D4 and SPE2R4D4 versus the fatigue life of as-welded specimen ASWEL001which was fatigue cycled without any repair until failure was reached.

Specimen SPE2R4D4 cracked at a repair end confirming the cracking pattern in short repairs. The crack was removed using R4D12L90 and the specimen was named S22R4D12. Although, MPI was used to verify that no crack remains were left after repair, the fatigue life extension obtained was negligible as it is shown from a=12 in figure 3.10. Thus, it was considered that the crack was not totally removed based on the crack growth obtained after repair. This consideration is based on the observation that the crack grew immediately after starting re-testing at the place where the deepest point of the original crack was found.

Specimen SPE3R4D4 also cracked at a repair end confirming again the cracking pattern of short repairs under bending. It was considered that more relevant data could be obtained from specimens of the other groups thus, to abbreviate testing time this specimen was not repaired nor re-tested

GROUP 4

This group is formed by specimens UPD4R2 and LPD4R2. These specimens are T-butt welded plates and both had an edge repair D4R2 (repair of constant section all across the specimen width) machined in as-welded condition. Specimen UPD4R2 was tested after repair and no subsequent repair was applied. Specimen LPD4R2 was shot peened after the repair was machined. Figure 3.18 shows the crack growth of these specimens, the legend in the figure provides the specimens thickness followed by the stress level in MPa used for testing. The purpose for testing these two specimens was to determine the benefit of compressive residual stresses induced by shot peening on the fatigue life of repaired specimens.

Both specimens were tested until failure and multiple cracking and coalescence was observed in the bottom of the edge repair. From the crack growth curves neither a direct comparison nor determination of the fatigue life extension due to compressive residual stresses is possible since, different nominal stress levels were used for testing. Analysis of compressive residual stresses by shot peening is made in chapter 4, section 4.3.2. Additional comments on fatigue life extension are made in the discussion in section 3.9.

GROUP 5

In this group only specimen MACHR4D4 is considered. This specimen is a machined T-butt with a weld toe radius of 4 mm. A centred repair R4D4L60 was machined on the specimen in as-machined conditions and fatigue cycling produced the characteristic repair ends cracking identified in short repairs. Figure 3.23 shows the crack growth of this specimen, the legend in the figure provides the stress level in MPa used for testing and the specimen thickness in mm. The aim of this group is to determine the fatigue life extension of a crack repair made by a ROV arm burr grinding procedure.

It was known after the ROV arm repair was made that crack remains were left. Thus, it was expected that the crack growth obtained from re-testing this specimen would show the same pattern observed re-testing specimen S22R4D12 of Group 3, see figure 3.10. Figure 3.29 shows the crack growth curves before and after the ROV arm repair, the legend in the figure provides the stress level in MPa used for testing and the specimen thickness in mm. Since the crack was not totally removed, a fatigue life extension was not obtained as in the case of specimen S22R4D12.

GROUP 6

This group is formed by four specimens TB300 series. This specimens are T-butt welded plates. Specimens TB300001 and TB300002 had prior to testing, the weld toes machined R4D0.5 except in a centred 30 mm long region on one side of the vertical attachment. Specimens TB300003 and TB300004 had prior to testing, disc cut machined repairs R4D6L60 and R4D9L60 respectively and the weld toes were left in as-welded condition on the repaired side of the attachment and machined R4D0.5 on the other side.

Figure 3.22 shows the crack growth curves for the four specimens TB3001-4, the legend in the figure provides the stress level in MPa used for testing and the specimen thickness in mm. It can be observed that the fatigue life increases as the nominal stress level is reduced. Repaired specimens TB300003 and TB300004 were tested under the same stress level but with a different repair depth therefore, the stress concentration produced by the repair was reflected in the fatigue life. Specimen TB300003 with shallower repair R4D6L60 showed a larger fatigue life than specimen TB300004 with deeper repair R4D9L60. The crack growth curve presented in figure 3.22 for the repaired specimens correspond to the crack initiation sites 30 for TB300004 and 130 for TB300003, which are located on the as-welded weld toes out of the repair groove at 20 mm from the repair ends, see figures 3.27 and 3.28.

Figures 3.25 and 3.26 show crack growth at the repair ends outside the repair groove (sites 30, 130) and in the bottom of the groove (site 80) for specimens TB300003 and TB300004 respectively. It can be observed that for both specimens crack growth initiated at sites 30 and 130 while at site 80 there is no initial crack growth. Figure 3.25 also shows that crack growth at site 80 only initiates after the crack at site 130 is approximately 5 mm deep, this is 1 mm before reaching the repair depth.

For specimen TB300003 crack initiation at site 80 starts after cracks initiated at sites 30 and 130 merge and continue growing as one crack, see crack growth evolution in figure 3.11. Unfortunately for specimen TB300004 it was not possible to determine crack growth in the repair groove region due to a high gain setting for the U10 crack Microgauge, causing voltage overflow. Analysis of fatigue life extension obtained is made in section 3.9.

GROUP 7

This group contains the ECM repaired specimens EM3R12D4, EM01R8D4 and ECM6R8D4. The only specimen that had the weld toes machined was ECM6R8D4 using a repair R8D0.5. This specimen developed surface cracks at the repair ends, confirming again this feature when using short repairs. However, this specimen was not successfully crack monitored during testing, thus a crack growth curve was not obtained. The other two specimens developed corner cracks initiated from weld defects located at the border of the specimens where the weld runs started. This situation invalidated the data collected. Although, it was not the aim of this group it was confirmed that weld toe improvement by machining can effectively remove weld defects producing a considerable improvement in the fatigue life of welded components.

3.7.2 Fatigue Crack Growth Rates

Crack growth rate is defined as the slope of a tangent line to a point on the crack growth curve and can be represented mathematically as da/dN. Graphs of da/dN versus a/T will be presented in chapter 4. In general, it was observed when reporting results of Group 6 that the crack growth rate is higher as stress level is increased, see figure 3.22.

The effect of the stress level on the crack growth rate can also be observed in figure 3.23 for butt specimens (LI2ASWB and LI3ASWB) and T-butts (NOW1, NOW3 and MACHR4D4).

Figures 3.25 and 3.26 show that crack growth rates are nil in the bottom of the repairs (sites 80) of specimens TB300003 and TB300004 for a considerable period. This is due to the effect of short repairs that force the cracking pattern in the repaired region to grow from the repair ends on the surface, extending first the repair longitudinally and then in depth. However, the crack growth rate cannot always be optimised as in the previous cases. For example, the crack growth rate is reduced after repair but it rapidly increased as was shown by specimen NOW1 in figure 3.23. For this particular specimen it has to be reminded that an equivalent stress lower than the original nominal stress was used for re-testing to consider the reduction in plate thickness across the with (edge repair). The stress equivalence is only valid during crack initiation and misrepresent the real stress distribution through the thickness during crack growth in a surface crack situation.

In the worst of the cases studied, the crack growth rate was not reduced at all after repair when the crack had not been removed entirely as described by the behaviour of specimens SPE2R4D4 in figure 3.10 and MACHR4D4 in figure 3.29.

3.7.3 Fatigue Crack Initiation

From the experimental results presented in figures 3.23, 3.25 and 3.26 it can be observed that for the purposes of life extension it is more effective if crack initiation after repair is located outside of the repair groove. This is because the new crack has again the total plate thickness for crack initiation and propagation. However, locating crack initiation outside the repair groove becomes increasingly less likely as the length of the repair increases. This will be addressed when explaining crack shape development in section 3.7.4.

Crack initiation life is usually considered the stage during which crack depth has not exceeded a certain value. Researching fatigue crack growth using the ACPD technique for crack depth monitoring revealed that Austin [3.16] measured crack depths from 0.05 mm deep. However, it is possible that a crack initiates between ACPD probe sites thus, the crack depth measured may not correspond to the precise place of initiation.

Figure 3.30 shows crack depth readings during crack initiation for specimen TB300003 on site 30 using spot welded probes with spacing of 10 mm. It can be observed that before 0.4 mm deep there is an average difference of +/- 0.05 mm between subsequent readings. When the ACPD array, see figure 3.7, which has spacing of 5mm was used the difference reduced considerably and consistent readings were obtained from 0.15 mm deep in specimen NOW3 as shown in figure 3.31.

Initiation life to total fatigue life ratios are not presented for all the specimens because not all the tests were continued to failure. Considering 0.4 mm as the crack depth for determining initiation life the initiation to total fatigue life ratios for the specimens series TB300 are presented in table 3.6. Figure 3.32 shows the trend of initiation to total fatigue life ratio for the specimens series TB300. It can be observed that although, specimens TB300003 and TB300004 were tested under the same stress level, the latter has a shorter initiation to total fatigue life ratio (Ni/Nt) as a result of the high stress concentration produced by a deeper repair (R4D9L60) with respect to specimen TB300003 (R4D6L60). Therefore, specimen TB300004 is outside the trend defined considering as-welded specimens and it can be inferred that its initiation life is less than an as-welded specimen under the same stress. However, it is worth noting that the weld toes of specimen TB300004 were in as-welded condition. Thus, it is expected that Ni/Nt would increase substantially if the weld toes are machined.

3.7.4 Crack Shape Development

The evolution of crack depth versus half crack length (a/c) is presented in this section. Determination of crack length and crack depth values were calculated graphically from crack depth contour plots (e.g. figure 3.11). Crack length was determined measuring the distance on the abscissa from the deepest crack section to the point where the crack contour plot approached the abscissa considering a difference of +/- 0.05 mm between subsequent readings observed during initiation.

In many cases a complete evolution until failure could not be obtained since either the specimens were not tested until failure or the spot welded probes only covered a short region of the specimen and the cracks extended outside the inspection area making it impossible to determine the total crack length. In the cases where the crack contour plot was short in length due to lack of probe sites and the trend was clearly defined, extrapolations were made manually until the plot approached the abscissa (+/- 0.4mm).

Crack shape evolution is presented in figure 3.33 where the code of each specimen corresponds to: aw for as-welded, mach for machined, R#D#L60 for the size of repair radius and repair depth used and the last numbers are the thickness in mm and one or more nominal stresses in MPa in the case the stress was increased during testing. In the same figure it is also presented the crack shape evolution of three T-butt specimens: AWC, SRE and AWE tested by Monahan [3.17] where each specimen is coded to give information about the heat treatment (AW for as-welded or SR for stress relieved), crack location (E for plate end or C for centre) and the nominal stress range in MPa.

In figure 3.33 it can be observed that Monahan's results show higher values of a/c as a consequence of a non uniform stress distribution along the specimen width. The stress was concentrated at the cracked section as a result of placing a short reaction roller under the specimen to avoid the development of edge cracks. It is also noticed that specimen ASWEL001 shows a characteristic drop in the crack shape development as a consequence of multiple initiation and coalescence enhanced by the uniform stress distribution along the width. With the exception of Monahan's specimens for the reason explained and specimens TB300004, TB300003 and MACHR4D4 after repair, little scatter is apparent in the crack shape evolution data for different tests in the range $0.01 < a/T < 0.28$. However, no consistency was found between the scatter and the nominal stress level.

Specimen MACHR4D4 after an incomplete crack removal shows high a/c values tending to decrease however, the specimen failed before a clear a/c decrease was observed.

The repaired specimens TB300003 and TB300004 show similar crack shape development as the initial a/c ratio falls to merge with the trend of the as-welded specimen TB300001. This is explained graphically in figures 3.27 and 3.28 which show that during early cracking the repair depth does not increase while cracks on the surface at both sides of the repair develop independently effectively increasing the c value without an increase in a (repair depth for this case). The a/c ratios of the repaired specimens merge with the as-welded trend when the cracks beside the repair have joined passing through the repair. At this stage the cracks beside the repair and the repair have become a single new crack, see figure 3.11. From the same figure it can be observed that the deepest point of the new crack lies approximately directly under the deepest section of the repair when failure is reached.

Scott and Thorpe [3.2] found that surface breaking fatigue cracks adopt preferred shapes as a function of fractional depth in both pure tension and bending. Initial cracks not of the preferred shape adjust towards it as crack growth proceeds. So, it can be deduced that in the case of a long repair groove with an initial a/c ratio less than that of the preferred shape, a crack would develop from the bottom of the groove to adjust with the preferred shape.

This situation was verified experimentally when T-butt specimens LPD4R2 and UPD4R2; which were both 30mm thick and 200mm wide with a groove D4R2 at the weld toe along the total specimen width were fatigue tested. It was found that an edge crack developed in the bottom of the groove. The initial a/c value is 4/100 = 0.04 and a/T value is 4/30 = 0.13 but it was not possible to determine an a/c evolution since the crack started almost simultaneously all along the specimen width in the bottom of the groove providing no information about the crack length development. However, locating a/c = 0.04 and a/T = 0.13 on figure 3.33 it can be observed that such values are close to the curve of specimen NOW3 which shows a trend to merge with the preferred crack shape of the as-welded specimen TB300001.

Finally, also shown on figure 3.33 is a curve representing a lower bound crack aspect ratio for tubular joints proposed by Dover et al [3.18] and described by the following equations:

$$a/c = a/T \qquad (3.8)$$
$$0 < a/T \leq 0.1$$

$$a/c = a/5T \qquad (3.9)$$
$$0.1 < a/T < 1.0$$

where

a/c crack aspect ratio (crack depth / crack length)

T plate thickness

The crack aspect ratios of the specimens tested in this work are generally close to the line described by equation (3.8).

3.7.5 S-N Data

An S-N diagram is a plot of alternating stress range versus cycles to failure. Since not all the tested specimens were cycled until failure, only the specimens that reached failure have been considered here.

From table 3.4 for the specimens coded with F (failure) a log-log plot of stress range in MPa versus cycles to failure can be produced and this is presented in figure 3.34. In the same figure a new basic design S-N curve for plates proposed for a new edition of the fatigue design guidance [3.19] is presented. Additionally, a mean line of fatigue performance of welded T-butt and cruciform joints in air with plate thickness in the range 20 to 30 mm is also shown. The mean line was obtained from a data base of experimental data used as a background to the new fatigue design guidance [3.20].

The design curve plotted is described by the equations:

$$\mathrm{Log}_{10}(N) = \mathrm{Log}_{10}(12.182) - 3\,\mathrm{Log}_{10}(S) \qquad N < 1\mathrm{x}10^{7} \text{ cycles} \tag{3.10}$$

$$\mathrm{Log}_{10}(N) = \mathrm{Log}_{10}(15.637) - 5\,\mathrm{Log}_{10}(S) \qquad N > 1\mathrm{x}10^{7} \text{ cycles} \tag{3.11}$$

where

N fatigue life in number of cycles

S stress range

The above curves are based upon a statistical analysis of experimental data which was taken to represent two standard deviations below the mean line. The design curve stress ranges in figure 3.34 were affected by a 1.34 multiplier which is a classification factor to account for the SCF associated with the local weld detail. It can be observed that four specimens lie below the design curve. However, the specimens UPD4R2 and LPD4R2 are very different compared with the rest since they have a constant depth repair groove across the width (edge repair) and their failure is not at the weld toe but in the bottom of the repair groove. An equivalent stress was calculated to locate them in the S-N plot since the edge repair makes the effective section thickness of 26 mm instead of 30 mm.

3.7.6 Fracture Surfaces

Examination of fracture surfaces was carried out on representative fatigue tested specimens to identify the characteristic patterns of failure found during the experiments. As explained before, only a region at the weld toe of each specimen had spot welded probes for ACPD crack monitoring or was covered by the ACPD array, therefore crack depth measurements are unavailable outside the inspection region. Final crack depth and length outside of the monitored region was estimated from examination of the fractured surfaces.

The basic patterns of failure found during testing were produced from cracks initiated as: surface cracks or corner cracks. Surface cracks in as-welded specimens under uniform stress coalesced and grew essentially as edge cracks. Surface cracks in some specimens were forced to initiate in a small region by leaving it as-welded and increasing the weld toe radius at both sides. In this case they grew as semi-elliptical cracks of low aspect ratio.

Fracture surfaces of edge cracks show an almost straight crack front until failure was reached. The deepest crack point was usually the place where the crack first initiated and then coalesced with others to form one crack front. Fracture surfaces of corner cracks show an inclined crack that varied from a total penetration through the thickness at one specimen end where the crack started to a partial penetration at the other end.

To complete a global description of the fracture surfaces found during fatigue testing three typical fractures will be described in detail to illustrate crack propagation from: repair with subsurface weld defects (specimen LI3ASWB), see figure 3.35, as-welded condition (specimen TB300001) see figure 3.36 and repaired condition (specimen TB300004) see figure 3.37.

As-welded specimen

Specimen:	TB300001 (see figure 3.36)
Test Description:	As-welded specimen cycled to failure.
Type of Joint:	T-butt weld, full penetration 45 ^{0}
Material:	BS 4360 50D
Plate width:	300mm
Thickness:	20 mm
Preparation:	In as-welded condition weld toes were ground R4D1 using a steel disc cutter driven by a numerically controlled machine except a 30 mm long region centred on one side of the

	specimen. Average weld toe radius of the remaining as-welded toe was 0.5 mm.
Loading:	4 Point Bending
Nominal stress:	300 MPa
R :	0.03
Crack Monitoring:	ACPD on 8 equally spaced spot welded sites at 10 mm. Reference distance = 10 mm. Site 40 was at the centre of the as-welded toe region.
Repair Dimensions:	No repair was made subsequent to fatigue testing.
Cracking History:	A crack developed from the as-welded toe and propagated towards both edges of the specimen. Test stopped due to large specimen deflections.

Post -Test Sectioning:

Crack initiated in the as-welded toe region and propagated almost symmetrically to both sides of the repair in a semielliptical shape until it reached the edges of the specimen. Broken ligaments on the top edge of the sectioned surface mark the direction of crack propagation however, the precise site where the crack initiated was not apparent.

ACPD crack monitoring shows that crack initiated at the centre of the as-welded toe region but crack growth was faster 20 mm away at the end of the test.

Repaired specimen

Specimen:	TB300004 (see figure 3.37)
Test Description:	Repair profile machined on as-welded specimen and cycled to failure.
Type of Joint:	T-butt weld, full penetration 45 ^{0}
Material:	BS 4360 50D

Plate width:	300mm
Thickness:	20 mm
Preparation:	Repair centred on the specimen in as-welded condition made by a steel disc cutter driven by a numerically controlled machine. Weld toes were ground R4D1 except 30 mm at both sides of the repair.
Loading:	4 Point Bending
Nominal stress:	200 MPa
R :	0.04
Crack Monitoring:	ACPD on 16 equally spaced spot welded sites at 10 mm. Reference distance = 10 mm. Site 80 at deepest section of the repair.
Repair Dimensions:	R4D9L60 repair was made from as-welded condition no subsequent repair was made.
Cracking History:	Cracks developed from the as-welded toes and propagated towards both edges of the specimen. Test stopped due to large specimen deflections.
Comments:	Since repair was made on as-welded condition this test specimen can be considered similar as a case of a specimen with a central surface crack totally removed and re-tested.

Post -Test Sectioning:

Crack initiated from the as-welded toes at both sides of the repair almost simultaneously, crack growth of both cracks was at a similar rate since the two crack fronts merged directly under the deepest point of the repair as can be seen by the discontinuity on the sectioned surface. Once both cracks merged the new crack propagated symmetrically at both sides of the repair in a semielliptical shape until it reached the edges of the specimen. Broken ligaments on the top edge of the sectioned surface mark the direction of crack propagation however, visually the precise site where the cracks initiated is not apparent.

ACPD crack monitoring shows that crack growth initiated at 20 mm and 10 mm from the ends of the repair respectively and that no other initiation sites developed. Crack acceleration was unchanged after the two cracks had merged.

Repaired specimen with subsurface weld defects

Specimen:	LI3ASWB (see figure 3.35)
Test Description:	Fatigue surface crack removed and specimen re-tested.
Type of Joint:	Butt weld, full penetration 45 ^{0}
Material:	BS 4360 50D
Plate width:	200mm
Thickness:	20 mm
Preparation:	Weld toes were ground R8D1 except 30 mm at the centre of one side of the weld. At the as-welded toe a small notch 1mm deep 16 mm long was made to force a crack to initiate at that site.
Loading:	4 Point Bending
Nominal stress:	180 MPa before and after repair
R :	0.07
Crack Monitoring:	ACPD on 8 spot welded sites. Same sites were used before and after repair.
Repair Dimensions:	R8D8L60 made by a steel disc cutter driven by a numerically controlled machine. After removing the crack weld toes were re-machined R8D0.5 to remove possible crack initiation regions.
Cracking History:	A crack developed from the machined notch. It was removed and the specimen re-tested. Long initiation life was obtained after repair and then crack initiation was observed from the repair side. Crack propagated towards one edge of

the specimen. Test stopped due to large specimen deflections.

Post -Test Sectioning:

A line of slag was found embedded in the weld when sectioning the specimen along the fracture. The slag line was located 5mm deep from the surface and ran along the specimen width. Although the lowest point of the repair was deeper than the slag line this was not seen on the repair surface since the slag line was located beside the repair almost in a tangent with the repair surface.

Broken ligaments in the slag line region which ran almost in a tangent with the repair surface reveal that two cracks developed: one above and other below the slag line . The crack below the slag line grew as an embedded flaw and did not break the surface. The crack above the slag line grew faster than the crack below due to the proximity with the stress concentration region produced by the repair surface. It is important to remember that the specimen was a butt weld and not a T-butt weld therefore, the stress concentration was located on the whole repair surface and not only at the surface ends of the repair.

It could be considered that the cracks below and above the slag line grew embedded maybe from the beginning of the test before the repair was made. However, other regions of the slag line do not show any sign of crack propagation therefore, this hypothesis can not be proved.

ACPD crack monitoring shows that the crack initiated in the region where the slag line was almost in a tangent with the repair surface confirming what was found on the sectioned surface. Additionally, crack growth data shows acceleration and deceleration that can be explained as the crack growing above the slag line and then below the slag line respectively.

3.8 Fatigue Life Extension of Crack Repaired Connections

In this section, an approximate determination of the fatigue life extension of crack repaired connections is proposed and observations for the convenience of implementing weld toe improvement by grinding before service are also made.

3.8.1 Approximate Determination of Fatigue Life Extension

It has been observed from the experimental results that fatigue life extension is only achieved when crack initiation is reinstalled by totally cutting out the crack. If the crack is not totally removed the fatigue life extension is negligible as shown by specimens SPE2R4D4 in figure 3.10 and MACHR4D4 in figure 3.29.

For the case when the crack is totally removed there are two possible cases of crack initiation after repair: a) initiation from the bottom of the repair and, b) initiation beside the repair ends outside the groove. The occurrence of one or the other depends on the repair shape as explained in section 3.7.4 but it can be simply established that case a) occurs in long repairs and case b) in short repairs. In both cases the crack follows a tendency to adjust to a preferred shape. It has also been observed from the experimental results that in case b), once the cracks at the repair ends have merged under the bottom of the repair, the new crack propagates at a high growth rate through the thickness, see figures 3.25.

From the behaviour presented above an approximate procedure to determine fatigue life extension after repair is proposed for the case when the crack has been totally removed and initiation occurs beside the repair ends outside of the groove. The procedure is as follows:

a) Choose a repair geometry using a combination of R, D and L that provides a SCF equal or less than the SCF in the as-welded condition. This is to assume that initiation life before and after repair would be approximately similar.
b) Consider that the life extension after repair is the same as the number of cycles to produce the initial crack. Since crack initiation would be similar and

knowing that once the cracks propagating from the repair ends have merged under the bottom of the repair, the remaining life is negligible, see figures 3.25.

A graphical description of the procedure is presented in figure 3.38. The procedure is basic but conservative since it is based on a real value of the fatigue life. It can not be assumed that is preferable to repair until cracks become deeper in order to extend fatigue life since, it is required to provide a repair with a SCF value at least equal to the as-welded SCF value. Thus, if D is large R has to increase to reduce the SCF but R is limited to a maximum value of 12mm or less in some cases since a substantial amount of weld is removed weakening the connection.

3.8.2 Weld Toe Improvement by Grinding

An additional fatigue life extension can be obtained reducing the SCF value at the weld toe. This can be achieved by controlled local machining or grinding to produce a smooth concave profile at the weld which blends smoothly with the parent material. An improvement of 2.2 on life using this procedure is proposed by the Health and Safety Executive (HSE) [3.21].

According to the HSE guidance during grinding weld toe defects should be removed, so grinding has to reach a depth of not less than 0.5 mm below the bottom of any visible undercut or defect. The maximum depth of local grinding should not exceed 2 mm or 5% of the plate thickness, whichever is less. An appropriate NDT technique should be used to ensure that no significant defects remain after grinding. The final ground surface should be protected against corrosion.

This weld toe improvement technique can be implemented while the crack is being repaired. Since it is easy to continue the machining process at both sides of the repair once the original surface has been reached, see figure 3.39. Quantification of the fatigue life improvement obtained with this technique was not made. However, fatigue life improvement was clearly observed when the technique was applied as a routine in all the specimens during the experimental work. A repair R4 or R8 with D0.5 along the total specimen width was made on the weld toes that did not have the crack repair. This was done to prevent cracking on the opposite side of the specimen and ensure that the fatigue life on the crack repaired side of the specimen was totally consumed, see figure 3.39.

3.9 Discussion

Calculations of the fatigue life extension obtained after crack repairing some of the experimentally tested specimens are presented here.

GROUP 1.

Before repair:

Specimen LI3ASWB (see figures 3.23 and 3.24 for reference)

for a=4, $N=1.1x10^6$

After repair:

Specimen LI3ASWB2 with repair R8D8L60 and weld toes machined R8D1

for a=4, $N=3.4x10^6$

Repair depth to plate thickness ratio: 100x(8/20)=40%

Fatigue life increment for a=4 is 3.4/1.1= 3.1

GROUP 2.

Before repair:

Specimen NOW1 (see figure 3.23 for reference)

for a=8, $N=2x10^5$ (approx. from extrapolation)

After repair:

Specimen NOW12 with repair R8D5.5+R4D4L60

for a=8, $N=4.1x10^5$

Repair depth to plate thickness ratio: 100x(9.5/20)=48%

Fatigue life increment for a=8 is 4.1/2= 2.0

Before repair:

Specimen NOW3 (see figure 3.23 for reference)

for a=3, $N=2.8x10^5$

After repair:

The specimen was repaired using R8D3 + R4D4L60

Specimen failed after $4.7x10^5$ accumulated cycles on the unrepaired side and no cracks were found on the repaired side.

Repair depth to plate thickness ratio: 100x(7/20)=35%

Fatigue life increment with no sign of cracking = 4.7/2.8 = 1.7

GROUP 6.

Calculation in this group will be based on the approximate cubic relation between stress ranges and fatigue life since different stress levels were used in as-welded and repaired conditions. For example, a prediction of fatigue life can be made for specimen TB300002 based on the fatigue life obtained from TB300001 as shown below.

For a=18 mm, see figure 3.22

Specimen	Stress range	$Nx10^5$
TB300001	300	1.5
TB300002	250	2.7 extrapolated

Applying the cubic relation described above, $(300/250)^3=1.73$. Thus, the estimated fatigue life for TB300002 at a=18 mm would be: $1.73x1.5x10^5=2.6x10^5$ which is very close to the extrapolated value obtained from figure 3.22.

For a=6 mm, see figure 3.22

Specimen	Stress range	$Nx10^5$
TB300001	300	0.8
TB300002	250	1.4

Applying the cubic relation, $(300/250)^3=1.73$. Thus, the estimated fatigue life for TB300002 at a=6 mm would be: $1.73x0.8x10^5=1.4x10^5$ which is the same value obtained from figure 3.22.

Using the cubic relation verified above, prediction of fatigue life extension after repair is presented for specimens TB300003 and TB300004.

For a repair depth D=6 mm, see figure 3.22.

Specimen	Stress range	$Nx10^5$
TB300001	300	0.8
TB300003	200	3.1

Applying the cubic relation, $(300/200)^3=3.38$. Thus, the estimated fatigue life for TB300003 at a=6 mm in as-welded condition would be: $3.38x0.8x10^5=2.7x10^5$ which is lower than the fatigue life obtained in the repaired condition, from figure 3.22.

Thus, after repair the fatigue life extension obtained would be (2.7+3.1)/2.7=2.1 times the as-welded fatigue life. The relation between repair depth and plate thickness is 100x(6/20)=30%

For a repair depth D=9 mm, see figure 3.22.

Specimen	Stress range	$Nx10^5$
TB300002	250	1.7
TB300004	200	2

Applying the cubic relation, $(250/200)^3=1.95$. Thus, the estimated fatigue life for TB300004 at a=9 mm in as-welded condition would be: $1.95x1.7x10^5=3.3x10^5$.

Thus, after repair the fatigue life extension obtained would be (3.3+2)/3.3=1.6 times the as-welded fatigue life. For this case the relation between repair depth and plate thickness is (9/20)x100=45%

It can be deduced from the limited results presented from Group 6 that a fatigue life extension after repair with as-welded weld toes equal to the fatigue in as-welded condition can only be obtained for repair depths up to 30% of the plate thickness. However, results from Groups 1 and 2 showed that machining the weld toes at the repair ends can still provide a fatigue life extension at least equal to the fatigue life in as-welded condition for repair depths up to 48% the plate thickness.

The results presented above are summarised in table 3.7. These results are based on limited experimental data, thus an extensive validation is recommended for its application in the industry.

GROUP 4.

The effect of compressive residual stresses by shot peening specimen LPD4R2 does not show a noticeable improvement in fatigue life. A rapid analysis of the S-N curve in figure 3.34 shows that if a line is drawn joining the data points corresponding to specimens UPD4R2 and LPD4R2, the line obtained is parallel to the Design Curve. However, if shot peening had made an improvement, the slope of the line would not be parallel to the Design Curve.

GROUP 5.

The ROV arm grinding trial and previous trials performed by IFREMER for the EDICS project are the very first crack repair trials carried out using an ROV arm and have demonstrated that grinding is recommended to be carried out under force control, otherwise tools can be damaged, increasing the time during repair due to tool replacement. Additionally, since during General Robotics Ltd and IFREMER trials, burrs have broken from the spindle it is maybe possible to consider the use of disc cutters since they are more robust tools to be driven by ROV arms.

Specimen MACHR4D4 was returned to UCL after ROV arm burr grinding. MPI inspection of the ground surface of the specimen did not reveal any crack trace but ACPD did detect a surface flaw. The reason is that the burr cutting teeth were not sharp thus, the texture left had the appearance of small scales of steel covering the surface making difficult to detect the crack by MPI, see figure 3.7.

GROUP 7.

Although, ECM was not deployed by an ROV when conducting the repairs presented in this chapter, it is considered that the technique is more suitable for deep water applications. This is due to the possibility of incorporating the ECM equipment in a self contained unit which can be deployed and positioned by the ROV arm where the repair is required. Thus, the ROV arm does not have to follow the repair contours since the ECM tool can be mounted on a cam. Electrolyte and electric current can be supplied from the surface using hoses and cables. For this alternative high precision is required to position the unit that contains the ECM equipment [3.13].

From the S-N data presented in figure 3.34, it can be observed that specimens EM3R12D4, EM01R8D4 and ECM6R8D4 are all above the Design Curve. Two of these specimens failed by corner cracking due to weld defects at the specimen ends. Thus for theses cases, the electrochemically machined repair did not produced a more severe notch than a weld defect that from visual inspection was not detectable. The third specimen showed surface cracks initiating at the repair ends, confirming again this feature when short repairs are used.

In the case where crack initiation is located at the repair ends outside the groove the surface quality of the repair groove is not especially important. This is because the crack has already initiated when the crack reaches the repair surface. Thus, the surface quality has no great influence on the crack propagation rate. Additionally, when crack initiates outside the repair groove, the fatigue life obtained is independent of the machining technique used to produce the repair groove. So, results obtained from disc cut repaired specimens can be considered valid for ECM repaired specimens.

From the crack shape evolution data in figure 3.33 it can be considered that if a 2 mm deep crack is detected when is in a plate 20 mm thick, a/T= 0.1. Considering the higher a/c ratio obtained in this experiments, a/c =0.1 thus 2c= 40 mm. Adding 2mm extra depth and 10 mm extra length considering for ECM, a total repair length of 50 mm is required. Corresponding repair shape parameters are: a/c = 4/25 = 0.16 and a/T = 4/20 = 0.2. The repair shape ratio forces crack initiation take place outside the repair groove, since a/c and a/T values from figure 3.33 locate a point above the trend found where behaviour of repaired specimens merge with crack initiation that takes place beside the repair ends.

Based on figure 3.33, it can be observed that for a given crack depth if the thickness of the cracked member is increased, the a/c ratio tends to decrease, thus the crack length increases and therefore, the repair length has to be increased as well.

3.10 Conclusions

The application of short repairs has experimentally demonstrated that the fatigue life of cracked welded connections can be extended by a factor of two in many cases. The successfulness of fatigue life extension using short repairs depends mainly on two considerations:

a) The crack is totally removed before it extends further than 30% of the plate thickness
b) The repair depth and length comply with a short repair profile to force crack initiation to take place at the repair ends

The experimental results obtained also showed that the application of short repairs in some cases can provide extensions of fatigue life larger than a factor of two. This is more likely to occur when the cracks are repaired in early stages of growth and the repair ends are machined to remove weld defects.

Machining the repair ends can be made easily by prolonging the cutting path of the same tool used to machine the short repair. For underwater conditions, this task appear especially suitable for the ECM technique.

In addition to the fatigue life extension, short repairs induce crack initiation outside the repair notch so, the total thickness for crack propagation is reinstated and easier access for inspection is provided. It has also been demonstrated that long repairs when compared with short repairs induce crack initiation in the bottom of the repair, thus fatigue life is expected to be shorted since thickness is consumed from the bottom. Long repairs might complicate inspection and subsequent repair operations. To produce a short repair the profile has to only remove the crack and the allowances. This situation leads to use a reliable inspection technique such as ACFM combined with MPI whist repairing.

ROV grind repair of fatigue cracked connections involves a considerable application of force thus, precise control of the trace is difficult and costly as time spent replacing broken burrs is probable. The ECM technique would be more suitable for ROV applications if it is incorporated as a self-contained unit to be deployed by the ROV.

3.11 References

[3.1] H.G.Morgan "The effect of section thickness on the fatigue performance of simple welded joints", *United Kingdom Atomic Energy Authority*, October 1983.

[3.2] Scott, P. M. and Thorpe, T. W., "A critical review of crack tip stress intensity factors for semi-elliptic cracks", *Fatigue of Engineering Materials and Structures*, Vol. 4, pp. 291-309, 1981.

[3.3] BS EN 10025:1993, "Hot rolled products in weldable fine grain structural steels", *British Standards Institution*, 1993. (This specification supersedes the BS 4360:1990)

[3.4] AWS, "Structural Welding Code Steel", *American Welding Society,* Thirteenth Edition, 1992.

[3.5] United Kingdom Offshore Steels Research Project-Phase I, *Final Report, OTH 88 282*, Prepared by the Safety and Reliability Directorate for the Department of Energy, 1988.

[3.6] Faulke, D.A., "PASCAL Programming Language, Test Control Routine", *University College London*, 1993.

[3.7] Metal Improvement Co. Inc., Navigation House, Hambridge Lane, Newbury, Berks RG14 5TU, UK., December 1996.

[3.8] ASTM E647-88, *Standard Test Method for Measurement of Fatigue Crack Growth Rates*, Appendix: Recommended Data Reduction Techniques, 1988.

[3.9] UKORSP, *United Kingdom Offshore Steels Research Project*, Final Report to the European Coal and Steel Community, 1979.

[3.10] T.R. Gurney, *Fatigue of Welded Structures*, Cambridge University Press, 1968, pp. 210.

[3.11] K. J. Marsh, *Shoot Peening: Techniques and Applications*, Engineering Materials Advisory Services Ltd., 1993

[3.12] K. Delderfield and M. Blackgrove, Private Communication, *Metal*

Improvement Co. Inc., Newbury, UK., December 1996.

[3.13] EDICS, "Evaluation of Diverless IRM for subsea Completions and deepsea Structures project", Cibernetix, Doris Engineering, General Robotics Ltd, IFREMER, Stolt Comex Seaway, Technical Software Consultants, University College London, *Final Technical Report*, UK September 1998.

[3.14] ARM, "Advanced Robotic Manipulator project", Mobil North Sea Ltd, Offshore Supplies Office, Slingsby Engineering Ltd, Technical Software Consultants Ltd, UK 1996.

[3.15] T. Larkum, E. Rodriguez and S. Rivas, "Trials on Grinding Weld Toes Using the ARM Manipulator System", *General Robotics Limited*, November 1998.

[3.16] J.A. Austin, "The role of corrosion fatigue crack growth mechanisms in predicting the fatigue life of offshore tubular joints", *PhD Thesis University College London*, 1994.

[3.17] Monahan, C. C., "Early Fatigue Crack Growth at Welds", *Computational Mechanics Publications*, Vol.26, Brebbia C.A. and Connor J.J Eds., 1995.

[3.18] W. D. Dover, X. Niu, A. Aaghaakouchak, R. Kare and D. Topp, "Fatigue Crack Growth in X Joints and Multi-brace Nodes", *Fatigue of Offshore Structures, Proceedings of a Conference held in London, UK*, 19th-20th September, 1988, Editors W. D. Dover and G. Glinka, EMAS.

[3.19] United Kingdom Department of Energy, *"Offshore Instalations: Guidance on Design and Construction"*, HMSO, 1984.

[3.20] United Kingdom Department of Energy, *"Background Notes to New Fatigue Design Guidance for Steel Welded Joints in Offshore Structures"*, HMSO, 1984.

[3.21] Health and Safety Executive, *"Offshore Installations: Guidance on design, construction and certification"*, Fourth edition, Amendment No.3, UK 1995.

Tables

C max.	Si	Mn max.	Nb max.	S max.	P max.	Supply condition
0.22	0.1/0.55	1.6	0.1	0.05	0.5	Normalized

Table 3.1. Chemical composition of steel BS EN 10025 Grade S355J2G4

Tensile Strength	Minimum Yield Strength for Thickness over 16mm	Minimum Charpy V-notch		
		Temperature	Energy min value	Thickness max
MPa	MPa	°C	Joules	mm
490/640	355	-20	27	40

Table 3.2. Mechanical properties of steel BS EN 10025 Grade S355J2G4

Specimen	Set	Stage 1			Stage 2		
		R-D	Shot Peening	Max Crack Depth(mm)	R-D	Shot Peening	Max Crack Depth(mm)
1		4-4					12
2		4-4	YES				12
3	1	4-4		7	4-9		12
4		4-4	YES	7	4-9	YES	12
5		8-4					12
6	2	8-4	YES				12
7		8-4		7	8-9		12
8		8-4	YES	7	8-9	YES	12
9		12-4					12
10	3	12-4	YES				12
11		12-4		7	12-9		12
12		12-4	YES	7	12-9	YES	12

Table 3.3. Proposed testing programme assuming crack initiation in the bottom of the repair

Specimen	Connection/ Manufacture	Dimensions T(mm)	W(mm)	Repair/ Procedure	Nominal Stress(MPa)	Life (million cycles)	R	Crack Monitoring	Comments	Line
TB300001	T-butt/A	20	300		300	0.195	0.03	ACPD-SW-8-10-10	AW, F,SC,FA	1
TB300002	T-butt/A	20	300		250	0.21	0.03	ACPD-SW-8-10-10	AW, BF,SC	2
TB300003	T-butt/A	20	300	R4D6L60/DC	200	0.384	0.04	ACPD-SW-16-10-10	F,SC	3
TB300004	T-butt/A	20	300	R4D9L60/DC	200	0.2525	0.04	ACPD-SW-16-10-10	F,SC,FA	4
NOW1	T-butt/M	20	200		300	0.18	0.04	ACPD-AR-6-5-5	AM, BF,EC	5
NOW12	T-butt/M	20	200	R4D4L60/DC	157	0.415	0.08	ACPD-AR-6-5-5	RR, BF,SC	6
NOW3	T-butt/M	20	200		300	0.28	0.04	ACPD-AR-6-5-5	AM, BF,SC	7
LI2ASWB	Butt/MW	20	200		180	0.81	0.07	ACPD-SW-8-10-10	AW,BF,SC	8
LI3ASWB	Butt/MW	20	200		180	1.08	0.07	ACPD-SW-8-10-10	AW,BF,SC	9
LI3ASWB2	Butt/MW	20	200	R8D8L60/DC	180	3.975	0.07	ACPD-SW-8-10-20	RR, F,SC,FA	10
MACHR4D4	T-butt/M	30	200	R4D4L60/DC	228	0.98	0.03	ACPD-SW-8-10-15	BF,SC	11
MACHR4D4	T-butt/M	27	200	R8D0-4L200/BG	228	1.045	0.03	ACPD-SW-16-10-10	RR,F,SC	12
SPE2R4D4	T-butt/MW	30	200	R4D4L60/DC	229/300	3.7/3.99	0.01	ACPD-SW-8-10-13	BF,SC	13
S22R4D12	T-butt/MW	30	200	R4D12L90/DC	300	4.062	0.01	ACPD-SW-8-10-13	RR, BF,SC	14
SPE3R4D4	T-butt/MW	30	200	R4D4L60/DC	108/122/228	4.21/4.94/5.29	0.03	ACPD-SW-8-10-10	SP,BF,SC	15
ASWEL001	T-butt/MW	30	200		133/161/179	3.6/4.8/5.1	0.2	ACPD-SW-8-10-10	AW,F,SC	16
UPD4R2	T-butt/MW	30	200	R2D4/DC	82	0.25	0.1	ACPD-SW-8-10-10	SP,F,EC	17
LPD4R2	T-butt/MW	30	200	R2D4/DC	112	0.125	0.1	ACPD-SW-8-10-10	SP,F,EC	18

Table 3.4. Fatigue tested specimens and relevant experimental parameters

Specimen	Connection/ Manufacture	Dimensions T(mm)	W(mm)	Repair/ Procedure	Nominal Stress(MPa)	Life (million cycles)	R	Crack Monitoring	Comments	Line
SPE4R4D4	T-butt/MW	30	200	D4R4L60/DC	228	0.98	0.03	ACPD-SW-16-10-15	SP,F,CC	19
EM3R12D4	T-butt/MW	30	200	D4R12L60/ECM	228	0.44	0.03	ACPD-AR-6-5-5	F,CC	20
EM01R8D4	T-butt/MW	30	200	D4R8L60/ECM	228	0.66	0.03	ACPD-AR-6-5-5	F,CC	21
SPE6R8D4	T-butt/MW	30	200	D4R8L60/DC	246	0.7	0.03		F,CC	22
SPE9R12D4	T-butt/MW	30	200	D4R12L60/DC	229	0.75	0.03		F,CC	23
SPE8D4R8	T-butt/MW	30	200	D4R8L60/DC	300	1.07	0.02	ACPD-AR-6-5-5	F,SC	24
ECM6R8D4	T-butt/MW	30	200	D4R8L60/ECM	300	0.85	0.02		F,SC	25

A=Automatic welding
M=Machined made
MW=Manually welded

DC=Disc cutter
ECM=Electrochemical Machining
BG=Arm Burr Grinded

SW- - - =Spot welding-No of sites-Spacing-Reference gap
AR- - - =Array probe-No of sites-Spacing-Reference gap
ACPD=Alternating Current Potential Difference

AW=As-welded tested
AM=As-machined tested
F=Specimen failed
BF=Test stopped before failure
RR=Repaired and retested
SP=Shot Peened
SC=Surface Crack
EC=Edge Crack
CC=Corner Crack
FA=Fracture surface analysed

Table 3.4. Fatigue tested specimens and relevant experimental parameters (cont.)

Specimen	Cutting Method	Differences in % Nominal vs. Measured		
		Repair Depth	Repair Length	Repair Positioning
ECM5(R4D4L60)	ECM	27.5	15.0	-0.4
ECM4(R4D4L60)	ECM	-25.0	-7.8	0.9
ECM2(R12D4L60)	ECM	8.7	-3.7	0.5
D4R8	DISC CUTTER	-1.3	-2.5	0.4
D6R4	DISC CUTTER	9.2	3.0	-0.1
LI2ASWB(R8D8L60)	DISC CUTTER	0.6	-0.7	-0.2

Table 3.5. Dimensional differences of three ECM and disc cut machined repairs

Specimen	Nominal Stress MPa	Fatigue Initiation Life (Ni)	Total Fatigue Life (Nt)	Ni/Nt
TB300001(As-welded)	300	22800	150000	0.15
*TB300002(As-welded)	250	60000	300000	0.20
TB300003(R4D6L60)	200	112000	383700	0.29
TB300004(R4D9L60)	200	50000	260000	0.19

*Extrapolated Total Fatigue Life

Table 3.6. Fatigue initiation life to total fatigue life ratios for specimens series TB300

Specimen	Repair Profile	Weld Toes	Nom. Stress (MPa)	Repair Depth-Thickness Ratio	Crack Depth after Repair(mm)	Fatigue Life Increment
LI3ASWB2	R8D8L60	R8D1	180	40%	4	3.1
NOW12	R4D4L60	R8D5.5	300	48%	8	2
NOW3	R4D4L60	R8D3	300	35%	0	1.7
TB300003	R4D6L60	As-welded	200	30%	6	2.1
TB300004	R4D9L60	As-welded	200	45%	9	1.6

Table 3.7. Fatigue life extension of crack repaired specimens

Figures

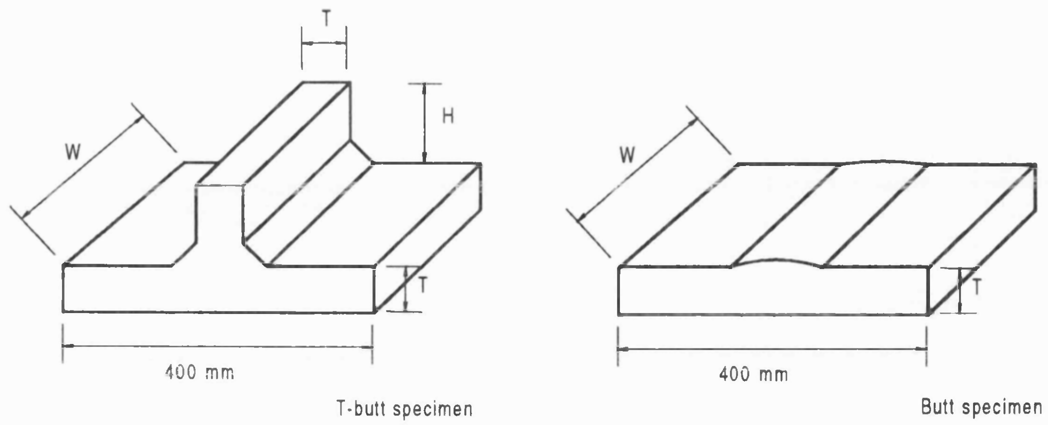

Manufacture	T	W	H
T-butts			
Automatic Welding	20	300	20
Machined	20	200	10
Machined	30	200	55
Manual Welding	30	200	55
Manual Welding	20	200	55
Butts			
Manual Welding	20	200	

Figure 3.1 T-butt and Butt specimens dimensions

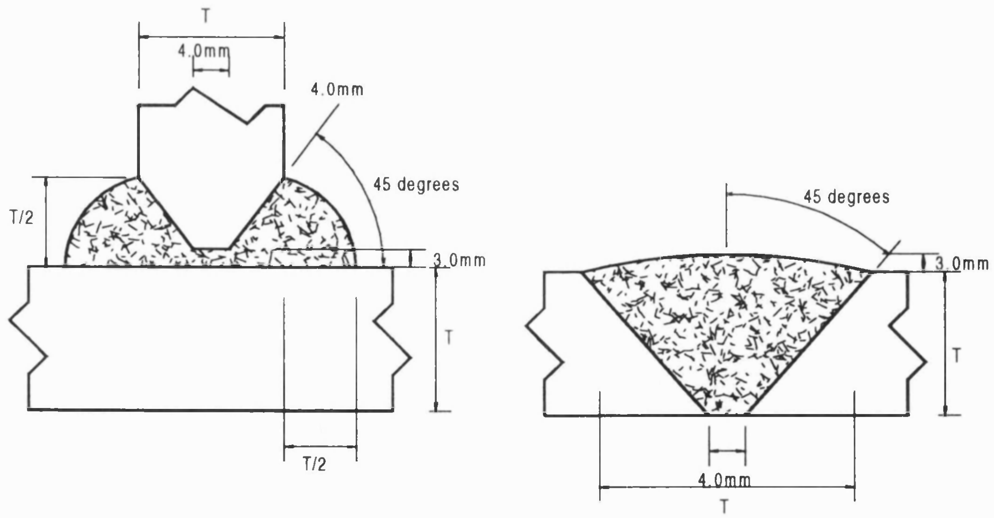

Figure 3.2 Weld dimensions

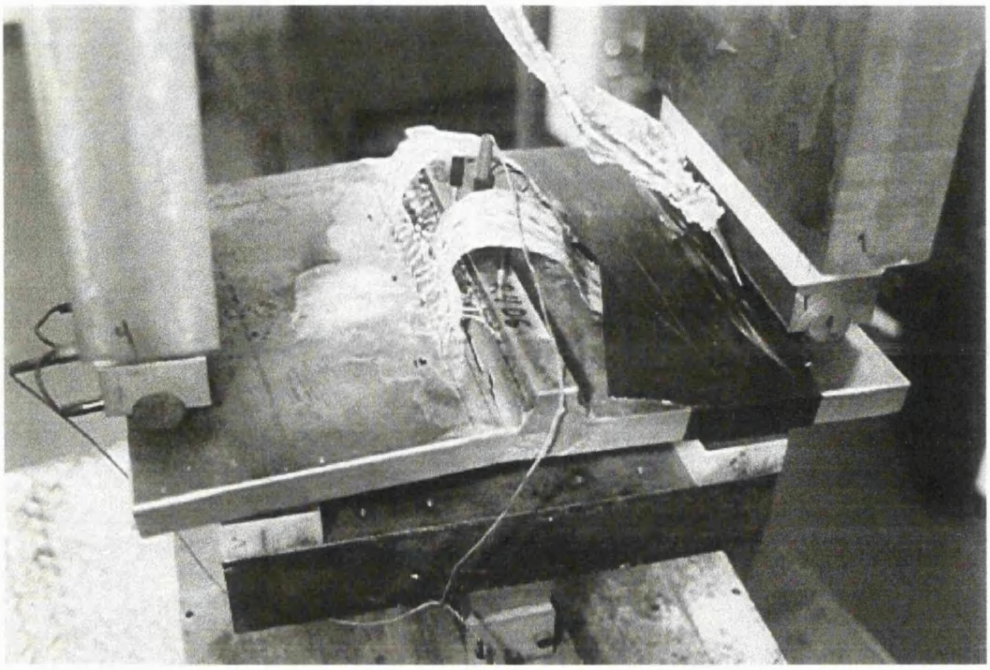

Figure 3.3 Loading set-up and spot welded T-butt specimen after failure

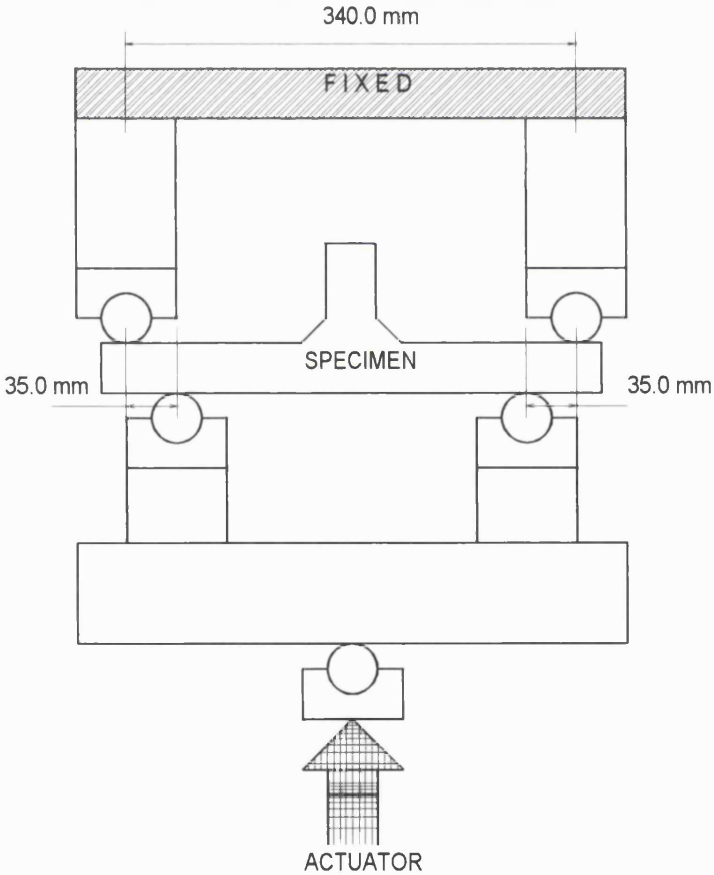

Figure 3.4 Loading set-up dimensions

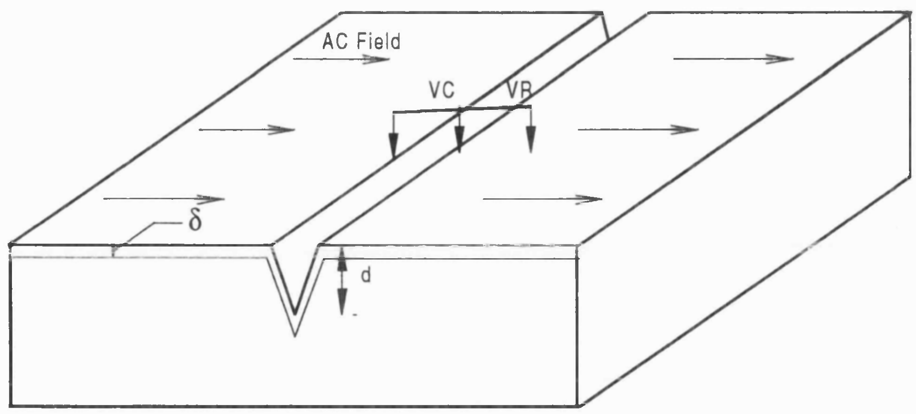

Figure 3.5 One dimensional crack depth measurement with ACPD

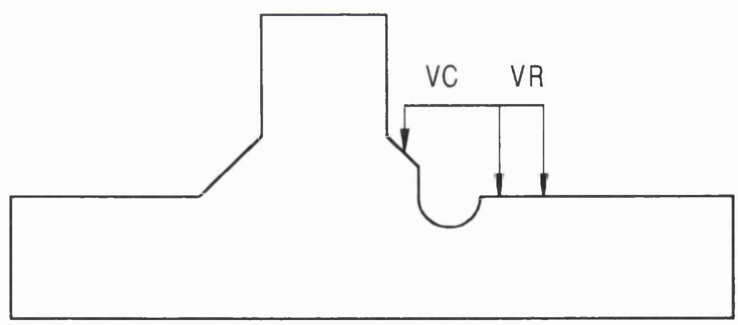

Figure 3.6 Spot welding on a repaired specimen

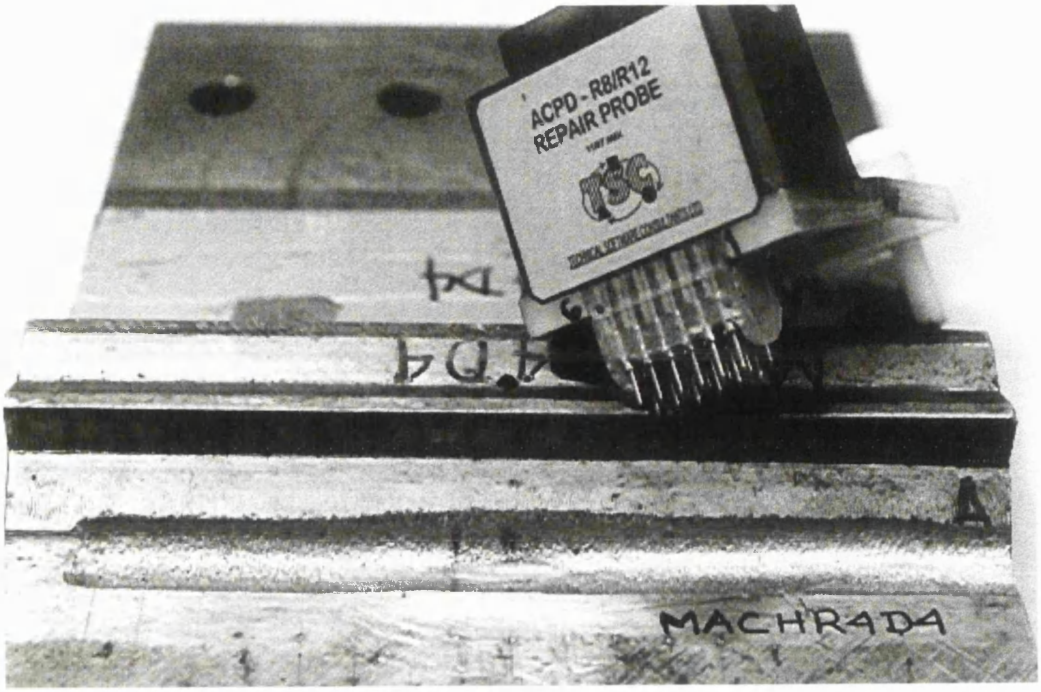

Figure 3.7 TSC ACPD Array and ROV arm ground specimen MACHR4D4

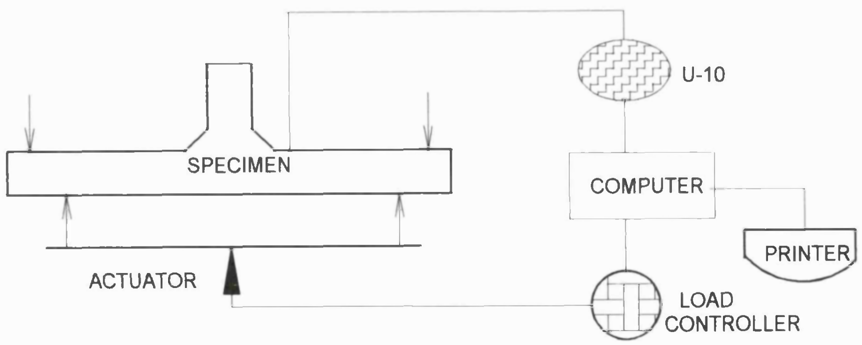

Figure 3.8 Testing system

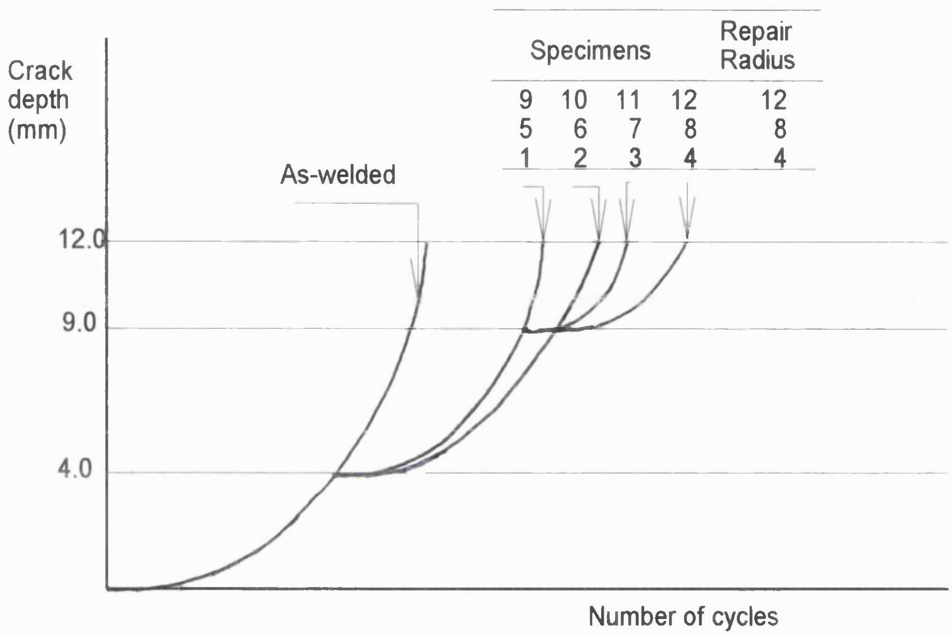

Figure 3.9 Experimental expected fatigue crack growth curves for proposed testing programme (see table 3.3)

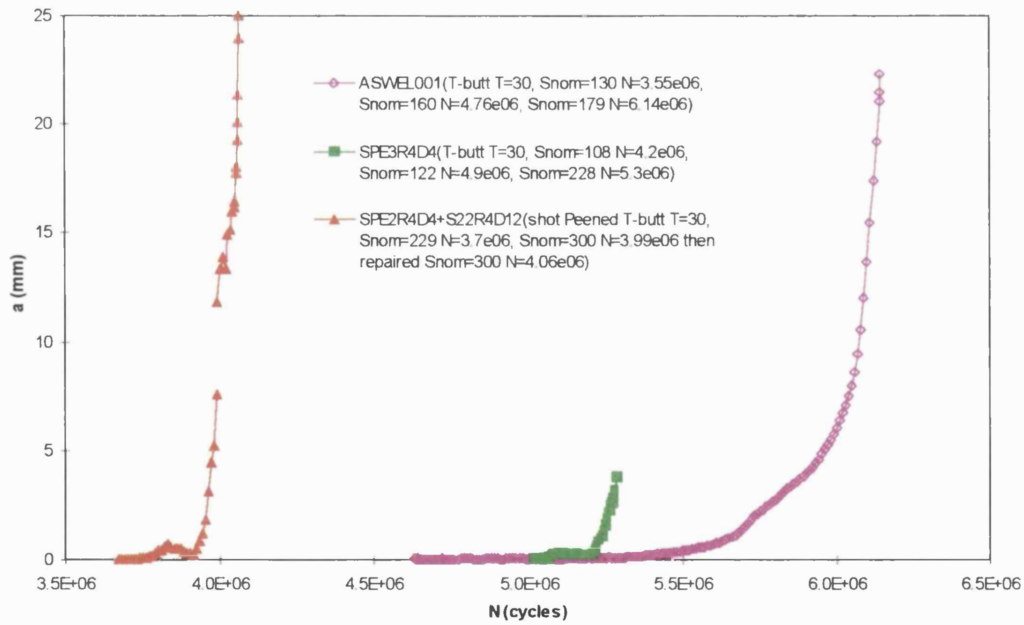

Figure 3.10 Fatigue crack growth increasing stress range for T-butt specimens

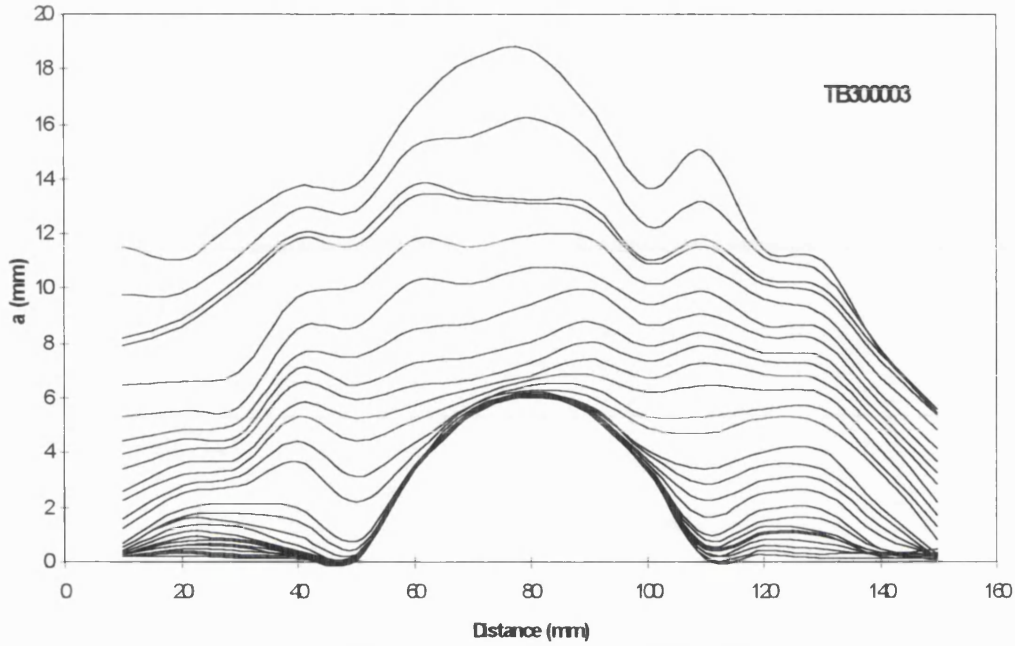

Figure 3.11 Fatigue crack growth evolution for repaired specimen TB300003

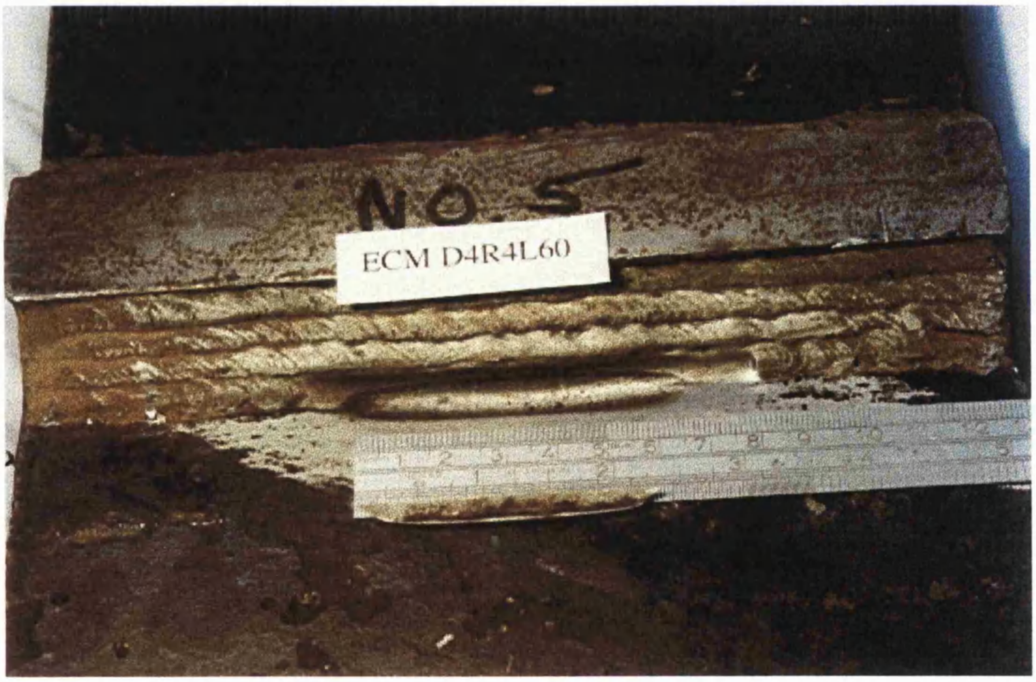

Figure 3.12 ECM repair profile D4R4L60 on ECM5 specimen

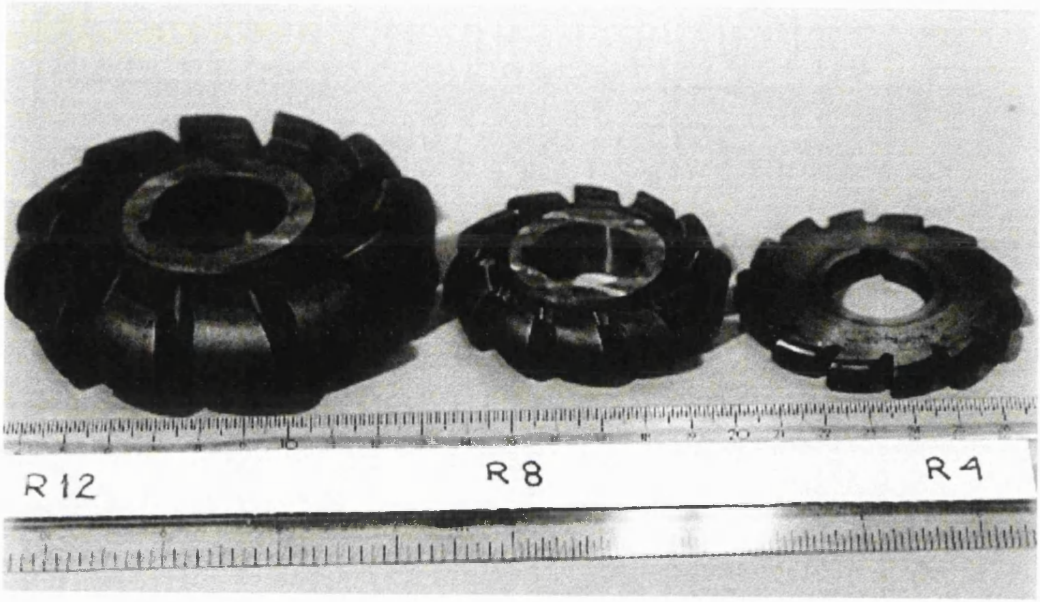

Figure 3.13 Disc cutters used for machining repair profiles

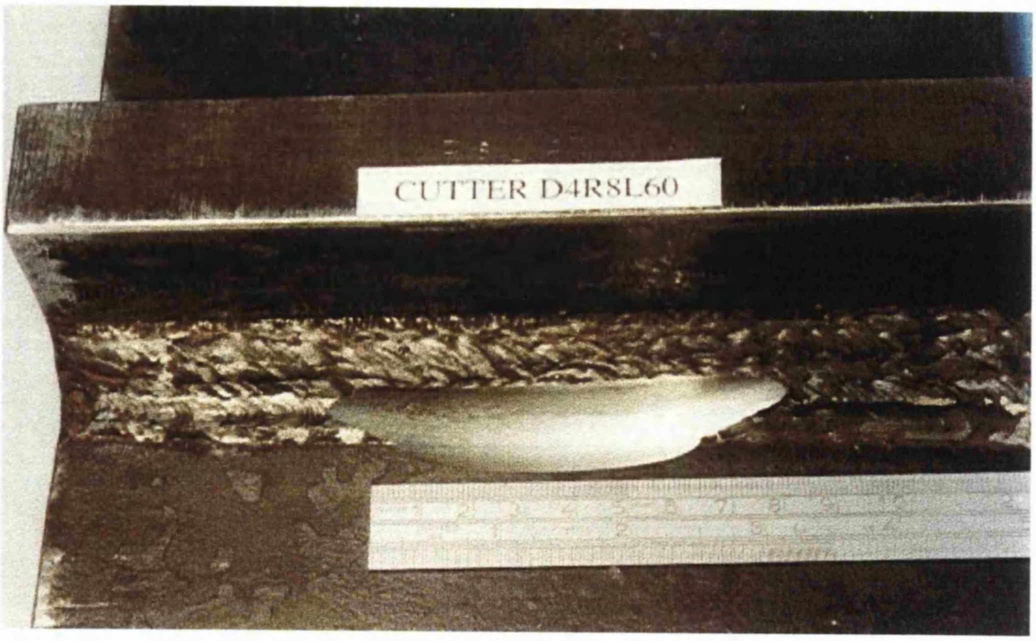

Figure 3.14 Disc cut repair profile R9D4L60 on T-butt specimen

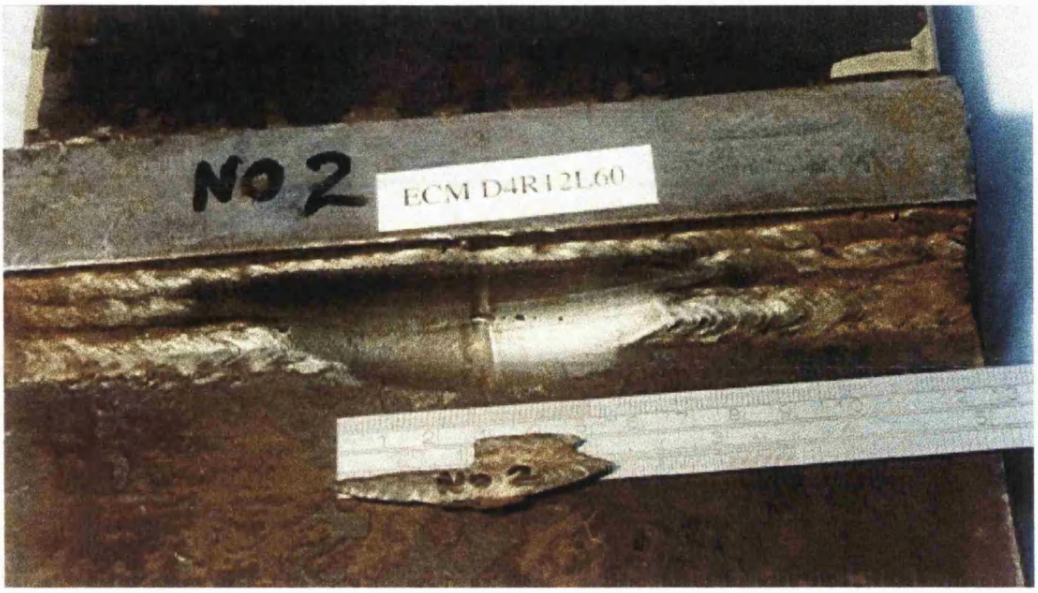

Figure 3.15 SpecimenECM2 showing poor repair surface quality due to welding inclusions found during ECM cutting

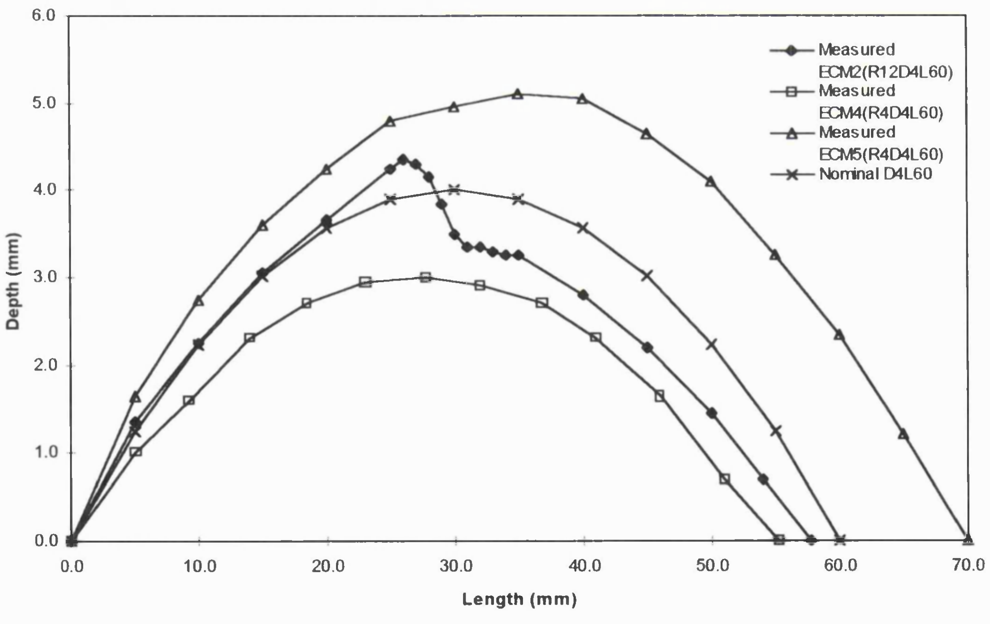

Figure 3.16 Depth and length differences of three ECM repairs

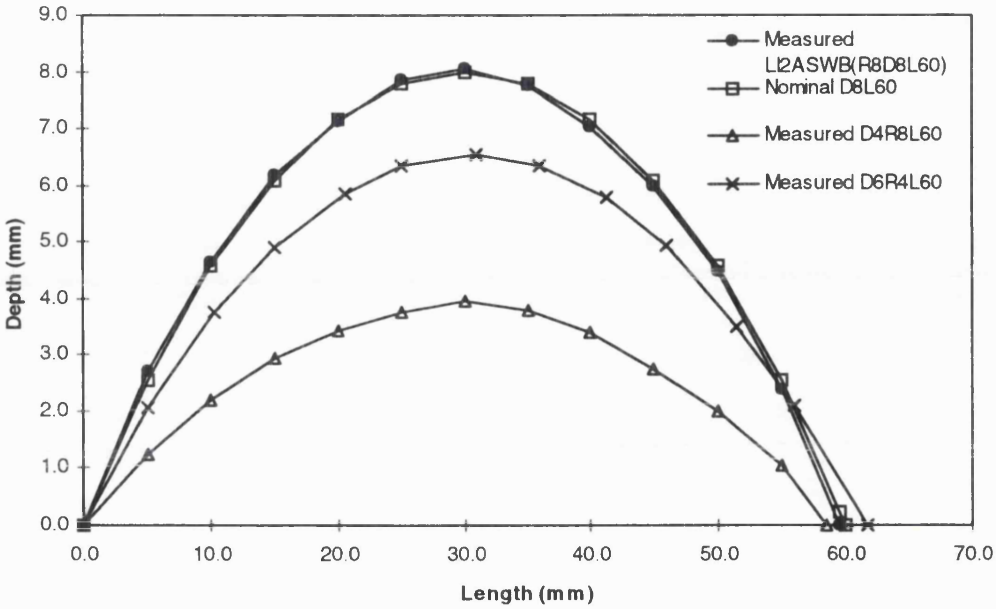

Figure 3.17 Depth and length differences of three disc cut repairs

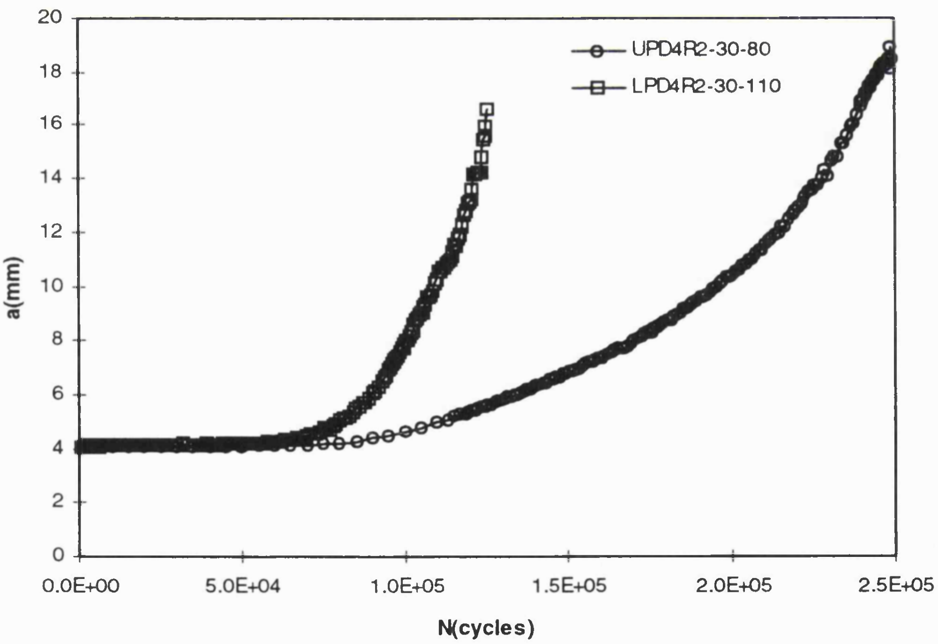

Figure 3.18 Crack growth of edge repaired specimens

Figure 3.19 Arm, grinder and tank during repair trials

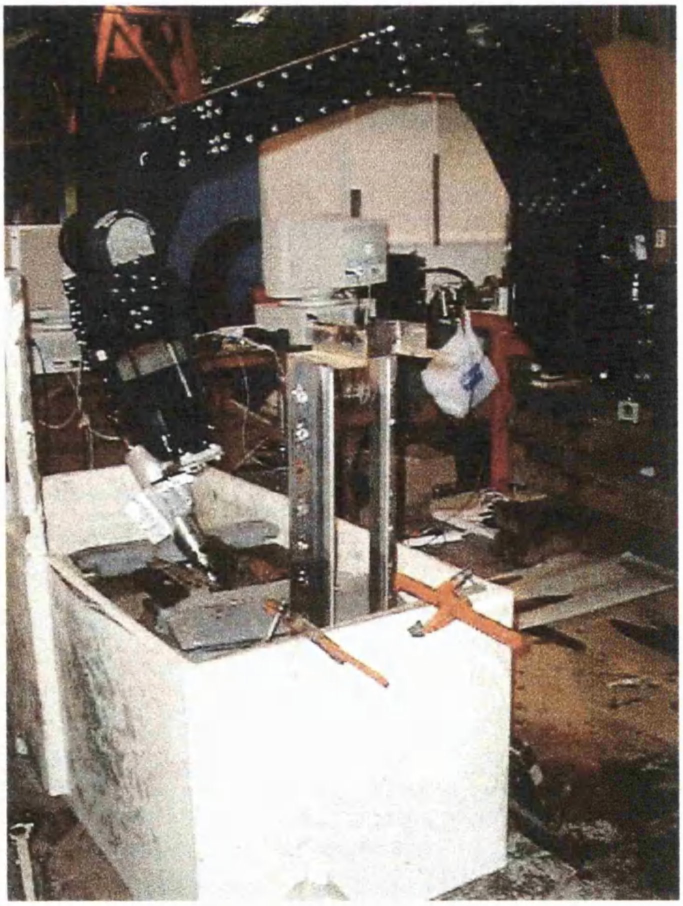

Figure 3.20 Arm configuration during repair trials

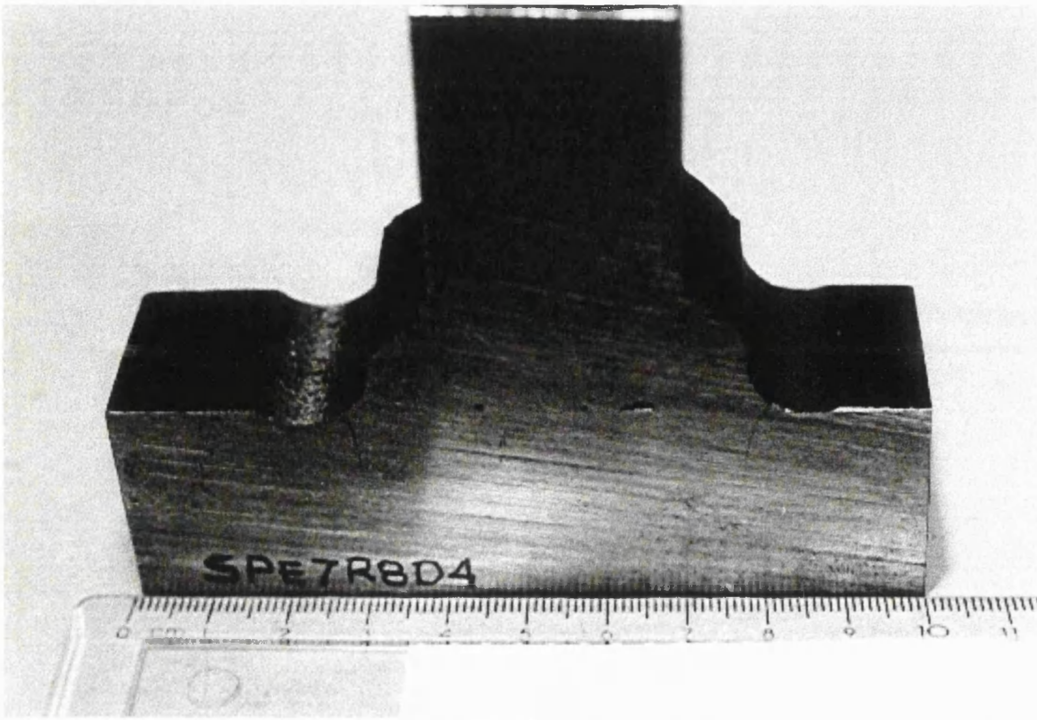

Figure 3.21 Slice of specimen SPE7R8D4 with cracks at the weld toes. On the right, surface produced by disc cutting. On the left, surface produced by ROV arm grinding

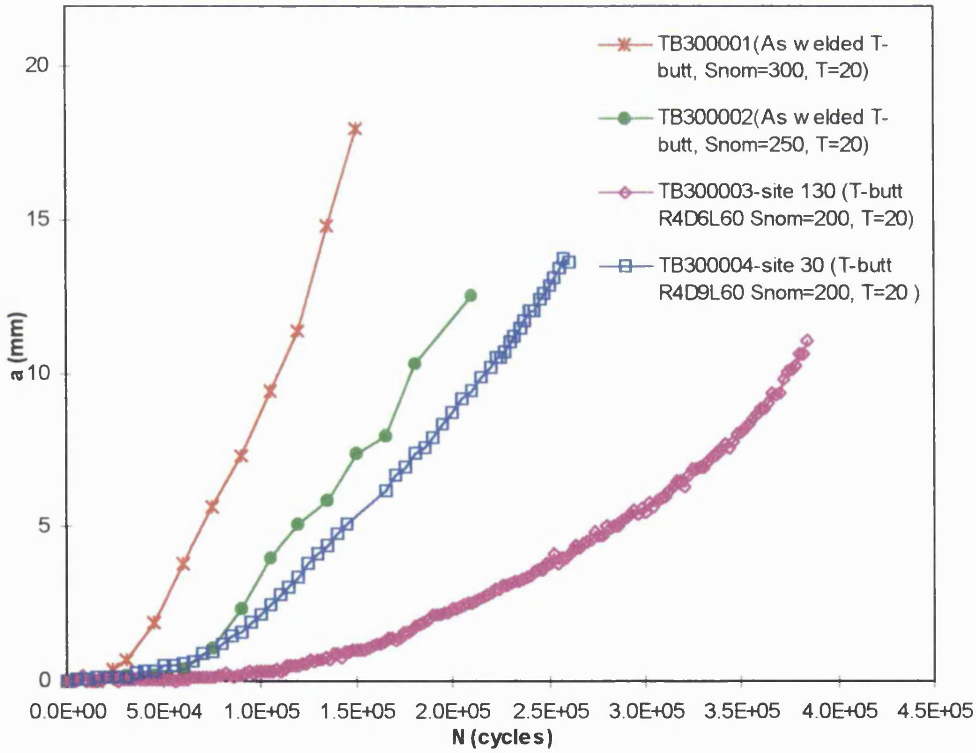

Figure 3.22. Fatigue crack growth for T-butt specimens series TB300

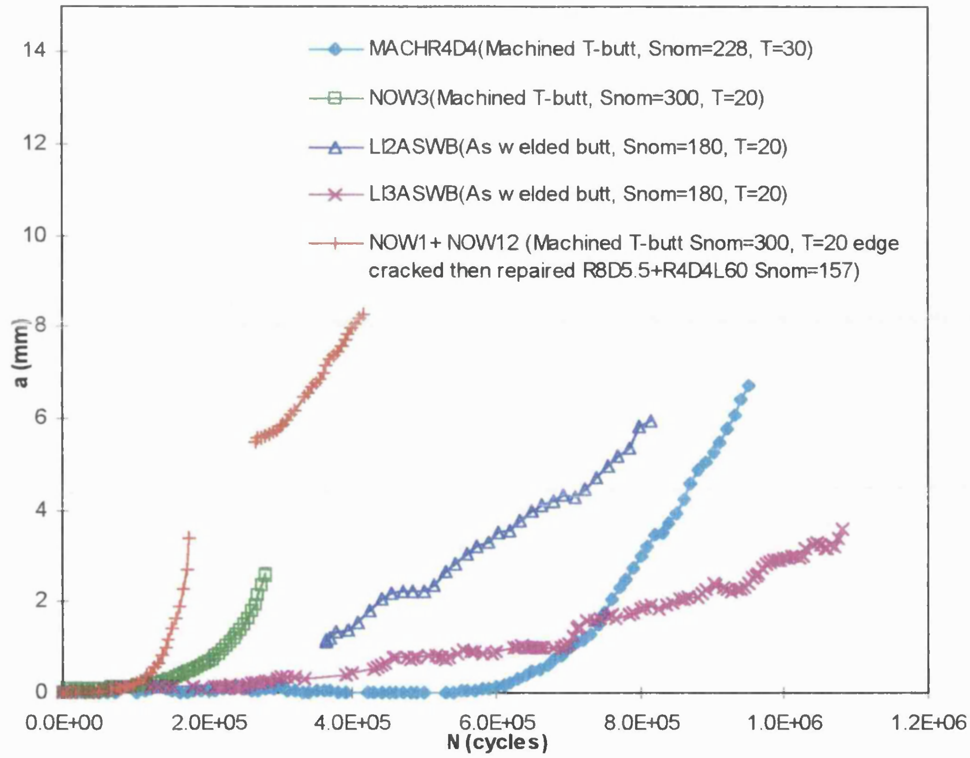

Figure 3.23 Fatigue crack growth for T-butt and butt specimens

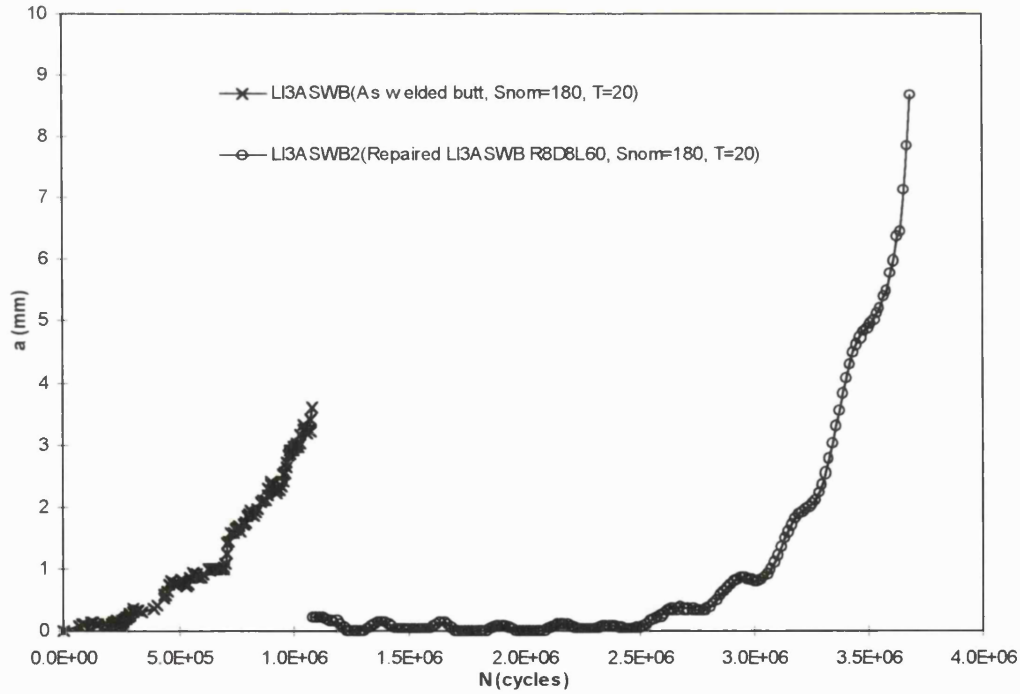

Figure 3.24 Fatigue crack growth for butt specimen LI3ASWB

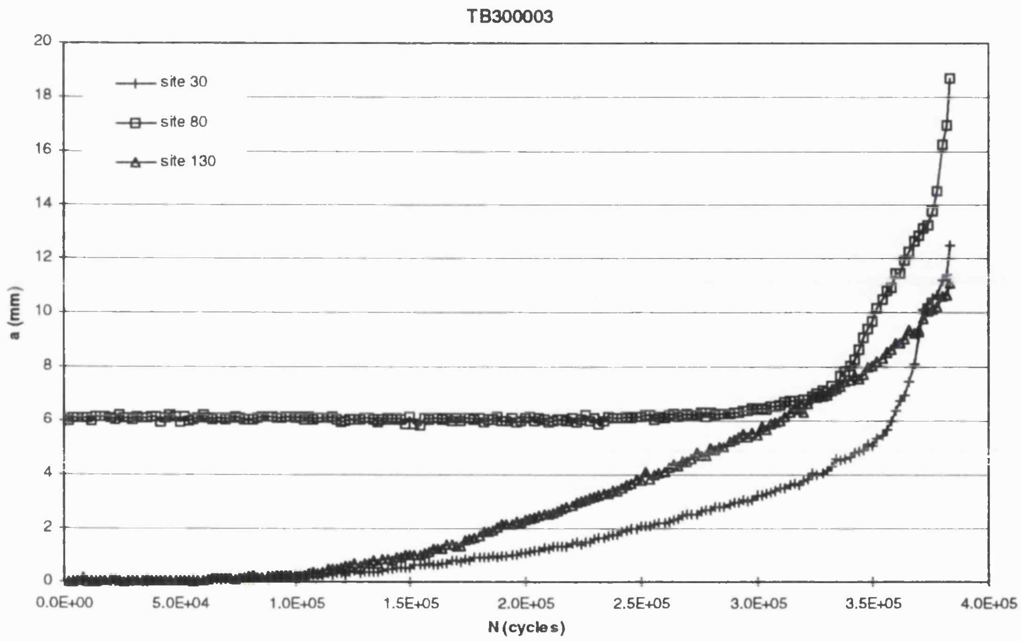

Figure 3.25 Fatigue crack growth at various sites for specimen TB300003

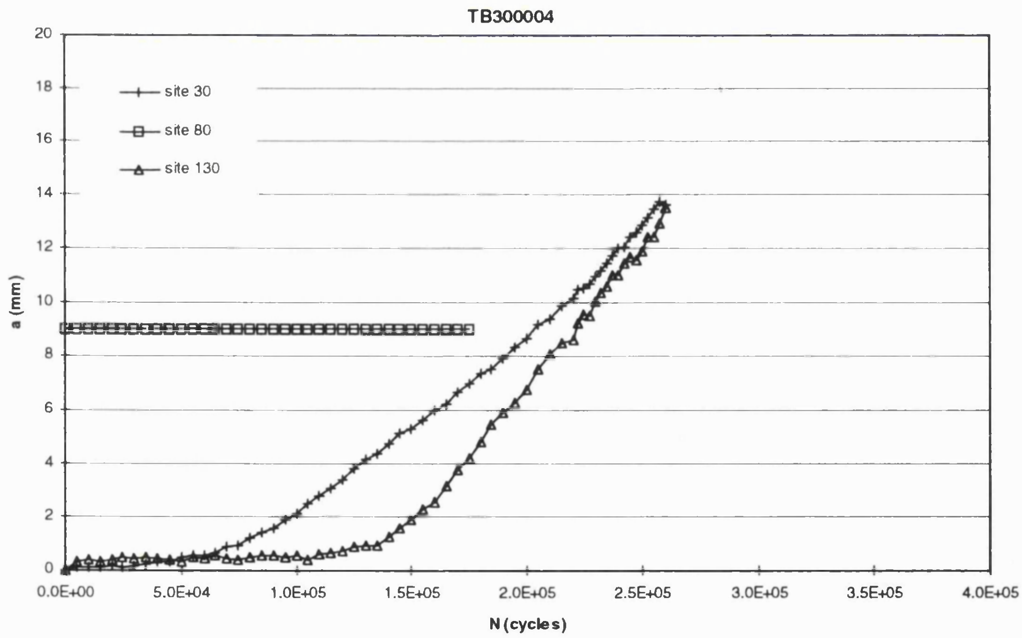

Figure 3.26 Fatigue crack growth at various sites for specimen TB300004

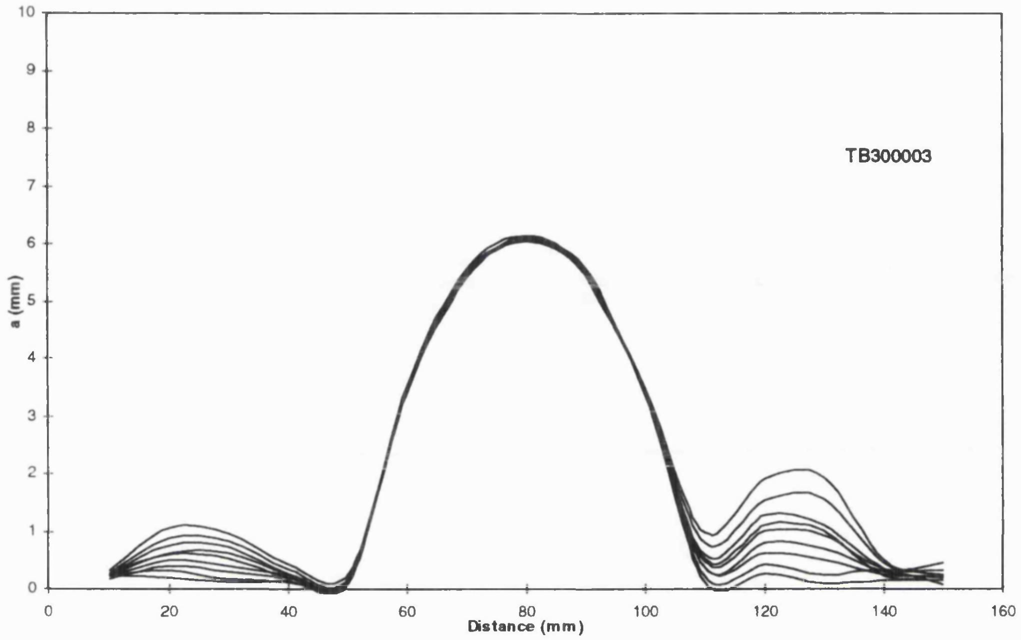

Figure 3.27 Fatigue crack initiation for specimen TB300003

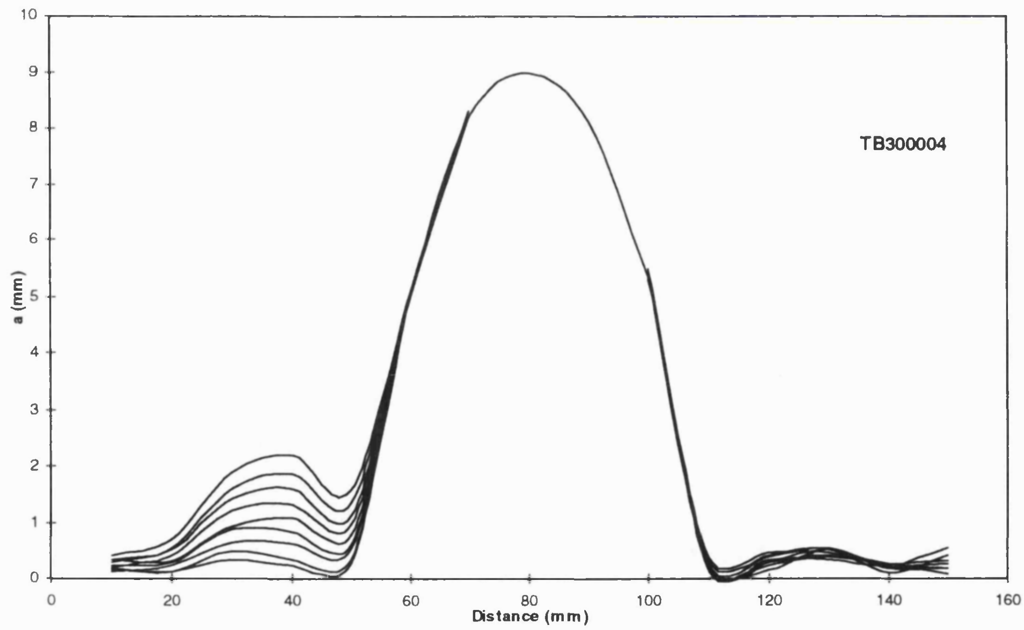

Figure 3.28 Fatigue crack initiation for specimen TB300004

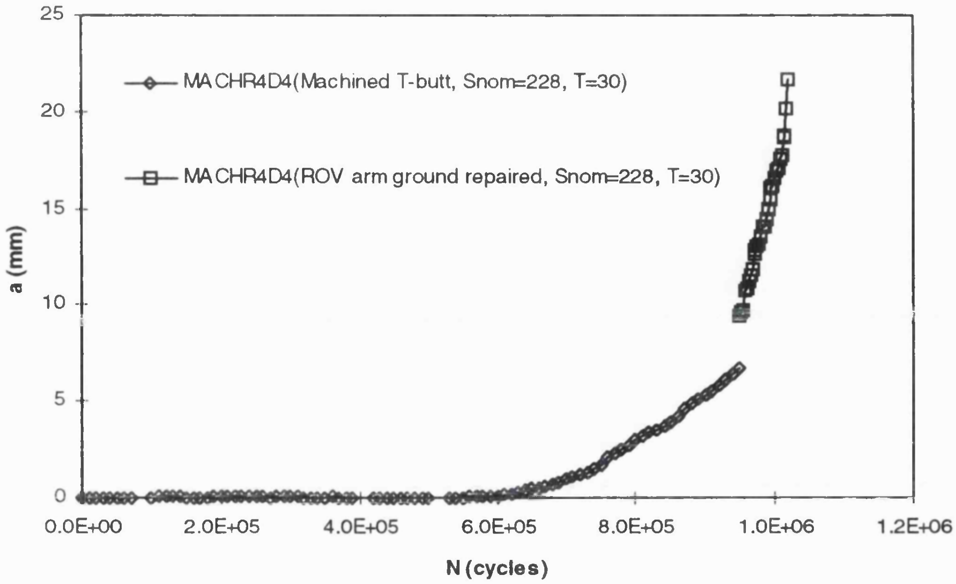

Figure 3.29 Fatigue crack growth curve of ROV arm ground specimen

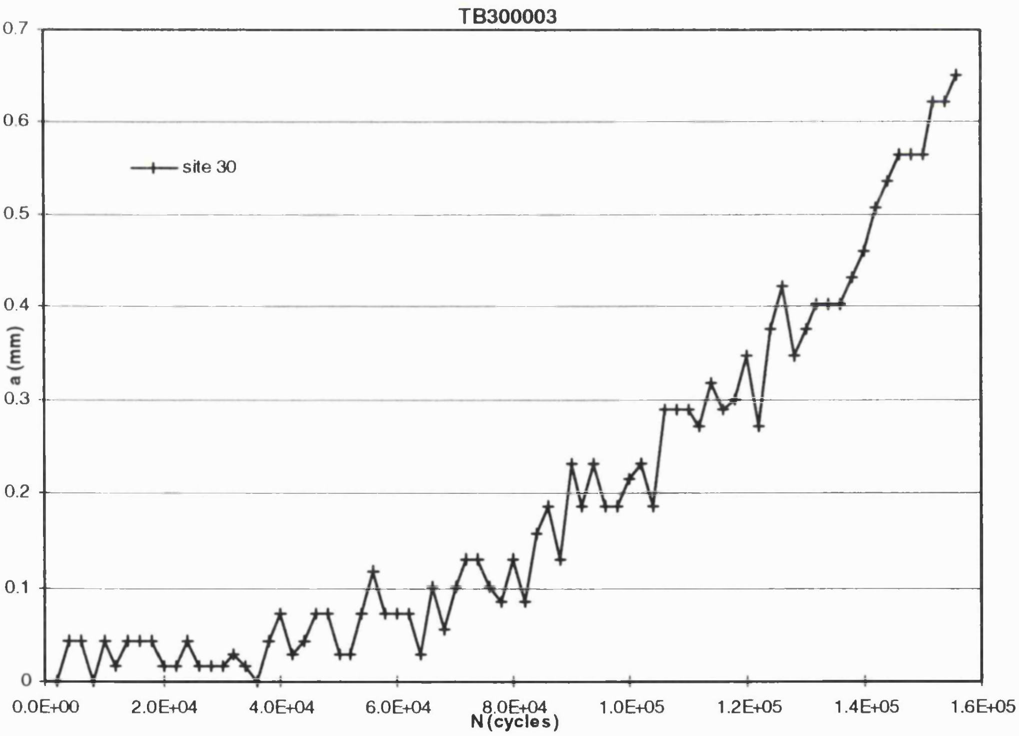

Figure 3.30 Fatigue crack growth during initiation for specimen TB300003

(Spot welding used for crack monitoring)

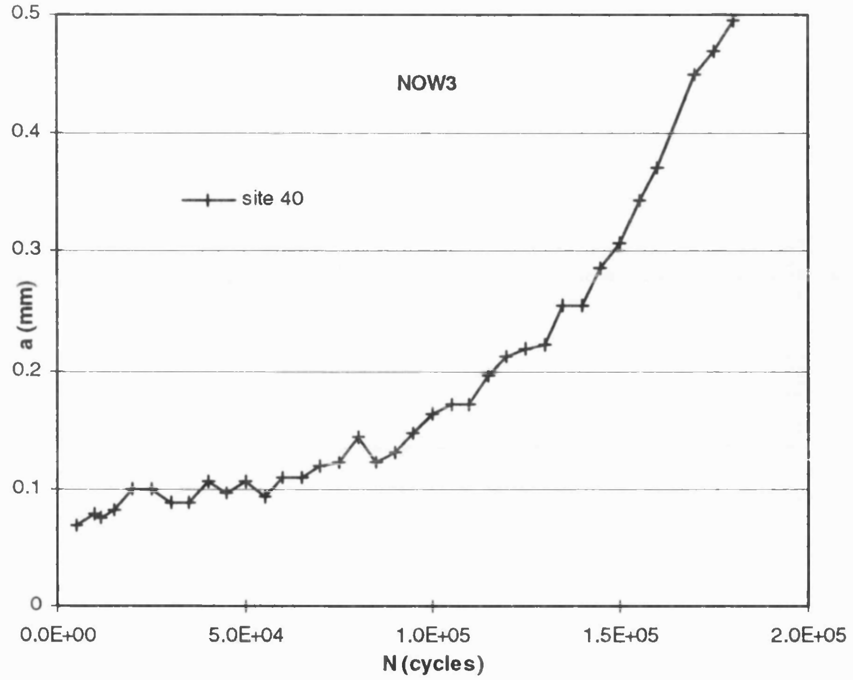

Figure 3.31 Fatigue crack growth during initiation for specimen NOW3 (TSC ACPD array used for crack monitoring)

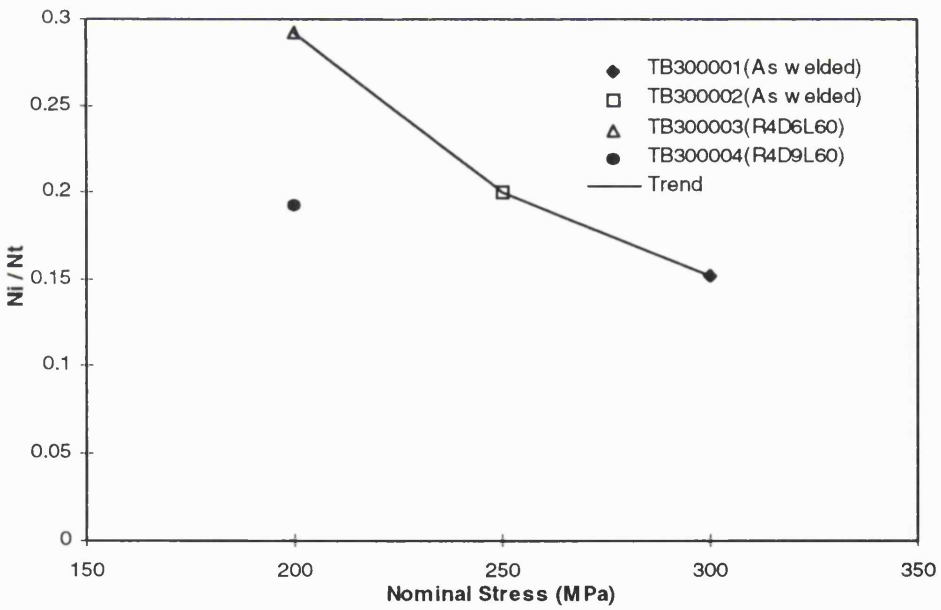

Figure 3.32 Fatigue initiation to total fatigue life ratios for T-butt specimens series TB300

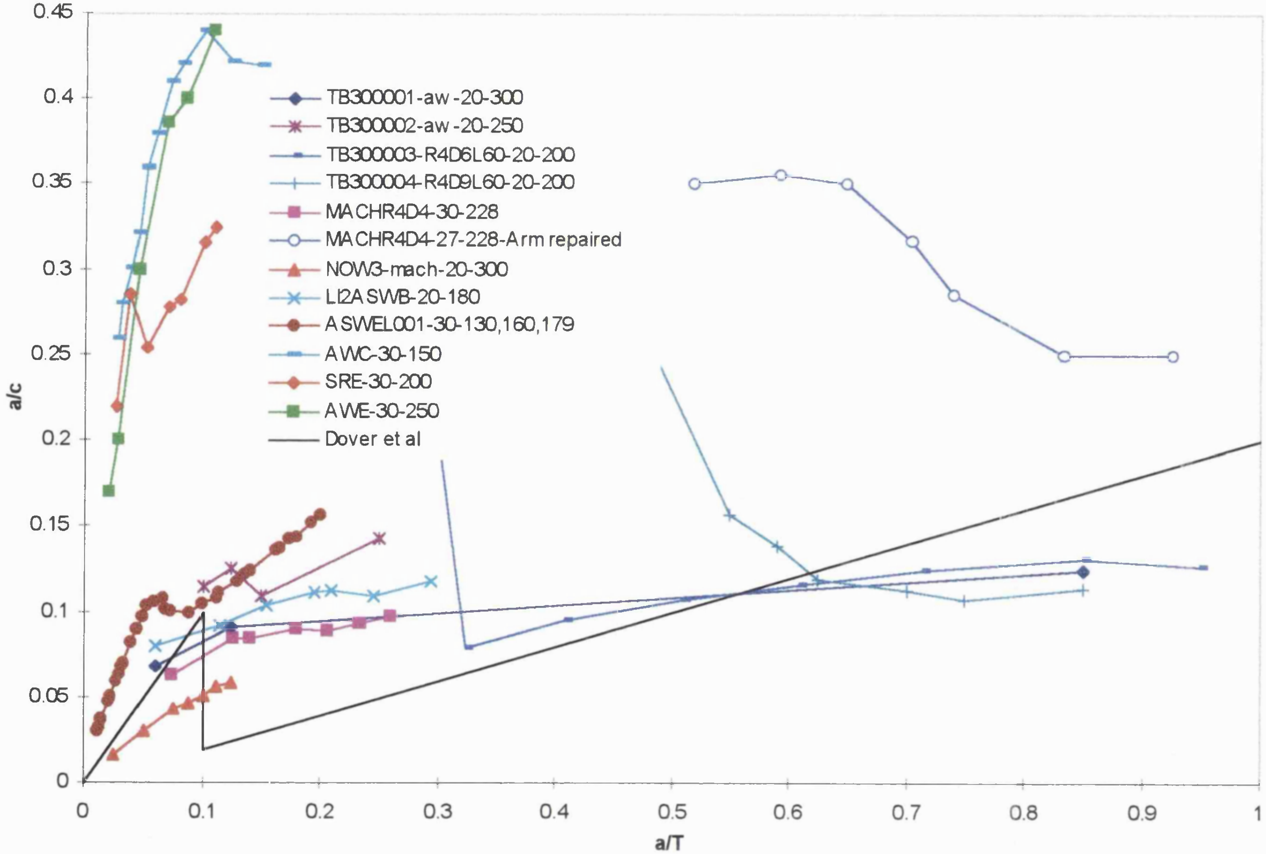

Figure 3.33 Fatigue crack shape evolution

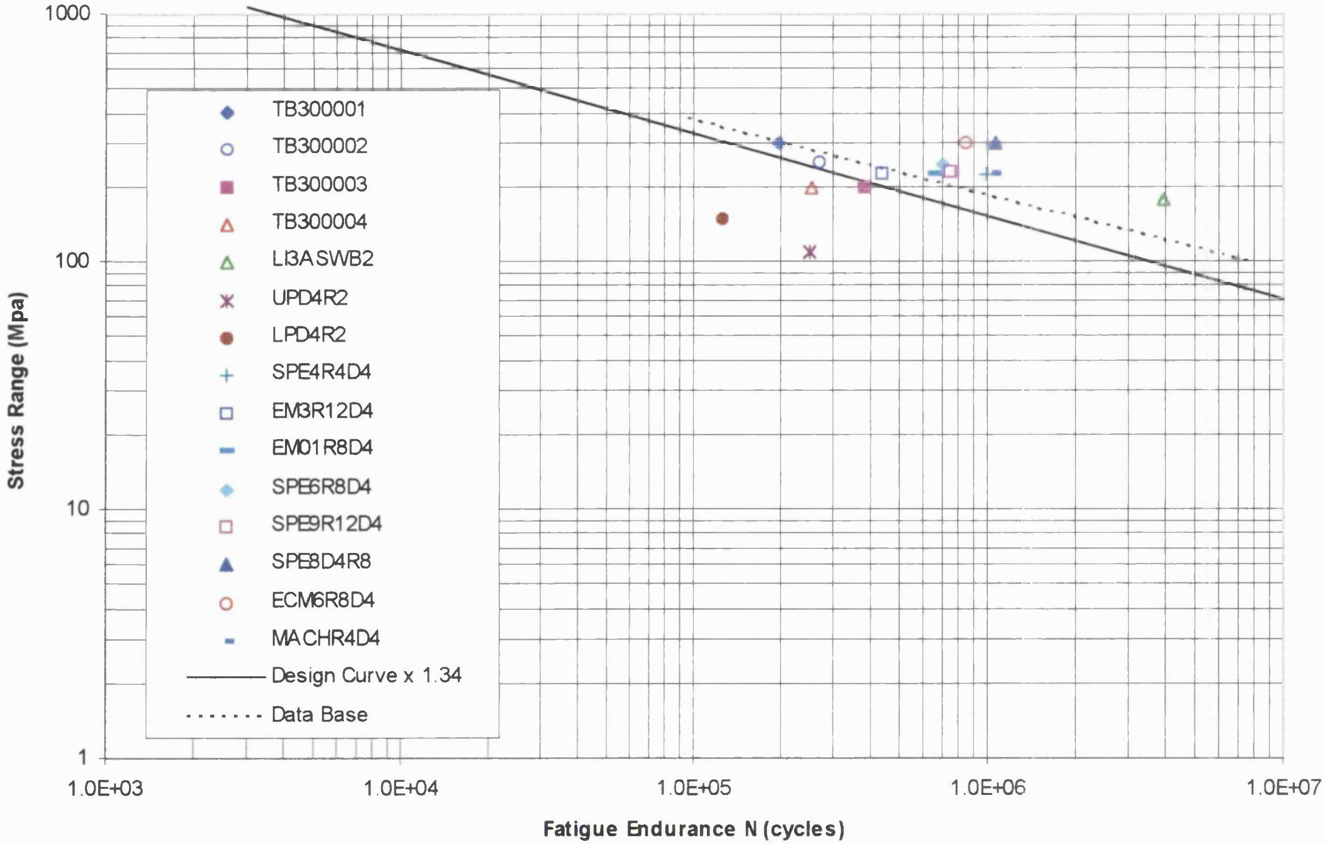

Figure 3.34 S-N values of T-butt and butt specimens experimentally tested

Figure 3.35 Fractured surface of specimen LI3ASWB
Crack initiation from subsurface weld defect (slag inclusions)

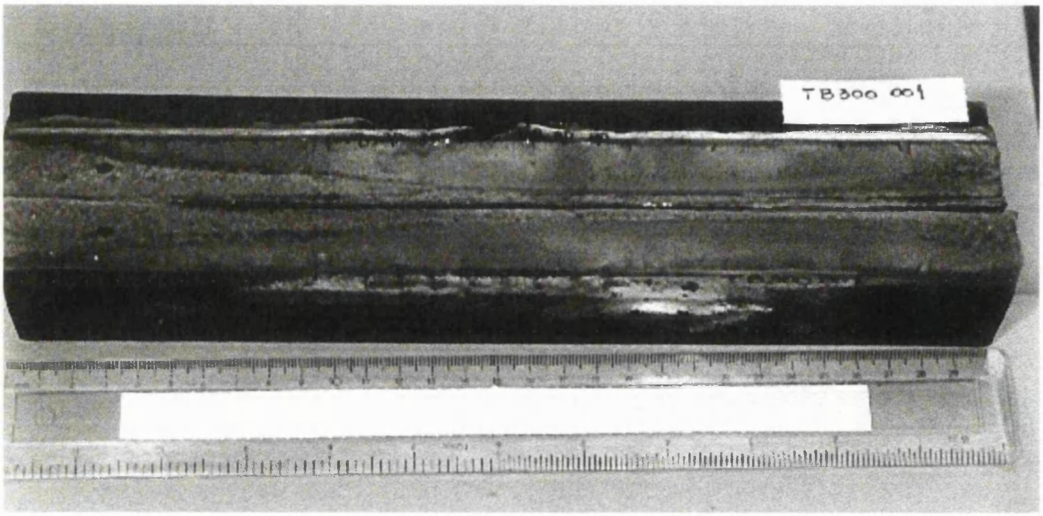

Figure 3.36 Fractured surface of specimen TB300001
Crack initiation from as-welded region

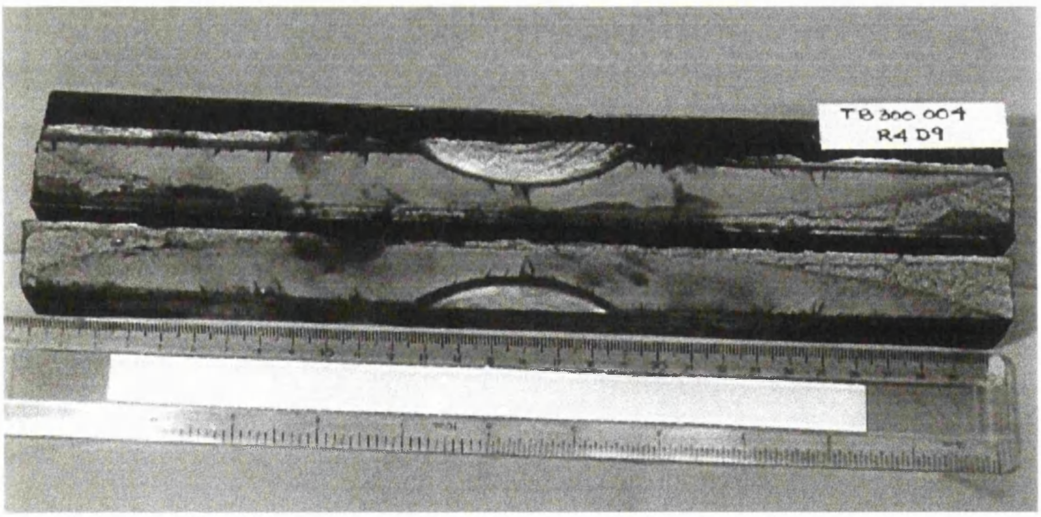

Figure 3.37 Fractured surface of specimen TB300004
Crack initiation from as-welded regions at both repair ends

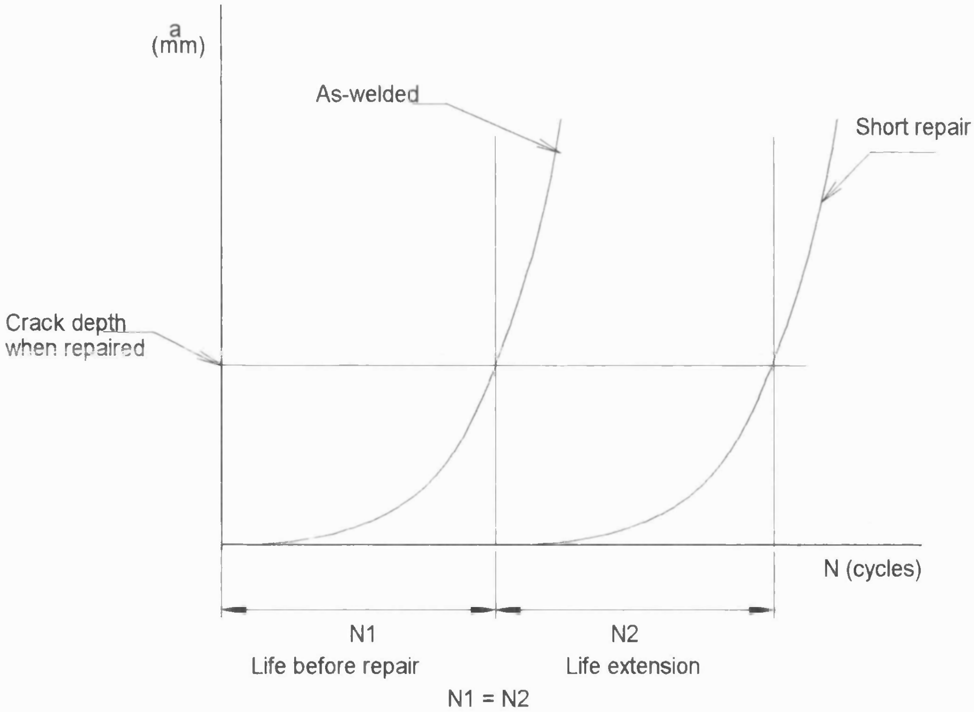

Figure 3.38 Approximate determination of fatigue life extension after repair

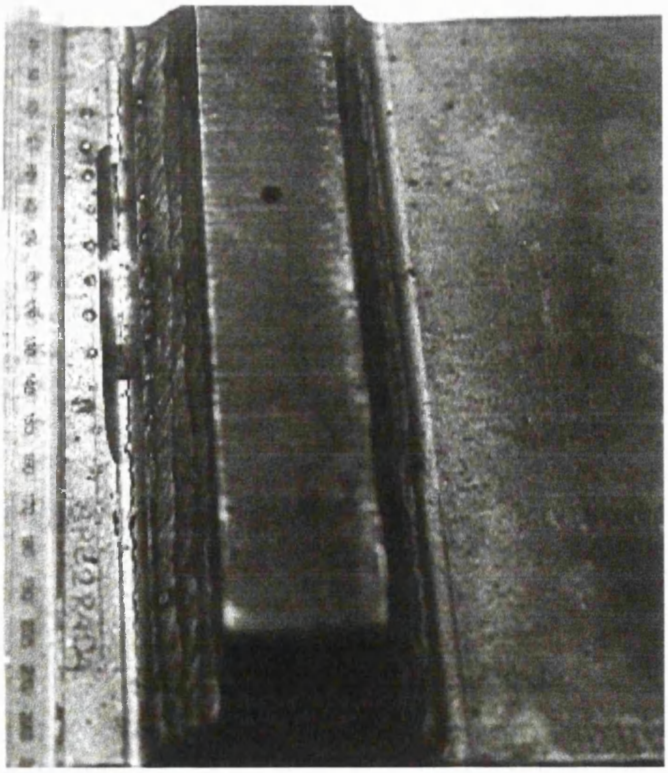

Figure 3.39 Cracking pattern after repair and re-testing specimen S22R4D12. Notice: weld toe improvement at both sides of the repair and on the other side of the vertical attachment.

CHAPTER FOUR

FRACTURE MECHANICS ANALYSIS OF FATIGUE REPAIRED JOINTS

4.1 Introduction

Fatigue life predictions based on fracture mechanics calculations are required to satisfy an increasing level of safety demanded by industry. These predictions are mainly used to schedule NDT inspections and with the data collected make structural integrity assessments. The periodic inspection-assessment process can lead to the implementation of the repair method presented in this thesis. Fracture mechanics analysis is used again to determine whether or not a repair will be effective. For the case of tubular joints, in offshore structures, once repairs have been shown to be ineffective it is usually required to install a clamp to maintain the continuity of the members of the joint if the structure is still required for production. This type of repair and its inspection is described in chapter 5.

In this chapter a fracture mechanics analysis of crack repaired joints based on Y factors is presented. The analysis is used to predict fatigue life after crack removal and is validated against the T-butts experimental data presented in chapter 3. The analysis is also extrapolated for the prediction of fatigue life of crack repaired tubular joints.

4.2 Stress Intensity Factors for T-Butt connections

Stress intensity factors were introduced in chapter 1 as a way to relate the localised crack tip stress response and the external conditions such as load, component geometry, boundary conditions, crack shape and crack size. The general form is given by

$$K = Y\sigma\sqrt{\pi a} \tag{4.1}$$

where σ is the nominal stress, a is the crack depth and Y is the stress intensity correction factor that accounts for the external conditions. Y factors can be obtained as the product of different effects and a recommended form is [4.1]

$$Y = Y_s Y_w Y_e Y_g Y_k Y_m \tag{4.2}$$

where

Y_s	Correction for a free front surface
Y_w	Correction for finite plate width
Y_e	Correction for crack geometry
Y_g	Correction for non uniform stress field
Y_k	Correction for the presence of geometrical discontinuity
Y_m	Correction for changes in structural restraint

For the calculation of Y factors various methods have been developed. These can be broadly classified as empirical and analytical methods.

4.3 Empirically Determined Y Factors

Empirical models are especially useful for the determination of Y factors for complex structural models such as tubular joints due to the analytical difficulty in considering multiple factors that effect crack growth and their interaction during crack growth evolution.

4.3.1 Extraction of Y Factors from Crack Growth Experimental Data

As explained in section 3.5.2 crack growth experimental data was processed to determine: crack growth rates, stress intensity factor range, crack shape characteristics and Y factors. In general, crack growth rates and ΔK are determined for the deepest point on the crack front for surface cracks and an average depth for edge cracks. Equations (4.3) and (4.4) were used to process the experimental data.

Paris equation:

$$\frac{da_i}{dN_i} = C(\Delta K_i)^m \tag{4.3a}$$

$$\Delta K_i = \left[\frac{1}{C}\left(\frac{da_i}{dN_i}\right)\right]^{\frac{1}{m}} \tag{4.3b}$$

where

$\frac{da_i}{dN_i}$ Fatigue crack growth rate 'i.'

C Crack growth coefficient (see section 3.5.2)

m Crack growth exponent (see section 3.5.2)

ΔK_i Stress intensity factor range 'i.'

N_i Number of cycles at ΔK_i and a_i

Knowing the values of ΔK_i and $\Delta\sigma_i$ a solution for the Y_i factors can be obtained from equation (4.4b).

$$\Delta K_i = Y_i \Delta\sigma_i \sqrt{\pi a_i} \tag{4.4a}$$

$$Y_i = \frac{\Delta K_i}{\Delta\sigma_i \sqrt{\pi a_i}} \tag{4.4b}$$

where

ΔK_i Stress intensity factor range 'i.'

Y_i Stress intensity calibration factor 'i.'

$\Delta\sigma_i$ Notch stress range 'i.'

a_i Crack depth 'i.'

In this chapter the parameters da/dN, ΔK and Y are presented for specimens which can provide useful understanding of fatigue crack growth of repaired connections.

Graphs of da/dN and ΔK obtained from the crack growth experimental data for specimen UPD4R2 are shown in figures 4.1 and 4.2. In the same figures, graphs determined using an analytical model which will be explained in 4.4.1 are also shown. A graph of experimentally determined Y factors for specimens LPD4R2 (lightly peened specimen) and UPD4R2 (unpeened) is shown in figure 4.3. In this figure Y factors are presented considering the bottom of the notch as the origin. This figure is particularly useful to demonstrate the effect of shot peening since a direct comparison of crack growth curves was not possible due to the different nominal stresses used for specimens UPD4R2 and LPD4R2.

4.3.2 Effect of Compressive Residual Stresses for Fatigue Improvement

Figure 4.3 compares the experimentally determined Y factors for an unpeened and lightly peened specimens and shows in general a lower value of Y for the peened specimen in the range $0 < a/(T-4) < 0.08$. This could mean that peening reduced the crack growth rate in this region. However, since the Y values are only slightly lower for the peened specimen it has to be considered that other factors may be involved that affected the Y values such as the crack aspect ratio or the accuracy of the measurement technique. It is for example possible that the presence of residual stress and its relaxation as the crack grows could have had an influence on the ACPD readings. Therefore, it is not possible to draw a firm conclusion from the experimental data obtained from only two specimens.

From figure 4.3 it can also be observed that the unpeened curve is smoother than that for the peened specimen in the range $0 < a/(T-4) < 0.08$; this may be explained by a multiple crack initiation effect, possibly caused by the mildly rough surface left by the shot particles. A final observation from the same figure can be obtained considering the point where the two curves intersect which is at $a/(T-4)=0.08$. At this point the crack is 2 mm deep this coincides with the approximate thickness of the residual stress compressive layer. This could be indicating the sensitivity of ACPD to residual stress.

A draft of the ISO code [4.2] recommends a fatigue life improvement factor of 4 when the toes of welded connections have been hammer peened. The objective of hammer peening is to obtain a smooth groove at the weld toe thus, manufacturing surface defects are eliminated, the transition between the parent and weld material is continuous and beneficial compressive residual stresses are induced at the surface. All of these contribute to the enhancement of the fatigue performance of the treated weld. Among other recommendations it is worth mentioning that the peened pit depth should be at least 0.5mm, but should not exceed 1.0mm. The pneumatic hammer bit tip radius should be about 3mm. Peened weld toes should be inspected directly after peening with MPI, [4.2].

Although, fatigue life improvement by shot peening was not determined, the Y factors of the peened specimens do not show any major difference compared with the unpeened specimens. Thus, it can be concluded that the considerable enhancement in fatigue performance of hammer peened welds recommended by the ISO code, relies more on the effect given by the metal work for the improvement of fatigue crack initiation resistance, rather than resistance to crack propagation.

Fatigue life improvement based on shot peening or hammer peening should be considered with care since variable amplitude loading can release residual compressive stresses [4.3].

4.3.3 Effect of Fatigue Crack Repair on Y Factors

Experimental Y factors for a representative sample of edge and surface repaired specimens is shown in figures 4.5 and 4.6. In these figures edge repairs are specified in the legend and the rest are surface repairs. The code in figures 4.5 and 4.6 that follows the specimen name corresponds to: aw for tested in as-welded condition, m for machined manufacture, R#D#L# for the size of radius, depth and length in mm of the surface repair machined on the specimen before testing, and the last numbers are the thickness in mm and the nominal stress in MPa. It is worth remembering that for a complete description of the specimen characteristics, table 3.4 should be consulted instead.

In figures 4.5 and 4.6, Y factor curves for edge repaired specimens are shifted to the right by a magnitude of a/T=4/30 (notch depth/thickness). This was done in order to consider the plate surface as a common origin for all the specimens. The same situation is presented by the Y curve of specimen TB300003 at site 80 which starts at a/T= 6/20 (notch depth/thickness). Figures 4.5 and 4.6 show that Y factors for surface repaired specimens for a/T>0.2 tend towards those for edge repaired specimens. However, the surface repaired specimens have longer fatigue lives than the edge repaired specimens, see figure 3.34. Thus, the extra life extension of a surface repair versus an edge repair is due to crack initiation taking place outside the repair notch, reinstalling the original plate thickness for crack propagation.

Experimental Y factors for various repaired specimens are presented in figure 4.6. In the figure it can be observed three typical Y factor curves: 1) Crack totally removed by the repair and crack initiation outside the repair notch propagating through the entire original thickness, see specimens LI3ASWB-LI3ASWB2 and TB300003 site 130. 2)Crack partially removed by the repair and propagation continuing from the bottom of the notch, see specimens MACHR4D4 and NOW1-NOW12. 3) Delayed crack initiation at the bottom of the repair notch by the effect of a short repair forcing initiation outside the repair notch, see specimen TB300003 site 80. From this particular case it can be deduced that for short repairs the Y factors for a crack growing in the bottom of the repair notch should follow the trend shown by specimen TB300003 at site 80 and for long repairs the crack can only grow in the bottom of the notch and should show the trend of specimens UPD4R2 and LPD4R2 presented in figure 4.5.

4.4 Analytically Determined Y Factors

The analytical methods for obtaining Y factors solutions are in general highly complex mathematical problems. So, other approaches as numerical solutions like the finite element analysis are frequently used instead. However, they can become expensive if solutions for multiple parametric variations are required. A practical analytical method for the determination of Y factors is the weight function method. This method is especially useful where various stress intensity factor solutions are required for a given geometry.

An analytical solution for the determination of Y factors for tubular joints is not currently available thus, Y solutions for plates have been extrapolated to tubular joints based on the relation presented in equation (4.2).

4.4.1 Weight Function

The weight function concept or also called Green's function was first introduced by Bueckner [4.4] based on analytical function representation of elastic fields for isotropic materials. He showed that the stress intensity factor due to an arbitrary but symmetrical set of applied loads can be obtained by integrating over crack length the product of the weight function and the through thickness stress distribution produced by the arbitrary set of applied loads at the potential crack plane but considering the body as uncracked.

$$K_{IS} = \int_0^a \sigma(x)m(a,x)dx \tag{4.5}$$

where

K_{Is} stress intensity factor sought

$\sigma(x)$ through thickness stress distribution in the uncracked body at the prospective crack site produced by a set of applied loads

$m(a,x)$ weight function

a crack length

x coordinate parallel to the crack

Rice [4.5] showed that the weight function is a universal function for a cracked body of any given geometry and material, regardless of the detailed way in which the body is loaded, and that knowledge of the stress intensity factor and crack face displacements as a function of crack length for a particular loading condition enables the determination of the stress intensity factor for the same body under any other loading producing the same cracking mode.

The weight function is given by

$$m(a,x) = \frac{H}{K_{Ik}}\left(\frac{\delta v(x)}{\delta a}\right) \tag{4.6}$$

where

H $E/(1+v^2)$for plane strain and E for plane stress

$v(x)$ known crack face displacements as a function of crack length at the loading point x in the direction of loading for the stress distribution analysed

K_{Ik} known stress intensity factor associated with the crack face displacements

Since weight functions can be obtained by differentiating the crack surface displacement with respect to crack length, a rational analytical approach to determining weight functions is to seek accurate representations of the crack opening displacements [4.6].

It is advantageous from a computational point of view to write equation (4.5) in a non-dimensional form. For this purpose a normalising stress σ, and a characteristic dimension which has to be defined individually for each cracked configuration are introduced and equation (4.5) can be rewritten as

$$Y = \int_0^a \frac{\sigma(x)}{\sigma}\frac{m(a,x)}{\sqrt{\pi a}}dx \tag{4.7}$$

and the stress intensity factor can be calculated as

$$K = Y\sigma\sqrt{\pi a W} \qquad (4.8)$$

where

W characteristic dimension that depends on the geometry of the component

Y factor that takes in account the geometric characteristics of the crack, component and type of loading.

σ nominal surface stress

a crack depth

K stress intensity factor

Carlsson and Wu using weight functions developed stress intensity factors for various crack geometries and among them the case of an edge crack at a semi-circular notch in a finite plate is presented in reference [4.6]. For this particular case Carlsson and Wu used reference solutions for stress intensity factors by Tan[4.7] and Nisitani [4.8]; and the crack line stress by Noda [4.9] and Manusell [4.10].

For this approach the load cases in plane bending and pure tension are presented here, see figure 4.4. The notch root stress is chosen as σ so:

$$\sigma = \frac{6K_t M}{B^2} \qquad \text{in plane bending} \qquad (4.9)$$

$$\sigma = \frac{K_t P}{B} \qquad \text{pure tension} \qquad (4.10)$$

where

M is the in plane bending moment referred to unit thickness

P is the total tensile force referred to unit thickness

K_t is the stress concentration factor, see figure 4.4

B is the plate thickness

Y values for equation (4.11) are shown in figure 4.4 as f values

$$K = Y\sigma\sqrt{\pi a R} \qquad (4.11)$$

where

R is the notch radius

4.4.2 Weight Function versus Experimental Y Factors

For the edge repair profile D4R2 used in only two specimens experimentally tested (UPD4R2 and LPD4R2) Y factors were determined using the weight function developed by Carlsson and Wu presented in figure 4.4. However, the previous weight function was developed for a notch geometry which has the notch radius centre on the plate surface and the repair profile D4R2 is a U-shape with the radius centre 2mm below the surface. Thus, theoretical Y factors were determined for a D4R4 notch geometry instead and compared with the experimentally determined Y factors for specimen LPD4R2 as shown in figure 4.7. The same procedure was applied to specimen UPD4R2 and from the theoretical Y factors stress intensity factor ranges and crack growth rates were determined using equations (4.4) and (4.3) respectively. The theoretical da/dN and ΔK values obtained for specimen UPD4R2 are shown graphically in figures 4.1 and 4.2 respectively.

For the application of weight function theory to the edge repaired specimens LPD4R2 and UPD4R2 no consideration of the weld geometry has been made and a semi-circular notch instead of a U-shaped notch was considered. This simplification of considering a U-shaped notch as a semicircle has no effect at all and the only effect is due to increasing the radius from 2 to 4 mm. This concept was explained when the equivalent notch configurations where presented in chapter 2. Since in the weight function solution, the weld geometry is not considered the Y factors are underestimated to some extent in early stages of crack growth as it can be seen in figure 4.7. However, the solution as a whole provides a close correlation with the experimentally determined parameters da/dN, ΔK and Y as shown in figures 4.1, 4.2 and 4.7.

4.4.3 Newman-Raju Equations

Stress intensity factor variation along the crack front for various crack shapes was determined using the finite element method and then presented in the form of an equation by Newman and Raju (N&R) in 1981, [4.11]. The empirical equation developed enables the calculation of stress intensity factors for a surface crack as a function of parametric angle, crack depth, crack length, plate thickness and plate width for tension and bending loadings. N&R quote in their paper that to account for the limiting behaviour as a/c approaches zero the results of Gross and Srawley [4.12] for a single edge crack were included in the equation. The N&R stress intensity factor solution is presented in the set of equations (4.12)

$$\mathrm{K_I} = (S_t + HS_b)\sqrt{\pi\frac{\mathrm{a}}{Q}}F(\frac{\mathrm{a}}{\mathrm{t}},\frac{\mathrm{a}}{\mathrm{c}},\frac{\mathrm{c}}{\mathrm{b}},\Phi) \tag{4.12}$$

where

$$Q = 1 + 1.464\left(\frac{\mathrm{a}}{\mathrm{c}}\right)^{1.65} \quad \text{for } \frac{\mathrm{a}}{\mathrm{c}} \leq 1$$

$$F = \left[\mathrm{M_1} + \mathrm{M_2}\left(\frac{\mathrm{a}}{\mathrm{t}}\right)^2 + \mathrm{M_3}\left(\frac{\mathrm{a}}{\mathrm{t}}\right)^4\right] f_\Phi g f_w$$

$$M_1 = 1.13 - 0.09\left(\frac{\mathrm{a}}{\mathrm{c}}\right)$$

$$M_2 = -0.54 + \frac{0.89}{0.2 + \left(\frac{\mathrm{a}}{\mathrm{c}}\right)}$$

$$M_3 = 0.5 - \frac{1.0}{0.65 + \left(\frac{\mathrm{a}}{\mathrm{c}}\right)} + 14\left(1.0 - \frac{\mathrm{a}}{\mathrm{c}}\right)^{24}$$

$$g = 1 + \left[0.1 + 0.35\left(\frac{\mathrm{a}}{\mathrm{t}}\right)^2\right](1 - \sin\Phi)^2$$

$$f_\Phi = \left[\left(\frac{a}{c}\right)^2 \cos^2\Phi + \sin^2\Phi\right]^{\frac{1}{4}}$$

$$f_w = \left[\sec\left(\frac{\pi c}{2b}\sqrt{\frac{a}{t}}\right)\right]^{\frac{1}{2}}$$

$$H = H_1 + (H_2 - H_1)\sin^p\Phi$$

$$p = 0.2 + \frac{a}{c} + 0.6\frac{a}{t}$$

$$H_1 = 1 - 0.34\frac{a}{t} - 0.11\frac{a}{c}\left(\frac{a}{t}\right)$$

$$H_2 = 1 + G_1\left(\frac{a}{t}\right) + G_2\left(\frac{a}{t}\right)^2$$

$$G_1 = -1.22 - 0.12\frac{a}{c}$$

$$G_2 = 0.55 - 1.05\left(\frac{a}{c}\right)^{0.75} + 0.47\left(\frac{a}{c}\right)^{1.5}$$

for the limits

$$0 < \frac{a}{c} \le 1.0$$

$$0 \le \frac{a}{t} < 1.0$$

$$\frac{c}{b} < 0.5$$

$$0 \le \Phi \le \pi$$

where

S_t	remote uniform tension stress in Pa
S_b	remote bending stress on outer fibre in Pa
b	half width of cracked plate in mm
h	half length of cracked plate
t	plate thickness
a	depth of surface crack in mm
c	half length of surface crack in mm
ϕ	parametric angle of ellipse in degrees
Q	shape factor for elliptical crack

The N&R solution was implemented in a spreadsheet and results using this solution are presented.

4.4.4 Proposed Crack Shape Design Curve

Fracture mechanics calculations for the prediction of remaining fatigue life require the determination of Y factors. Y factors for numerous geometries and loading conditions can be found in the literature however, for the particular U-shaped short repair notch considered in this work a Y factor solution was not found. So, the N&R solution was used to determine the Y factors. However, for the determination of Y factors crack shape evolution behaviour through the thickness needs to be defined. A proposed crack shape (a/c) design curve is presented in equations (4.13) and (4.14).

$$a/c = a/T \tag{4.13}$$

for $0 < a/T \leq 0.12$

$$a/c = 0.25 \tag{4.14}$$

for $a/T > 0.12$

Although, the N&R solution was developed for flat plates it was compared with the experimental Y factors determined for T-butts to investigate the weld effect on Y factors. The input dimensions used for the N&R solution were 300mm wide and 20mm thick. It can be observed that experimental Y factors for surface and edge repaired specimens in the range $0<a/T<0.2$ are under predicted by the N&R solution when considering the proposed a/c design curve (Y N&R+DC) as shown in figure 4.8. It can also be seen from figure 4.8 that Y N&R+DC merge with the experimental Y factor curves after the weld has no longer an influence on the crack growth, this is at approximately $a/T=0.2$.

Figure 4.8 also shows that edge repaired specimens LPD4R2 and UPD4R2 have a steeper gradient of the Y factor curve in the range $0<a/T<0.2$ than the other specimen results. This is due to the reduced effect of the weld geometry on a crack growing in the bottom of an edge repair compared with the case of a crack growing at the weld toe as in the case of a surface repair.

Corrections to Y N&R+DC to consider the weld effect are presented in the following section.

4.4.5 Weld Geometry Correction Factor

A similar procedure to that followed by Monahan [4.13] is presented here for the determination of the correction applied to Y N&R+DC to consider the effect of the weld. Y factors were determined using a stress intensity factor calculation procedure developed by Albrecht and Yamada [4.14]. This procedure allows the determination of stress intensity factors for intermediate crack sizes and the corresponding Y factors in the following manner:

1) Determine the stresses along the crack line but in the uncracked condition
2) Determine K by integration of the stresses determined in step 1 over the length of the crack
3) Repeat step 2 for any desired crack length

The value of K in step 2) is determined using the solution for a central crack of length 2a in an infinite plate with two equal pairs of splitting forces P, applied at $x=\pm b$ as proposed by Tada et al [4.15] as shown in figure 4.11.

$$K = \frac{2P}{\sqrt{\pi a}} \frac{a}{\sqrt{a^2 - b^2}} \tag{4.15}$$

Replacing the concentrated forces by a symmetrical distributed stress field about the centre of the crack, the splitting forces can be expressed as the product of stress over a length and equation (4.15) becomes (4.16).

$$K = \sqrt{\pi a}\, \frac{2}{\pi} \int_0^a \frac{\sigma_b}{\sqrt{a^2 - b^2}}\, db \tag{4.16}$$

where

σ_b stress in the uncracked body over infinitesimal length db

Using the notation in figure 4.11 on equation (4.16) leads to

$$K = \sqrt{\pi a}\frac{2}{\pi}\sum_{i=1}^{n}\sigma_{bi}\int_{bi}^{bi+1}\frac{1}{\sqrt{a^2 - b^2}}db \tag{4.17}$$

the discrete stress σ_{bi} is applied over the element width from b_i to b_{i+1}. The integration is carried out over the element width and the summation over the number of elements from the centre of the crack to the crack tip. Integrating and factoring

$$K = \sigma\sqrt{\pi a}\frac{2}{\pi}\sum_{i=1}^{n}\frac{\sigma_{bi}}{\sigma}\left(\arcsin\frac{b_{i+1}}{a} - \arcsin\frac{b_i}{a}\right) \tag{4.18}$$

From inspection of equation (4.18) it is apparent that the geometry correction factor Yg is

$$Y_g = \frac{2}{\pi}\sum_{i=1}^{n}\frac{\sigma_{bi}}{\sigma}\left(\arcsin\frac{b_{i+1}}{a} - \arcsin\frac{b_i}{a}\right) \tag{4.19}$$

where

σ stress uniformly distributed over the plate thickness

In equation (4.19) $\frac{\sigma_{bi}}{\sigma}$ represents the ratio of the non uniform stress distribution along the line of the crack to a uniformly distributed stress thus, this value can be interpreted as a SCF. Therefore, Yg accounts for the effect on the stress intensity factor (K) from a stress concentration produced by a structural detail.

For the application of the procedure described above the uncracked stress distribution trough the plate thickness at the weld toe section is required. Stress at the weld toe is a function of the weld geometry thus, the weld geometry of specimen TB300004 is used in the calculations. The average weld toe radius was 0.8 mm so, the weld toe radius to plate thickness ratio is $\rho/T= 0.04$. Sharples et al [4.15] fitted equations to the results of finite element calculated weld toe stresses in uncracked T-plates under three point bending. The weld angle considered is 45^0 and the reported results for $\rho/T= 0.05$ expressed in equations (4.20a) and (4.20b) are used here.

$$SCF_W = \frac{\sigma_W(x/T)}{\sigma_{no}} = 2.0476e^{-55x/T} + (0.8624 - 1.8624x/T) \qquad (4.20a)$$

for $x/T \leq 0.4$

$$SCF_W = \frac{\sigma_W(x/T)}{\sigma_{no}} = 0.8624 - 1.8624x/T \qquad (4.20b)$$

for $x/T > 0.4$

where

SCF_W	weld toe stress concentration factor
$\sigma_W(x/T)$	weld toe stress at a non-dimensional depth to thickness ratio x/T
σ_{no}	nominal surface stress at the weld toe

A flat plate under bending has a linear stress distribution described by

$$SCF = \frac{\sigma(x/T)}{\sigma_{no}} = 1 - 2x/T \qquad (4.21)$$

Although, equations (4.20) were derived for three point bending they are used here to correct Y N&R+DC in order to compare with experimental Y factors obtained from four point bending. It has been observed in practice that the mode II contribution can be neglected for fatigue crack growth predictions [4.20].
Plotting the non-uniform and linear stress distributions described by equations (4.20) and (4.21) the weld influence can be clearly seen in figure 4.9.

A Y factor solution for a flat plate (Y_{lin}) is given by

$$Y_{lin} = 1 - 1.273\ a/T \qquad (4.22)$$

Using equations (4.20) and (4.19) non uniform stress correction factors were obtained (Yg) and a comparison with Y_{lin} is shown in figure 4.10. From figures 4.9 and 4.10 it can be seen that the weld influence extends deeper for the Y factor than for the stress distribution in the uncracked body. Additionally, as was initially seen from the experimental data in figures 4.5 and 4.6 and explained above the weld effect on Y factors is negligible after $a/T>0.2$. Therefore, the correction to Y N&R will be only applied for $0<a/T \leq 0.2$.

Since the Y N&R solution was developed for flat plates it is on its own Y_{lin} so, the correction to account for the non uniform stress (NSC) effect produced by the weld is

$$NSC = \frac{Y_g}{Y_{lin}} \tag{4.23}$$

Applying the NSC correction to Y N&R+DC denoted as Y N&R+DC+NSC allows the development of an approximate Y factor solution for a T-butt plate in four point bending. The results are shown in figure 4.8 with the legend N&R+DC+NSC.

Y N&R+DC+NSC were developed for the deepest point along the crack front, this is $\phi=90^0$ in the Newman and Raju solution. Predictions using this approach have to correspond to this location on the crack line. This approach is intended to be applied to predict fatigue life from the repair ends to determine when the effect of the repair has disappeared, this is a = repair depth. This was graphically explained in figures 3.25 and 3.26 where it is shown that crack growth is nil in the bottom of the repair until the lateral cracks join under the bottom. Figures 3.27 and 3.28 also show that the cracks growing from the repair ends have a crack front that allows the application of Y N&R+DC+NSC.

4.5 Fatigue Crack Growth Predictions

Prediction of crack growth was made integrating the Paris equation (4.3) over the crack length and considering the Y N&R+DC+NSC

$$N = \int_{ai}^{af} \left(\frac{1}{C(\Delta K)^m} \right) da \tag{4.24}$$

substituting equation (4.19) and factoring constant values

$$N = \frac{1}{C(\Delta S\sqrt{\pi})^m} \int_{ai}^{af} \left(\frac{1}{Y_g \mathrm{a}^{\frac{m}{2}}} \right) da \tag{4.25}$$

where

C	2.88×10^{-12} in MPa
m	3.23
a_i	initial crack size in metres
a_f	final crack size in metres
ΔS	nominal stress range in MPa
Y_g	Y N&R+DC+NSC
N	fatigue life in cycles

The C and m values presented above were obtained from least squares geometric regression analysis of experimental data for steel Grade 50D in the United Kingdom Offshore Steel Research Project [4.16]. They are not the same that were used for the determination of experimental Y factors (C= 4.5×10^{-12} and m=3.3). The values used for the calculation of experimental Y factors correspond to an upper bound. Therefore, for predictions of crack growth and comparison with experimental crack growth the C and m obtained by regression are considered more appropriate.

It is well documented that the fatigue life estimation is strongly dependent on a_i, and generally not sensitive to a_f when $a_i \ll a_f$. Large changes in a_f result in small changes of fatigue life [4.17]. From observation of figure 3.30 which shows crack growth during initiation of specimen TB300003 the value a_i=0.1mm was considered appropriate. This value will be used for the rest of the specimens series TB300 since all of them were welded in the same conditions (automatic welding) and the weld toe radii had similar dimensions (ρ/T= 0.04).

For the integration of equation (4.25), Simpson's rule [4.18] was coded in a spreadsheet. During the selection of the crack shape design curve proposed in section 4.4.3 it was noticed that fatigue life prediction is highly sensitive to minor differences in the Yg curve used.

To reproduce the experimental crack growth curve of specimen TB300004 at the repair ends (sites 30 or 130) an a_i=0.1 mm and the experimental nominal stress range of 190 MPa were used. Inserting Y determined experimentally (Yexp) at site 30 in equation (4.25) allows to reproduce the experimental crack growth of such site. The reproduced (Yexp) and experimental fatigue crack growths (legend ending with exp.) are shown in figure 4.12 and a difference is clearly noticeable. In the same figure it is also shown the predicted fatigue life using Y N&R+DC+NSC in equation (4.25).

To verify that an appropriate number of intervals had been used in the Simpson's rule a different approach to reproduce the crack growth data was used. Using experimentally determined growth rates for the crack front the following approximation was made

$$\left(\frac{da}{dN}\right)_{\dot{a}} = \frac{a_{i+1} - a_i}{N_{i+1} - N_i} \tag{4.26}$$

so,

$$N_{i+1} = \frac{a_{i+1} - a_i}{\left(\frac{da}{dN}\right)_{\dot{a}}} + N_i \tag{4.27}$$

where

$$\dot{a} = \frac{a_{i+1} + a_i}{2} \tag{4.28}$$

The value of $\left(\frac{da}{dN}\right)_{\dot{a}}$ was determined from the smoothed experimental data. This crack growth reproduction (Yda/dN) from experimental crack growth rates was compared in figure 4.12 with the previous crack growth reproduction based on Y exp. Since both reproductions were similar, the integration of Paris law using Simpson's rule was considered valid.

Before predicting the fatigue life of specimen TB300003 it is worth remembering that this specimen was tested under the same nominal stress level of specimen TB300004 and both had a very similar weld toe radius however, the fatigue life of specimen TB300003 was larger, see figures 3.25 and 3.26. This situation was identified in chapter 3 as the effect of the shallower repair in specimen TB300003 (R4D6L60) causing a lower stress concentration at the repair ends compared with the repair in specimen TB300004 (R4D9L60). Prediction of fatigue life of specimen TB300003 using YN&R+DC+NSC in equation (4.25) gave the same prediction as for TB300004 since the same input values were used (nominal stress and a_i). Comparison of prediction versus experimental crack growth for specimen TB300003 is shown in figure 4.13.

It became evident from the results presented above that the T-butt as-welded stress distribution considered in the development of Y N&R+DC+NSC do not represent the case of repaired T-butts. Since the same stress distribution through the thickness is applied regardless of the repair dimensions.

Comparison of figures 4.12 and 4.13 show that using Y N&R+DC+NSC the effect of the repair on the scatter of the fatigue life predictions reduces as the repair depth (D) is reduced. The only difference in the repairs between specimens TB300004 and TB300003 is the repair depth for the former is D9 and D6 for the latter. The prediction that involves D6, see figure 4.13 is closer than the prediction with D9 , see figure 4.12. It is clear that a shallower repair has a more similar stress distribution through the thickness compared with the T-butt as-welded stress distribution used to develop YN&R+DC+NSC.

For fatigue life predictions of specimens TB300004 and TB300003 it is required to determine the stress distributions through the thickness from a finite element stress analysis and obtain a particular Yg for each specimen.

Since Y N&R+DC+NSC was developed using a T-butt as-welded stress distribution, fatigue life predictions using equation (4.25) were compared versus experimental crack growth obtained from as-welded specimens. The specimens considered were TB300001 and TB300002 and the experimental stress ranges used were 285 MPa and 238 MPa respectively. The fatigue life predictions versus the experimental crack growth is presented in figures 4.14 and 4.15. These predictions are very accurate considering the scatter in the experimental data in almost identical situations, see sites 30 and 130 for the same specimen in figures 4.12 and 4.13. Note that this predictions were made using a proposed design crack shape curve and not using the particular crack shape data of the specimens.

The procedure proposed for the fatigue life prediction of repaired T-butts was based on the determination of the fatigue life until the cracks at the repair ends join under the bottom of the repair, a = D (repair effect has disappeared). However, from a = D the stress distribution through the thickness is no longer affected by the repair geometry and YN&R+DC+NSC can be used as it has been presented in this section.

4.6 Extrapolation of Y factors to Tubular Joints

The repair procedure presented in this thesis was initially conceived for the repair of fatigue cracks in tubular welded joints like those used in the oil and gas offshore industry. So, extrapolation of the stress intensity calibration factor (Y) determined for fatigue crack repaired T-butt plates to tubular joints is required.

The extrapolation of Y from plates is a normal procedure for the determination of Y for tubular joints. In fact the majority of the theoretical Y equations for tubulars were developed from plates and then affected by a moment release procedure [4.19]. The moment release procedure is used to consider the so called load shedding effect present during crack growth in tubular joints, this effect is not present in crack growth of plates. The load shedding effect is based on the observation that in circular sections as the crack grows through the thickness, the bending moment decreases while the membrane force remains constant. Therefore, the bending stress has to be corrected by a reduction function known as moment release. Aaghaakouchak et al [4.19] proposed a linear moment release function to account for this effect

$$\sigma_b = \sigma_{bo}(1 - \frac{a}{T}) \tag{4.29}$$

where

σ_b bending stress at the crack tip

σ_{bo} bending stress at the surface

Including the expression (1-a/T) in the proposed Y N&R+DC+NSC for T-butts under bending provides a Y curve that could be applicable to the bending component of tubular joints. The proposed Y curves for bending for T-butts and tubular joints with weld geometries $\alpha = 45^0$ and $\rho/T = 0.05$ are shown in figure 4. 16. Note that a) for fatigue life prediction of repaired tubular joints Y N&R+DC+NSC has to be recalculated to consider the stress distribution through the thickness at the repair ends following the procedure described above and b) a proposed crack shape design curve based on T-butt fatigue experimental data was used during the development of YN&R+DC+NSC so, Y factors of non-repaired tubular joints have to be compared with Y factors shown in figure 4.5 to verify the procedure for tubular joints. However, as was mentioned in chapter 3, the crack shape evolution behaviour in T-butts appears to be similar to the crack shape behaviour found in tubular joints, see figure 3.33.

4.7 Discussion

Although, no experimental work was carried out on hammer peened specimens it can be infered from the experimental work on shot peened specimens that hammer peening is more suitable for offshore structures. This is based on the fact that with hammer peening a smooth grove at the weld toe can be obtained. Additionally, major benefits were observed when removing the weld defects at the weld toes by machining. Despite the fact that hammer peening does not remove the weld defects, the deformation produced on the surface can modify their shape. Reshape of weld defects at the weld toes may retard or eliminate growth of cracks already present. However, this needs to be verified experimentally.

Experimental Y values obtained for the specimens TB300 series are shown in figure 4.5. Specimens TB300001 and TB300002 were tested in an as-welded condition and TB300003 and TB300004 in a repaired condition. It can be seen that the effect of the notch is minimal since the as-welded and repaired specimen's Y values show very low scatter. However, the trend of the Y values obtained from the bottom of the repair is very different, see figure 4.5 specimen TB300003 at site 80. This trend is due to the absence of crack at site 80 until the cracks at both ends of the repair have joined.

It is clear that the stress distribution through the thickness used to determine NSC should be obtained considering the repair geometry. However, the use of a stress distribution through the thickness of a non repaired T-butt plate was intended to be assessed as it is a simpler calculation than a three dimensional finite element analysis of the repaired T-butt and allowed the identification of the methodology to follow.

When the cracks growing from the repair ends have joined under the repair bottom the stress distribution may be considered to be that of the as-welded condition. Thus, for fatigue life predictions of repaired T-butts (N for a = D) it is essential to determine the stress distribution at the repair ends through the thickness.

From the predictions made for the as-welded specimens it can be considered that the proposed design crack shape curve is not unrealistic and could be used for preliminary predictions.

4.8 Conclusions

It is essential to determine the stress distribution through the thickness at the repair ends of short repairs for the calculation of the Y factor for the fatigue life prediction of repaired connections. Short repairs induce crack initiation at the repair ends.

A crack shape design curve has been proposed for as-welded and repaired welded connections. This design curve when included in solutions to determine Y factors like the one proposed by Newman and Raju provides a reasonable correlation with Y empirical factors obtained from experimental testing of welded T-butts. However, low scatter in Y factors does not mean low scatter in fatigue life predictions.

4.9 References

[4.1] BS PD 6493: 1991, *Guidance on Methods for Assessing the Acceptability of Flaws in Welded Structures*, British Standards Institution, London 1991.

[4.2] *ISO TC67/SC7/WG3/P3*, Technical core group joints, Draft code provisions Revision R4, Section F Fatigue strength of connections, December 1997.

[4.3] *ICON User Group Meeting,* University College London, May 1998.

[4.4] H.F. Bueckner, "A novel principle for the computation of stress intensity factors", *Math. Mech.* 1970, 50, 529.

[4.5] J. R. Rice, "Some remarks on elastic crack tip stress fields"*, Int. J. Solids Structures*, 8, 751, 1972.

[4.6] X. R. Wu and A. J. Carlsson, *Weight Functions and Stress Intensity Factor Solutions*, Pergamon Press, 1991

[4.7] P. W. Tan, I.S. Raju, and J. C. Newman, "Boundary force method for analyzing two dimensional cracked bodies", *NASA TM-87725*, 1986.

[4.8] H. Nisitani, "Solutions of notch problems by body force method", *Mechanics of Fracture 5*, Stress Analysis of Notch Problems, Ed. G. C., Sih, Noordhoff Int. Publishing, Leyden, 1973.

[4.9] N.A. Noda and H. Nisitani, "Stress concentration of a strip with a single edge notch", *Engng. Fract. Mech.* 1987, 28, 223.

[4.10] F.G. Maunsell, "Stress in a notched plate under tension", *Phil. Magazine* 1936, 21, series 7, 765.

[4.11] J. C. Newman and I. S. Raju, "An Empirical Stress Intensity Factor Equation for the Surface Crack", *Engineering Fracture Mechanics*, Vol. 15, No. 1-2, 1981.

[4.12] B. Gross and J.E. Srawley, "Stress intensity factors for a single edge notch specimen in bending or combined bending and tension by boundary collocation of a stress function". *NASA TN D-2603*, 1965.

[4.13] C.C. Monahan, "Early Fatigue Crack Growth at Welds", *Computational*

Mechanics Publications, Vol.26, Brebbia C.A. and Connor J.J Eds., 1995, pp. 48.

[4.14] P. Albrecht and K. Yamada, "Rapid Calculation of Stress Intensity Factors", *Journal of the Structural Division,* 1977.

[4.15] H. Tada, P. Paris and G.R. Irwin, *"The Stress Analysis of Cracks Handbook"*, Del Research Corporation, Hellertown, Pa., 1973.

[4.16] UKORSP, *United Kingdom Offshore Steels Research Project*, Final Report to the European Coal and Steel Community, 1979.

[4.17] J.A.Bannantine, J.J. Comer, J.L. Handrock, *Fundamentals of Metal Fatigue Analysis*, Prentice Hall, 1990.

[4.18] E. Kreyszig, *Advanced Engineering Mathematics*, John Wiley, 1983.

[4.19] A.A. Aaghaakouchack, G. Glinka and S. Dharmavasan, "A load shedding model for fracture mechanics analysis of fatigue cracks in tubular joints," *OMAE 89 Conference*, The Hague, Netherlands, 1989.

[4.20] X. Niu and G. Glinka, "The weld profile effect on stress intensity factors in weldments", *International Journal of Fatigue,* Vol. 35, pp3-20, 1987.

Figures

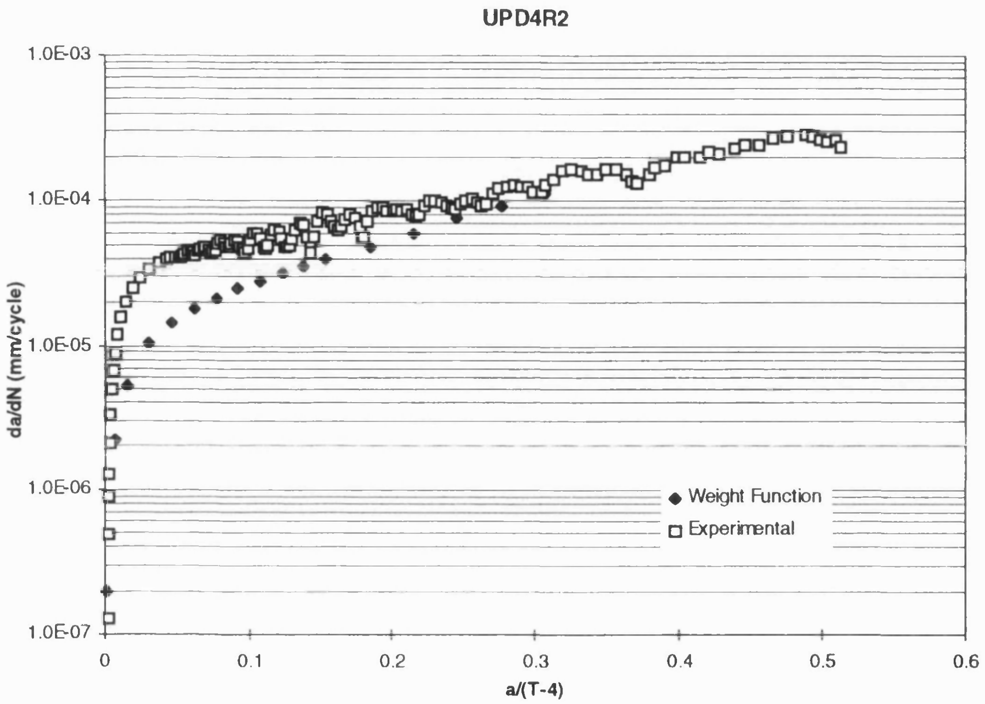

Figure 4.1 Crack growth rate versus a/T for specimen UPD4R2

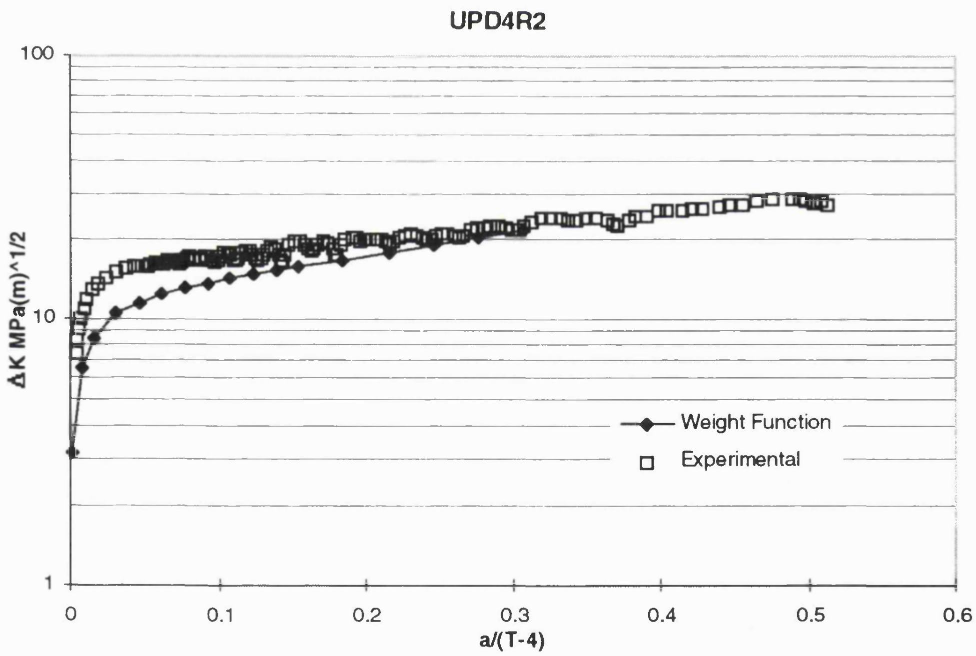

Figure 4.2 Stress intensity factor range versus a/T for specimen UPD4R2

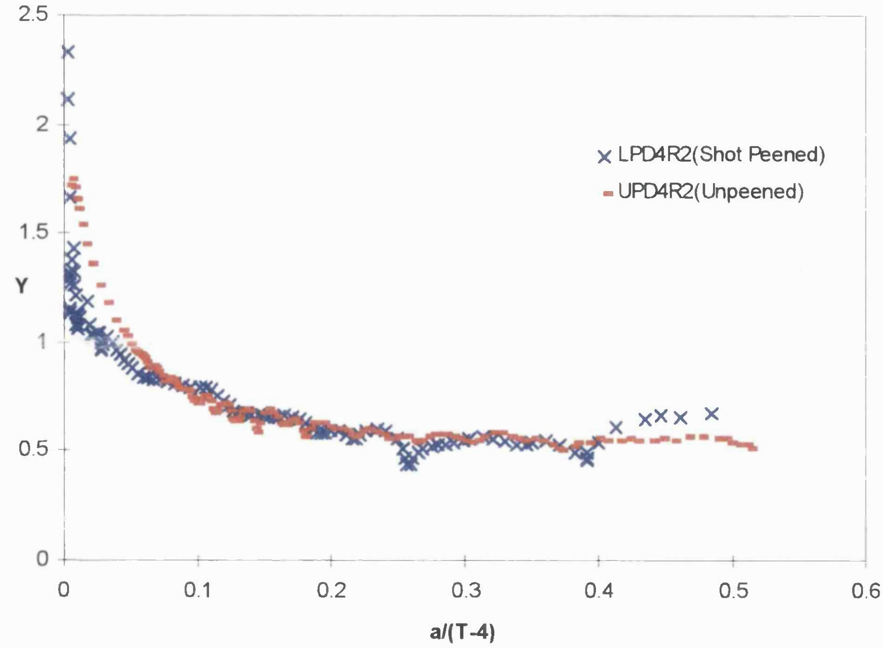

Figure 4.3 Experimentally determined Y factors versus a/T for edge repaired specimens UPD4R2 and LPD4R2

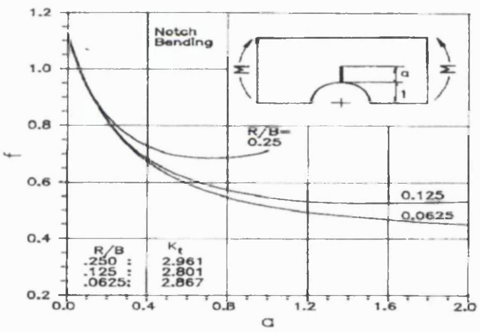

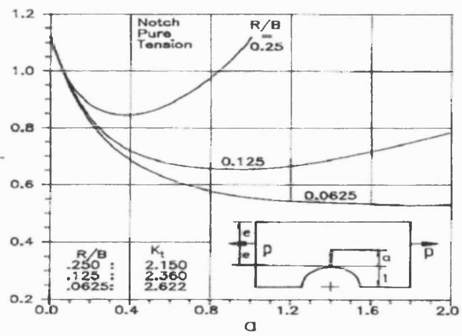

Figure 4.4 Y factors (denoted as f) for an edge crack at a semi-circular notch in an infinite plate subjected to: in plane bending (top) and pure tension (bottom), R is notch radius and B is plate thickness, [4.5].

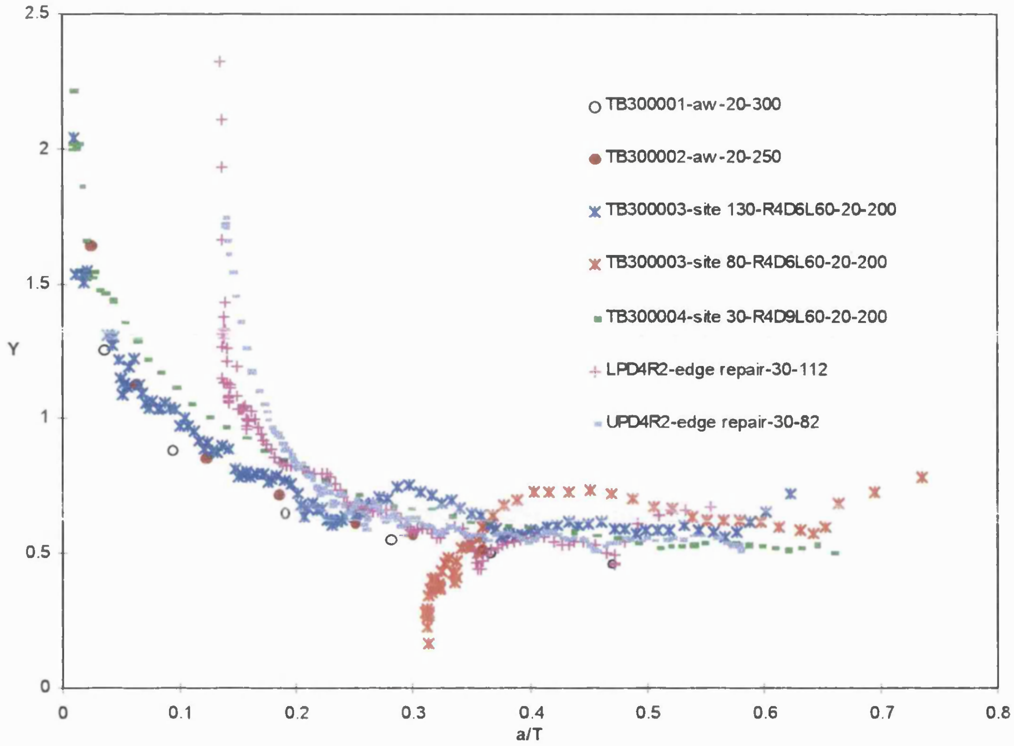

Figure 4.5 Comparison of experimental Y factors for specimens TB300 and edge repaired

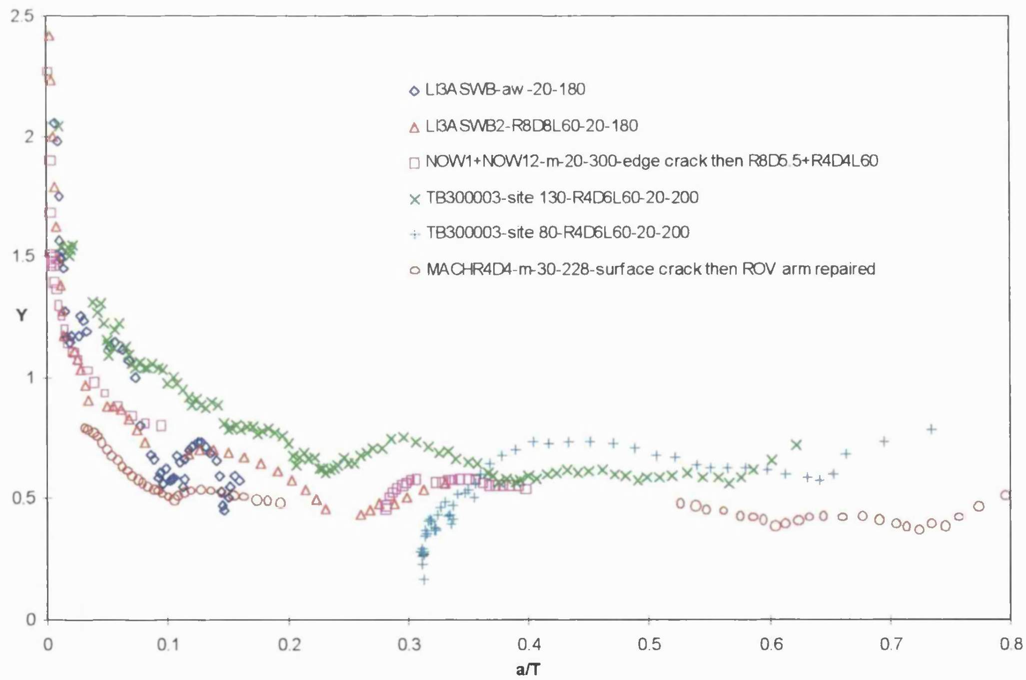

Figure 4.6 Comparison of experimental Y factors solution for various repaired specimens

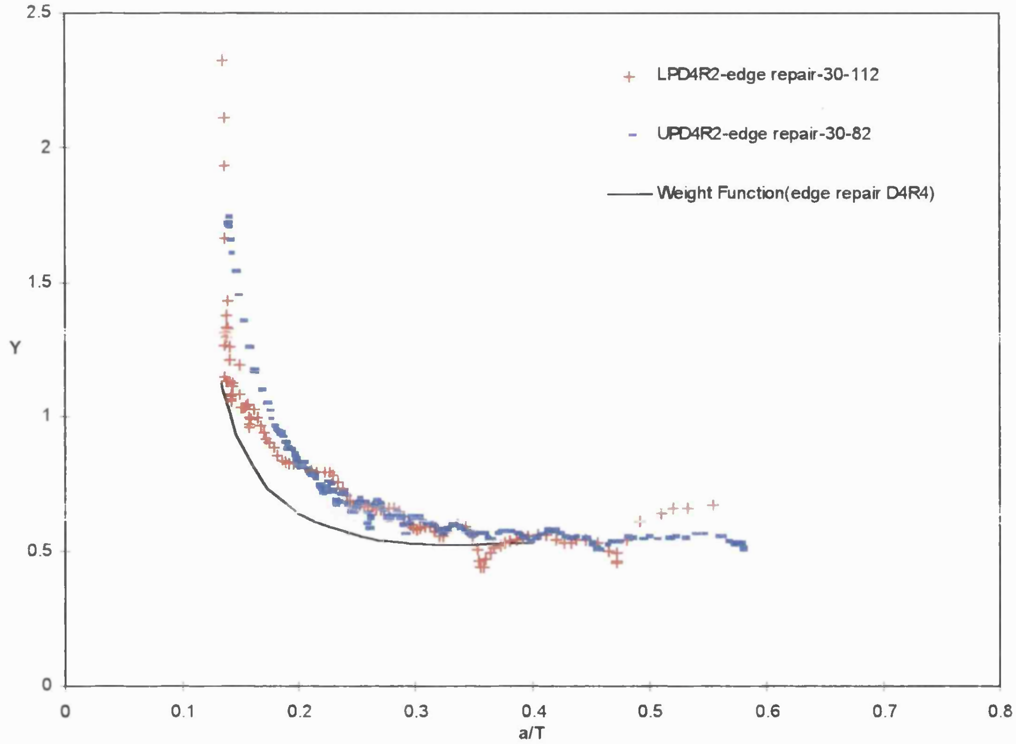

Figure 4.7 Comparison of experimental Y factors of edge repaired specimens versus weight function solution

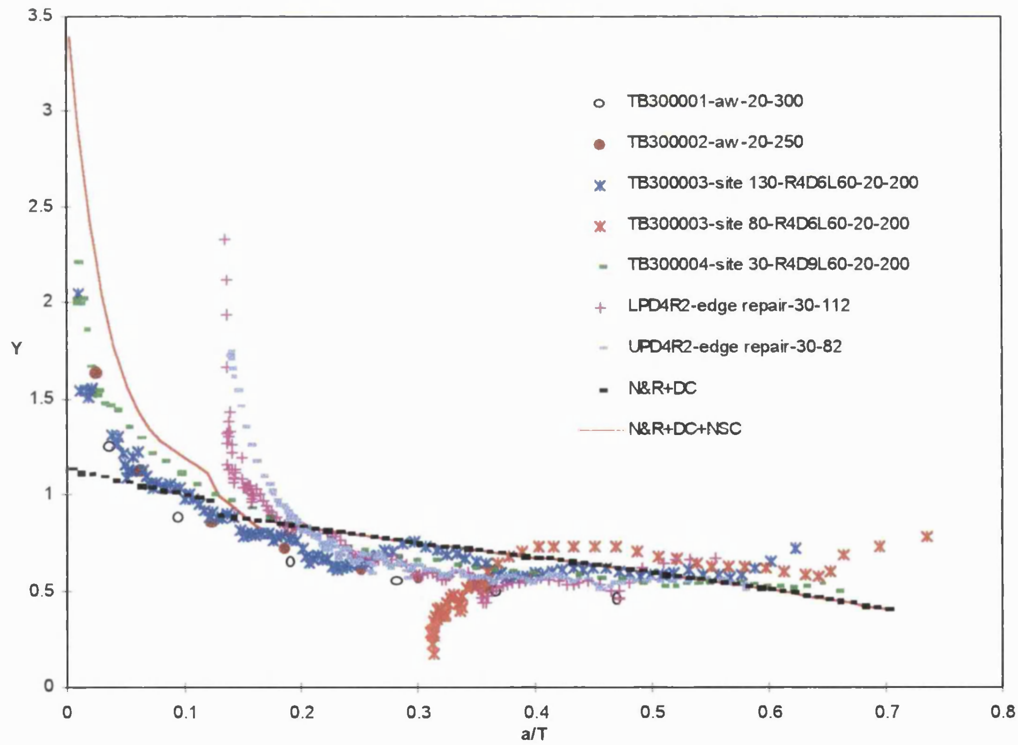

Figure 4.8 Comparison of experimental Y factors versus corrected Newman&Raju solution (specimens TB300 and edge repaired)

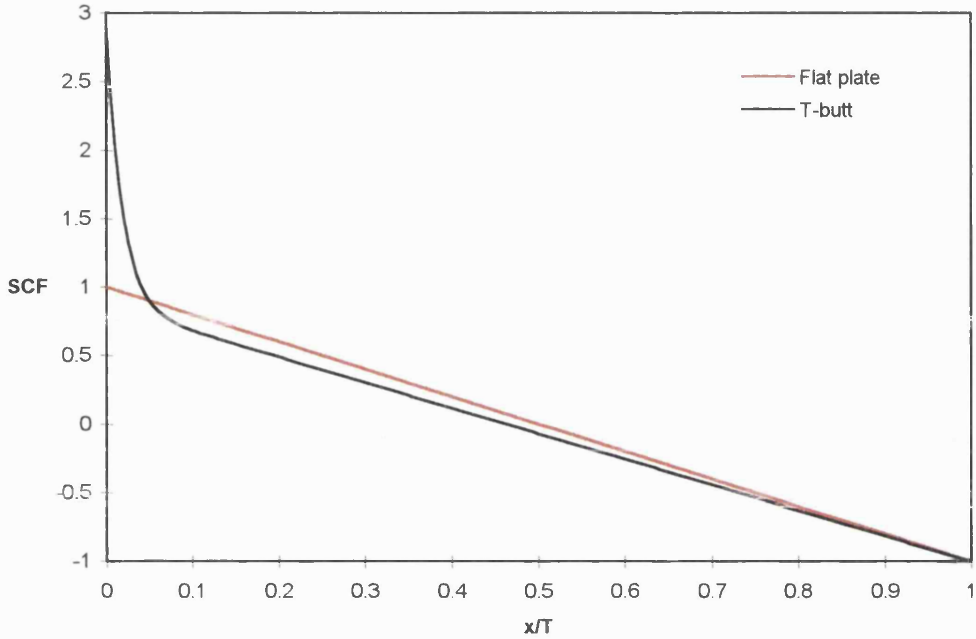

Figure 4.9 Weld influence on the stress distribution in a T-butt under bending ($\alpha=45^0$ and $\rho/T=0.05$)

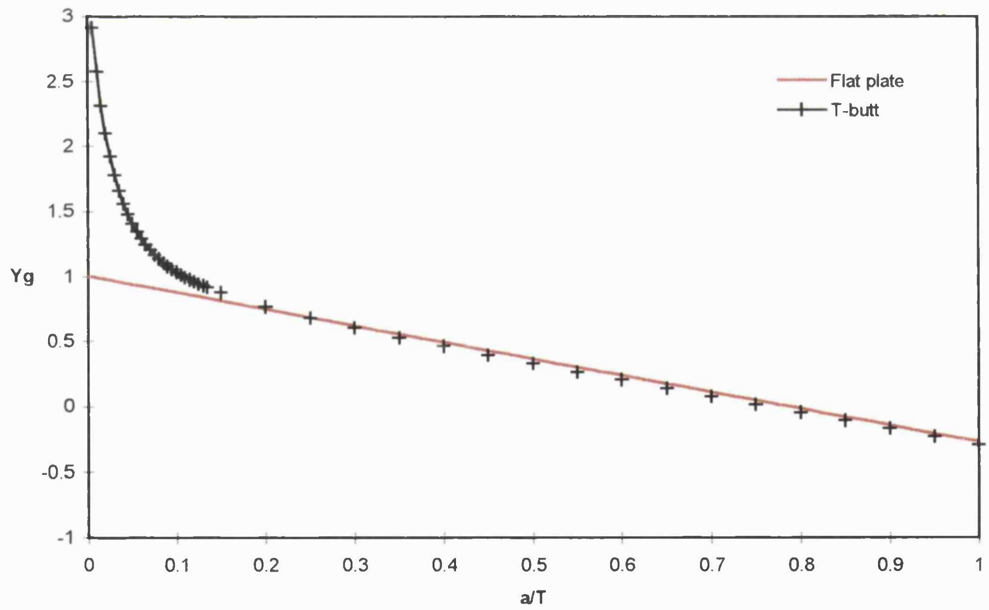

Figure 4.10 Weld influence on the Y factor in a T-butt under bending ($\alpha=45^0$ and $\rho/T=0.05$)

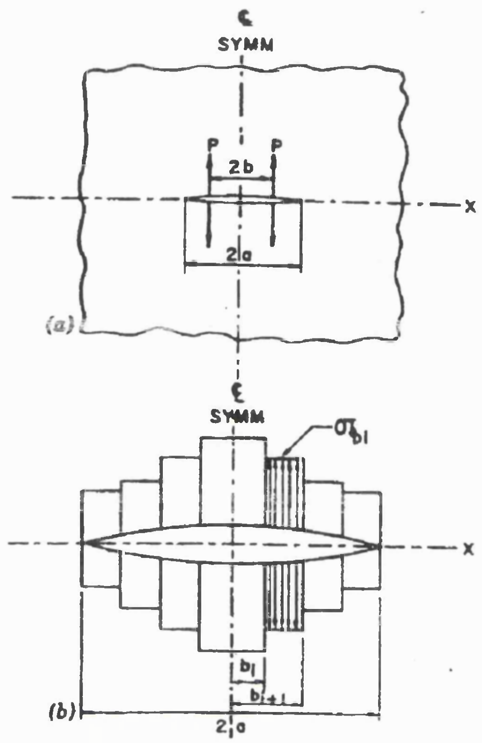

Figure 4.11 Crack in infinite plate under (a) Two pairs of equal splitting forces and (b)Pairs of discrete stresses [4.13]

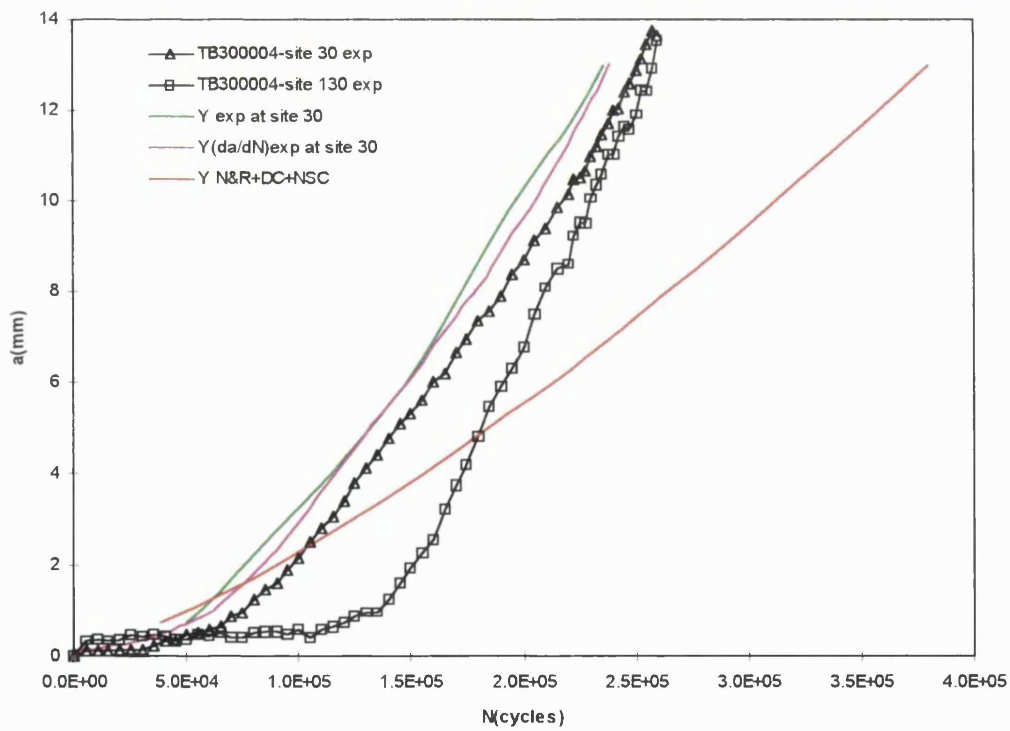

Figure 4.12 Experimental, reproduced and predicted crack growth curves for specimen TB300004 (R4D9L60) at the repair ends (sites 30 and 130)

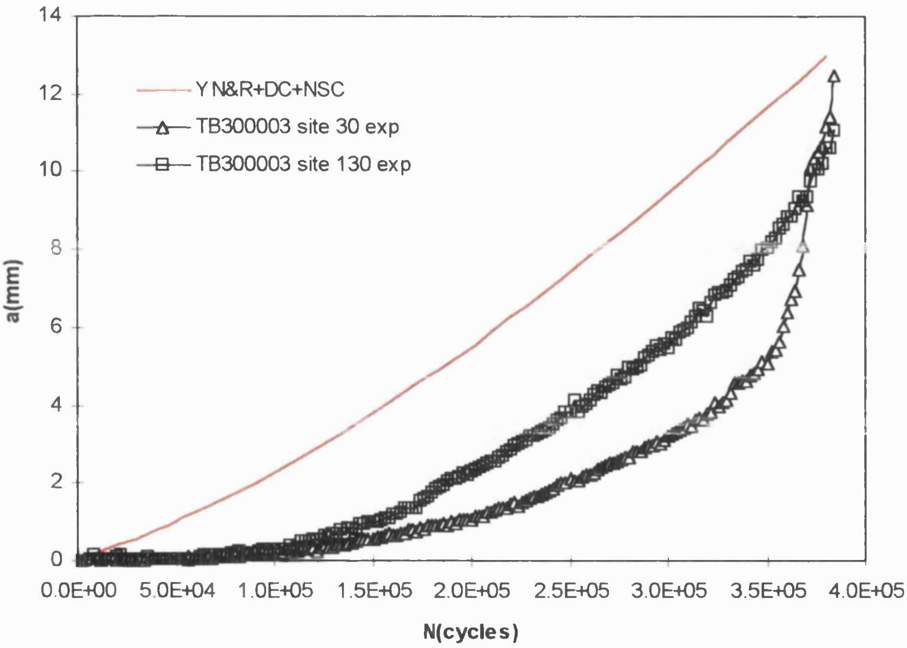

Figure 4.13 Experimental and predicted crack growth curves for specimen TB300003(R4D6L60) at the repair ends (sites 30 and 130)

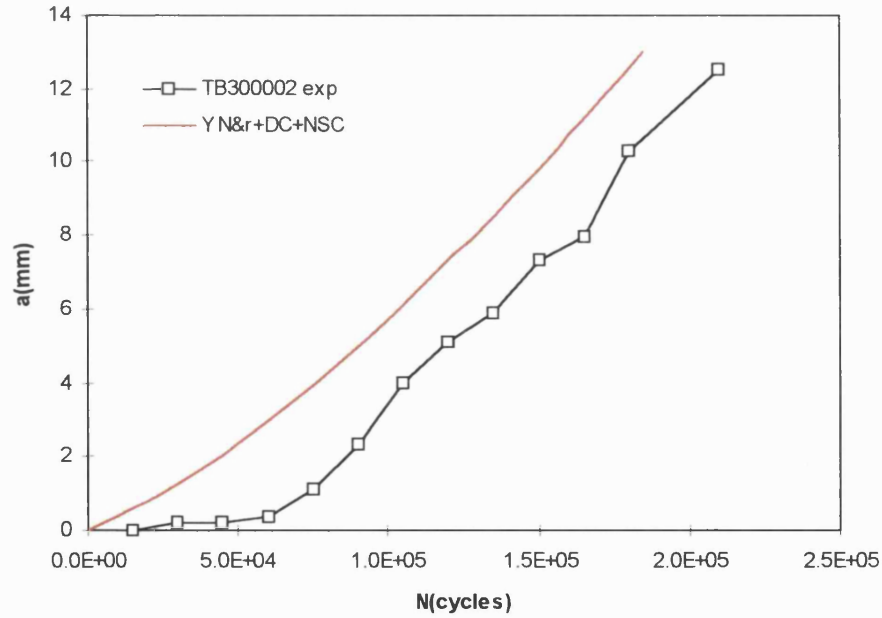

Figure 4.14 Experimental and predicted crack growth curves for specimen TB300002 at the deepest crack point

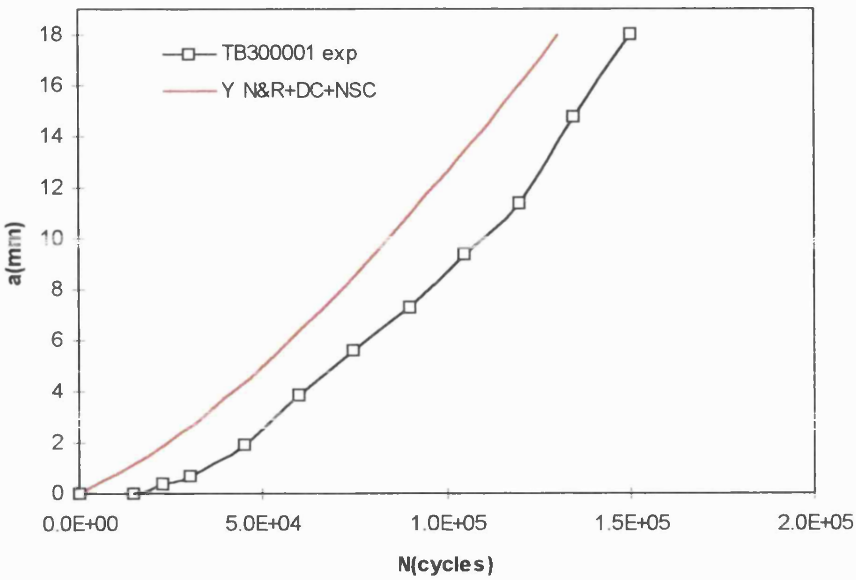

Figure 4. 15 Experimental and predicted crack growth curves for specimen TB300001 at the deepest crack point

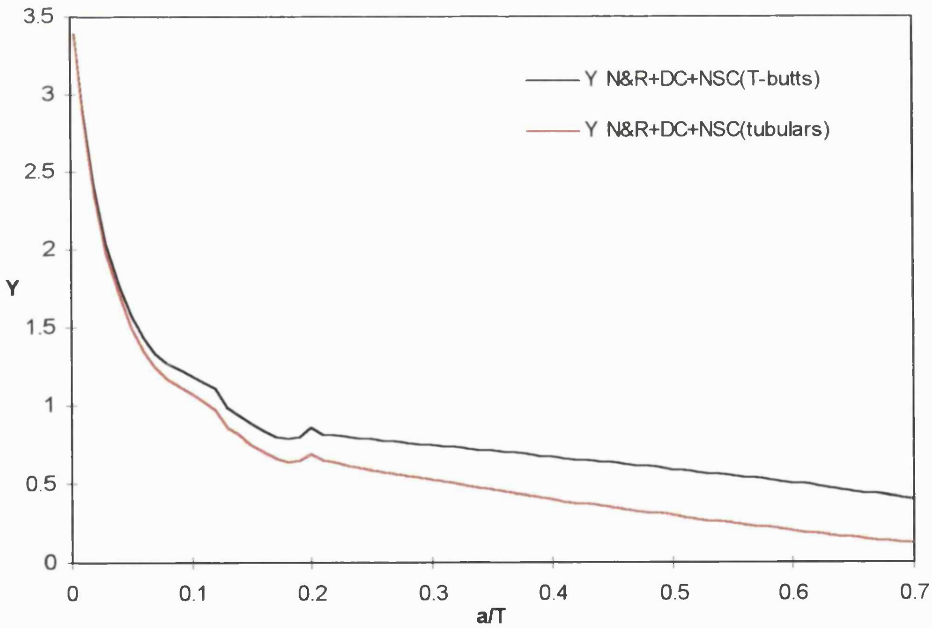

Figure 4.16 Proposed Y curves for bending for T-butts and tubular joints with weld geometries $\alpha = 45^{0}$ and $\rho/T = 0.05$

CHAPTER FIVE

REPAIR AND INSPECTION OF SEVERELY CRACKED TUBULAR OFFSHORE STRUCTURES

5.1 Introduction

Fatigue crack repair by removing the crack preferably with a short repair profile as presented in chapter 2 can only be applied to cracks before they reach advanced stages of growth. An alternative option to repair severely cracked components is cutting out the crack using an almost edge repair. However, depending on the crack depth, this could be inefficient since the repair depth required may be large leading to a high stress concentration with a short initiation life and fast propagation, as was observed in the experimental results presented in chapter 3. From the experimental results obtained in this work, the severely cracked state in T-butt welded joints can be identified when the remaining uncracked thickness is less than 40% of the original thickness.

Predictions of the remaining fatigue life after repair are required to schedule inspection of the repair. The inspection data can be used to update the fatigue life predictions and so forth.

Crack repair by mechanical strengthening is recommended for severely cracked components. For the case of tubular joints the mechanical strengthening is achieved by the use of clamps formed from two or more segments held together by long threaded studs. Clamps rely on the friction between the tubular member and the clamp to provide the load path. The clamping force between the clamp segments and the tubular member provided by the studs has to remain within certain limits so, that the load path is provided. This situation means there is a requirement to inspect the studs regularly and determine the axial load carried on each one. A novel application of the Alternating Current Stress Measurement (ACSM) technique for load determination on clamp studs and assessment of the technique on a underwater full scale clamp trial using an ROV arm manipulator is presented in this chapter.

5.2 Repair by Mechanical Strengthening

For the repair of a severely cracked offshore tubular joints it is necessary to provide an alternative parallel load path between the chord and brace. This can be achieved by placing a clamp around the cracked joint. Clamps can sit directly on the joint or can sit on cementitious material injected in the annular space between clamp and joint before or after tensioning the studs. The former type of clamp is called mechanical clamp and the latter ones grouted and stress grouted clamps respectively. This chapter will only consider the case of mechanical clamps since the intention is to give relevance to the measurement of axial loads on studs using the ACSM technique rather than the study of clamps. Extensive design data for the design of clamps can be obtained from reference [5.1].

5.2.1 Mechanical Clamps

A mechanical clamp can be used to strengthen an existing tubular joint. It is formed in two or more segments which are placed around the tubular joint. The segments are clamped together to provide a load path between the clamp and the joint. The clamping forces are induced by long studs reacting against widely spaced flanges welded to the clamp.

This type of clamp is quicker to fabricate and install than an equivalent stressed grouted clamp. However, a precise survey of the joint is required before the fabrication. Possible reasons that could lead to the application of clamps or other repair techniques are: fatigue, increased code requirements, ship impacts and impact by debris.

Mechanical clamps can also be used for not to strengthen but to hold attachments required after the installation of the structure such as anodes, bumpers, equipment for monitoring etc. This type of clamp is not commonly placed around a joint but on a straight tubular member. Figure 5.1 shows the mechanical clamp used during the trials described in this chapter. The clamp was used to hold an anode from a straight member thus, does not have the geometry of a tubular joint. However, for the purposes of measuring loads on studs it is equally representative of a mechanical clamp for strengthening a tubular joint.

The strength of a mechanical clamp is obtained from the steel to steel friction which is developed by means of the stressed studs applying a normal compressive force on the tubular joint/clamp interface. Therefore, the strength obtained is dependent on the magnitude of the normal force and the coefficient of friction between the two contact surfaces [5.1].

The segments of a mechanical clamp react against a chord or a chord and brace for the case of a clamp for a joint. The chord and brace have a relative flexibility under the pressure of the clamp. Thus, fluctuating hoop stresses on chord and brace due to external forces reduce the clamp contact pressure and can cause fluctuating strains in the stud-bolts. Increasing the stud-bolts length reduces the magnitude of the strain for a given change in diameter of the chord and hence reduces the possibility of the nuts loosening and stud-bolt fatigue damage [5.1]. For the reason explained above it is necessary to use continuous top plates to employ long stud-bolts rather than discontinuous top plates, see figure 5.2.

There was no data available on load attenuation of stud-bolts in mechanical clamps when the Joint Industry Repairs Research Project (JIRRP) concluded in 1984, (JIRRP is reported in reference [5.1]). A literature search did not reveal any other study of load attenuation of stud-bolts in mechanical clamps.

Results from tests on stressed grouted clamps suggest that observed losses were due entirely to grout shrinkage and therefore it is expected that losses in mechanical clamps will be minimal [5.1]. A clamp has to be designed to be stiff since this reduces the stud-bolt load fluctuations minimising the possibility of fatigue in the clamp.

The calculation of stud-bolt load is based on the knowledge of the forces and moments resolved into those terms which require friction for their transfer and those which do not. Figure 5.3 illustrates load components for the design of a mechanical clamp for a T-joint.

5.2.2 Stud-bolt Load Attenuation

Losses in stud bolts of mechanical clamps can be divided into two categories [5.1]:

I. Short term losses. This are caused by bedding down of threads and top plate bending.
II. Long term losses. This are caused by relaxation and as mentioned above, they were found to be minimal.

Losses due to bedding down can be reduced by repeated stud-bolt stressing until the nut does not break free from the clamp to plate under the applied jack load. Losses due to plate bending occur at transfer load from the reaction nut sitting on the jack (stiff), to the nut sitting on the clamp top plate (flexible compared with the jack). The losses due to top plate bending can be minimised by using stiff top plates or thick washers. It is considered that the use of two spherical thick washers reduces entirely the loss due to top plate bending.

Additionally, spherical washers are recommended in conjunction with long stud-bolts as misalignment and angular tolerances of stressed flanges can result in large bending stresses. However, spherical washers only take out initial tolerances prior to loading. Once the stud-bolt is loaded, friction prevents the washer from rotating.

The JIRRP reported that a 10% excess pre-load is adequate to account for the effects of relaxation on mechanical clamps. For the case of stressed grouted clamps, grout shrinkage is an additional cause for loosing stud-bolt load. The

JIRRP also reported that load lost was approximately 5%, and after one month of grouting it is expected that minimum or no further grout shrinkage occurs. Therefore, it is likely that re-tensioning the stud-bolts of stressed grouted clamps after a one year period will reduce subsequent losses to a negligible amount.

5.3 Inspection of Clamps

After a clamp has been installed it has to be inspected according to the inspection philosophy used by the operator. This is to ensure that the clamp performs in a satisfactory manner. All available levels of inspection ranging from visual to MPI, ultrasonic thickness measurement and crack depth measurement using the ACFM technique may be involved.

5.3.1 Inspection of Stud-bolt Load Attenuation

It is clear that a procedure for verifying the load level on stud-bolts by releasing the load and re-tightening is not recommended since the short term losses described above could reoccur. Additionally, the level of corrosion and marine growth may impede the use of the same studs for re-tightening. There is also the possibility that the stud-bolt load was within acceptable limits and the operation was not required. This might result in considerable unnecessary costs considering the high costs involved in underwater operations

Stud-bolt load measurement is a specialist application and there is little commercial equipment available to perform this task underwater. Therefore, the verification of the load level on stud-bolts has been always left to the judgement of an inspection engineer who typically uses sometimes unscientific methods for this purpose. The procedures vary in complexity but the simplest one reported is hitting the stud-bolt with a spanner to judge the tightness from the sound emitted, this practice is totally unreliable.

In the following sections the ACSM technique for measuring stress on stud-bolts and the application of the technique in a underwater full scale clamp trial using an ROV arm manipulator are presented.

5.4 The ACSM Technique for Measuring Load on Clamp Studs

It has been observed when using the ACPD technique that noticeable variations of the reference voltage are obtained when readings are taken under different stress levels. For this reason the specimens were scanned under mean stress for crack sizing as was described in chapter 3. For the case of the Alternating Current Field Measurement (ACFM) technique which is the non-contacting version of ACPD, variations of the B_x signal have also been observed under different stress levels. The B_x signal is one of the three signals (B_x, B_y and B_z) used for crack detection and sizing during crack inspection. Therefore, the possibility of adapting the ACFM technique for obtaining a non-contacting stress measurement technique was considered and developed by TSC Ltd. and the UCL NDE Centre. The new technique for stress measurement is known as Alternating Current Stress Measurement (ACSM). In the following sections laboratory experiments during the validation of the ACSM technique and full scale trials are reported.

5.4.1 ACSM Background

The ACSM technique is based on the physical phenomenon known as magnetostriction. This is the spontaneous strain caused by the alignment of atomic magnetic moments within magnetically orderd regions called domains. In a ferromagnetic material, domains are separated from each other by walls. Each domain has a direction of magnetisation rotated 180^0 and 90^0 with respect to each other. The net magnetisation is the resultant of all the domains. Domain directions in a ferromagnetic material can change due to the effect of a magnetic field or mechanical stress.

So, the measurement of magnetisation of a ferromagnetic surface can be related to the measurement of stress. This method of stress measurement is known as inverse magnetostriction. The measurement of magnetisation is generally carried out with alternating magnetic fields of constant amplitude. The relation between magnetic field and magnetisation is given by:

$$M = \mu H \tag{5.1}$$

where

H magnetic field

M magnetisation

μ permeability

For a constant magnetic field or applied stress the magnetisation becomes proportional to the permeability [5.2]. Permeability is a material property that relates the disposition of being magnetised. Measurement of magnetisation caused by stress under low magnetic fields can provide different values under the same stress depending if readings were taken during loading or unloading. This stress hysteresis can be overcome when stress measurements are taken after demagnetisation [5.3].

Chen and Brennan [5.4] experimenting on the inverse magnetostriction effect induced a low alternating magnetic field near the surface of a loaded mild steel specimen and then picked up the influences of applied stresses on that field using the ACFM equipment supplied by TSC Ltd. [5.5]. Additionally, a mathematical model of half-space electromagnetic induction [5.6] was combined with previously published fundamental relationships between stress and magnetisation giving a new model that allowed the interpretation of a relation between the ACFM readings and the applied stresses obtained from the tests. This confirmed that the ACFM technology can be further developed into an ACSM technique.

5.4.2 ACSM Determination of Load on Clamp Studs

The application of the ACSM technique for the measurement of load level on clamp studs relies on the stress measurement at the stud surface. Then, assuming that the stress distribution is uniform across the stud section and knowing the stud cross section area, the load can be determined.

Although the ACFM technique requires no calibration, the ACSM technique for stress measurement does. Therefore, it is currently not possible to determine the stress level at a point on a stud surface without making reference to a unstressed second point on the same stud. This can be overcome by measuring an unstressed point between the stud ends and the nuts. However, it has to be noted that both readings should be taken under the same conditions of stud surface, i.e. threaded or plain surface.

5.5 ROV ACSM Trials on a Full Scale Clamp

Underwater ROV arms are very capable when used for pick and place operations. Therefore, ACSM was identified as a suitable technique to be deployed by an ROV arm since during the inspection, the probe only needs to be placed, held in position and removed. Hence, ACSM was considered in the European project Evaluation of Diverless IRM for subsea Completions and deepsea Structures (EDICS) [5.7]. The following sections describe the ACSM inspection trial conducted at IFREMER testing tank in Brest, France on the 11th December, 1997 on a full scale anode clamp at 20m water depth.

5.5.1 Description of Clamp and Trials

A anode clamp formed in two segments was obtained from Elf UK and although, this clamp was not used for mechanical strengthening of a severely cracked tubular joint, the studs are tightened and held in a same manner. Figure 5.1 illustrates the clamp geometry with dimensions in millimetres and the holes where the studs were inserted.

The clamp was designed to use one inch diameter studs but in order to investigate other diameter sizes 1.125" diameter studs were used for the trial. The ends of all the studs were machined down to 1" to fit the clamp holes and threaded to fit the hydraulic tensioning puller jacks supplied by Hydra-Tight Limited. The studs were made from BS970 EN 19T steel. Mechanical properties are given in table 5.1.

In practice the six studs are tensioned at the same time however, the trial was designed to maintain a constant load in the four corner studs while the two middle studs were tensioned and released to test the recording of stress. This prevented the possibility of the clamp moving. In laboratory conditions at the UCL NDE Centre during the system check, the four corner studs were tensioned injecting 900 Bar of oil pressure in the hydraulic jacks, then the nuts were tightened and the two middle studs were loaded and unloaded in steps in the range 0 Bar - 700 Bar - 0 Bar. After checking, the tube with the clamp fitted on it were mounted on I-beams and transported to IFREMER.

At IFREMER the arrangement of clamp, tube, studs, hydraulic jacks and I-beam supports was mounted on a test rig that simulated a section of an offshore tubular structure, see figure 5.4. The studs shown in the previous figure can be labelled as top, middle and bottom. The four corner bars were tensioned to 900 Bars and then the pressure hoses were connected only to the middle hydraulic jacks. The new arrangement was installed in the tank at 20 metres water depth. A Stolt Comex Seaways ROV and Cybernetix arm were used for the ACSM inspection, figure 5.5 shows the ROV being launched into the tank holding the ACSM probe. A close view of the Cybernetix arm and the ACSM probe is shown in figure 5.6.

The ROV was driven to the test rig assisted with fixed cameras mounted on the front and with an additional eye ball camera which could be positioned as required, this camera proved invaluable during docking operations. The Cybernetix arm deployed the ACSM probe on the centre stud. The ACSM probe had installed proximity sensors to assist the arm operator to position the probe correctly on the bar. Stress measurements were collected after demagnetising for various loading steps up to 800 Bar and downloading to 0 Bar. Figure 5.7 shows the TSC U9 topside unit under the portable PC, beside it is the demagnetising unit and at the right end is the power supply unit. The empty socket on the demagnetising unit is to connect the ACSM probe.

To verify the dexterity of positioning the ACSM probe, it was located on the top, middle and bottom studs in sequence. It was found that taking stress measurements for load and unload conditions was possible and without any difficulty. To determine the effect of wave loading on the system a wave generator was used to cause movement on the ROV. The Cybernetix arm was not affected during placing the probe on the studs under wave loading and stress measurements were successfully taken on the middle stud. A complete report of the trial can be found in reference [5.8]

5.5.2 ACSM Data analysis

The data collected during the trial consisted of ACSM readings and oil pressure injected to the hydraulic jacks. The load applied by each jack was determined by the product P x Ap where P is the applied pressure and Ap is the area of the jack piston. The stress on each stud was determined by (P x Ap)/As where As is the cross sectional area of the stud. Figure 5.8 shows the percentage change of the ACSM readings obtained in the trial for the centre stud versus stress.

In order to continue with the assessment of the ACSM technique for stress measurement the clamp, tube, studs and hydraulic jacks were brought back to the UCL NDE Centre. An exhaustive study under laboratory conditions was undertaken in which the ACSM results were compared against stresses calculated from a strain analysis using electrical resistance strain gauges. The ACSM readings obtained in the EDICS trial were reproduced and confirmation was made that the underwater conditions and ROV arm deployment do not affect results.

The additional study looked for example at probe positioning accuracy. This showed that a forty percent loss in sensitivity (percent change in Bx per MPa) can be expected with a probe inclined at 2.5 degrees and ten percent with a probe inclined at 0.5 degrees to the surface of the stud [5.9]. The result demonstrated the importance of the proximity sensors fitted for probe positioning. The study also provided information about the importance of using appropriate ACSM probes since a probe with good sensitivity on unthreaded regions may not be sensitive on threads. ACSM of threaded regions requires the increase of the demagnetisation current to take account of the lift off from the stressed core of the stud.

5.6 Discussion

The problem of load attenuation within studs is more relevant in stress grouted clamps than in mechanical clamps due to the grout shrinkage. So, the application of the ACSM technique is more recommended in the former case and for the later case a small excess pre-load may be applied to compensate for the minimal loss of load attenuation in stud-bolts. However, in both cases an independent measure of stress/load would be an extremely valuable quality check.

For the application of the ACSM technique there is no need to remove coatings and only severe marine fouling should be removed from the studs for stress measurement. However, as in the case of threads an increase in demagnetisation may be required to take into account the probe lift-off.

The TSC Ltd. ACSM probe manufactured for the EDICS trial showed low sensitivity on threaded regions, see reference [5.9], thus a new probe was manufactured for that purpose. The new probe applied stronger demagnetisation and showed more sensitivity measuring stresses on the threaded regions, however when used on unthreaded regions showed lower sensitivity than the probe used in the EDICS trial.

Due to the sensitivity of the ASCM technique for a particular setting (probe, leads, temperature, material, etc.) comparison of the readings obtained currently has to be made in absolute terms for various locations and subsequent inspections.

5.7 Conclusions

Structural safety of severely cracked tubular joints of offshore structures relies on the application of mechanical strengthening methods such as clamps. The clamp is only efficient as a strengthening method if the studs are tensioned with the designed load. However, no stud load measurement instrument is commonly available in the offshore industry. This important offshore inspection deficiency could be addressed with the application of the ACSM technique for load measurement.

It has been demonstrated that the ACSM technique can provide a reliable estimation of the stress in uni-axially loaded circular studs in laboratory and field conditions. The measured stresses have to be interpreted with care since the system is sensitive to the particular settings present during the inspection. The practical application of the technique to underwater conditions is novel thus, it can be upgraded and its application extended to other structural members.

5.8 References

[5.1] Wimpey Offshore Engineers & Constructors Ltd., "Grouted and Mechanical Strengthening and Repair of Tubular Steel Offshore Structures", *Offshore Technology Report, UK Department of Energy,* OTH 88 283, 1988.

[5.2] A. Yoshinaga, "Study on the measurement of the residual stress by the magnetostriction method", Ship Res. Inst. Rep., Vol. 17, 1979.

[5.3] S. Tiitto, "Magnetic methods". *Handbook of Measurement of Residual Stress*, Society of Experimental Mechanics, Bethel, Pennsylvania., Chapter 8, 1996.

[5.4] K. Chen and F.P. Brennan, "A theoretical and experimental study of alternating current stress measurement under different loading modes", *Journal of Strain Analysis*, Vol. 33, No. 4, 1998.

[5.5] TSC Ltd., "Technical Software Consultants", 6 Mill Square, Featherstone Road, Wolverton Mill, Milton Keynes, MK12 5RB, England, UK.

[5.6] J. Zhou, R. Collins and D.H. Michael, "Half space induction by a rectangular coil with rounded corners: local uniformity and ACFM", *Rev. Prog. in Quantitative Non-destructive Evaluation*, Vol. 13, 1994.

[5.7] EDICS, "Evaluation of Diverless IRM for subsea Completions and deepsea Structures project", Cibernetix, Doris Engineering, General Robotics Ltd, IFREMER, Stolt Comex Seaway, Technical Software Consultants, University College London, *Final Technical Report,* UK September 1998.

[5.8] W. D. Dover, J.E. Rodriguez, K. Chen, J. Zhou and R.F. Kare, "ACSM Trials on an Anode Clamp", *EDICS,* UCL NDE Centre, January 1998.

[5.9] F.P. Brennan, "A Laboratory Assessment of the TSC Ltd. Anode Clamp ACSM System", *NDE Centre* (internal report), September 1998.

Tables

	Heat Treatment	σ_y (MPa)	σ_{UTS} (MPa)	% EL	HB
BS970EN 19T	Q&T	800	940	15	305

Table 5.1 Mechanical Properties of BS970 EN 19T steel

Figures

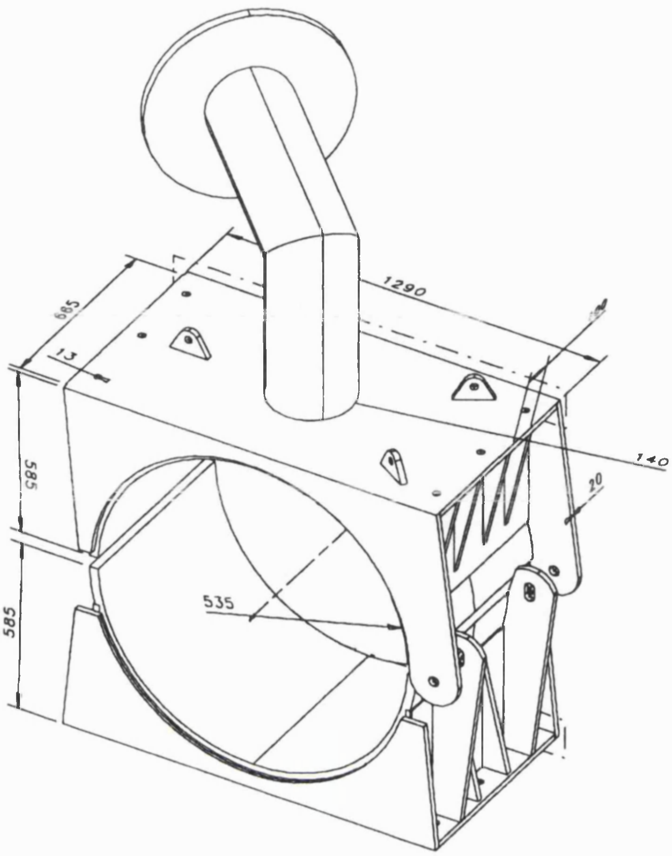

Figure 5.1 Anode clamp used in the EDICS Trials, studs are not shown. [5.8]

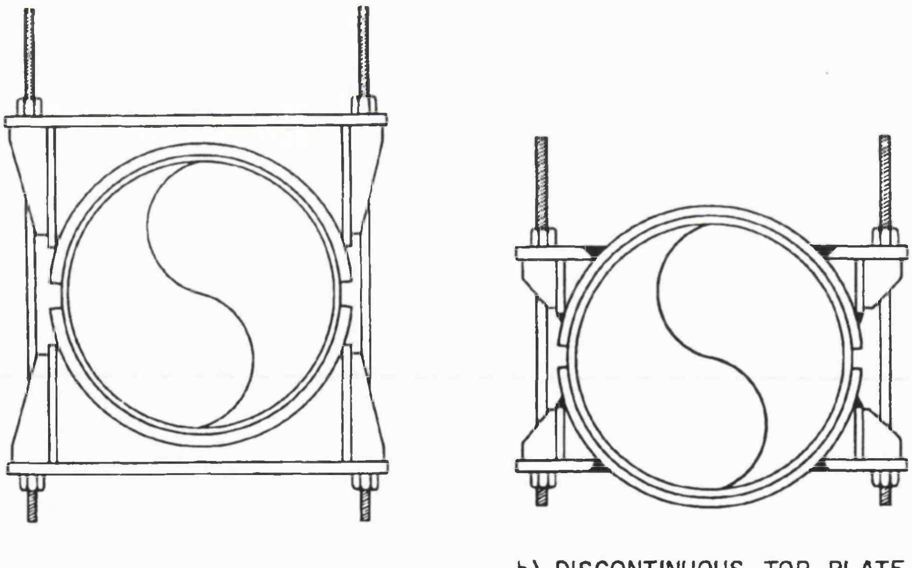

Figure 5.2 Types of mechanical clamps [5.1]

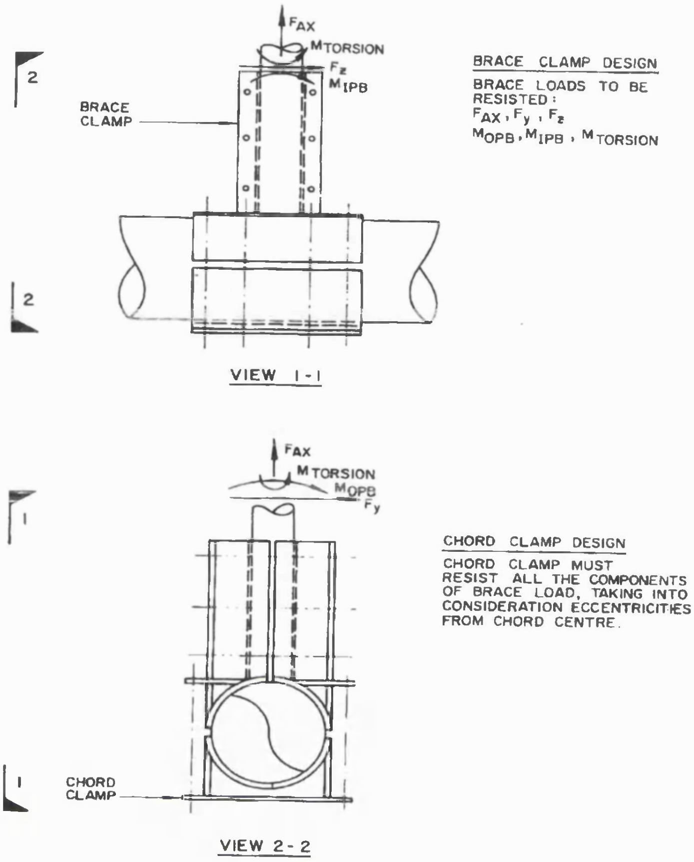

Figure 5.3 Brace member loads considered for the design of a mechanical or stressed grouted clamp [5.1]

Figure 5.4 Clamp, tube, studs and hydraulic jacks on a test rig prior to installation at 20 meters water depth in IFREMER's water tank.

Figure 5.5 Stolt Comex Seaways ROV and Cybernetix arm during launching

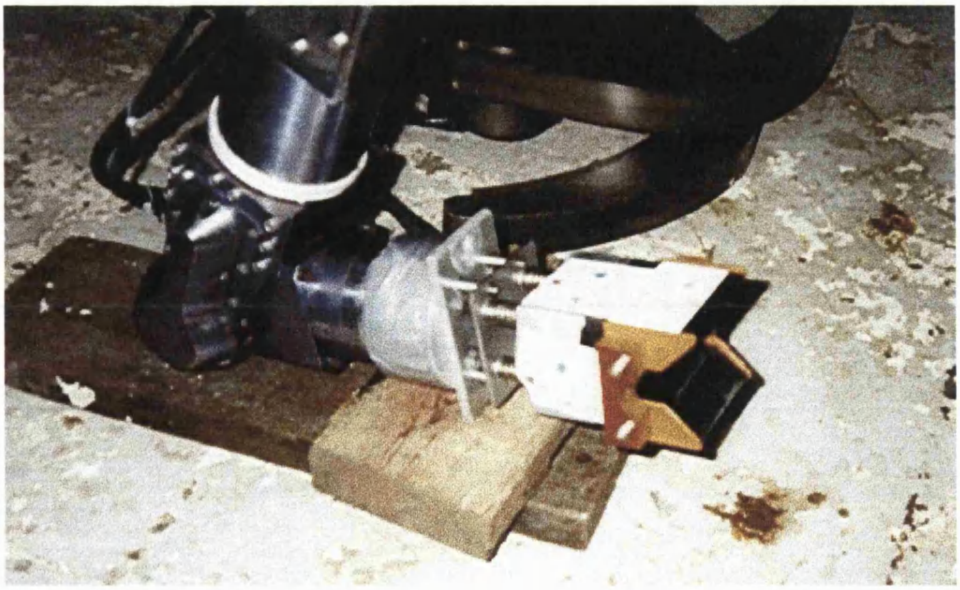

Figure 5.6 Cybernetix arm holding the ACSM probe

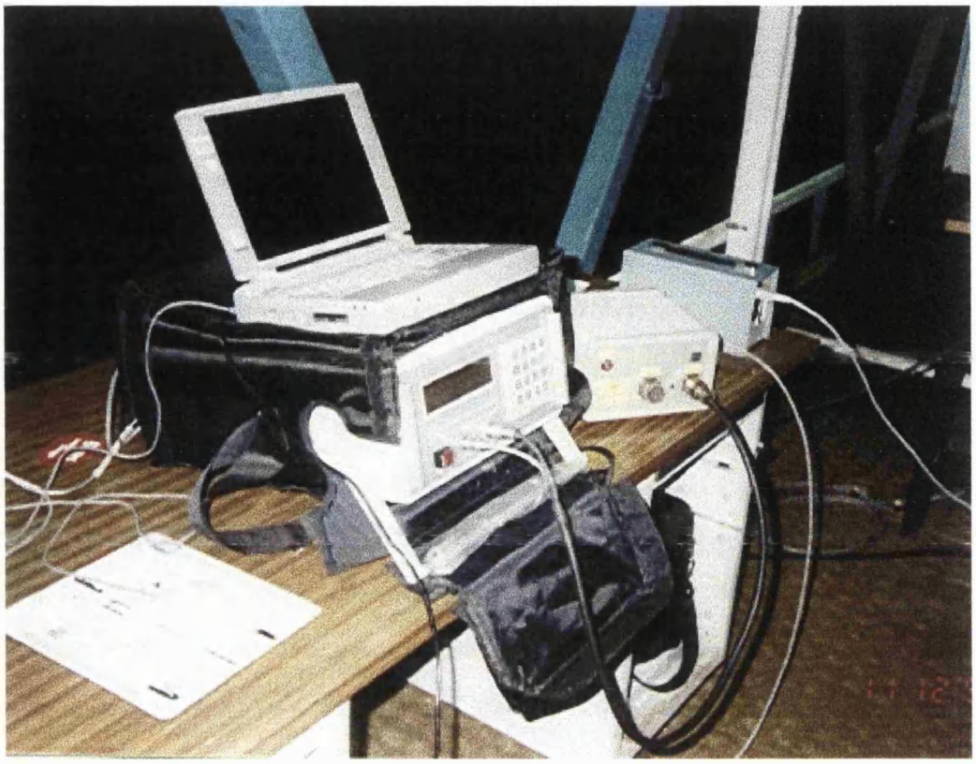

Figure 5.7 From left to right. TSC U9 topside unit under laptop, demagnetising unit (empty socket is for ACSM probe lead) and power supply unit.

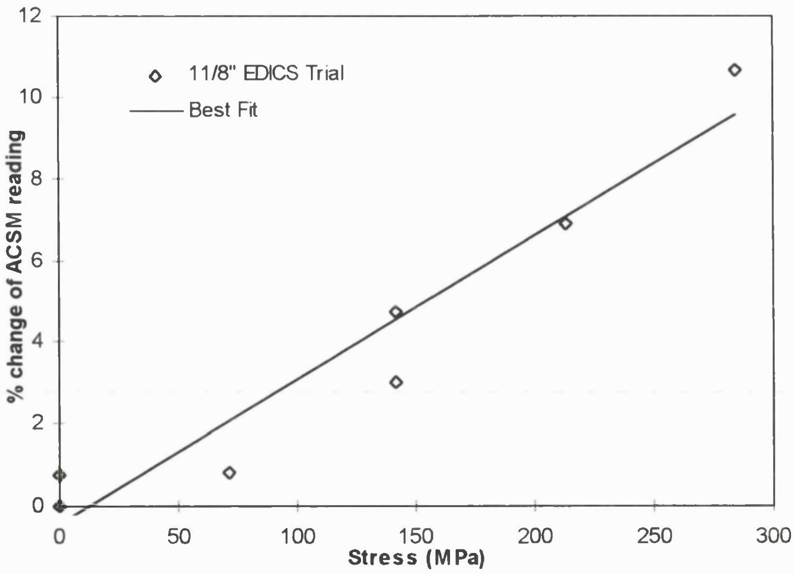

Figure 5.8 ACSM readings on 11/8" unthreaded central stud of EDICS Trial

CHAPTER SIX
SUMMARY, CONCLUSIONS AND RECOMMENDATIONS

In chapter 1 generalities of fatigue cracks in tubular joints and analytical approaches for the analysis of crack repairs were presented. The concept of clamping a severely crack joint was identified for the cases when crack removal cannot be successfully achieved.

In chapter 2 a comprehensive finite element analysis of crack repairs was made. This analysis allowed the identification of stress distributions in short and long repair profiles. The short repair stress distributions gave expectations for providing large fatigue life extension for crack repaired connections. This was due to the higher SCF values at the repair ends forcing crack initiation to take place in these regions where plate thickness remains intact.

In chapter 3 the experimental work presented confirmed in many occasions that crack initiation takes place at the repair ends in short repairs and in the bottom of the repair for long repairs (edge repairs). Crack removal and re-testing provided valuable data for the determination of fatigue life extension. The benefits of removing weld toe defects were clearly identified. The following three methods for crack removal were applied: Disc cutting, Electrochemical machining and ROV arm burr grinding. Pros and cons were identified and comparisons were also made. The effects of compressive residual stresses by shot peening were also briefly addressed. To conclude the chapter an approximate procedure for the determination of fatigue life extension after repair was introduced.

In chapter 4 the experimental data was processed to extract stress intensity correction factors (Y factors). Based on the Y factor values the effect of the compressive residual stress induced by shot peening was analysed. The crack repair effect on the Y factors trend was also observed. Analytical determination of Y factors was presented considering the weight function approach and the Newman-Raju solution. A crack shape design curve applicable to a crack repair and as-welded conditions was proposed. The crack shape design curve inserted in the Newman-Raju solution allowed the determination of a Y factor curve. The Y factor curve was corrected to consider non-uniform stress distributions and it was used to make crack growth predictions on T-butts. Predicted and experimental crack growth curves were compared. Finally, the load shedding effect is considered in the Y factor curve for the prediction of crack growth on tubular joints.

Chapters 2, 3 and 4 completed the work on fatigue crack repair by crack removal. Thus it was felt necessary, for a complete view of the problem, to include in this thesis a brief study about repairing severely cracked tubular joints by clamping.

In chapter 5 it was identified that clamps rely on the friction between the clamp and the tubular joint for providing an alternate load path. The friction is provided by the compressive force induced by the studs. Thus, the clamp effectiveness for repairing a severely cracked joint depends on the studs load level. Unfortunately, there is a lack of measurement instruments for determining load/stress on studs in underwater conditions. In this chapter a novel application of the ACSM technique for measuring load/stress on studs was presented. Finally, the experimental work developed for the validation was also addressed.

In this thesis, fatigue crack repair for offshore structures is aimed to extend the service life of structural fatigue cracked members by means of crack removal or clamping cracked tubular joints. Conclusions obtained from the work presented are as follows:

- The analytical and experimental results obtained from T-butt specimens showed that it is recommended to use short repairs for the removal of fatigue cracks. This recommendation comes from the observation that fatigue cracks in short repairs initiate where the repair ends merge with the original plate surface, thus the original plate thickness is reinstalled for crack propagation. This feature facilitates crack inspection and provides the possibility of a subsequent crack repair without the need to increase the repair depth if detection is made in early stages of growth. The fatigue life of short repairs is substantially improved by machining the weld toes at both sides of the repair ends.

- Fatigue life extensions equal to the as-welded fatigue life can be achieved by welded connections repaired with short repairs when cracks are removed before they reach 30% of the plate thickness. This extension can be increased by machining the weld toes at both sides of the repair ends.

- For removing a fatigue crack by using a short repair, the crack can be detected in any stage of growth. Short repairs can still be applied when cracks have exceeded 30% of the plate thickness. The only condition to satisfy for designing a short repair is verify that the repair shape ratios (D/T and 2D/L) located on the crack shape evolution plot (figure 3.33) are above the trend. The repair dimensions should include the inspection-repair allowances presented in chapter 3.

- The benefits of short repairs are heightened when just the crack and inspection-repair allowances are machined. This can be achieved by the support of a combination of inspection techniques like ACFM and MPI whilst machining.

- Fatigue crack repair by ROV grinding is possible and satisfactory crack repairs can be obtained. However, results can be greatly improved if new technology is incorporated to operate the ROV arm under force control. This would avoid the application of the considerable forces that occurred in the trials causing burr tools to wear rapidly and break prematurely. Additionally, this would reduce the time offshore spent on tool replacement.

- Fatigue crack removal by machining a short repair using the ECM technique has been demonstrated to provide the same results as an ideal technique like disc cutting. Although, the surface quality obtained using disc cutters is considerably better than that obtained using ECM technique, this does not have any effect on the fatigue life extension since crack initiation takes place outside of the repair groove.

- A design crack shape curve has been proposed for preliminary predictions of crack shape evolution on T-butts and tubular joints in as-welded and repaired conditions. The design curve can be incorporated into models to determine stress intensity correction factors (Y factors) for the prediction of crack growth evolution. The crack growth predictions made did not differ greatly from the experimental results. However it is recommended to determine the stress distribution through the thickness for accurate predictions of crack growth after crack removal. Predictions of fatigue life using the fracture mechanics procedure presented in chapter 4 can assist when determining whether a crack removal or a clamp is more suitable for a particular fatigue cracked connection.

- The application of the ACSM technique for stress measurement allows the determination of the stress magnitude on clamp studs with a good accuracy by simply placing a probe on the metal surface. Successful probe deployment by ROV arms was proved in underwater trials.

From the work presented in this thesis the following recommendations for future work can be made:

- In general terms in tubular joints the stress distribution at the weld toe around the perimeter of the member is not uniform as opposed to the stress distribution along the weld toe of T-butts. This situation motivated Dover et al to remove cracks in tubular joints using a repair with long run-outs until regions of lower stress are reached by the repair ends. The extrapolation of the behaviour of short repairs found in T-butts to tubular joints appear to be valid. However further analysis and experimentation is required on tubular joints with short repairs to validate the benefits found in T-butts.

- Although, ROV deployment of the ECM technique for crack removal was not made, it is considered that ECM crack removal could be more suitable for ROV applications than grinding. The ECM is a self contained unit; thus, the ROV is only required for deployment and positioning. Further experimentation is required to confirm this consideration.